

Second Edition

Well Productivity Handbook

Vertical, Fractured, Horizontal, Multilateral,
Multi-fractured, and Radial-Fractured Wells

Boyun Guo



Well Productivity Handbook

Vertical, Fractured, Horizontal,
Multilateral, Multi-Fractured,
and Radial-Fractured Wells

Second Edition

Boyun Guo

*Professor, University of Louisiana at Lafayette, Lafayette, LA,
United States*



Gulf Professional Publishing
An imprint of Elsevier

Gulf Professional Publishing is an imprint of Elsevier
50 Hampshire Street, 5th Floor, Cambridge, MA 02139, United States
The Boulevard, Langford Lane, Kidlington, Oxford, OX5 1GB, United Kingdom

Copyright © 2019 Elsevier Inc. All rights reserved.

No part of this publication may be reproduced or transmitted in any form or by any means, electronic or mechanical, including photocopying, recording, or any information storage and retrieval system, without permission in writing from the publisher. Details on how to seek permission, further information about the Publisher's permissions policies and our arrangements with organizations such as the Copyright Clearance Center and the Copyright Licensing Agency, can be found at our website: www.elsevier.com/permissions.

This book and the individual contributions contained in it are protected under copyright by the Publisher (other than as may be noted herein).

Notices

Knowledge and best practice in this field are constantly changing. As new research and experience broaden our understanding, changes in research methods, professional practices, or medical treatment may become necessary.

Practitioners and researchers must always rely on their own experience and knowledge in evaluating and using any information, methods, compounds, or experiments described herein. In using such information or methods they should be mindful of their own safety and the safety of others, including parties for whom they have a professional responsibility.

To the fullest extent of the law, neither the Publisher nor the authors, contributors, or editors, assume any liability for any injury and/or damage to persons or property as a matter of products liability, negligence or otherwise, or from any use or operation of any methods, products, instructions, or ideas contained in the material herein.

Library of Congress Cataloging-in-Publication Data

A catalog record for this book is available from the Library of Congress

British Library Cataloguing-in-Publication Data

A catalogue record for this book is available from the British Library

ISBN: 978-0-12-818264-2

For information on all Gulf Professional Publishing publications visit our website at
<https://www.elsevier.com/books-and-journals>

Publisher: Brian Romer

Senior Acquisition Editor: Katie Hammon

Editorial Project Manager: Ali Afzal Khan

Production Project Manager: R.Vijay Bharath

Cover Designer: Greg Harris

Typeset by TNQ Technologies



This book is dedicated to my wife Huimei for her understanding and encouragement that were as responsible as the experience and knowledge that have been inscribed herein.

Boyun Guo

List of symbols

A = cross-sectional area for fluid flow, or drainage area

A_{in} = choke port area

$^{\circ}API$ = API gravity of stock tank oil

A_1 = upstream hydraulic flow area

A_2 = downstream hydraulic flow area

B_o = formation volume factor of oil

B_g = formation volume factor of gas

B_w = formation volume factor of water

c = polytropic constant

C_A = drainage area shape factor

c_d = choke discharge coefficient

c_L = specific heat of liquid

c_t = total compressibility

c_p = specific heat of gas at constant pressure

C_v = control valve coefficient

c_v = specific heat of gas at constant volume

c_{vg} = gas heat capacity at constant volume

c_{vo} = oil heat capacity at constant volume

c_{vw} = water heat capacity at constant volume

C_d = drag coefficient

D = inner diameter in feet, or non-Darcy flow coefficient

d = inner diameter

d_{choke} = choke port ID

D_H = hydraulic diameter

d_h = equivalent diameter of the drain hole

$D\rho v$ = inertial force

d_1 = upstream hydraulic ID

E_k = kinetic energy per unit volume of gas

E_{km} = minimum required kinetic energy

F_{CD} = fracture conductivity

f_F = Fanning friction factor

F_g = correction factor for gas production rate

f_M = Darcy-Wiesbach (Moody) friction factor

F_o = correction factor for oil production rate

- f_{2F} = two-phase friction factor
 g = gravitational acceleration
 g_c = gravitational conversion factor
 G_2 = mass flux at downstream
 h = pay zone thickness
 I_{ani} = anisotropy index
 J = productivity indexd
 J^* = productivity index at and above bubble-point
 J_O = productivity index of non-fractured well
 k = effective horizontal permeability, or heat specific ratio
 k_f = fracture permeability
 k_H = horizontal permeability
 k_V = vertical permeability
 L = length
 ΔL = length change
 M = liquid mass flow rate
 m_i = mass flow rate from/into layer i
 M_{G2} = gas phase mass flow rate at downstream
 M_{L2} = liquid phase mass flow rate at downstream
 m_t = total mass flow rate
 M_W = molecular weight of gas
 m_{wh} = mass flow rate at wellhead
 M_2 = mixture mass flow rate at downstream
 n = polytropic exponent for gas
 N_D = pipe diameter number
 N_L = liquid viscosity number
 N_{Re} = Reynolds number
 N_{Vg} = gas velocity number
 N_{VL} = liquid velocity number
 p = pressure
 p_a = atmospheric pressure
 p_b = oil bubble-point pressure
 p_{dst} = downstream pressure
 p_e = reservoir pressure
 p_{hf} = wellhead flowing pressure
 p_i = initial reservoir pressure

P_{kf} = pressure at kick-out point
 p_L = average pressure in the inner region
 p_m = pressure at the mid-depth
 P_{outlet} = pressure at choke outlet
 P_{pr} = pseudoreduced pressure
 p_{sc} = standard pressure
 P_{up} = upstream pressure
 p_{wf} = flowing bottom-hole pressure
 p_{wH} = pressure at the heel of drain hole
 \bar{p} = reservoir pressure
 Δp = pressure increment
 P_1 = pressure at point 1
 P_2 = pressure at point 2
 p_1 = upstream pressure
 p_2 = downstream pressure
 q = liquid flow rate
 q_g = gas production rate
 Q_{gpm} = liquid flow rate
 $gslM$ = minimum gas flow rate
 q_i = flow rate from/into layer i
 q_o = critical oil rate
 q_s = sand production rate
 q_w = water production rate
 R = universal gas constant
 r_e = radius of drainage area of vertical well
 r_{eH} = radius of drainage area of horizontal well
 r_L = equivalent radius of the inner region
 R_s = solution gas-oil ratio
 r_w = wellbore radius
 S = skin factor
 S_o = skin factor of the non-fractured well
 T = temperature in °R
 t = temperature in °F
 T_{av} = average temperature
 T_{pr} = pseudoreduced temperature
 T_{sc} = standard temperature

- T_{up} = upstream gas temperature
 u = fluid velocity
 u_m = mixture velocity
 u_{SG} = superficial velocity of gas phase
 u_{SL} = superficial velocity of liquid phase
 u_1 = mixture fluid velocity at upstream
 u_2 = mixture fluid velocity at downstream
 V = volume of the pipe segment
 V_{G1} = upstream gas specific volume
 V_{G2} = downstream gas specific volume
 V_{gas} = gas volume in standard condition
 V_L = upstream liquid specific volume
 V_{oil} = oil volume in stock tank condition
 V_{sc} = gas volume in standard condition
 v_{sl} = terminal slip velocity
 V_{st} = oil volume in stock tank condition
 w = fracture width
 x_g = free gas in-situ quality at upstream
 x_o = oil in-situ quality at upstream
 x_w = water in-situ quality at upstream
 x_f = fracture half-length
 x_1 = free gas quality at upstream
 y = downstream-to-upstream pressure ratio
 y_a = actual downstream-to-upstream pressure ratio
 y_b = distance of boundary from drain hole
 y_c = critical downstream-to-upstream pressure ratio
 y_e = half drainage length perpendicular to horizontal wellbore
 y_L = liquid holdup
 z = gas compressibility factor
 \bar{z} = average gas compressibility factor
 z_e = half of the distance between fractures
 z_{up} = upstream gas compressibility factor
 Δz = elevation change
 β = upstream-downstream fluid velocity ratio
 ε = relative roughness
 ϕ = porosity

γ = specific gravity of the liquid relative to water

γ_g = gas specific gravity

γ_O = oil specific gravity

γ_S = specific gravity of produced solid

γ_w = water specific gravity

ρ = fluid density

$\bar{\rho}$ = average mixture density

ρ_{air} = density of air

ρ_g = gas density

ρ_{G1} = upstream gas density

ρ_{G2} = downstream gas density

ρ_i = density of fluid from/into layer i

ρ_L = liquid density

ρ_{m2} = mixture density

ρ_o = oil density

$\rho_{o,st}$ = density of stock tank oil

ρ_w = water density

ρ_{wh} = density of fluid at wellhead

$\Delta\rho$ = density difference

ρ_1 = mixture density at top of tubing segment

ρ_2 = mixture density at bottom of segment

λ = parameter group

σ = liquid-gas interfacial tension

μ = fluid viscosity

μ_G = gas viscosity

$\bar{\mu}_g$ = average gas viscosity

μ_J = Joule-Thomson coefficient

μ_L = liquid viscosity

μ_o = oil viscosity

List of figures

Figure 1.1	A naturally flowing well produces oil and gas by its own pressure.	4
Figure 1.2	The hydrocarbon phase diagram shows how the liquid or gas phases of hydrocarbons are related to temperature and pressure.	5
Figure 1.3	In a water drive reservoir, pressure exerted at the water–oil contact (WOC) forces the oil up and toward the wellbore.	6
Figure 1.4	In a gas-cap drive reservoir, pressure is exerted on the oil by the overlying gas cap, forcing it toward and into the wellbore.	6
Figure 1.5	In a dissolved-gas drive reservoir, production pressure comes from the gas that emerges from the oil when reservoir pressure falls below the bubble point.	7
Figure 1.6	A typical flowing oil well requires specific equipment from the bottom of the wellbore to the producing wellhead.	7
Figure 1.7	The wellhead is the link between casing and tubing within the wellbore and the surface production equipment.	9
Figure 1.8	A “Christmas Tree” is used to regulate well fluid flow passively, through surface chokes, or actively, through valves.	10
Figure 1.9	Either wellhead or down-hole chokes can be used to regulate well fluid flow.	10
Figure 1.10	Water coning in a vertical well with partial perforation.	11
Figure 1.11	Horizontal well completion with predrilled liner equipped with external casing packers in which a casing patch is run to permanently isolate a segment of the wellbore.	12
Figure 1.12	Illustration of a multifractured horizontal well completed with plug and perf method.	13
Figure 1.13	Sketch of radial fractures around a vertical wellbore created by blast fracturing.	13
Figure 2.1	Parameters for a horizontal wellbore.	41
Figure 2.2	Measured bottom-hole pressures and oil production rates during a pressure draw-down test.	45
Figure 2.3	Log–log diagnostic plot of test data.	45
Figure 2.4	Semilog plot for vertical radial flow analysis.	46
Figure 2.5	Square-root time plot for pseudo-linear flow analysis.	46
Figure 2.6	Semilog plot for horizontal pseudo-radial flow analysis.	47
Figure 2.7	Model-match to the measured pressure response.	48
Figure 3.1	A reservoir model illustrating radial flow: (A) lateral view, (B) top view.	55
Figure 3.2	A reservoir model illustrating a constant-pressure boundary.	57
Figure 3.3	Pressure and flow conditions of a reservoir with no-flow boundaries.	57

Figure 3.4	Shape factors for closed drainage areas with low-aspect ratios.	59
Figure 3.5	Shape factors for closed drainage areas with high-aspect ratios.	60
Figure 3.6	An example of reservoir pressure distribution near a long fracture.	63
Figure 3.7	A typical inflow performance relationship curve for an oil well.	65
Figure 3.8	Transient inflow performance relationship curve for Sample Problem 3-2.	67
Figure 3.9	Steady-state inflow performance relationship curve for Sample Problem 3-2.	68
Figure 3.10	Pseudo—steady-state inflow performance relationship curve for Sample Problem 3-2.	69
Figure 3.11	Inflow performance relationship curve for Sample Problem 3-3.	71
Figure 3.12	Generalized Vogel inflow performance relationship model for partial two-phase reservoirs.	72
Figure 3.13	Inflow performance relationship curve for Sample Problem 3-4.	74
Figure 3.14	Inflow performance relationship curves for Sample Problem 3-5, Well A.	76
Figure 3.15	Inflow performance relationship curves for Sample Problem 3-5, Well B.	77
Figure 3.16	Inflow performance relationship curves for Sample Problem 3-6.	79
Figure 3.17	Inflow performance relationship curves of individual oil-bearing strata.	83
Figure 3.18	Composite inflow performance relationship (IPR) curve for all strata open to flow.	84
Figure 3.19	Inflow performance relationship curves for Sample Problem 3-8.	86
Figure 3.20	Inflow performance relationship curves for Sample Problem 3-9.	89
Figure 4.1	Parameters used to characterize flow along a tubing string.	94
Figure 4.2	Darcy—Wiesbach friction factor diagram.	96
Figure 4.3	Pressure profile given by the spreadsheet program <i>HagedornBrownCorrelation.xls</i> for Sample Problem 4.5.	113
Figure 4.4	Calculated tubing pressure profile for Sample Problem 4.6.	116
Figure 5.1	Inflow performance relationship (IPR) and tubing performance relationship (TPR) curves given by the spreadsheet program <i>Transient Production Forecast.xls</i> .	126
Figure 5.2	Inflow performance relationship (IPR) and tubing performance relationship (TPR) curves given by the spreadsheet program <i>Pseudosteady-2Phase Production Forecast.xls</i> .	128
Figure 5.3	Inflow performance relationship (IPR) and tubing performance relationship (TPR) curves given by the spreadsheet program <i>Steady-2Phase Production Forecast.xls</i> .	130

Figure 5.4	Inflow performance relationship (IPR) and tubing performance relationship (TPR) curves given by the spreadsheet program <i>Dry Gas Transient Production Forecast.xls</i> .	134
Figure 5.5	Curves given by the spreadsheet program <i>Pseudosteady Production of Single-Fractured Well.xls</i> . IPR, inflow performance relationship; TPR, tubing performance relationship.	143
Figure 5.6	Curves given by the spreadsheet program <i>Pseudosteady-2Phase Horizontal Well Production Forecast.xls</i> . IPR, inflow performance relationship; TPR, tubing performance relationship.	147
Figure 5.7	Calculated annular pressure distributions with and without inflow control device (ICD) installations.	151
Figure 5.8	Calculated oil influx distributions with and without inflow control device (ICD) installations.	151
Figure 5.9	Curves given by the spreadsheet program <i>Horizontal Dry Gas Well Production Forecast.xls</i> . IPR, inflow performance relationship.	154
Figure 6.1	Schematic of a typical root well.	166
Figure 6.2	Schematic of a reservoir section drained by a fishbone well.	166
Figure 6.3	Curves given by the spreadsheet program <i>Pseudosteady Production of Fishbone Oil Well.xls</i> . IPR, inflow performance relationship; TPR, tubing performance relationship.	169
Figure 6.4	A simplified multilateral well structure.	172
Figure 6.5	Symbols used to describe a multilateral well.	173
Figure 7.1	A reservoir section drained by a multifractured horizontal wellbore.	184
Figure 7.2	Fluid flow in a fracture to a horizontal wellbore.	184
Figure 7.3	Curves given by spreadsheet program <i>Pseudosteady Production of Multi-Fractured Well.xls</i> . IPR, inflow performance relationship; TPR, tubing performance relationship.	188
Figure 7.4	Tortuous fractures in the near-wellbore area.	190
Figure 7.5	Twelve fracture trends developed from 12 perforation clusters in three stages of fracturing.	191
Figure 7.6	Model-predicted well productivity curves for a volume-fractured horizontal oil well given by spreadsheet program <i>Volume-Fractured Oil Well.xls</i> .	193
Figure 7.7	Model-predicted well productivity curves for a volume-fractured horizontal gas well given by spreadsheet program <i>Volume-Fractured Gas Well.xls</i> .	194
Figure 8.1	Radial propagation of fractures in EF and HEGF. EF, explosive fracturing; HEGF, high-energy gas fracturing.	198
Figure 8.2	A sketch of radial fractures created in blast fracturing.	198

Figure 8.3	A sketch of radial fractures created in hydraulic re-fracturing.	199
Figure 8.4	Effect of fracture penetration on productivity index of a blast-fractured oil well.	201
Figure 8.5	Effect of fracture conductivity on productivity of a high-energy gas fracturing oil well.	203
Figure E.1	A planar schematic of fluid flow from a quadrant of matrix volume V to a fracture.	220
Figure F.1	A sketch of radial fracture configuration around a wellbore.	228

List of tables

Table 2.1	Composition of a typical petroleum fluid.	18
Table 2.2	Results given by the spreadsheet program OilProperties.xls.	22
Table 2.3	Results given by the spreadsheet program MixingRule.xls.	25
Table 2.4	Results given by the spreadsheet program Carr-Kobayashi-Burrows-GasViscosity.xls.	27
Table 2.5	Results given by the spreadsheet program Brill-Beggs-Z.xls.	30
Table 2.6	Results given by the spreadsheet program Hall-Yarborough-Z.xls.	31
Table 2.7	Coefficients of correlations for parachors of hydrocarbons.	35
Table 3.1	Summary of test points for eight oil-bearing layers.	83
Table 3.2	Comparison of commingled and strata-grouped productions.	84
Table 4.1	Results given by spreadsheet program Poettmann-CarpenterBHP.xls for Sample Problem 4.3	104
Table 4.2	Results given by spreadsheet program Guo-GhalamborBHP.xls for Sample Problem 4.4	106
Table 4.3	Result given by spreadsheet program HagedornBrownCorrelation.xls for Sample Problem 4.5	111
Table 4.4	Spreadsheet program AverageTZ.xls—Data input and result sections.	115
Table 4.5	Spreadsheet program Cullender-Smith.xls—data input and result sections.	118
Table 5.1	Data given by the spreadsheet program Transient Production Forecast.xls.	126
Table 5.2	Data generated by the spreadsheet program Pseudosteady-2Phase Production Forecast.xls.	128
Table 5.3	Data given by the spreadsheet program Steady-2Phase Production Forecast.xls.	129
Table 5.4	Data given by the spreadsheet program Dry Gas Production Forecast.xls.	133
Table 5.5	Data given by the spreadsheet program Wet Gas Pseudosteady Production Forecast.xls.	135
Table 5.6	Result given by the spreadsheet program TurnerLoading.xls.	138
Table 5.7	Results given by the spreadsheet program GasWellLoading.xls.	141
Table 5.8	Data given by the spreadsheet program Pseudosteady Production of Single-Fractured Well.xls.	143
Table 5.9	Data given by the spreadsheet program Fractured Gas Well Production Forecast.xls.	145
Table 5.10	Data given by the spreadsheet program Pseudosteady-2Phase Horizontal Well Production Forecast.xls.	146
Table 5.11	Designed inflow control device locations and sizes.	152

Table 5.12	Data given by the spreadsheet program Horizontal Dry Gas Well Production Forecast.xls.	153
Table 6.1	Results given by spreadsheet Program Pseudosteady Production of Fishbone Gas Well.xls.	172
Table 6.2	Given data for a four-lateral root-type oil well.	175
Table 6.3	Reservoir property data.	176
Table 6.4	Fluid property data.	176
Table 6.5	Well data for vertical sections.	177
Table 6.6	Well data for curved sections.	177
Table 6.7	Well data for horizontal sections.	177
Table 6.8	Summary of calculated lateral and well production rates.	178
Table 6.9	Given data for a four-lateral root-type gas well.	178

Preface

Several new types of oil and gas wells with complex completions have been developed and used in the energy industry since the publication of the first edition of this book a decade ago. The author realized that there is a real need for the second edition of the book that documents the productivity models of both traditional and the new well types.

This book is written primarily for reservoir and production engineers, and college students at senior as well as graduate levels. It is not the authors' intention to simply duplicate general information that can be found elsewhere. This book gathers the authors' experience gained through years of teaching production engineering and reservoir simulation courses in the petroleum industry and at the university level. The mission of the book is to provide reservoir and production engineers with a handy reference for modeling oil and gas production wells with simple and complex completions. The original manuscript of this book has been used as a petroleum engineering textbook for undergraduate and graduate students in petroleum engineering programs.

This book is intended to cover the full *scope* of the productivity of naturally flowing wells, with all types of completions. But the well inflow models presented here are also valid for wells that require artificial lift. Following a sequence from simple to complex well completions, this book presents its *contents* in eight chapters:

- Chapter 1 presents an introduction to petroleum production wells.
- Chapter 2 outlines methods for estimating petroleum fluid and rock properties that are essential for analyzing and modeling performance of wells.
- Chapter 3 discusses modeling of inflow performance of wells producing different types of fluids.
- Chapter 4 presents and illustrates different mathematical models for describing wellbore/tubing performance when delivering single or multiphase production fluid.
- Chapter 5 describes the principle of well productivity analysis and shows how to predict productivity of wells with simple trajectories.
- Chapter 6 demonstrates methods for predicting productivity of multilateral wells.
- Chapter 7 illustrates methods for predicting productivity of multifractured wells.
- Chapter 8 presents methods for predicting productivity of radial-fractured wells.

Because the substance of this book is virtually boundless in depth, knowing what to omit was the greatest difficulty with its editing. The authors believe that it would require many books to fully cover the basics of well productivity modeling. To counter any deficiency that might arise from space limitations, the book contains a list of reference books and papers at the end of each chapter, so that readers should experience little difficulty in pursuing each topic beyond the presented scope.

Regarding *presentation*, this book focuses on presenting and illustrating the engineering principles used for well productivity modeling, rather than covering in-

depth theories. The derivation of mathematical models is beyond the scope of this book. Applications are illustrated by solving sample problems using computer spreadsheet programs except for very simple problems. All the computer programs are provided with the book. Although the US field units are used in the text, the option of using SI units is provided in the computer spreadsheet programs.

This book is based on numerous documents, including reports and papers accumulated through years of industry and academic work by the authors. We are grateful to the University of Louisiana at Lafayette for permission to publish its materials. Special thanks are due to Chevron Corporation for providing Chevron I and Chevron II professorships during the editing of this book. Our thanks are due to Mr. Rashid Shaibu of University of Louisiana at Lafayette who made a thorough review and editing of this book manuscript. On the basis of collective experience, the author expects this book to be of value to reservoir and production engineers in the petroleum industry. Below is a link to a list of Excel spreadsheets that accompany the book's material, helping the petroleum engineer practice and be more efficient in every day decisions.

<https://www.elsevier.com/books/well-productivity-handbook/guo/9780128182642>

Boyun Guo, PhD

June 10, 2019

Lafayette, Louisiana

Well productivity basics

1

This section of the book presents basic data and knowledge required for predicting productivity of oil and gas wells with conventional structures.

Chapter 1 presents an introduction to petroleum production wells, covering a brief description of oil and gas reservoirs, types of well completion, and the concept of well productivity.

Chapter 2 outlines methods for estimating petroleum fluid and reservoir properties, covering oil properties, gas properties, production water properties, fluid interfacial properties, and reservoir rock properties.

Chapter 3 provides basic knowledge for constructing well inflow performance relationship (IPR) of conventional well structures including nonfractured vertical wells, fractured vertical wells, and horizontal wells. Deliverability of oil and gas wells in reservoirs with single-phase, two-phase, and partial two-phase flow is described.

Chapter 4 describes tubing/wellbore performance relationship (TPR) for single- and multiphase flow in oil and gas wells.

Chapter 5 illustrates the principle of NODAL analysis in well productivity forecast. It shows how to combine well IPR and TPR to predict productivity of conventional well structures including nonfractured vertical wells, fractured vertical wells, and horizontal wells.

Introduction

Chapter outline

1.1 Oil and gas wells and reservoirs	3
1.2 Types of well completions	9
1.2.1 Conventional well completions.....	11
1.2.2 Unconventional well completions.....	11
1.3 Well productivity	14
1.4 Summary	15
1.5 Problems	15
References	15

1.1 Oil and gas wells and reservoirs

Oil and gas wells are used for extracting crude oil and natural gas from oil and gas reservoirs. There are three types of wells: oil, gas condensate, and gas. Their classification depends on the producing gas—oil ratio (GOR). Gas wells produce at a GOR greater than 100,000 scf/stb; gas condensate wells produce at a GOR less than 100,000 scf/stb but greater than 5000 scf/stb; and oil wells produce at a GOR less than 5000 scf/stb. Unit conversion factors for the SI systems are provided in Appendix A.

A naturally flowing well consists of a reservoir segment, wellbore, and wellhead (Fig. 1.1).

The reservoir segment supplies the wellbore with production fluids (crude oil and/or natural gas). The wellbore provides a path for the fluids to flow from bottom hole to the surface. The wellhead permits control of the fluid production rate.

An oil or gas reservoir is a single porous and permeable underground rock formation, containing an individual bank of fluid hydrocarbons, and confined by impermeable rock or water barriers. It contains a single natural pressure system. An oil or gas field is an underground region consisting of one or more reservoirs, all related to the same structural feature. An oil or gas pool is a more extensive region containing one or more reservoirs, in isolated structures.

Engineers classify oil, gas condensate, and gas reservoirs on the basis of the initial reservoir condition and hydrocarbon composition. Oil that is at a pressure above its bubble point is called undersaturated oil because it can dissolve more

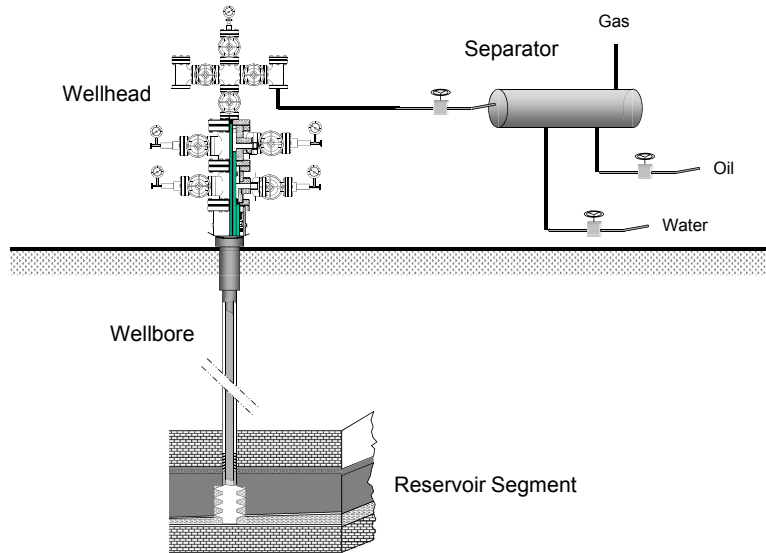


FIGURE 1.1

A naturally flowing well produces oil and gas by its own pressure.

gas if available at the temperature (Fig. 1.2). Oil that is at its bubble-point pressure is called saturated oil because it can dissolve no more gas at the temperature. Single (liquid)-phase flow occurs in an undersaturated oil reservoir. Two-phase (liquid oil and free gas) flow occurs in a saturated oil reservoir.

Oil reservoirs are further classified on the basis of boundary type, which determines the driving mechanism. The three types of reservoirs include the following:

- Water drive
- Gas-cap drive
- Dissolved-gas drive

In water drive reservoirs, the oil zone is connected through a continuous pressure path to a ground water system (aquifer). The pressure due to the water column forces the oil and gas to the top of the reservoir against the impermeable barrier that restricts further migration (the trap boundary). This pressure forces the oil and gas toward the wellbore. Under a constant oil production rate, an active water drive reservoir will maintain reservoir pressure longer, compared with other driving mechanisms. Edge-water drive reservoirs are better producers than bottom-water drive reservoirs. The reservoir pressure remains at its initial value above bubble-point pressure for longer, maintaining single-phase liquid flow in the reservoir for maximum productivity. An edge-water drive reservoir can also maintain steady-state flow condition for a significantly longer time before water breakthrough in

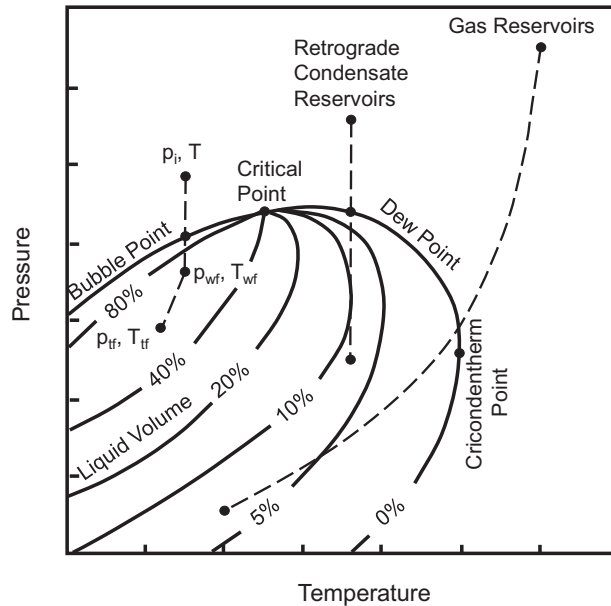


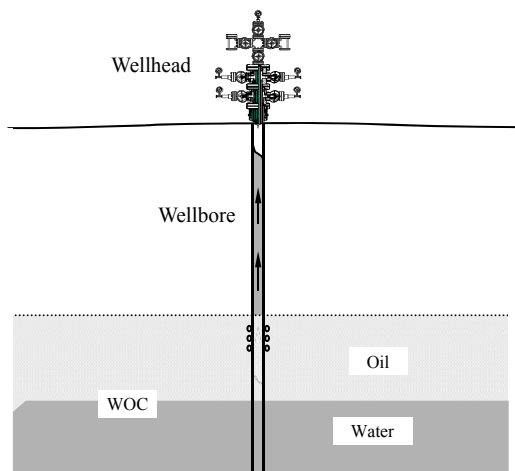
FIGURE 1.2

The hydrocarbon phase diagram shows how the liquid or gas phases of hydrocarbons are related to temperature and pressure.

the well. Bottom-water drive reservoirs are more troublesome because of water coning problems that affect oil production economics due to water treatment and disposal issues (Fig. 1.3).

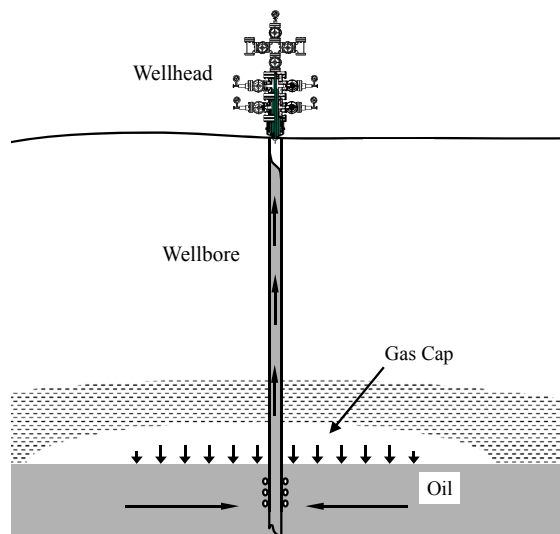
In gas-cap drive reservoirs, the gas in the gas cap expands and compensates for pressure depletion in the oil zone due to production (Fig. 1.4). Thus, the oil below the gas cap will produce naturally and longer. If the gas in the gas cap is extracted early in field development, the reservoir pressure will decrease rapidly. Some oil reservoirs display both water and gas-cap driving mechanisms.

A dissolved-gas drive reservoir is also called a solution-gas drive reservoir (Fig. 1.5). The oil reservoir has a fixed volume, bounded by impermeable structures or layers (faults or pinch-outs). In dissolved-gas drive oil reservoirs, the driving mechanism is gas held in solution in the oil (and water, if any). During production, the dissolved gas expands and partially compensates for the inevitable pressure decline in reservoir production. Dissolved-gas drive is a weaker mechanism in a volumetric reservoir than either water drive or gas drive. If the reservoir pressure drops to a value below the bubble-point pressure of the oil, gas escapes from the oil, and oil–gas two-phase competing flow begins. This reduces the effective permeability of the reservoir to the oil, increases the viscosity of the remaining oil, and thus reduces well productivity and ultimate oil recovery. Early attention to pressure maintenance can increase ultimate oil recovery in the solution-gas drive reservoir.

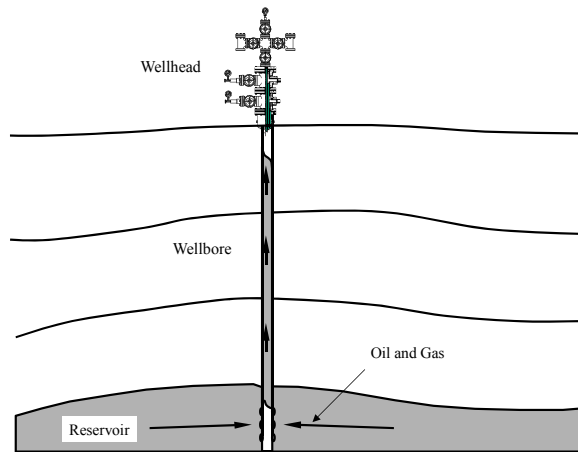
**FIGURE 1.3**

In a water drive reservoir, pressure exerted at the water–oil contact (WOC) forces the oil up and toward the wellbore.

For a typical oil well that delivers fluids to the surface solely due to the natural pressure of the reservoir, a completed wellbore is composed of casings, tubing, packers, and optional down-hole chokes (Fig. 1.6).

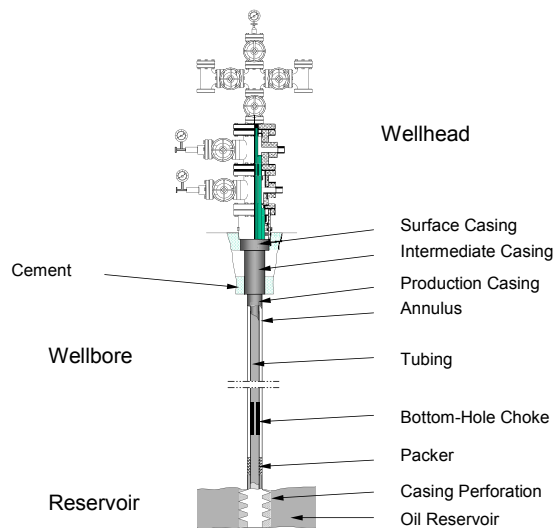
**FIGURE 1.4**

In a gas-cap drive reservoir, pressure is exerted on the oil by the overlying gas cap, forcing it toward and into the wellbore.

**FIGURE 1.5**

In a dissolved-gas drive reservoir, production pressure comes from the gas that emerges from the oil when reservoir pressure falls below the bubble point.

A wellbore is like an upside-down telescope. The large-diameter borehole section is at the top of the well. Each successive section of the wellbore is cased to the surface using narrower and narrower strings of nested casing. Lastly, a liner is inserted down the well that laps over the last casing at its upper end. Each casing

**FIGURE 1.6**

A typical flowing oil well requires specific equipment from the bottom of the wellbore to the producing wellhead.

or liner is cemented into the well (usually up to at least where the cement overlaps the previous cement job).

The final casing in the well is the production casing (or production liner). Once this casing has been cemented, production tubing is run down the well. A packer is usually used near the bottom of the tubing to isolate the annulus between tubing and casing, and to guide the produced fluids into the tubing. Packers can be actuated mechanically or hydraulically. The production tubing is often provided with a bottom-hole choke (particularly during initial well flow) to control the well flow and restrict overproduction.

Tubing strings are installed in most production wells. A tubing string provides a good seal and allows gas expansion to help lift the oil to the wellhead. The American Petroleum Institute (API) defines tubing size using nominal diameter and weight per foot. The nominal diameter refers to the inside diameter of the tubing. The tubing outside diameter determines the tubing's weight per foot. Steel grade used in tubing is designated H-40, J-55, C-75, L-80, N-80, C-90, and P-105, where the numbers represent minimum yield strength in units of 1000 psi. The minimum performance properties of production tubing are given in Appendix B.

The wellhead is the surface equipment set below the master valve and includes multiple casing heads and a tubing head. A casing head is a mechanical assembly used for hanging a casing string. The lowermost casing head is threaded, flanged, or studded into the surface casing (Fig. 1.7). Depending on the casing programs used during drilling, several casing heads might be installed. The casing head has a bowl which supports the casing hanger, which is threaded into the top of the production casing (or utilizes friction grips to hold the casing). As in the case of the production tubing, the production casing is suspended in tension so that the casing hanger actually supports it down to the freeze point. In a similar manner, the intermediate casings are supported by their respective casing hangers and bowls. The casing heads are all supported by the surface casing, which is in compression and cemented to the surface. A well completed with three casing strings will have two casing heads. The uppermost casing head supports the production casing, while the lowermost casing head is attached to and is supported by the surface casing.

The tubing string is supported at the surface by the tubing head, which is supported, in turn, by the production casing head. The tubing string is in tension all the way down to the packer.

The "Christmas Tree" is connected to the tubing head by an adaptor and regulates fluid flow from the well (Fig. 1.8). The Christmas Tree may have one flow outlet (a tee) or two flow outlets (a cross). A typical Christmas Tree consists of a master valve, wing valves, and a needle valve, located just below the tubing pressure gauge. The master valve and wing valves can close the well partially or completely when needed, but to replace the master valve itself, the tubing must be plugged. At the top of the "Christmas Tree," a pressure gauge indicates tubing pressure when the needle valve is open.

Surface chokes are restrictions in the flow line and control the flow rate in their respective lines (Fig. 1.9). In most naturally flowing wells, the oil production rate is regulated by changing the choke size. The choke (plus any other restrictions in the

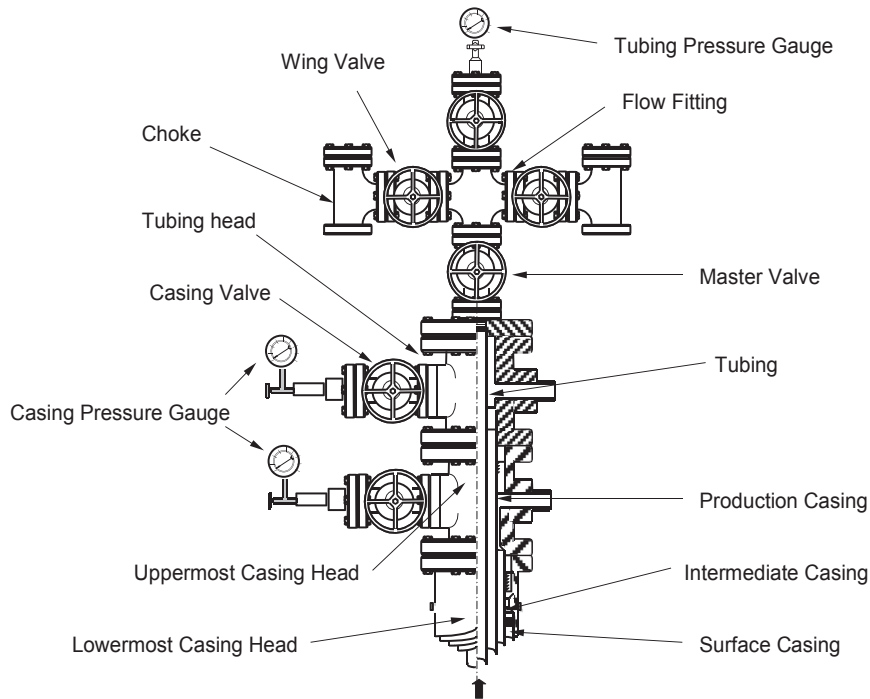


FIGURE 1.7

The wellhead is the link between casing and tubing within the wellbore and the surface production equipment.

flow line) causes backpressure in the line, which increases the flowing bottom-hole pressure. Increasing this flowing bottom-hole pressure decreases the pressure draw-down from the reservoir to the wellbore, in turn decreasing the fluid production rate of the well.

In some wells, chokes are installed in the lower section of tubing strings (Fig. 1.9). This arrangement reduces wellhead pressure and increases the oil production rate due to gas expansion in the tubing string. For gas wells, the use of down-hole chokes minimizes any gas hydrate problems in the well stream. A major disadvantage of the down-hole choke arrangement is that they are more expensive to replace than those chokes installed in the Christmas Tree.

1.2 Types of well completions

Well completion has revolutionized in the last 40 years from the conventional vertical wells through horizontal wells to the modern multilateral and multifractured horizontal wells. Radial fractured wells are anticipated to be the next generation of oil and gas wells.

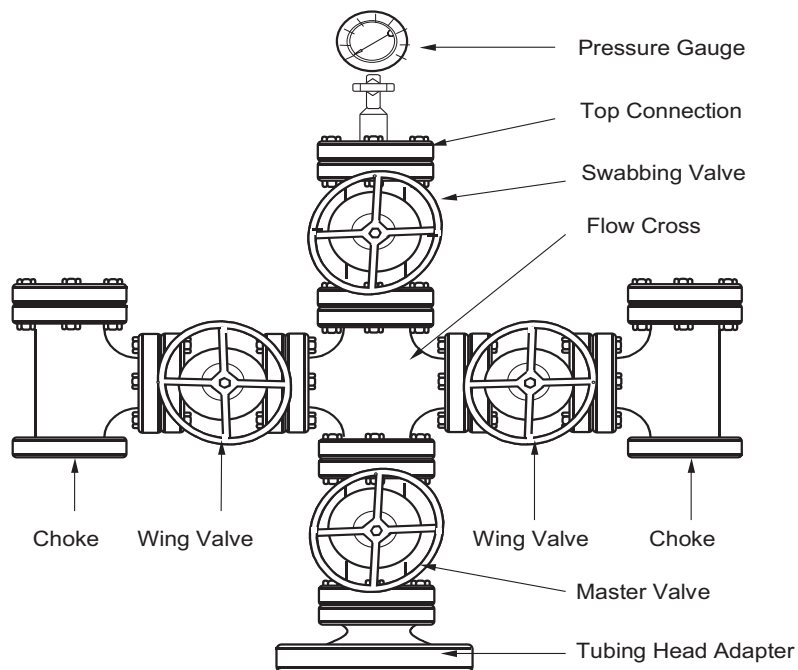


FIGURE 1.8

A “Christmas Tree” is used to regulate well fluid flow passively, through surface chokes, or actively, through valves.

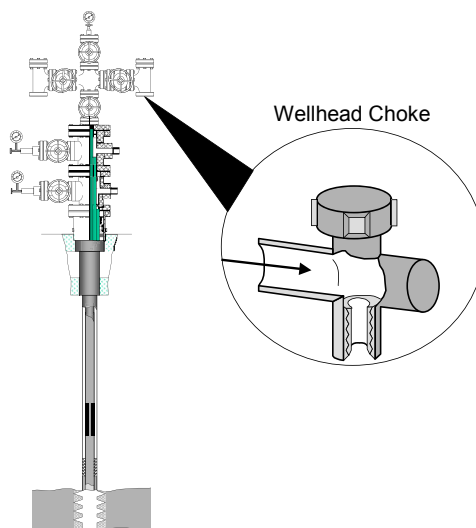


FIGURE 1.9

Either wellhead or down-hole chokes can be used to regulate well fluid flow.

1.2.1 Conventional well completions

Oil and gas wells were conventionally completed by open and cased hole methods before the 1980s. Pay zone thickness is the major factor affecting deliverability of vertical wells if the pay zones are fully opened. However, the pay zones are often partially opened to reduce water and gas production in water coning and gas coning reservoirs (Fig. 1.10). When the vertical wells are hydraulically fractured, fracture geometry and conductivity dominate well deliverability. Horizontal well drilling revolutionized the energy industry in the last decade of the 20th century. Horizontal wells can be completed as open holes, open holes with pre-drilled/slot liners with or without external casing packers (Fig. 1.11), and prepacked screens and liners. When horizontal wells are completed as cased holes, they are usually subjected to further well stimulations such as hydraulic fracturing and acidizing. Horizontal wellbore length is the key parameter controlling horizontal well productivity. Deliverability of horizontal wells can be adjusted if inflow control devices or inflow control valves are utilized in completion (Guo et al., 2008).

1.2.2 Unconventional well completions

Unconventional well completions are for multilateral wells, multifractured horizontal wells, and radial fractured wells. Multilateral wells fall into two categories, namely root type for reaching multiple production zones and fishbone type for

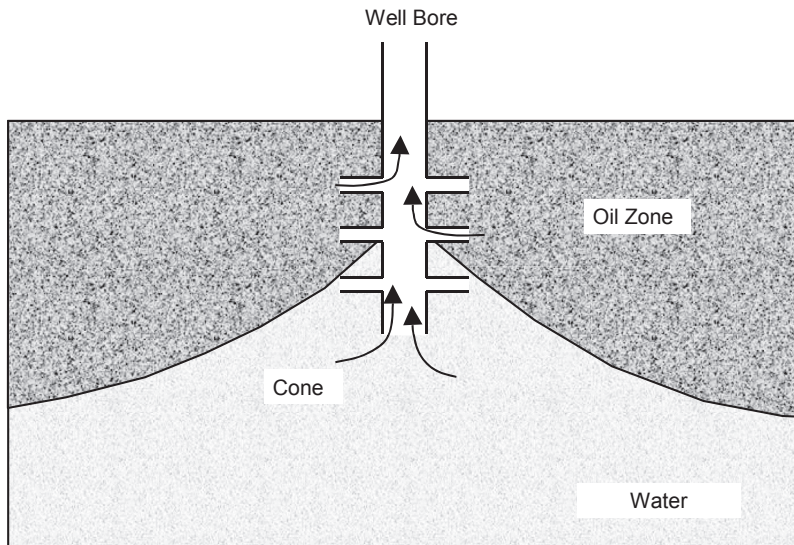


FIGURE 1.10

Water coning in a vertical well with partial perforation (Guo et al., 2008).

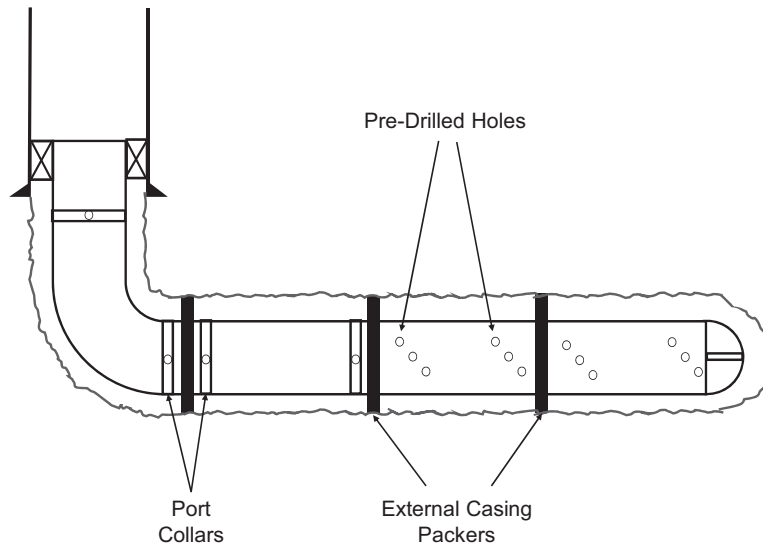


FIGURE 1.11

Horizontal well completion with predrilled liner equipped with external casing packers in which a casing patch is run to permanently isolate a segment of the wellbore.

reaching different regions in the same production zone. Multilateral wells are completed in six levels of technologies based on junction types (Hill et al., 2008). They are (1) open lateral with unsupported junction, (2) cased trunk with open lateral, (3) cased and cemented trunk with cased but not cemented lateral, (4) cemented trunk and lateral at junction, (5) pressure integrity at junction achieved with completion, and (6) pressure integrity at junction achieved with casing. Deliverability of multilateral wells depends on the fluid deliverability of individual laterals.

Multifractured horizontal wells are wells completed with multistage hydraulic fracturing technique mainly for improving productivity of wells in low-perm reservoirs such as tight sands, tight gas, shale gas, and shale oil plays. The vast majority of these types of horizontal wells are currently completed using cemented sleeves (ball or coiled tubing activated) or the “plug and perf” method (Fig. 1.12). Deliverability of multifractured horizontal wells depends on many factors including matrix permeability, number of fractures, fracture spacing, fracture geometry, and fracture conductivity.

Radial fractured wells are those wells completed with blast fracturing (Guo et al., 2014), high-energy gas fracturing (Li et al., 2018), and refracturing (Shan et al., 2018) methods. Deliverability of radial fractured wells depends on matrix permeability, number of fractures created, and fracture geometry (Fig. 1.13).

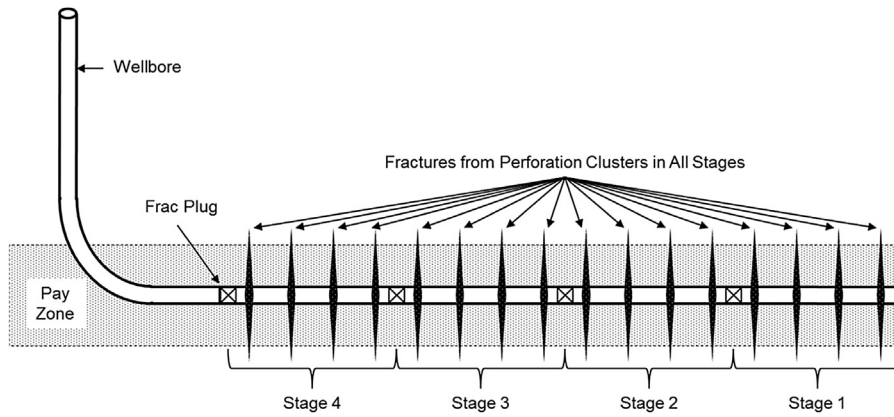
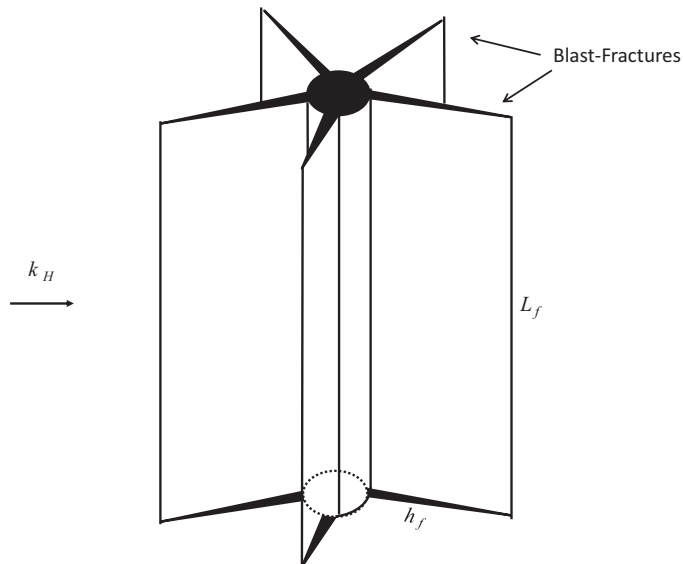
**FIGURE 1.12**

Illustration of a multifractured horizontal well completed with plug and perf method (Guo et al., 2017).

**FIGURE 1.13**

Sketch of radial fractures around a vertical wellbore created by blast fracturing (Guo et al., 2014).

1.3 Well productivity

The past three decades have seen rapid changes in field development methods. The traditional way to develop oil and gas fields has been to drill and complete vertical wells with specific well spacing chosen to correspond with the properties of the specific oil and gas reservoirs being developed. New technologies in well construction and stimulation introduced over the last 30 years include horizontal well drilling (Joshi, 1991), multilateral well drilling (Hill et al., 2008), and multistage hydraulic fracturing (Guo et al., 2017). These newer technologies permit drilling fewer wells to develop oil and gas fields, with lower costs and improved oil and gas recovery.

Numerical reservoir simulators have revolutionized oil and gas field development. A development strategy targeting maximum oil and gas recovery can be designed using reservoir simulation in a few days to a few weeks. However, reservoir simulators are subject to GIGO (garbage-in, garbage-out). They require realistic well models and reliable input data for the specific reservoir and fluid properties. This book addresses both the well model and input data quality issues and emphasizes the realistic well models that should be used in both reservoir and production simulation.

Reservoir productivity is not the same as well productivity. The former is usually described using the inflow performance relationship (IPR), which predicts the oil or gas production rate at a specified bottom-hole pressure. While reservoir productivity refers to the reservoir's ability to deliver oil and gas to the wellbore, well productivity refers to the production rate of oil or gas by a well against a specified wellhead pressure. Thus the well productivity is the well's ability to deliver oil and gas to the wellhead. Obviously, well productivity is determined by both reservoir productivity and wellbore performance (flow resistance). This book presents well models and productivities of various types of wells at designed wellhead pressures.

For simple well trajectories such as vertical and horizontal wells, NODAL analysis (a Schlumberger patent) can predict well productivity. Although NODAL analysis can be performed using any point in the system as a solution node, it is usually conducted using either the bottom hole or wellhead as the solution node. This is because measured pressure data are normally available at these two points, and these data can be used for evaluating the predictions of NODAL analysis. This book illustrates the principle of NODAL analysis using bottom-hole as the solution node where IPR is readily available for predicting the productivities of wells with simple trajectories.

For more complicated well trajectories, such as multilateral wells, an iteration procedure proposed by Guo et al. (2006) can predict well productivity. It uses a trial-and-error method to couple pressures, flow rates, and fluid properties in different wellbore branches and equipment such as down-hole chokes to estimate oil and gas production at the surface.

1.4 Summary

This chapter provides an introduction to oil and gas wells, well completion methods, and defines the concept of well productivity.

1.5 Problems

- 1-1 What are the advantages and disadvantages of using down-hole chokes rather than wellhead chokes?
- 1-2 What do the digits in the tubing specification represent (e.g., H-40, J-55, C-75, L-80, N-80, C-90, and P-105)?

References

- Guo, B., Liu, X., Tan, X., 2017. *Petroleum Production Engineering*, second ed. Elsevier, Cambridge.
- Guo, B., Shan, J., Feng, Y., April 14, 2014. Productivity of blast-fractured wells in liquid-rich shale gas formations. *Journal of Natural Gas Science and Engineering* 18C, 360–367.
- Guo, B., Sun, K., Ghalambor, A., 2008. *Well Productivity Handbook*. Gulf Publishing Company, Houston.
- Guo, B., Zhou, J., Ling, K., and Ghalambor, A.: “A rigorous composite-IPR model for multi-lateral wells,” Paper SPE 100923, Presented at the SPE Annual Technical Conference & Exhibition (24–27 September 2006), San Antonio, TX.
- Hill, D., Zhu, D., Economides, M.J., 2008. *Multilateral Wells*. Society of Petroleum Engineers, Richardson.
- Joshi, S.D., 1991. *Horizontal Well Technology*. PennWell Publishing Company, Tulsa, OK.
- Li, J., Cao, L., Guo, B., Zhang, X., 2018. Prediction of productivity of high energy gas-fractured oil wells. *Journal of Petroleum Science and Engineering* 160, 510–518.
- Shan, L., Guo, B., Weng, D., Liu, Z., Chu, H., 2018. Posteriori assessment of fracturing propagation in Re-fractured vertical oil wells by pressure transient analysis. *Journal of Petroleum Science and Engineering*. PETROL12431.

Petroleum reservoir properties

Chapter outline

2.1 Introduction	18
2.2 Reservoir fluid properties	18
2.2.1 Properties of oil.....	19
2.2.1.1 <i>Solution gas–oil ratio</i>	19
2.2.1.2 <i>Oil density</i>	19
2.2.1.3 <i>Oil formation volume factor</i>	20
2.2.1.4 <i>Oil viscosity</i>	21
2.2.1.5 <i>Oil compressibility</i>	22
2.2.2 Properties of natural gas	23
2.2.2.1 <i>Gas-specific gravity</i>	23
2.2.2.2 <i>Gas pseudocritical pressure and temperature</i>	24
2.2.2.3 <i>Gas viscosity</i>	26
2.2.3 Gas compressibility factor	28
2.2.3.1 <i>Gas density</i>	30
2.2.3.2 <i>Gas formation volume factor</i>	32
2.2.3.3 <i>Gas compressibility</i>	33
2.2.4 Properties of produced water	33
2.2.4.1 <i>Density, specific gravity, and salinity</i>	33
2.2.4.2 <i>Water viscosity</i>	33
2.2.4.3 <i>Water formation volume factor</i>	34
2.2.4.4 <i>Water compressibility</i>	34
2.2.5 Fluid interfacial tension	34
2.3 Reservoir rock properties	36
2.3.1 Lithology	36
2.3.2 Reservoir porosity	37
2.3.3 Reservoir total compressibility	37
2.3.4 Reservoir permeability	38
2.3.5 Effective permeability	39
2.3.5.1 <i>Flow regimes</i>	40
2.3.5.2 <i>Permeability determination</i>	41
2.3.6 Skin factor.....	44

2.4 Summary	47
2.5 Problems	48
References	50
Further reading	51

2.1 Introduction

Crude oil, natural gas, and produced water are petroleum fluids, which are characterized by their physical and chemical properties. Lithology, porosity, and permeability are rock properties used to characterize petroleum reservoirs. Understanding these properties is essential for predicting well productivity, which is the subject of this book. This chapter presents definitions of these fluid and rock properties and nonexperimental methods for obtaining their values. Applications of the fluid and rock properties appear in the later chapters.

2.2 Reservoir fluid properties

Any naturally occurring petroleum is a fluid mixture of hundreds of different hydrocarbons and a few inorganic compounds. These components exist in gas, liquid, and solid phases. PVT laboratories usually report hydrocarbons as a number of groups, typically less than 20. Table 2.1 summarizes the composition of a typical petroleum fluid. Because methane (C_1), ethane (C_2), propane (C_3), and nitrogen (N_2) are gases at atmospheric and relatively low pressures, and the major component of the fluid mixture defined in the table is methane, this petroleum fluid is considered a natural gas. As shown in Fig. 1.2 in Chapter 1, phase changes of a petroleum fluid are

Table 2.1 Composition of a typical petroleum fluid.

Component	Mole fraction
C_1	0.775
C_2	0.083
C_3	0.021
$i-C_4$	0.006
$n-C_4$	0.002
$i-C_5$	0.003
$n-C_5$	0.008
C_6	0.001
C_{7+}	0.001
N_2	0.050
CO_2	0.030
H_2S	0.020

characterized by its pseudocritical point, bubble-point pressure locus, dew point pressure locus, and grade curves within a phase envelope. Petroleum fluids are further characterized by the properties of the oil, its dissolved gas, and the produced water.

2.2.1 Properties of oil

Oil properties include its solution gas–oil ratio (GOR), density, formation volume factor, viscosity, and compressibility. The latter four properties are interrelated through the first.

2.2.1.1 Solution gas–oil ratio

The solution GOR is the fundamental parameter used to characterize oil. It is defined as the volume of gas, normalized to standard temperature and pressure (STP), which will dissolve in a unit volume of oil at the prevailing pressure and temperature of the actual reservoir. That is,

$$R_s = \frac{V_{gas}}{V_{oil}} \quad (2.1)$$

where

$$\begin{aligned} R_s &= \text{solution GOR (scf/stb),} \\ V_{gas} &= \text{gas volume at STP (scf), and} \\ V_{oil} &= \text{oil volume at STP (stb).} \end{aligned}$$

In most states in the United States, STP is defined as 14.7 psia and 60°F. At a given temperature, the solution GOR of a particular oil remains constant at pressures greater than bubble-point pressure. In the pressure range less than the bubble-point pressure, the solution GOR decreases as the pressure decreases.

PVT laboratories can provide actual solution GORs from direct measurement, or empirical correlations can be made based on PVT laboratory data. One of the correlations is expressed as

$$R_s = \gamma_g \left[\frac{p}{18} \frac{10^{0.0125(^{\circ}\text{API})}}{10^{0.00091t}} \right]^{1.2048} \quad (2.2)$$

where γ_g and $^{\circ}\text{API}$ are gas-specific gravity and oil-API gravity (defined in later sections of this chapter), and p and t are pressure and temperature in psia and °F, respectively.

Solution GORs are often used for volumetric oil and gas calculations in reservoir engineering, and as a base parameter for estimating other fluid properties such as oil density.

2.2.1.2 Oil density

Oil density is defined as the mass of oil per unit volume, or lb_m/ft^3 in US field units. It is widely used in hydraulics calculations, such as those for wellbore performance (see Chapter 4).

Because of the dissolved gas content, oil density is pressure- and temperature-dependent. Oil density at STP (stock tank oil or dead oil) is evaluated using its °API gravity. The relationship between the density of a stock tank oil and its API gravity is given by

$$^{\circ}\text{API} = \frac{141.5}{\gamma_o} - 131.5 \quad (2.3)$$

and

$$\gamma_o = \frac{\rho_{o,st}}{\rho_w} \quad (2.4)$$

where

°API = API gravity of stock tank oil (freshwater equals 10),
 γ_o = specific gravity of stock tank oil (freshwater equals 1),
 $\rho_{o,st}$ = density of stock tank oil (lb_m/ft^3), and
 ρ_w = density of freshwater ($62.4 \text{ lb}_m/\text{ft}^3$).

The density of oil at elevated temperatures and pressures can be estimated based on empirical correlations developed by a number of investigators, summarized by [Ahmed \(1989\)](#). Engineers should select and validate the correlations carefully against actual measurements before adopting any of them.

[Standing \(1981\)](#) presented a correlation for estimating the oil formation volume factor as a function of solution GOR, specific gravity of stock tank oil, specific gravity of solution gas, and temperature. By coupling the mathematical definition of the oil formation volume factor with Standing's correlation, [Ahmed \(1989\)](#) proposed the following expression for the density of live oil at elevated pressures and temperatures:

$$\rho_o = \frac{62.4\gamma_o + 0.0136R_s\gamma_g}{0.972 + 0.000147 \left[R_s \sqrt{\frac{\gamma_g}{\gamma_o} + 1.25t} \right]^{1.175}} \quad (2.5)$$

where

t = temperature (°F) and
 γ_g = specific gravity of gas (air equals 1).

2.2.1.3 Oil formation volume factor

The formation volume factor of oil is defined as the volume occupied by the oil in the reservoir at the prevailing pressure and temperature by the volume of oil in stock tank conditions (STP) plus its dissolved gas. That is,

$$B_o = \frac{V_{res}}{V_{ST}} \quad (2.6)$$

where

B_o = formation volume factor of oil (rb/stb),
 V_{res} = oil volume under reservoir conditions (rb), and
 V_{st} = oil volume under stock tank conditions (STP, stb).

The formation volume factor of oil is always greater than one because oil will dissolve more gas under prevailing reservoir conditions than under stock tank conditions (STP). At a given reservoir temperature, the oil formation volume factor remains nearly constant at pressures greater than its bubble-point pressure. In pressure ranges less than the bubble-point pressure, the oil formation volume factor decreases as pressure decreases due to released gas.

PVT laboratories also measure the formation volume factor of oil, and numerous empirical correlations are available based on accumulated experimental data. One correlation was developed by [Standing \(1981\)](#):

$$B_o = 0.9759 + 0.00012 \left(R_s \sqrt{\frac{\gamma_g}{\gamma_o} + 1.25t} \right)^{1.2} \quad (2.7)$$

The formation volume factor of oil is often used for oil volumetric calculations and well inflow performance calculations, as well as a base parameter for estimating other oil properties.

2.2.1.4 Oil viscosity

Viscosity is an empirical parameter that describes the resistance of a fluid to flow. Oil viscosity is used in well inflow and hydraulics calculations in reservoir and production engineering. While PVT laboratories can measure actual oil viscosity, it is often estimated using empirical correlations developed by a number of investigators, including [Beal \(1946\)](#), [Beggs and Robinson \(1975\)](#), [Standing \(1981\)](#), [Glaso \(1985\)](#), [Khan \(1987\)](#), and [Ahmed \(1989\)](#), who also provides a summary. As with oil density, engineers should select and validate a correlation with actual measurements before using it. [Standing's \(1981\)](#) correlation for dead oil is expressed as

$$\mu_{od} = \left(0.32 + \frac{1.8 \times 10^7}{API^{4.53}} \right) \left(\frac{360}{t + 200} \right)^A \quad (2.8)$$

where

$$A = 10 \left(0.43 + \frac{8.33}{API} \right) \quad (2.9)$$

and μ_{od} is the viscosity of dead oil in cp.

[Standing's \(1981\)](#) correlation for **gas-saturated crude oil** is expressed as

$$\mu_{ob} = 10^a \mu_{od}^b \quad (2.10)$$

where μ_{ob} is the viscosity of saturated crude oil in cp, and

$$a = R_s(2.2 \times 10^{-7} R_s - 7.4 \times 10^{-4}) \quad (2.11)$$

$$b = \frac{0.68}{10^c} + \frac{0.25}{10^d} + \frac{0.062}{10^e} \quad (2.12)$$

$$c = 8.62 \times 10^{-5} R_s \quad (2.13)$$

$$d = 1.10 \times 10^{-3} R_s \quad (2.14)$$

$$e = 3.74 \times 10^{-3} R_s \quad (2.15)$$

Standing's (1981) correlation for **undersaturated crude oil** is expressed as

$$\mu_o = \mu_{ob} + 0.001(p - p_b) (0.024\mu_{ob}^{1.6} + 0.38\mu_{ob}^{0.56}) \quad (2.16)$$

where p_b is bubble-point pressure in psi.

2.2.1.5 Oil compressibility

Oil compressibility is defined as

$$c_o = -\frac{1}{V} \left(\frac{\partial V}{\partial p} \right)_T \quad (2.17)$$

where T and V denote temperature and volume, respectively. Oil compressibility is measured in PVT laboratories and is often used in modeling well inflow performance and reservoir simulation. Its value is in the order of 10^{-5} psi $^{-1}$.

2.1 Sample problem

The solution GOR of oil is 600 scf/stb at 4475 psia and 140°F. Given the following PVT data, estimate density and viscosity of the crude oil at the following pressure and temperature:

Bubble-point pressure: 2745 (psia),

Oil gravity: 35 (°API), and

Gas-specific gravity: 0.77 (1.0 for air).

Solution

This problem may be quickly solved using the spreadsheet program **OilProperties.xls** in which Standing's correlation for oil viscosity has been coded. Input data and program output are shown in [Table 2.2](#).

Table 2.2 Results given by the spreadsheet program **OilProperties.xls**.

OilProperties.xls		
Description:	This spreadsheet calculates density and viscosity of a crude oil.	
Instruction:	(1) Click a unit box to choose a unit system; (2) Update parameter values in the "Input Data" section; (3) View result in the "Solution" section.	
Input Data:	US Field Units	
Pressure (p):	4475	psia
Temperature (t):	140	°F
Bubble-point pressure (p _b):	2745	psia

Table 2.2 Results given by the spreadsheet program **OilProperties.xls**.—*cont'd*

OilProperties.xls		
Stock tank oil gravity (API):	35	°API
Solution gas–oil ratio (R_s):	600	scf/stb
Gas specific gravity (γ_g):	0.77	Air = 1
Solution:		
$\gamma_o = \frac{141.5}{API+131.5}$	= 0.8498	H ₂ O = 1
$\rho_o = \frac{62.4\gamma_o + 0.0136R_s\gamma_g}{0.972 + 0.000147 \left[R_s \sqrt{\frac{\gamma_g}{\gamma_o} + 1.25t} \right]^{1.175}}$	= 44.90	1b _m /ft ³
$A = 10^{(0.43+8.33/API)}$	= 4.6559	
$\mu_{od} = \left(0.32 + \frac{1.8 \times 10^7}{API^{1.53}} \right) \left(\frac{360}{t+200} \right)^A$	= 2.7956	cp
$a = R_s(2.2 \times 10^{-7} R_s - 7.4 \times 10^{-4})$	= -0.3648	
$c = 8.62 \times 10^{-5} R_s$	= 0.0517	
$d = 1.10 \times 10^{-3} R_s$	= 0.6600	
$e = 3.74 \times 10^{-3} R_s$	= 2.2440	
$b = \frac{0.68}{10^6} + \frac{0.25}{10^2} + \frac{0.062}{10^6}$	= 0.6587	
$\mu_{ob} = 10^a \mu_{od}^b$	= 0.8498	cp
$\mu_o = \mu_{ob} + 0.001(p - p_b)(0.024\mu_{ob}^{1.6} + 0.38\mu_{ob}^{0.56})$	1.4819	cp

2.2.2 Properties of natural gas

Natural gas properties include gas specific gravity, gas pseudocritical pressure and temperature, gas viscosity, gas compressibility factor, gas density, gas formation volume factor, and gas compressibility. The first three depend on natural gas composition. The remainder depends on composition, pressure, and temperature.

2.2.2.1 Gas-specific gravity

Gas-specific gravity is defined as the ratio of the apparent molecular weight of the gas to that of air. The molecular weight of air is usually taken as 28.97 (approximately 79% nitrogen and 21% oxygen). Therefore, the gas-specific gravity can be expressed as

$$\gamma_g = \frac{MW_a}{28.97} \quad (2.18)$$

where MW_a is the apparent molecular weight of the gas, which can be calculated on the basis of its composition. Gas composition is usually determined in laboratories and is reported in mole fractions of the gas components. For example, if y_i is the

mole fraction of component i , the apparent molecular weight of the gas can be calculated using the mixing rule:

$$MW_a = \sum_{i=1}^{N_c} y_i MW_i \quad (2.19)$$

where MW_i is the molecular weight of component i , and N_c is the number of components in the gas. The necessary molecular weights of compounds can be found in textbooks on organic chemistry or petroleum fluids, such as that by [Ahmed \(1989\)](#). Gas-specific gravity varies between 0.55 and 0.9.

2.2.2.2 Gas pseudocritical pressure and temperature

In a similar way to determining gas apparent molecular weight by using the gas composition data, the mixing rule can also be used to estimate the critical properties of a gas on the basis of the critical properties of the compounds it contains. The gas critical properties determined in such a way are called pseudocritical properties. Gas pseudocritical pressure (p_{pc}) and pseudocritical temperature (T_{pc}) are, respectively, expressed as

$$p_{pc} = \sum_{i=1}^{N_c} y_i p_{ci} \quad (2.20)$$

and

$$T_{pc} = \sum_{i=1}^{N_c} y_i T_{ci} \quad (2.21)$$

where p_{ci} and T_{ci} are the critical pressure and the critical temperature of compound i , respectively.

2.2 Sample problem

For the gas composition given in [Table 2.1](#), estimate the gas apparent molecular weight, specific gravity, pseudocritical pressure, and pseudocritical temperature of the gas.

Solution

This problem may be solved using the spreadsheet program **MixingRule.xls**, as shown in [Table 2.3](#).

If the gas composition is not known, but gas-specific gravity is given, the pseudocritical pressure and temperature can be estimated using various charts or correlations that have been developed empirically. Two simple correlations are

$$p_{pc} = 709.604 - 58.718\gamma_g \quad (2.22)$$

$$T_{pc} = 170.491 + 307.344\gamma_g \quad (2.23)$$

which are valid for sweet gases—that is, those in which $H_2S < 3\%$, $N_2 < 5\%$, and the total content of inorganic compounds is less than 7%.

Corrections for impurities in sour gases are always necessary and can be determined using either charts or correlations. One is the [Wichert-Aziz \(1972\)](#) correction, expressed as

Table 2.3 Results given by the spreadsheet program **MixingRule.xls**.

MixingRule.xls							
Description: This spreadsheet calculates gas apparent molecular weight, specific gravity, pseudocritical pressure, and pseudocritical temperature based on gas composition.							
Instruction: (1) Update gas composition data (y_i); (2) view result.							
Compound	y_i	MW_i	$y_i MW_i$	p_{ci} (psia)	$y_i p_{ci}$ (psia)	T_{ci} (°R)	$y_i T_{ci}$ (°R)
C_1	0.775	16.04	12.43	673	521.58	344	266.60
C_2	0.083	30.07	2.50	709	58.85	550	45.65
C_3	0.021	44.10	0.93	618	12.98	666	13.99
$i-C_4$	0.006	58.12	0.35	530	3.18	733	4.40
$n-C_4$	0.002	58.12	0.12	551	1.10	766	1.53
$i-C_5$	0.003	72.15	0.22	482	1.45	830	2.49
$n-C_5$	0.008	72.15	0.58	485	3.88	847	6.78
C_6	0.001	86.18	0.09	434	0.43	915	0.92
C_{7+}	0.001	114.23	0.11	361	0.36	1024	1.02
N_2	0.050	28.02	1.40	227	11.35	492	24.60
CO_2	0.030	44.01	1.32	1073	32.19	548	16.44
H_2S	0.020	34.08	0.68	672	13.45	1306	26.12
	1.000	$MW_a =$	20.71	$p_{pc} =$	661	$T_{pc} =$	411
		$\gamma_g =$	0.71				

$$A = y_{H_2S} + y_{CO_2} \quad (2.24)$$

$$B = y_{H_2S} \quad (2.25)$$

$$\varepsilon_3 = 120(A^{0.9} - A^{1.6}) + 15(B^{0.5} - B^{4.0}) \quad (2.26)$$

$$T'_{pc} = T_{pc} - \varepsilon_3(\text{corrected } T_{pc}) \quad (2.27)$$

$$P'_{pc} = \frac{P_{pc} T'_{pc}}{T_{pc} + B(1-B)\varepsilon_3} (\text{corrected } p_{pc}) \quad (2.28)$$

Other correlations with impurity corrections to compensate for inorganic components are also available (Ahmed, 1989):

$$p_{pc} = 678 - 50(\gamma_g - 0.5) - 206.7y_{N_2} + 440y_{CO_2} + 606.7y_{H_2S} \quad (2.29)$$

$$T_{pc} = 326 + 315.7(\gamma_g - 0.5) - 240y_{N_2} - 83.3y_{CO_2} + 133.3y_{H_2S} \quad (2.30)$$

Applications of the pseudocritical pressure and temperature are normally found in petroleum engineering using pseudo-reduced pressure and temperature, defined as

$$p_{pr} = \frac{p}{P_{pc}} \quad (2.31)$$

$$T_{pr} = \frac{T}{T_{pc}} \quad (2.32)$$

2.2.2.3 Gas viscosity

Petroleum engineers usually measure dynamic viscosity (μ_g) in centipoises (cp). Dynamic viscosity is related to kinematic viscosity (ν_g) through density (ρ_g):

$$\nu_g = \frac{\mu_g}{\rho_g} \quad (2.33)$$

For a new gas, engineers prefer to measure gas viscosity directly. If the gas composition (y_i) and the viscosities of the gas components are known, the mixing rule can be used to estimate the viscosity of the mixed gas:

$$\mu_g = \frac{\sum(\mu_{gi}y_i\sqrt{MW_i})}{\sum(y_i\sqrt{MW_i})} \quad (2.34)$$

Gas viscosity is often estimated using charts or correlations derived experimentally. The gas viscosity correlation of Carr et al. (1954) involves a two-step procedure. First, the gas viscosity at STP is estimated from the specific gravity of the gas and its inorganic compound content. The STP value is then adjusted to local pressure conditions using a correction factor that compensates for the increased gas temperature and pressure. Gas viscosity at atmospheric pressure (μ_1) can be expressed as

$$\mu_1 = \mu_{1HC} + \mu_{1N_2} + \mu_{1CO_2} + \mu_{1H_2S} \quad (2.35)$$

where

$$\begin{aligned} \mu_{1HC} = & 8.188 \times 10^{-3} - 6.15 \times 10^{-3} \log(\gamma_g) \\ & + (1.709 \times 10^{-5} - 2.062 \times 10^{-6} \gamma_g) T \end{aligned} \quad (2.36)$$

$$\mu_{1N_2} = [9.59 \times 10^{-3} + 8.48 \times 10^{-3} \log(\gamma_g)] y_{N_2} \quad (2.37)$$

$$\mu_{1CO_2} = [6.24 \times 10^{-3} + 9.08 \times 10^{-3} \log(\gamma_g)] y_{CO_2} \quad (2.38)$$

$$\mu_{1H_2S} = [3.73 \times 10^{-3} + 8.49 \times 10^{-3} \log(\gamma_g)] y_{H_2S} \quad (2.39)$$

Dempsey (1965) developed the following correlation for determining gas viscosity at elevated pressures:

$$\begin{aligned} \mu_r = \ln\left(\frac{\mu_g T_{pr}}{\mu_1}\right) = & a_0 + a_1 p_{pr} + a_2 p_{pr}^2 + a_3 p_{pr}^3 \\ & + T_{pr} (a_4 + a_5 p_{pr} + a_6 p_{pr}^2 + a_7 p_{pr}^3) \\ & + T_{pr}^2 (a_8 + a_9 p_{pr} + a_{10} p_{pr}^2 + a_{11} p_{pr}^3) \\ & + T_{pr}^3 (a_{12} + a_{13} p_{pr} + a_{14} p_{pr}^2 + a_{15} p_{pr}^3) \end{aligned} \quad (2.40)$$

where

$$\begin{aligned}
 a_0 &= -2.46211820 \\
 a_1 &= 2.97054714 \\
 a_2 &= -0.28626405 \\
 a_3 &= 0.00805420, \\
 a_4 &= 2.80860949 \\
 a_5 &= -3.49803305 \\
 a_6 &= 0.36037302 \\
 a_7 &= -0.01044324 \\
 a_8 &= -0.79338568 \\
 a_9 &= 1.39643306 \\
 a_{10} &= -0.14914493 \\
 a_{11} &= 0.00441016 \\
 a_{12} &= 0.08393872 \\
 a_{13} &= -0.18640885 \\
 a_{14} &= 0.02033679, \text{ and} \\
 a_{15} &= -0.00060958.
 \end{aligned}$$

Once the value of μ_r is determined using the right-hand side of the equation, the gas viscosity at an elevated pressure can be readily calculated using the following relation:

$$\mu_g = \frac{\mu_1}{T_{pr}} e^{\mu_r} \quad (2.41)$$

Other correlations for gas viscosity include those of [Dean-Stiel \(1958\)](#) and [Lee-Gonzalez-Eakin \(1966\)](#).

2.3 Sample problem

A natural gas has a specific gravity of 0.65 and contains 10% nitrogen, 8% carbon dioxide, and 2% hydrogen sulfide. Estimate the viscosity of the gas at 10,000 psia and 180°F.

Solution

This problem may be solved using the spreadsheet program **Carr-Kobayashi-Burrows-GasViscosity.xls**, as shown in [Table 2.4](#).

Table 2.4 Results given by the spreadsheet program **Carr-Kobayashi-Burrows-GasViscosity.xls**.

Carr-Kobayashi-Burrows-GasViscosity.xls		
Description: This spreadsheet calculates gas viscosity with correlation of Carr, Kobayashi, and Burrows.		
Instruction: (1) Select a unit system; (2) Update data in the "Input Data" section; (3) Review result in the "Solution" section.		
Input Data:	US Field Units	
Pressure:	10,000	psia
Temperature:	180	°F

Continued

Table 2.4 Results given by the spreadsheet program **Carr-Kobayashi-Burrows-GasViscosity.xls**.—*cont'd*

Carr-Kobayashi-Burrows-GasViscosity.xls		
Gas specific gravity:	0.65	Air = 1
Mole fraction of N ₂ :	0.1	
Mole fraction of CO ₂ :	0.08	
Mole fraction of H ₂ S:	0.02	
Solution:		
Pseudocritical pressure	= 697.164	psia
Pseudocritical temperature	= 345.357	°R
Uncorrected gas viscosity at 14.7 psia	= 0.012174	cp
N ₂ correction for gas viscosity at 14.7 psia	= 0.000800	cp
CO ₂ correction for gas viscosity at 14.7 psia	= 0.000363	cp
H ₂ S correction for gas viscosity at 14.7 psia	= 0.000043	cp
Corrected gas viscosity at 14.7 psia (μ_1)	= 0.013380	cp
Pseudo-reduced pressure	= 14.34	
Pseudo-reduced temperature	= 1.85	
$\ln(\mu_g/\mu_1 \cdot T_{pr})$	= 1.602274	
Gas viscosity	= 0.035843	cp

2.2.3 Gas compressibility factor

The gas compressibility factor is also called the deviation factor or z-factor. Its value reflects how much the real gas behavior deviates from that of an ideal gas at a given pressure and temperature. The compressibility factor is expressed as

$$z = \frac{V_{actual}}{V_{ideal \text{ gas}}} \quad (2.42)$$

Introducing the z-factor to the gas law for an ideal gas results in the gas law for a real gas as

$$pV = nzRT \quad (2.43)$$

where n is the number of moles of gas. When pressure p is entered in psia, volume V in ft³, and temperature in °R, the gas constant R is equal to:

$$10.73 \frac{\text{psia} - \text{ft}^3}{\text{mole} - ^\circ \text{R}}$$

PVT laboratories can determine the gas compressibility factor from measurements. For a given amount of gas, if temperature is kept constant and the volume

is measured both at 14.7 psia and at an elevated pressure p_1 , the z-factor can be determined using the following formula:

$$z = \frac{p_1}{14.7} \frac{V_1}{V_0} \quad (2.44)$$

where V_0 and V_1 are the gas volumes measured at 14.7 psia and p_1 , respectively.

Very often the z-factor is estimated using a chart developed by [Standing and Katz \(1954\)](#), which has been adapted for computer solution by a number of individuals. [Brill and Beggs's correlation \(1974\)](#) gives z-factor values accurate enough for many engineering calculations. The correlation is expressed as

$$A = 1.39(T_{pr} - 0.92)^{0.5} - 0.36T_{pr} - 0.10 \quad (2.45)$$

$$B = (0.62 - 0.23T_{pr})p_{pr} + \left(\frac{0.066}{T_{pr} - 0.86} - 0.037 \right) p_{pr}^2 + \frac{0.32p_{pr}^6}{10^E} \quad (2.46)$$

$$C = 0.132 - 0.32 \log(T_{pr}) \quad (2.47)$$

$$D = 10^F \quad (2.48)$$

$$E = 9(T_{pr} - 1) \quad (2.49)$$

$$F = 0.3106 - 0.49T_{pr} + 0.1824T_{pr}^2 \quad (2.50)$$

and

$$z = A + \frac{1 - A}{e^B} + Cp_{pr}^D \quad (2.51)$$

2.4 Sample problem

A natural gas with a specific gravity of 0.65 contains 10% N₂, 8% CO₂, and 2% H₂S. Estimate z-factor of the gas at 5000 psia and 180°F using the Brill and Beggs' correlation.

Solution

This problem may be solved using the spreadsheet program **Brill-Beggs-Z.xls**, as shown in [Table 2.5](#).

[Hall and Yarborough \(1973\)](#) presented a more accurate correlation to estimate the z-factor of natural gases, which may be summarized as

$$t_r = \frac{1}{T_{pr}} \quad (2.52)$$

$$A = 0.06125 t_r e^{-1.2(1-t_r)^2} \quad (2.53)$$

$$B = t_r(14.76 - 9.76t_r + 4.58t_r^2) \quad (2.54)$$

$$C = t_r(90.7 - 242.2t_r + 42.4t_r^2) \quad (2.55)$$

$$D = 2.18 + 2.82t_r \quad (2.56)$$

and

$$z = \frac{Ap_{pr}}{Y} \quad (2.57)$$

Table 2.5 Results given by the spreadsheet program **Brill-Beggs-Z.xls**.

Results given by the spreadsheet program Brill-Beggs-Z.xls		
Description: This spreadsheet calculates gas compressibility factor based on Brill and Beggs correlation.		
Instruction: (1) Select a unit system; (2) Update data in the "Input Data" section; (3) Review result in the "Solution" section.		
Input Data:	US Field Units	
Pressure:	5000	psia
Temperature:	180	°F
Gas specific gravity:	0.65	air = 1
Mole fraction of N ₂ :	0.1	
Mole fraction of CO ₂ :	0.08	
Mole fraction of H ₂ S:	0.02	
Solution:		
Pseudocritical pressure =	697	psia
Pseudocritical temperature =	345	°R
Pseudo-reduced pressure =	7.17	
Pseudo-reduced temperature =	1.95	
A =	0.6063	
B =	2.4604	
C =	0.0395	
D =	1.1162	
Gas compressibility factor z =	0.9960	

where Y is the reduced density, determined from

$$f(Y) = \frac{Y + Y^2 + Y^3 - Y^4}{(1 - Y)^3} - Ap_{pr} - BY^2 + CY^D = 0 \quad (2.58)$$

If Newton–Raphson’s iterative method is used to solve Eq. (2.58) for Y , the following derivative is needed:

$$\frac{df(Y)}{dY} = \frac{1 + 4Y + 4Y^2 - 4Y^3 + Y^4}{(1 - Y)^4} - 2BY + CDY^{D-1} \quad (2.59)$$

An example of using the Hall and Yarborough’s correlation is shown in the next section, covering gas density prediction.

2.2.3.1 Gas density

Because gas is compressible, its density is a function of its pressure and temperature. In addition to direct laboratory measurement, gas density can be predicted from the gas law for real gases with acceptable accuracy:

$$\rho_g = \frac{m}{V} = \frac{MW_a p}{zRT} \quad (2.60)$$

where m is mass of gas and ρ_g is gas density. Taking air molecular weight as 29, and the gas constant R as equal to

$$10.73 \frac{\text{psia} - \text{ft}^3}{\text{mole} - ^\circ R}$$

Eq. (2.60) may be rearranged to yield

$$\rho_g = \frac{2.7\gamma_g p}{zT} \quad (2.61)$$

where the gas density is expressed in lb_m/ft^3 .

2.5 Sample problem

A gas with a specific gravity of 0.65 contains 10% N_2 , 8% CO_2 , and 2% H_2S . Estimate the z -factor and gas density at 5000 psia and 180°F.

Solution

This problem may be solved using the spreadsheet program **Hall-Yarborough-Z.xls**, as shown in Table 2.6.

Table 2.6 Results given by the spreadsheet program **Hall-Yarborough-Z.xls**.

Hall-Yarborough-Z.xls		
Instruction: This spreadsheet computes gas compressibility factor with Hall-Yarborough method.		
Instruction: (1) Select a unit system; (2) Update data in the "Input Data" section; (3) Click "Solution" button; 4) View result.		
Input Data:	US Field Units	
Temperature:	180	°F
Pressure:	5000	psia
Gas specific gravity:	0.65	air = 1
Nitrogen mole fraction:	0.1	
Carbon dioxide fraction:	0.08	
Hydrogen sulfite fraction:	0.02	
Solution:		
$T_{pc} = 326 + 315.7(\gamma_g - 0.5)$ $- 240y_{N_2} - 83.3y_{CO_2} + 133.3y_{H_2S}$	= 345.357	°R
$p_{pc} = 678 - 50(\gamma_g - 0.5) - 206.7y_{N_2}$ $+ 440y_{CO_2} + 606.7y_{H_2S}$	= 697.164	psia
$T_{pr} = \frac{T}{T_{pc}}$	= 1.853155	
$t_r = \frac{1}{T_{pr}}$	= 0.53962	
$p_{pr} = \frac{p}{p_{pc}}$	= 7.171914	
$A = 0.06125 t_r e^{-1.2(1-t_r)^2}$	= 0.025629	
$B = t_r(14.76 - 9.76t_r + 4.58t_r^2)$	= 5.842446	

Continued

Table 2.6 Results given by the spreadsheet program **Hall-Yarborough-Z.xls**.—*cont'd*

Hall-Yarborough-Z.xls		
$C = t_r(90.7 - 242.2t_r + 42.4t_r^2)$	= -14.9203	
$D = 2.18 + 2.82t_r$	= 3.701729	
Y = result in trial and error	= 0.183729	
$f(Y) = \frac{Y+Y^2+Y^3-Y^4}{(1-Y)^3} - Ap_{pr} - BY^2 + CY^D = 0$	= -2.6E-05	
$z = \frac{Ap_{pr}}{Y}$	= 1.000445	
$\rho_g = \frac{2.7\gamma_g P}{zT}$	= 13.70484	1b _m /ft ³

2.2.3.2 Gas formation volume factor

Gas formation volume factor is defined as the ratio of gas volume under reservoir conditions to the gas volume at STP, expressed as

$$B_g = \frac{V}{V_{sc}} = \frac{p_{sc}}{p} \frac{T}{T_{sc}} \frac{z}{z_{sc}} = 0.0283 \frac{zT}{p} \tag{2.62}$$

where

- B_g = formation volume factor of gas (ft³/scf),
- V = gas volume under reservoir conditions (ft³),
- V_{sc} = gas volume under standard conditions (STP, ft³),
- p = pressure (psia),
- p_{sc} = standard pressure (psia),
- T = temperature (°R),
- T_{sc} = standard temperature (°R),
- z = gas compressibility factor, and
- z_{sc} = 1.0, gas compressibility factor under standard conditions (STP).

If expressed in rb/scf, Eq. (2.62) can be simplified to

$$B_g = 0.00504 \frac{zT}{p} \tag{2.63}$$

The gas formation volume factor is frequently used in mathematical modeling of the gas well inflow performance relationship (IPR). Another way to express this parameter is to use the gas expansion factor, defined in scf/ft³ as

$$E = \frac{1}{B_g} = 35.3 \frac{P}{zT} \tag{2.64}$$

or in scf/rb as

$$E = 198.32 \frac{P}{zT} \tag{2.65}$$

The gas expansion factor is normally used for estimating gas reserves.

2.2.3.3 Gas compressibility

Gas compressibility is defined as

$$c_g = -\frac{1}{V} \left(\frac{\partial V}{\partial p} \right)_T \quad (2.66)$$

Because the gas law for real gases gives $V = \frac{nzRT}{p}$,

$$\left(\frac{\partial V}{\partial p} \right) = nRT \left(\frac{1}{p} \frac{\partial z}{\partial p} - \frac{z}{p^2} \right) \quad (2.67)$$

Substituting Eq. (2.67) into Eq. (2.66) yields

$$c_g = \frac{1}{p} - \frac{1}{z} \frac{\partial z}{\partial p} \quad (2.68)$$

Because the second term in the right-hand side is usually small, gas compressibility is approximately equal to the reciprocal of pressure.

2.2.4 Properties of produced water

Water properties that are frequently used in oil and gas field management include density, specific gravity, salinity, viscosity, formation volume factor, and compressibility. These properties are easy to measure in laboratories.

2.2.4.1 Density, specific gravity, and salinity

The density of pure water (H₂O) is 62.4 lbm/ft³ at STP. The density of produced water is higher than this value due to impurities, mostly salts. Water-specific gravity is defined as the ratio of density of the produced water to that of pure water. In practice, the water density, specific gravity, and salinity are interconvertible, as their relationships depend on the types of salts dissolved in the water. For typical oil field brines, the data from McCain (1973) provides the following correlation:

$$\rho_w = 62.4 + 0.48C_s \quad (2.69)$$

where

ρ_w = density of brine (lbm/ft³) and

C_s = total dissolved solids (%)

2.2.4.2 Water viscosity

The viscosity of water is affected by its salinity, dissolved gas content, pressure, and temperature, with temperature being the most significant factor. For typical oil field brines, the data from McCain (1973) provides the following correlation:

$$\mu_w = \frac{70.42}{t} \quad (2.70)$$

where

μ_w = viscosity of brine (cp) and

t = temperature (°F)

2.2.4.3 Water formation volume factor

Like oil, the formation volume factor of produced water is defined as the volume occupied in the reservoir at the prevailing reservoir pressure and temperature, divided by the volume of water plus its dissolved gas at surface conditions (STP), expressed as

$$B_w = \frac{V_{res}}{V_{st}} \quad (2.71)$$

where

B_w = formation volume factor of water (rb/stb),
 V_{res} = water volume in reservoir condition (rb), and
 V_{st} = water volume at surface conditions (STP, stb).

For typical oil-field brines, formation volume factors are very close to one.

2.2.4.4 Water compressibility

Water compressibility is defined as

$$c_w = -\frac{1}{V} \left(\frac{\partial V}{\partial p} \right)_T \quad (2.72)$$

Water compressibility is measured in laboratories, with values in the order of 10^{-6} psi^{-1} . Water compressibility is often used in modeling well inflow performance and in reservoir simulation.

2.2.5 Fluid interfacial tension

The interfacial tension (IFT) between liquid (oil or water) and gas phases is an important parameter in multiphase flow calculations for wellbore and pipeline design. For a given pair of fluids, IFT is a function of pressure and temperature. [Schechter and Guo \(1998\)](#) proposed the following relation for estimating IFT of hydrocarbons based on modern physics:

$$\sigma = \left[\sum_{i=1}^n P_i \left(x_i \frac{\rho_l}{M_l} - y_i \frac{\rho_v}{M_v} \right) \right]^{3.88} \quad (2.73)$$

where

σ = interfacial tension (dyne/cm²),
 n = number of compounds in the system,
 i = index of compound,
 P_i = parachor of compound i , dimensionless,
 x_i = mole fraction of compound i in the liquid phase,
 y_i = mole fraction of compound i in the vapor phase,

ρ_l = density of liquid phase (g/cm^3),
 ρ_v = density of vapor phase (g/cm^3),
 M_l = apparent molecular weight of the liquid phase, and
 M_v = apparent molecular weight of the vapor phase.

Schechter and Guo (1998) presented values for parachor for single compounds and oil cuts. They also proposed the following correlation for mixtures of compounds:

$$P = aM + b \quad (2.74)$$

where M is apparent molecular weight of fluid mixture. The correlation coefficients a and b are given in Table 2.7.

The IFT between water and gas phases is a strong function of temperature and weak function of pressure. Lyons et al. (2009) presented the following correlation for IFT for temperatures between 74°F and 280°F:

$$\sigma = \sigma_{74} - \frac{(\sigma_{74} - \sigma_{280})(t - 74)}{206} \quad (2.75)$$

where the temperature t is in °F, or

$$\sigma = \sigma_{74} - \frac{(\sigma_{74} - \sigma_{280})(1.8t_C - 42)}{206} \quad (2.76)$$

where temperature t_C is in °C. The IFT at 74°F is given by

$$\sigma_{74} = 75 - 1.108p^{0.349} \quad (2.77)$$

and the IFT at 280°F is given by

$$\sigma_{280} = 53 - 0.1048p^{0.637} \quad (2.78)$$

where pressure p is in psi, or

$$\sigma_{74} = 75 - 6.323p_{MPa}^{0.349} \quad (2.79)$$

Table 2.7 Coefficients of correlations for parachors of hydrocarbons.

Hydrocarbons	a	b	SEOE ^a
Normal paraffins	2.9799	18.1763	4.617
Alkanes	2.987	11.7344	5.884
Alkanes, alkenes, and alkadienes	2.9792	12.7057	10.022
Alkanes, alkenes, alkadienes, and alkynes	2.9769	11.3715	12.594
Alkanes, alkenes, alkadienes, alkynes, and cyclic compounds	2.9764	5.06389	16.022
Alkanes, alkenes, alkadienes, alkynes, cyclic, and aromatic compounds	2.9518	3.71917	21.941

^a SEOE = standard error of estimate for parachor.

and

$$\sigma_{280} = 53 - 2.517p_{MPa}^{0.637} \quad (2.80)$$

where pressure p_{MPa} is in MPa.

2.3 Reservoir rock properties

Petroleum reservoir rock properties include pay zone thickness, lithology, rock porosity, rock total compressibility, and rock permeability. These properties affect fluid flow within the reservoir and thus well productivity. Reservoir engineers must understand these properties to simulate reservoir behavior and to predict well productivity. Reservoir pay zone thickness is usually determined from open-hole logs, which are not addressed in this book. This chapter presents definitions of the remaining reservoir properties and the methods for obtaining their values. Applications of reservoir properties will be covered in Chapters 5–8, which deal with reservoir deliverability.

2.3.1 Lithology

Lithology is a geological term used to describe the types of formation rocks. Three main types are commonly defined: sedimentary, metamorphic, and igneous. In reservoir analysis, the lithology is identified by geologists using core samples taken from the exploration wells.

Sedimentary rocks are rocks formed after compaction of settled solid particles in water. For millions of years, the earth has been eroded—broken down and worn away by wind and water. The resulting small particles are washed downstream where they settle to the bottom of the rivers, lakes, and oceans in layer after layer. These layers are pressed down through time, until heat and pressure slowly turn the lower layers into rock. Gravels, sandstones, siltstones, shales, and mudstones are some of the subclasses of sedimentary rocks. These subclasses are generally porous and can contain water and hydrocarbons. Geologists believe that most hydrocarbons are formed in shales and subsequently migrated into sandstones over geologic time.

Carbonate rocks are a subclass of sedimentary rocks composed primarily of carbonate minerals. Two major types of carbonate rocks are limestone and dolomite, composed of calcite (CaCO_3) and the mineral dolomite ($\text{CaMg}(\text{CO}_3)_2$), respectively. Chalk and tufa are minor sedimentary carbonates. Carbonate rocks are very tight—that is, they display low porosity and permeability—but are highly fractured and may contain water and hydrocarbons.

Igneous rocks may be formed either underground or at the surface by the freezing or crystallization of molten rock. Subsurface molten rock is called magma and becomes igneous rock as it is trapped underground and crystallizes slowly. Igneous rocks are also formed as volcanoes erupt. When the magma rises to the surface, it is

called lava, both as a molten and a solid rock. Igneous rocks are very tight and are not usually reservoir rocks. Exceptions include naturally fractured igneous rocks.

Metamorphic rocks are composed of sedimentary, igneous, or even previously metamorphosed rocks that have been chemically altered by heat, pressure, and deformation while buried deep in the earth's crust. These rocks show changes in mineral composition, texture, or both. This area of rock classification is highly specialized and complex. Marble and quartz are typical metamorphic rocks. These types of rocks are not porous and thus do not form hydrocarbon-bearing reservoirs.

2.3.2 Reservoir porosity

Porosity of reservoir rock is defined as the pore fraction of the rock—that is, the ratio of pore space volume to bulk volume of the rock. Porosity is usually expressed as a percentage:

$$\phi = \frac{V_{pore}}{V_{bulk}} \quad (2.81)$$

Fluid-productive sandstones display porosities ranging between 0.05 and 0.4, or 5%–40%. Although the porosity of carbonate base material is practically zero, the overall porosity of carbonate rocks can be significant due to natural fractures within the rocks. The base materials of igneous rocks have no porosity, but their natural fractures form some degree of overall porosity in which hydrocarbons have been discovered in recent years.

Reservoir rock porosity can be measured in laboratories through core sample analysis. It may also be estimated using open-hole well logs. The porosity factor is often used to estimate hydrocarbon reserves.

2.3.3 Reservoir total compressibility

Total reservoir compressibility is defined as

$$c_t = -\frac{1}{V} \left(\frac{\partial V}{\partial p} \right)_T \quad (2.82)$$

For gas reservoirs, its value is close to gas compressibility. For undersaturated oil reservoirs, its value can be estimated using fluid saturations and the compressibilities of reservoir fluids, expressed as

$$c_t = c_o S_o + c_w S_w + c_f \quad (2.83)$$

where c_f is formation rock compressibility, and S_o and S_w are oil and water saturations in the pore space, respectively. The following values are typical:

$$c_o = 10 \times 10^{-6} \text{ psi}^{-1}$$

$$c_w = 3 \times 10^{-6} \text{ psi}^{-1}$$

$$c_f = 6 \times 10^{-6} \text{ psi}^{-1}$$

The most reliable way to determine total reservoir compressibility is by using pressure transient test analysis. Total reservoir compressibility data are crucial for well productivity during the transient flow period.

2.3.4 Reservoir permeability

Permeability refers to a rock's ability to transmit fluids. Permeable formations are those that transmit fluids readily, such as sandstones, and tend to have many large, well-connected pores. Impermeable formations, such as shales and siltstones, tend to be finer grained or of mixed grain size, with smaller, fewer, or less interconnected pores.

Consider a fluid with viscosity μ flowing horizontally in a cylindrical rock body of length ΔL and cross-sectional area A . The relationship between the pressure drop Δp across the rock and volumetric flow rate q obeys Darcy's law:

$$q = k \frac{A \Delta p}{\mu \Delta L} \quad (2.84)$$

where the proportionality factor k is called permeability.

If the pore space in the rock is filled with one fluid such as water, the permeability is called the *absolute* permeability (k_a). Thus the absolute permeability is equal to the measured permeability when a single fluid, or fluid phase, is present in the rock. The absolute permeability of rock sample can therefore be determined experimentally. If μ , ΔL , A , Δp , and q are measured in cp, cm, cm², atm, and cm³/s, respectively, the absolute permeability of the rock sample in darcies can be calculated from the measurements by

$$k_a = \frac{q \mu \Delta L}{A \Delta p} \quad (2.85)$$

The absolute permeability may be different when different types of fluids (water, oil, or gas, etc.) are used in the experiments. This is due to rock's wetting preference for different fluids, and the Klinkenberg effect for gas flow.

If more than one fluid or fluid phase is present in the pore space, Darcy's law applies to each phase. The permeability parameter is called the *effective* permeability. The effective permeability is the ability to preferentially flow or transmit a particular fluid through a rock when other immiscible fluids are also present. If water, oil, and gas are present in the pore space, the relationship is expressed as

$$q_w = k_w \frac{A \Delta p}{\mu_w \Delta L} \quad (2.86)$$

$$q_o = k_o \frac{A \Delta p}{\mu_o \Delta L} \quad (2.87)$$

$$q_g = k_g \frac{A \Delta p}{\mu_g \Delta L} \quad (2.88)$$

where k_w , k_o , and k_g are the effective permeability to water, oil, and gas, respectively. The effective permeability of the rock to any phase is proportional to the absolute permeability of the rock, where the proportionality factor is called the *relative permeability*. The effective permeabilities to water, oil, and gas, respectively, are expressed as

$$k_w = k_{rw} k_a \quad (2.89)$$

$$k_o = k_{ro} k_a \quad (2.90)$$

$$k_g = k_{rg} k_a \quad (2.91)$$

where k_{rw} , k_{ro} , and k_{rg} are the relative permeabilities to water, oil, and gas, respectively. In addition to the nature of the rock, the relative saturations (pore volume fractions) of the fluids also influence effective permeability. That is,

$$k_{rw} = f(S_w) \quad (2.92)$$

$$k_{ro} = \phi(S_o) \quad (2.93)$$

$$k_{rg} = \psi(S_g) \quad (2.94)$$

where S_w , S_o , and S_g are saturations of water, oil, and gas, respectively. If a single fluid is present in a rock, its relative permeability is 1.0. Generally, relative permeability increases with the corresponding phase saturation, but the relationship between them must be established experimentally for any given rock. Calculating relative permeabilities permits comparison of the abilities of different fluids with flow in multifluid systems because the presence of more than one fluid generally inhibits flow.

2.3.5 Effective permeability

The effective permeabilities determined by using laboratory measurement of the absolute permeability and relative permeability from well cores are only accurate at the small scale of the well core. Their accuracy breaks down at the larger scales of well and field levels. The effective permeability data required for well productivity prediction are often obtained by analyzing pressure transient data from actual well testing.

In pressure transient data analyses, the effective reservoir permeability controlling a well's deliverability should be derived from the flow regime that prevails in the reservoir for long-term production. To better understand the flow regimes, the commonly used equations describing flow in oil reservoirs are summarized first in the following subsection. Similar equations for gas reservoirs can be found in the literature.

2.3.5.1 Flow regimes

Common regimes of fluid flow in reservoirs identifiable for extracting effective permeability include horizontal radial flow, horizontal linear flow, vertical radial flow, horizontal pseudo-linear flow, and horizontal pseudo-radial flow.

2.3.5.1.1 Horizontal radial flow

For vertical wells that fully penetrate nonfractured reservoirs, horizontal radial flow can be mathematically described in consistent units as

$$p_{wf} = p_i - \frac{qB\mu}{4\pi k_h h} \left[\ln \left(\frac{k_h t}{\phi \mu c_t r_w^2} \right) + 2S + 0.80907 \right] \quad (2.95)$$

where

- p_{wf} = flowing bottom-hole pressure,
- p_i = initial reservoir pressure,
- q = volumetric liquid production rate,
- B = formation volume factor,
- μ = fluid viscosity,
- k_h = average horizontal permeability,
- h = pay zone thickness,
- t = flow time,
- ϕ = porosity,
- c_t = total reservoir compressibility,
- r_w = wellbore radius, and
- S = total skin factor.

2.3.5.1.2 Horizontal linear flow

For hydraulically fractured wells, horizontal linear flow can be mathematically described in consistent units as

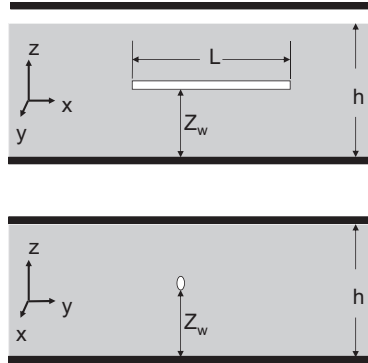
$$p_{wf} = p_i - \frac{qB\mu}{2\pi k_y h} \left[\sqrt{\frac{\pi k_y t}{\phi \mu c_t x_f^2}} + S \right] \quad (2.96)$$

where x_f is fracture half-length and k_y is the permeability in the direction perpendicular to the fracture surface.

2.3.5.1.3 Vertical radial flow

For the horizontal well depicted in Fig. 2.1, initial vertical radial flow can be mathematically described in consistent units as

$$p_{wf} = p_i - \frac{qB\mu}{4\pi k_{yz} L} \left[\ln \left(\frac{k_{yz} t}{\phi \mu c_t r_w^2} \right) + 2S + 0.80907 \right] \quad (2.97)$$

**FIGURE 2.1**

Parameters for a horizontal wellbore.

where L is the horizontal wellbore length and k_{yz} is the arithmetic mean of horizontal and vertical permeabilities, expressed as

$$k_{yz} = \sqrt{k_y k_z} \quad (2.98)$$

2.3.5.1.4 Horizontal pseudo-linear flow

Pseudo-linear fluid flow toward a horizontal wellbore can be mathematically described in consistent units as

$$p_{wf} = p_i - \frac{qB\mu}{2\pi k_y (h - Z_w)} \left[\sqrt{\frac{4\pi k_y t}{\phi \mu c_t L^2}} + S \right] \quad (2.99)$$

2.3.5.1.5 Horizontal pseudo-radial flow

Pseudo-radial fluid flow toward a horizontal wellbore can be mathematically described in consistent units as

$$p_{wf} = p_i - \frac{qB\mu}{4\pi k_h h} \left[\ln \left(\frac{k_h t}{\phi \mu c_t r_w^2} \right) + 2S + 0.80907 \right] \quad (2.100)$$

2.3.5.2 Permeability determination

For vertical wells fully penetrating nonfractured reservoirs, it is usually the average (geometric mean) of horizontal permeabilities, k_h , that dominates long-term production performance. The average horizontal permeability may be derived from data obtained during the horizontal radial flow regime. For wells draining relatively small portions of hydraulically fractured reservoir segments, it is usually the permeability in the direction perpendicular to the fracture surface that controls long-term production performance. This permeability may be derived from the horizontal linear flow regime. For horizontal wells draining relatively large portions of nonfractured

reservoir segments, it is usually again the geometric mean of horizontal permeabilities that dominates long-term production performance. This average horizontal permeability can be derived from the pseudo-radial flow regime. For vertical wells partially penetrating nonfractured reservoirs, both horizontal and vertical permeabilities influence long-term production performance. These permeabilities can usually be derived from the so-called hemispherical flow regime.

Flow regimes are usually identified using the diagnostic pressure derivative p' , expressed as

$$p' = \frac{d\Delta p}{d \ln(t)} = t \frac{d\Delta p}{dt} \quad (2.101)$$

where t is time and Δp is defined as

$$\Delta p = p_i - p_{wf} \quad (2.102)$$

for drawdown tests where p_i and p_{wf} are initial reservoir pressure and flowing bottom-hole pressure, respectively. For pressure buildup tests, the Δp is defined as

$$\Delta p = p_{sw} - p_{wfe} \quad (2.103)$$

where p_{ws} and p_{wfe} are shut-in bottom-hole pressure and the flowing bottom-hole pressure at the end of flow (before shut-in), respectively.

For any type of radial flow—that is, horizontal radial flow, vertical radial flow, and horizontal pseudo-radial flow—the diagnostic derivative is derived from Eqs. (2.95), (2.97), and (2.100) as

$$p' = \frac{d\Delta p}{d \ln(t)} = \frac{qB\mu}{4\pi\bar{k}H_R} \quad (2.104)$$

where \bar{k} is the average permeability in the flow plane (k_h or k_{yz}) and H_R is the distance of radial flow (h or L). Apparently, the diagnostic derivative is constant over the radial flow time regime. The plot of p' versus t data should show a straight line parallel to the t -axis.

For linear flow—that is, flow toward a hydraulic fracture—the diagnostic derivative is derived from Eq. (2.96) as

$$p' = \frac{d\Delta p}{d \ln(t)} = \frac{qB}{4hx_f} \sqrt{\frac{\mu t}{\pi\phi c_t k_y}} \quad (2.105)$$

For pseudo-linear flow—that is, flow toward a horizontal well—the diagnostic derivative is derived from Eq. (2.99) as

$$p' = \frac{d\Delta p}{d \ln(t)} = \frac{qB}{2L(h - z_w)} \sqrt{\frac{\mu t}{\pi\phi c_t k_y}} \quad (2.106)$$

Taking the logarithm of Eqs. (2.105) and (2.106) gives

$$\log(p') = \frac{1}{2} \log(t) + \log\left(\frac{qB}{4hx_f} \sqrt{\frac{\mu}{\pi\phi c_t k_y}}\right) \quad (2.107)$$

and

$$\log(p') = \frac{1}{2} \log(t) + \log\left(\frac{qB}{2L(h-z_w)} \sqrt{\frac{\mu}{\pi\phi c_t k_y}}\right) \quad (2.108)$$

Eqs. (2.107) and (2.108) indicate that the defining characteristic of a linear flow regime is the half slope on the log–log plot of diagnostic derivative versus time.

Once the flow regimes are identified, slope analysis can be used to calculate reservoir permeabilities. For any type of radial flow, Eqs. (2.95), (2.97), and (2.100) indicate that plotting bottom-hole pressure against time on a semilog scale will show a trend with constant slope m_R , where

$$m_R = -\frac{qB\mu}{4\pi\bar{k}H_R} \quad (2.109)$$

The average permeability in the flow plane (k_h or k_{yz}) can then be estimated by

$$\bar{k} = -\frac{qB\mu}{4\pi H_R m_R} \quad (2.110)$$

For any type of linear flow, Eqs. (2.96) and (2.99) indicate that plotting bottom-hole pressure against the square root of time will show a trend of constant slope m_L where

$$m_L = -\frac{qB}{H_L X_L} \sqrt{\frac{\mu}{\pi\phi c_t k_y}} \quad (2.111)$$

where $H_L = h$ and $X_L = 2x_f$ for linear flow, and $H_L = h - z_w$ and $X_L = L$ for pseudo-linear flow, respectively. The permeability in the flow direction can then be estimated by

$$k_y = \frac{\mu}{\pi\phi c_t} \left(\frac{qB}{m_L H_L X_L}\right)^2 \quad (2.112)$$

If a horizontal well is tested for long enough for a pseudo-radial flow regime to become established, then it is possible to estimate other directional permeabilities by

$$k_x = \frac{k_h^2}{k_y} \quad (2.113)$$

and

$$k_z = \frac{k_{yz}^2}{k_y} \quad (2.114)$$

Although k_x and k_z are not used in well productivity analysis, they can provide insight about reservoir anisotropy and can also be used in petroleum reservoir simulation.

2.3.6 Skin factor

Skin factor is a constant used to adjust flow equations derived from theoretically ideal conditions of homogeneous and isotropic porous media to suit applications under nonideal conditions. It is a general factor designed to account for the lumped effects of several real-world variables not included in the derivation of the ideal flow equations. The skin factor can be derived from pressure transient test analysis using Eqs. (2.95)–(2.97), (2.99), and (2.100). But the practical definition of S is not the same under different flow regimes. A general expression of the skin factor is

$$S = S_D + S_{C+\theta} + S_P + \sum S_{PS} \quad (2.115)$$

where S_D is the damage skin component created during drilling, cementing, well completion, fluid injection, and even oil and gas production, due to physical plugging of pore space by external or internal solid particles and fluids. This component of skin factor can be removed or prevented in well stimulation operations. The $S_{C+\theta}$ is the skin component due to partial completion and deviation angle, which modifies the flow pattern near the wellbore from an ideal radial flow pattern. This skin component is not removable in water-coning and gas-coning systems. The S_P is the skin component due to nonideal flow conditions near the perforations made during cased-hole completion. It depends on a number of parameters, including perforation density, phase angle, perforation depth, diameter, compacted zone, etc. This component can be minimized by optimizing perforating techniques. The $\sum S_{PS}$ represents pseudo-skin components due to non-Darcy flow effects, multiphase effects, and flow convergence near the wellbore. These components cannot be eliminated.

It is essential to know the magnitude of the components of the skin factor S derived from pressure transient test data analysis. Commercial software packages are available for decomposition of the skin factor for different well completion methods, such as WellFlo (EPS, 2005).

2.6 Sample problem

A horizontal wellbore is placed in a 100-ft-thick oil reservoir of 0.23 porosity. Oil formation volume factor and viscosity are 1.25 rb/stb and 1 cp, respectively. The total reservoir compressibility factor is 10^{-5} psi^{-1} . The well is tested following the schedule shown in Fig. 2.2, which also shows the measured flowing bottom-hole pressures. Estimate the directional permeabilities and the skin factors from the test data.

Solution

Fig. 2.3 presents a log–log diagnostic plot of well test data. It clearly indicates initial vertical radial flow, intermediate pseudo-linear flow, and the beginning of final pseudo-radial flow.

The semilog analysis for the vertical radial flow is shown in Fig. 2.4, which gives $k_{yz} = 0.9997 \text{ md}$ and near-wellbore skin factor $S = -0.0164$.

The square-root time plot analysis for the pseudo-linear flow is shown in Fig. 2.5, which gives the effective wellbore length of $L = 1082.75 \text{ ft}$ and a skin factor due to convergence of $S = 3.41$.

The semilog analysis for the horizontal pseudo-radial flow is shown in Fig. 2.6, which gives $k_h = 1.43 \text{ md}$ and a pseudo-skin factor $S = -6.17$.

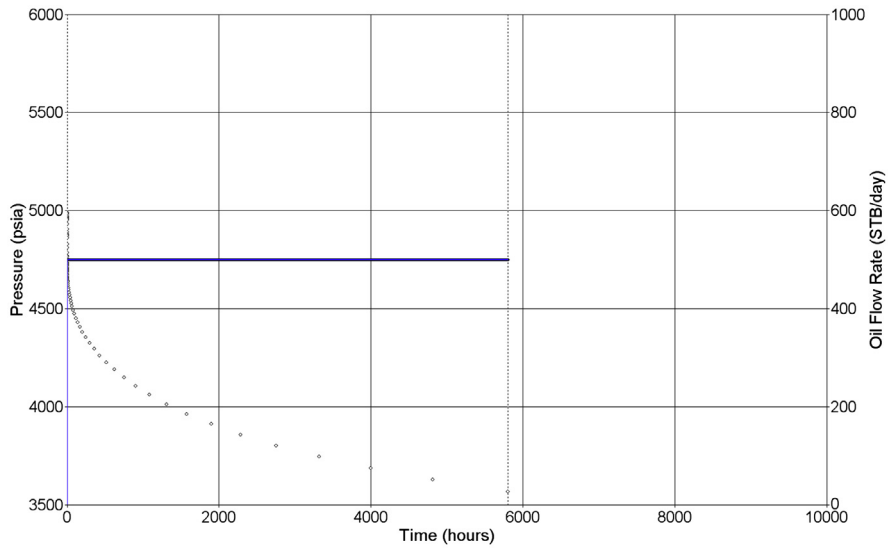


FIGURE 2.2

Measured bottom-hole pressures and oil production rates during a pressure draw-down test.

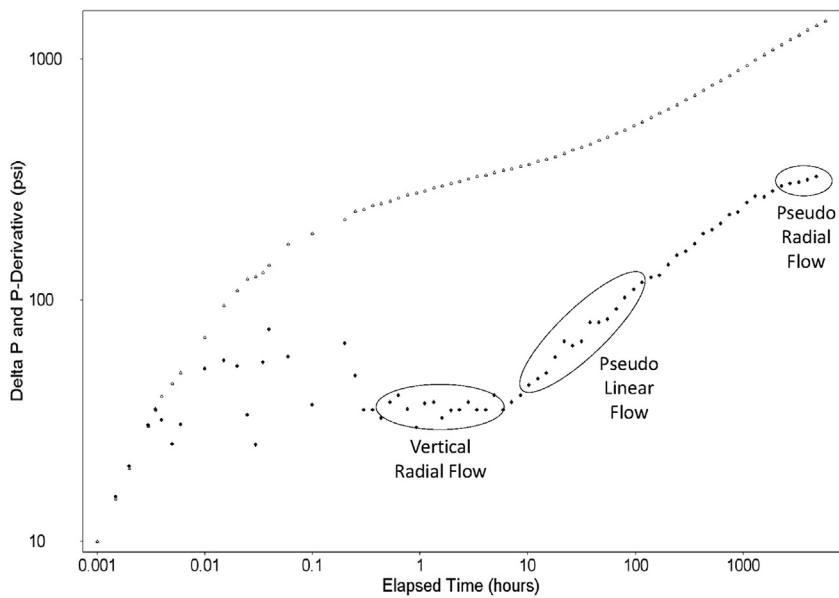


FIGURE 2.3

Log-log diagnostic plot of test data.

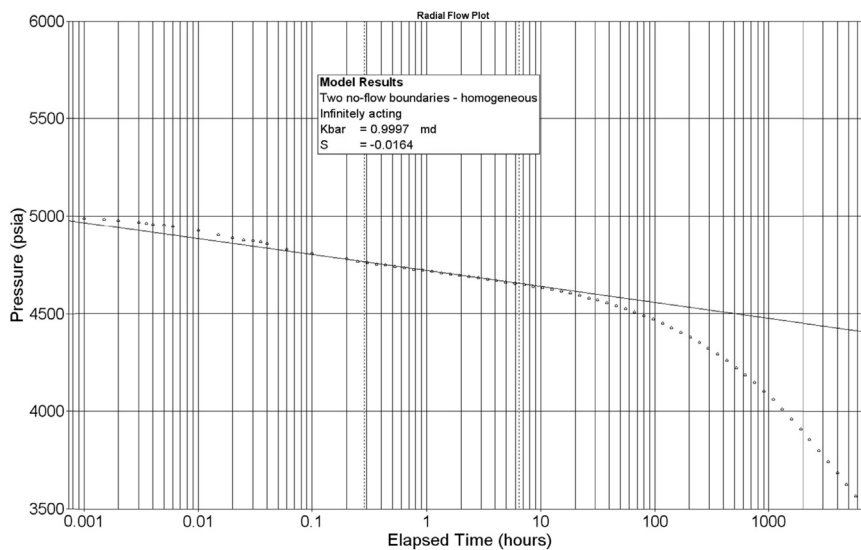


FIGURE 2.4

Semilog plot for vertical radial flow analysis.

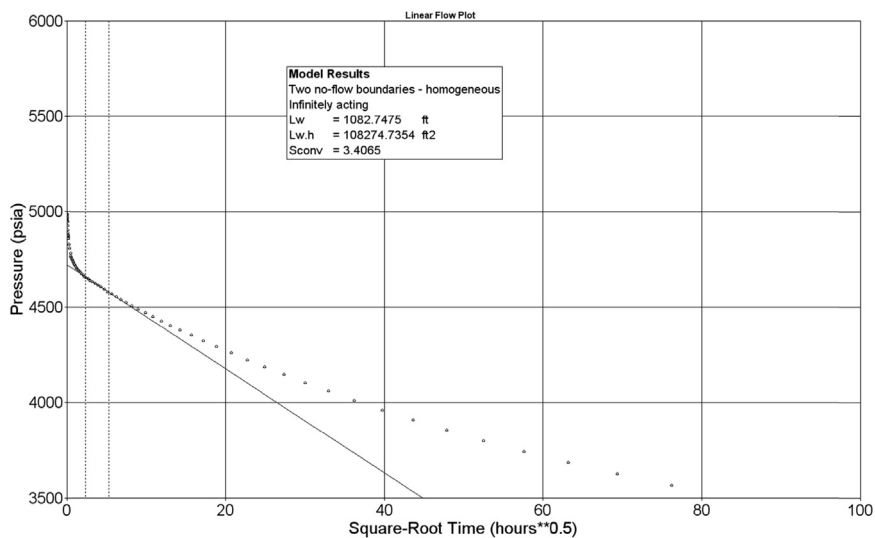
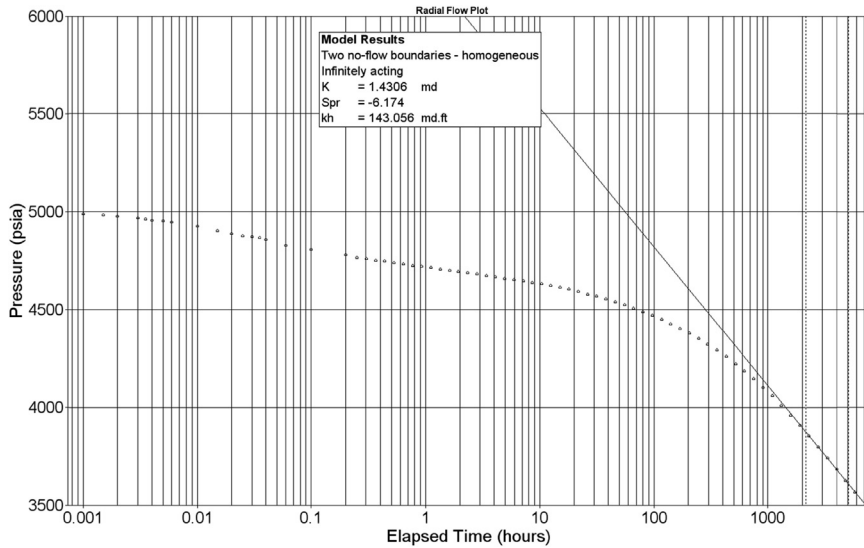


FIGURE 2.5

Square-root time plot for pseudo-linear flow analysis.

**FIGURE 2.6**

Semilog plot for horizontal pseudo-radial flow analysis.

Fig. 2.7 shows a match between measured and predicted pressures, obtained using the following parameter values:

$$k_h = 1.29 \text{ md,}$$

$$k_z = 0.80 \text{ md,}$$

$$S = 0.06, \text{ and}$$

$$L = 1243 \text{ ft.}$$

To estimate the long-term productivity of this horizontal well, the $k_h = 1.29$ md and $S = 0.06$ should be used in the well inflow equation to be presented in Chapter 5.

2.4 Summary

This chapter defined relevant properties of oil, natural gas, and produced water and provided several techniques for using empirical correlations to estimate their values. These correlations are coded in spreadsheet programs included with this book. Applications of these fluid properties will be presented in later chapters. This chapter also defined parameters used for characterizing reservoir properties. The effective permeabilities determined on the basis of absolute permeability and relative permeability from core measurements are only accurate at the small scale of the well core. The effective permeability data required to predict well productivity are often obtained by analyzing pressure transient data obtained by actual well testing. In pressure transient data analyses, the effective reservoir permeability that controls a

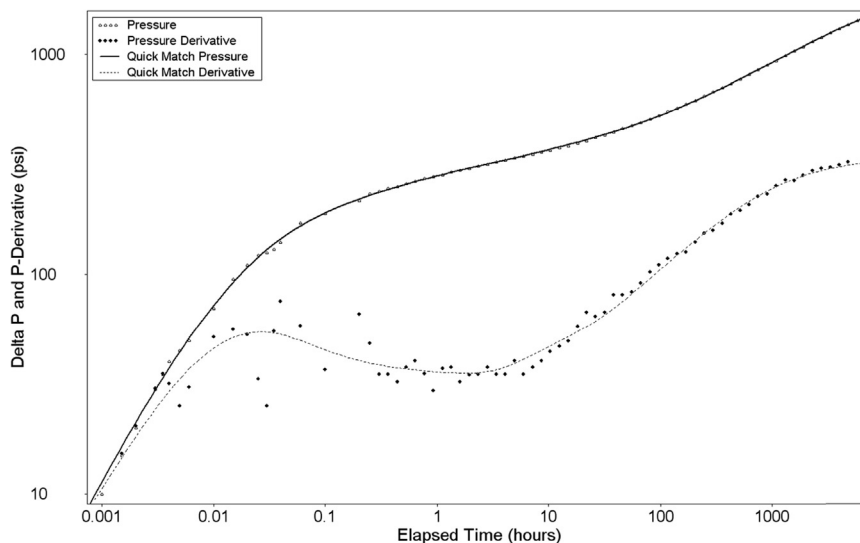


FIGURE 2.7

Model-match to the measured pressure response.

well's deliverability should be derived from the flow regime that prevails in the reservoir for best long-term production.

2.5 Problems

- 2.1** Estimate the density of a 35-API gravity dead oil at 90°F.
- 2.2** The solution gas—oil ratio of a crude oil is 800 scf/stb at 3000 psia and 110°F. Given the following PVT data:
 Bubble-point pressure: 2550 psia,
 Oil gravity: 45 °API,
 Gas specific gravity: 0.70 air = 1,
 Estimate the density and viscosity of the crude oil at 110°F: at 2550 psia and at 3000 psia.
- 2.3** For the gas composition given below, determine the apparent molecular weight, specific gravity, pseudocritical pressure, and pseudocritical temperature of the gas.

Component	Mole fraction
C_1	0.665
C_2	0.123
C_3	0.071
$i-C_4$	0.006
$n-C_4$	0.002

Component	Mole fraction
<i>i</i> -C ₅	0.003
<i>n</i> -C ₅	0.008
C ₆	0.001
C ₇₊	0.001
N ₂	0.060
CO ₂	0.040
H ₂ S	0.020

- 2.4** Estimate the gas viscosity of a 0.72 specific gravity gas at 150°F at 100 psia, 1000 psia, 5000 psia, and 10,000 psia.
- 2.5** Use the Hall-Yarborough method to estimate the gas compressibility factor and density of a 0.75 specific gravity gas at 150°F at 50 psia, 500 psia, and 5000 psia. Compare the results with those given by the Brill and Beggs' correlation. What is your conclusion?
- 2.6** Estimate the density of a 0.8 specific gravity dead oil at 45°C.
- 2.7** The solution gas–oil ratio of a crude oil is 4200 sm³/m³ at 20 MPa and 50°C. Given the following PVT data:
Bubble-point pressure: 15 MPa
Oil specific gravity: 0.8 water = 1
Gas specific gravity: 0.72 air = 1
Estimate density and viscosity of the crude oil at 50°C at 15 MPa and at 20 MPa.
- 2.8** For the gas composition given below, determine the apparent molecular weight, specific gravity, pseudocritical pressure, and pseudocritical temperature of the gas.

Component	Mole fraction
C ₁	0.715
C ₂	0.093
C ₃	0.031
<i>i</i> -C ₄	0.006
<i>n</i> -C ₄	0.002
<i>i</i> -C ₅	0.003
<i>n</i> -C ₅	0.008
C ₆	0.001
C ₇₊	0.001
N ₂	0.070
CO ₂	0.050
H ₂ S	0.020

- 2.9** Estimate the gas viscosity of a 0.75 specific gravity gas at 85°C at 1 MPa, 5 MPa, 10 MPa, and 50 MPa.
- 2.10** Using the Hall-Yarborough method, calculate the gas compressibility factor and density of a 0.73 specific gravity gas at 80°C at 1 MPa, 5 MPa, 10 MPa, and 50 MPa. Compare the results with those given by the Brill and Beggs' correlation. What is your conclusion?

- 2.11 What are the major differences between sandstone and carbonate rocks?
- 2.12 What is the maximum possible value of sandstone porosity?
- 2.13 What is the difference between absolute permeability and effective permeability?
- 2.14 What flow regimes should be used to determine effective horizontal permeability using pressure transient test data?
- 2.15 How would you determine the practical value for skin factor that truly reflects formation damage?

References

- Ahmed, T., 1989. *Hydrocarbon Phase Behavior*. Gulf Publishing Company, Houston.
- Beal, C., 1946. The viscosity of air, water, natural gas, crude oils and its associated gases at oil field temperatures and pressures. *Transactions of the Metallurgical Society of AIME* 165, 94–112.
- Beggs, H.D., Robinson, J.R., September 1975. Estimating the viscosity of crude oil systems. *Journal of Petroleum Technology* 1140–1141.
- Brill, J.P., Beggs, H.D., 1974. *Two-Phase Flow in Pipes*. INTERCOMP Course, The Hague.
- Carr, N.L., Kobayashi, R., Burrows, D.B., 1954. Viscosity of hydrocarbon gases under pressure. *Transactions of the Metallurgical Society of AIME* 201, 264–272.
- Dean, D.E., Stiel, L.I., 1958. The viscosity of non-polar gas mixtures at moderate and high pressures. *AIChE Journal* 4, 430–436.
- Dempsey, J.R., August 16, 1965. Computer routine treats gas viscosity as a variable. *Oil & Gas Journal* 141.
- EPS, 2005. *FloSystem User Manual*. E-Production Services, Inc, Edinburgh.
- Glaso, O., May 1985. Generalized pressure-volume-temperature correlations. *Journal of Petroleum Technology* 785–795.
- Hall, K.R., Yarborough, L., June 18, 1973. A new equation of state for Z-factor calculations. *Oil & Gas Journal* 82.
- Khan, S.A.: “Viscosity Correlations for Saudi Arabian Crude Oils,” Paper SPE 15720, Presented at the 50th Middle East Conference and Exhibition (7–10 March 1987), Manama, Bahrain.
- Lee, A.L., Gonzalez, M.H., Eakin, B.E., August 1966. The viscosity of natural gases. *Journal of Petroleum Technology* 997–1000.
- Lyons, W.C., Guo, B., Graham, R.L., Hawley, G.D., 2009. *Air and Gas Drilling Manual*, third ed. Elsevier Publishing Company, Amsterdam.
- McCain Jr., W.D., 1973. *Properties of Petroleum Fluids*. PennWell Books, Tulsa.
- Schechter, D.S., Guo, B., 1998 Jun 1. Parachors based on modern physics and their uses in IFT prediction of reservoir fluids. *SPE Reservoir Evaluation & Engineering Journal* 1 (03), 207–217.
- Standing, M.B., 1981. *Volume and Phase Behavior of Oil Field Hydrocarbon Systems*, ninth ed. Society of Petroleum Engineers, Dallas.
- Standing, M.B., Katz, D.L., 1954. Density of natural gases. *Transactions of the Metallurgical Society of AIME* 146, 140–149.
- Wichert, E., Aziz, K., May 1972. Calculate z_s for sour gases. *Hydrocarbon Processing* 51, 119.

Further reading

- Chaudhry, A.C., 2004. Oil Well Testing Handbook. Gulf Professional Publishing, Burlington.
- Dake, L.P., 2002. Fundamentals of Reservoir Engineering. Elsevier, Amsterdam.
- Economides, M.J., Hill, A.D., Ehlig-Economides, C., 1994. Petroleum Production Systems. Prentice Hall PTR, New Jersey.
- EPS, 2004. PanSystem User Manual. E-Production Services, Inc, Edinburgh.
- Fekete, F.A.S.T., 2003. WellTest User Manual. Fekete Associates, Inc, Calgary.
- Horne, R.N., 1995. Modern Well Test Analysis: A Computer-Aided Approach. Petroway Publishing, New York.
- Lee, J.W., Rollins, J.B., Spivey, J.P., 2003. Pressure Transient Testing. Society of Petroleum Engineers, Richardson.

Reservoir deliverability

Chapter outline

3.1 Introduction	53
3.2 Vertical wells	54
3.2.1 Transient flow	54
3.2.2 Steady-state flow	56
3.2.3 Pseudo–steady-state flow.....	57
3.3 Fractured wells	59
3.4 Horizontal wells	63
3.5 Inflow performance relationship	65
3.5.1 IPR for single (liquid)-phase reservoirs	65
3.5.2 IPR for two-phase reservoirs	69
3.5.3 IPR for partial two-phase oil reservoirs.....	72
3.6 Construction of IPR curves using test points	74
3.7 Composite IPR of stratified reservoirs	79
3.7.1 Composite IPR models.....	80
3.7.1.1 <i>Single-phase liquid flow</i>	80
3.7.1.2 <i>Two-phase flow</i>	81
3.7.1.3 <i>Partial two-phase flow</i>	81
3.7.2 Applications.....	82
3.8 Predicting future IPR	84
3.8.1 Using Vogel's method to predict future IPR.....	85
3.8.2 Using Fetkovich's method to predict future IPR	86
3.9 Summary	89
3.10 Problems	89
References	91

3.1 Introduction

Reservoir deliverability is the oil or gas production rate that can be achieved from a reservoir at a given bottom-hole pressure and is a major factor affecting well deliverability. Reservoir deliverability determines which types of completion and which artificial lift methods must be used. A thorough understanding of it is essential for accurately predicting well productivity.

Reservoir deliverability depends on the following factors:

- Reservoir pressure
- Pay zone thickness
- Effective permeability
- Reservoir boundary type and distance
- Wellbore radius
- Reservoir fluid properties
- Near-wellbore conditions

Reservoir engineers assume transient flow, steady-state flow, and pseudo-steady-state flow to construct mathematical models predicting reservoir deliverability. Knowing the flow pattern permits engineers to formulate an analytical relationship between bottom-hole pressure and production rate, called inflow performance relationship (IPR). This chapter addresses the procedures used to establish the IPR of vertical, fractured, and horizontal wells producing oil and gas from reservoirs.

3.2 Vertical wells

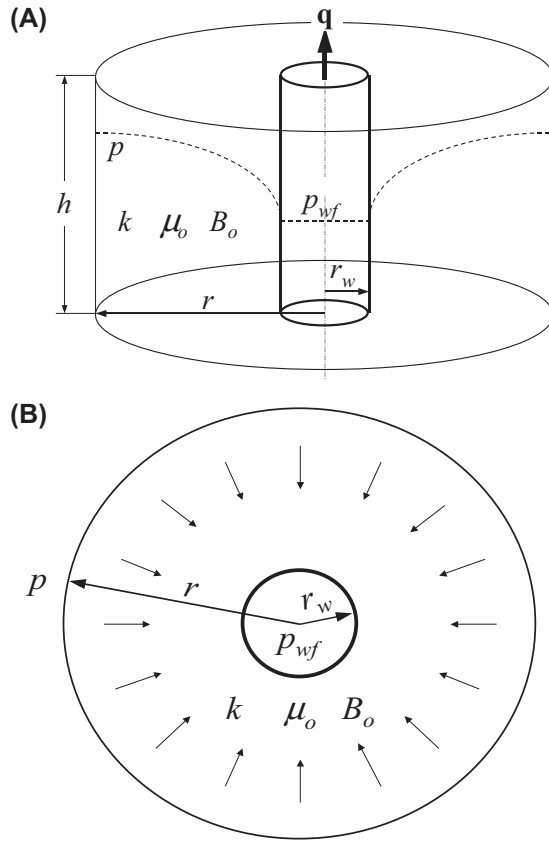
As a vertical well produces oil at production rate q , it creates a pressure funnel of radius r around the wellbore, as illustrated by the dotted curve in Fig. 3.1A. In this reservoir model, h is the reservoir thickness, k is the effective horizontal reservoir permeability to oil, μ_o is the oil viscosity, B_o is the oil formation volume factor, r_w is the wellbore radius, p_{wf} is the flowing bottom-hole pressure, and p is the pressure in the reservoir at the distance r from the wellbore centerline. The flow stream lines in the cylindrical region form the horizontal radial flow pattern depicted in Fig. 3.1B.

3.2.1 Transient flow

Transient flow is defined as a flow condition under which the radius of pressure wave propagation from the wellbore has not reached the boundaries of the reservoir. During transient flow the developing pressure funnel is small, relative to the reservoir size. Therefore, the transient pressure behaves as if the reservoir were infinitely large.

Assuming single-phase oil flow in the reservoir, several analytical solutions have been developed for describing transient flow behavior. These are available from classic textbooks, such as [Dake \(1978\)](#). A constant-rate solution expressed by Eq. (3.1) is frequently used in reservoir engineering:

$$p_{wf} = p_i - \frac{162.6qB_o\mu_o}{kh} \left(\log t + \log \frac{k}{\phi\mu_o c_t r_w^2} - 3.23 + 0.87S \right) \quad (3.1)$$

**FIGURE 3.1**

A reservoir model illustrating radial flow: (A) lateral view, (B) top view.

where

- p_{wf} = flowing bottom-hole pressure (psia),
- p_i = initial reservoir pressure (psia),
- q = oil production rate (stb/day),
- μ_o = viscosity of oil (cp),
- k = effective horizontal permeability to oil (md),
- h = reservoir thickness (ft),
- t = flow time (hours),
- ϕ = porosity (fractional),
- c_t = total compressibility (psi^{-1}),
- r_w = wellbore radius to the sand face (ft),
- S = skin factor, and
- Log = 10-based logarithm (\log_{10}).

The fixed choke size used in typical production oil wells results in constant wellhead pressure, which, in turn, results in constant bottom-hole pressure. A constant-bottom-hole pressure solution is therefore more desirable for well inflow performance analysis. Using an appropriate inner boundary condition arrangement, Earlougher (1977) developed a constant-bottom-hole pressure solution, which is similar to Eq. (3.1), expressed as

$$q = \frac{kh(p_i - p_{wf})}{162.6B_o\mu_o \left(\log t + \log \frac{k}{\phi\mu_o c_t r_w^2} - 3.23 + 0.87S \right)} \quad (3.2)$$

which is used for transient well performance analysis in reservoir engineering.

Eq. (3.2) indicates that at a constant-bottom-hole pressure, the oil production rate decreases with flow time. This is because the radius of the pressure funnel (over which the pressure drawdown $(p_i - p_{wf})$ acts) increases with time. In other words, the overall pressure gradient in the drainage area decreases with time.

For gas wells, the transient solution is expressed as

$$q_g = \frac{kh[m(p_i) - m(p_{wf})]}{1638T \left(\log t + \log \frac{k}{\phi\mu_g c_t r_w^2} - 3.23 + 0.87S \right)} \quad (3.3)$$

where q_g is the production rate in Mscf/d, k is the effective permeability to gas in md, T is the temperature in °R, μ_g is the gas viscosity in cp, and $m(p)$ is the real-gas pseudo-pressure, defined as

$$m(p) = \int_{p_b}^p \frac{2p}{\mu_g z} dp \quad (3.4)$$

where p_b is the base pressure, usually taken as 14.7 psia. The real-gas pseudo-pressure can be readily determined using spreadsheet program **PseudoPressure.xls**.

3.2.2 Steady-state flow

Steady-state flow is defined as a flow condition under which the pressure at any point in the reservoir remains constant over time. This flow condition prevails when the pressure funnel shown in Fig. 3.1 has propagated to a constant-pressure boundary. The constant-pressure boundary might be the edge of an aquifer, or the region surrounding a water injection well. A sketch of this reservoir model is shown in Fig. 3.2, where p_e represents the pressure at the constant-pressure boundary. Under steady-state flow conditions due to a circular constant-pressure boundary at distance r_e from the wellbore centerline, assuming single-phase flow, the following theoretical relationship for an oil reservoir can be derived from Darcy's law:

$$q = \frac{kh(p_e - p_{wf})}{141.2B_o\mu_o \left(\ln \frac{r_e}{r_w} + S \right)} \quad (3.5)$$

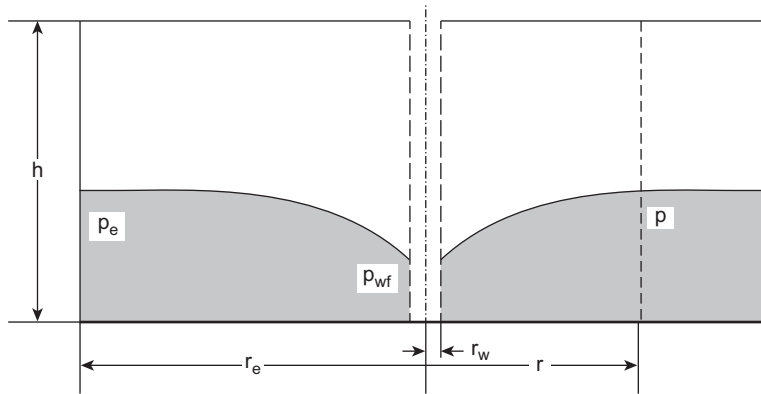


FIGURE 3.2
A reservoir model illustrating a constant-pressure boundary.

where “ln” denotes 2.718-based natural logarithm (\log_e). The derivation of Eq. (3.5) is left to the reader as an exercise.

3.2.3 Pseudo—steady-state flow

Pseudo—steady-state flow is defined as a flow condition under which the pressure at any point in the reservoir declines at the same constant rate over time. This flow condition prevails after the pressure funnel shown in Fig. 3.1 has propagated to all adjacent no-flow boundaries. A no-flow boundary can be a sealing fault, a pinch-out of the reservoir pay zone, or the boundaries of drainage areas of production wells. A sketch of this reservoir model is shown in Fig. 3.3 where p_e represents the pressure

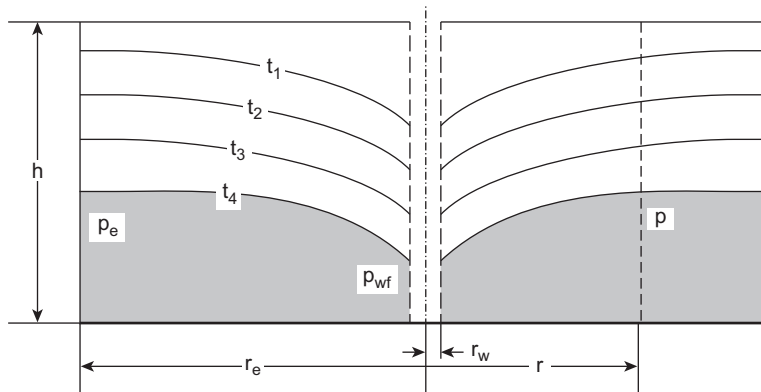


FIGURE 3.3
Pressure and flow conditions of a reservoir with no-flow boundaries.

at the no-flow boundary at time t_d . Under pseudo-steady-state flow conditions due to a circular no-flow boundary at distance r_e from wellbore centerline, assuming single-phase flow, the following theoretical relationship for an oil reservoir can be derived from Darcy's law:

$$q = \frac{kh(p_e - p_{wf})}{141.2B_o\mu_o \left(\ln \frac{r_e}{r_w} - \frac{1}{2} + S \right)} \quad (3.6)$$

The flow time required for the pressure funnel to reach the circular boundary can be expressed as

$$t_{pss} = 1200 \frac{\phi\mu_o c_t r_e^2}{k} \quad (3.7)$$

Since the value of reservoir pressure, p_e , in Eq. (3.6) is usually not known, the following expression using the average reservoir pressure is more useful:

$$q = \frac{kh(\bar{p} - p_{wf})}{141.2B_o\mu_o \left(\ln \frac{r_e}{r_w} - \frac{3}{4} + S \right)} \quad (3.8)$$

where \bar{p} is the average reservoir pressure, estimated by pressure transient data analysis or predicted by reservoir simulation. The derivations of Eqs. (3.6) and (3.8) are left to the reader as an exercise.

If the no-flow boundaries delineate a noncircular drainage area, use the following equation to predict the pseudo-steady-state flow:

$$q = \frac{kh(\bar{p} - p_{wf})}{141.2B_o\mu_o \left(\frac{1}{2} \ln \frac{4A}{\gamma C_A r_w^2} + S \right)} \quad (3.9)$$

where

A = drainage area (ft²),

$\gamma = 1.78 = e^{0.5572}$ (where 0.5572 is Euler's constant), and

C_A = drainage area shape factor (31.6 for a circular boundary).

An appropriate value of the shape factor C_A can be found from Figs. 3.4 and 3.5.

For a gas well located at the center of a circular drainage area, the pseudo-steady-state solution is expressed as

$$q_g = \frac{kh[m(\bar{p}) - m(p_{wf})]}{1424T \left(\ln \frac{r_e}{r_w} - \frac{3}{4} + S + Dq_g \right)} \quad (3.10)$$

where

D = non-Darcy flow coefficient, d/Mscf.


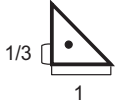
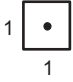
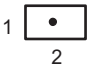

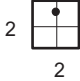

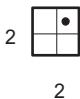
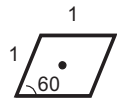

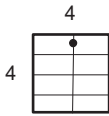

Reservoir Shape & Well Location	Shape Factor C_A	Reservoir Shape & Well Location	Shape Factor C_A
	31.6		21.9
	30.9		22.6
	31.6		12.9
	27.6		4.5
	27.1		In water-drive reservoirs 19.1
	3.39		In reservoirs of unknown production character 25

FIGURE 3.4

Shape factors for closed drainage areas with low-aspect ratios (Dietz, 1965).

3.3 Fractured wells

Hydraulically created fractures receive fluids from the reservoir matrix and provide channels for it to flow into the wellbore. Apparently, the productivity of fractured wells depends on two stages: (1) receiving fluids from the formation by the fractures and (2) transporting the received fluid to wellbore along the fractures. Usually, one of the stages is a limiting factor that controls well production rate. The efficiency of the first stage depends on fracture dimension (length and height), and the efficiency

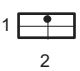
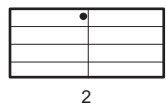
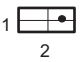

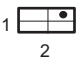
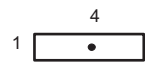

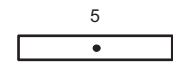

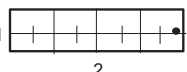

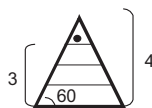
Reservoir Shape & Well Location	Shape Factor C_A	Reservoir Shape & Well Location	Shape Factor C_A
	10.8		3.13
	4.86		0.607
	2.07		5.38
	2.72		2.36
	0.232		0.111
	0.115		0.098

FIGURE 3.5

Shape factors for closed drainage areas with high-aspect ratios (Dietz, 1965).

of the second stage depends on fracture permeability. The relative importance of each can be analyzed using the concept of fracture conductivity (Argawal et al., 1979; Cinco-Ley and Samaniego, 1981) defined as

$$F_{CD} = \frac{k_f w}{k x_f} \tag{3.11}$$

where

F_{CD} = fracture conductivity (dimensionless),
 k_f = fracture permeability (md),

w = fracture width (ft), and
 x_f = fracture half-length (ft).

In situations where the fracture length is much smaller compared with the drainage area of the well, the long-term productivity of a fractured well can be estimated assuming pseudo-radial flow in the reservoir. In that case, the inflow equation for steady-state flow can be expressed as

$$q = \frac{kh(p_e - p_{wf})}{141.2B\mu \left(\ln \frac{r_e}{r_w} + S_f \right)} \quad (3.12)$$

where S_f is the equivalent skin factor for the fractured well and takes negative values. The factor of increase in reservoir deliverability can be expressed as

$$\frac{J}{J_o} = \frac{\ln \frac{r_e}{r_w}}{\ln \frac{r_e}{r_w} + S_f} \quad (3.13)$$

where

J = productivity of fractured well (stb/d-psi) and
 J_o = productivity of nonfractured well (stb/d-psi).

The effective skin factor S_f can be determined based on fracture conductivity. [Cinco-Ley and Samanigo \(1981\)](#) showed that the parameter $S_f + \ln(x_f/r_w)$ approaches a constant value of about 0.7 in the range of $F_{CD} > 100$, that is,

$$S_f \approx 0.7 - \ln(x_f/r_w) \quad (3.14)$$

This indicates that the equivalent skin factor of fractured wells depends only on fracture length for high-conductivity fractures, not fracture permeability and width. This is the situation where the first stage is the limiting factor. On the other hand, their chart indicates that the parameter $S_f + \ln(x_f/r_w)$ declines linearly with $\log(F_{CD})$ in the range of $F_{CD} < 1$, that is,

$$S_f + \ln(x_f/r_w) \approx 1.52 - 1.545 \log(F_{CD}) \quad (3.15)$$

which gives

$$S_f \approx 1.52 + 2.31 \log(r_w) - 1.545 \log\left(\frac{k_f w}{k}\right) - 0.765 \log(x_f) \quad (3.16)$$

Comparing the coefficients of the last two terms in this relation indicates that the equivalent skin factor of a fractured well is more sensitive to fracture permeability and width than to fracture length for low-conductivity fractures. This is the situation in which the second stage is the limiting factor.

The previous analyses reveal that low-permeability reservoirs would benefit most from increased fracture length, while high-permeability reservoirs benefit more from increased fracture permeability and width.

Valko et al. (1997) converted Cinco-Ley and Samanigo's (1981) chart in the whole range of fracture conductivity to the following correlation:

$$S_f + \ln(x_f/r_w) = \frac{1.65 - 0.328u + 0.116u^2}{1 + 0.180u + 0.064u^2 + 0.05u^3} \quad (3.17)$$

where $u = \ln(F_{CD})$.

3-1 Sample problem

A gas reservoir has a permeability of 1 md. A vertical well with a radius of 0.328 ft drains a reservoir area of 160 acres. If the well is hydraulically fractured to create a 2000-ft-long, 0.12-inch-wide fracture of 200,000 md permeability around the center of the drainage area, what is the expected factor of increase in reservoir deliverability?

Solution

Radius of the drainage area:

$$r_e = \sqrt{\frac{A}{\pi}} = \sqrt{\frac{(43,560)(160)}{\pi}} = 1490 \text{ ft}$$

Fracture conductivity:

$$F_{CD} = \frac{k_f w}{k x_f} = \frac{(200,000)(0.12/12)}{(1)(2000/2)} = 2$$

Eq. (3.17) yields

$$S_f + \ln(x_f / r_w) \approx 1.2$$

which gives

$$S_f \approx 1.2 - \ln(x_f/r_w) = 1.2 - \ln(1000/0.328) = -6.82$$

The factor of increase in reservoir deliverability is therefore

$$\frac{J}{J_o} = \frac{\ln \frac{r_e}{r_w}}{\ln \frac{r_e}{r_w} + S_f} = \frac{\ln \frac{1490}{0.328}}{\ln \frac{1490}{0.328} - 6.82} = 5.27$$

The above principle is also valid for pseudo-steady flow, in which the average reservoir pressure should be used. In that case, Eq. (3.12) becomes

$$q = \frac{kh(\bar{p} - p_{wf})}{141.2B_o\mu_o \left(\frac{1}{2} \ln \frac{4A}{\gamma C_A r_w^2} + S_f \right)} \quad (3.18)$$

Eq. (3.13) assumes radial flow and may result in significant error if used in situations where the fracture length is comparable with the drainage area of the well ($x_f > 0.5r_e$). In these cases, long-term reservoir deliverability may be estimated assuming bilinear flow in the reservoir and fracture. Pressure distribution in a linear flow reservoir with linear flow in a fracture of finite conductivity is

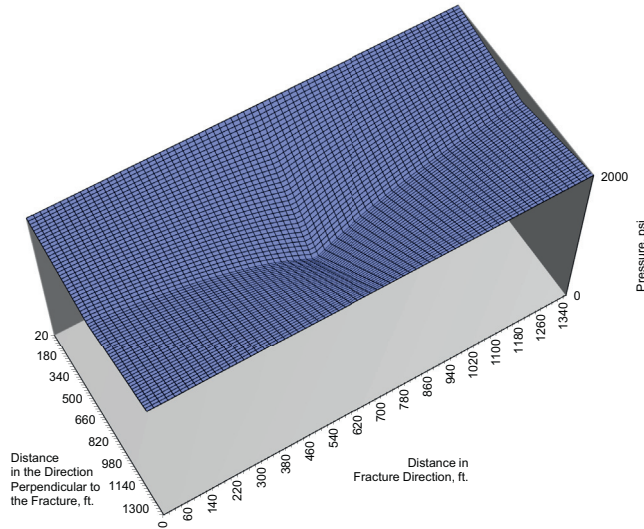


FIGURE 3.6

An example of reservoir pressure distribution near a long fracture.

illustrated in Fig. 3.6. An analytical solution for estimating the factor of increase in reservoir deliverability was presented by Guo and Schechter (1999), as follows:

$$\frac{J}{J_o} = \frac{0.72 \left(\ln \frac{r_e}{r_w} - \frac{3}{4} + S_o \right)}{z_e \sqrt{c \left(\frac{1}{1 - e^{-\sqrt{c}x_f}} - \frac{1}{2x_f \sqrt{c}} \right)}} \quad (3.19)$$

where $c = \frac{2k}{z_e w k_f}$ and

J = productivity index of fractured well (stb/d-psi),

J_o = productivity index of nonfractured well (stb/d-psi),

S_o = skin factor of the nonfractured well (dimensionless), and

z_e = distance between the fracture and the flow boundary (ft).

3.4 Horizontal wells

The transient flow, steady-state flow, and pseudo–steady-state flow can also exist in reservoirs penetrated by horizontal wells. Different mathematical models are available from literature. Joshi (1988) presented a mathematical model considering steady-state flow of oil in the horizontal plane and pseudo–steady-state flow in the vertical plane. Joshi’s equation was modified by Economides et al. (1991) to include the effect of reservoir anisotropy. Guo et al. (2007) pointed out that Joshi’s equation is optimistic for high-productivity reservoirs due to neglecting the effect of frictional pressure in the horizontal wellbore. Guo et al.

(2007) suggests that the following modified Joshi equations be applied to estimating horizontal well inflow performance.

For oil wells,

$$q = \frac{k_H h (p_e - p_{wf})}{141.2 B_o \mu_o \left\{ \ln \left[\frac{a + \sqrt{a^2 - (L/2)^2}}{L/2} \right] + \frac{I_{ani} h}{L} \ln \left[\frac{I_{ani} h}{r_w (I_{ani} + 1)} \right] + S \right\}} F_o \quad (3.20)$$

For gas wells,

$$q_g = \frac{k_H h (p_e^2 - p_{wf}^2)}{1424 \bar{\mu}_g \bar{z} T \left\{ \ln \left[\frac{a + \sqrt{a^2 - (L/2)^2}}{L/2} \right] + \frac{I_{ani} h}{L} \ln \left[\frac{I_{ani} h}{r_w (I_{ani} + 1)} \right] + s + D q_g \right\}} F_g \quad (3.21)$$

where

$$a = \frac{L}{2} \sqrt{\frac{1}{2} + \sqrt{\left[\frac{1}{4} + \left(\frac{r_{eH}}{L/2} \right)^4 \right]}} \quad (3.22)$$

and

q = oil production rate (stb/day) and
 q_g = gas production rate (Mscf/day).

$$I_{ani} = \sqrt{\frac{k_H}{k_V}}$$

k_H = the average horizontal permeability (md),

k_V = vertical permeability (md),

r_{eH} = radius of drainage area of horizontal well (ft),

L = length of horizontal wellbore ($L/2 < 0.9 r_{eH}$) (ft),

F_o = correction factor for oil production rate (dimensionless),

F_g = correction factor for gas production rate (dimensionless),

T = reservoir temperature ($^{\circ}\text{R}$),

$\bar{\mu}_g$ = average gas viscosity (cp),

\bar{z} = average gas compressibility factor (dimensionless),

s = skin factor (dimensionless), and

D = non-Darcy flow coefficient (day/Mscf).

The methods for obtaining the correction factors F_o and F_g will be presented in Appendix C and Appendix D, respectively.

3.5 Inflow performance relationship

Engineers use the IPR to evaluate deliverability in reservoir and production engineering. The IPR curve is a graphical presentation of the relationship between the flowing bottom-hole pressure and the liquid production rate. A typical IPR curve is shown in Fig. 3.7. The magnitude of the slope of IPR curve is called productivity index (PI or J), expressed as

$$J = \frac{q}{(p_e - p_{wf})} \quad (3.23)$$

where J is productivity index. Apparently J is not a constant in a two-phase flow reservoir.

The well IPR curves are usually constructed using reservoir inflow models, which can be derived theoretically or from empirical formulation. It is essential to validate these models with test points in field applications.

3.5.1 IPR for single (liquid)-phase reservoirs

All reservoir inflow models presented earlier in this chapter were derived assuming single-phase flow. This assumption is valid for undersaturated oil reservoirs or for reservoir regions where the pressure is greater than the bubble-point pressure. The following equations define the productivity index (J^*) for flowing bottom-hole pressures greater than the bubble-point pressure.

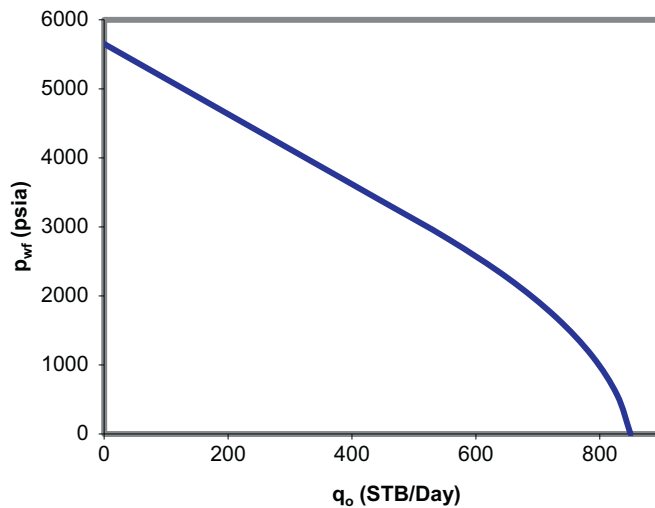


FIGURE 3.7

A typical inflow performance relationship curve for an oil well.

For **radial transient** flow around a **vertical** well,

$$J^* = \frac{q}{(p_i - p_{wf})} = \frac{kh}{162.6B_o\mu_o \left(\log t + \log \frac{k}{\phi\mu_o c_t r_w^2} - 3.23 + 0.87S \right)} \quad (3.24)$$

For **radial steady-state** flow around a **vertical** well,

$$J^* = \frac{q}{(p_e - p_{wf})} = \frac{kh}{141.2B_o\mu_o \left(\ln \frac{r_e}{r_w} + S \right)} \quad (3.25)$$

For **pseudo—steady-state** flow around a **vertical** well,

$$J^* = \frac{q}{(\bar{p} - p_{wf})} = \frac{kh}{141.2B_o\mu_o \left(\frac{1}{2} \ln \frac{4A}{\gamma C_A r_w^2} + S \right)} \quad (3.26)$$

For **steady-state** flow around a **fractured** well,

$$J^* = \frac{q}{(p_e - p_{wf})} = \frac{kh}{141.2B_o\mu_o \left(\ln \frac{r_e}{r_w} + S_f \right)} \quad (3.27)$$

For **steady-state** flow around a **horizontal** well,

$$J^* = \frac{q}{(p_e - p_{wf})} = \frac{k_H h}{141.2B_o\mu_o \left\{ \ln \left[\frac{a + \sqrt{a^2 - (L/2)^2}}{L/2} \right] + \frac{I_{ani} h}{L} \ln \left[\frac{I_{ani} h}{r_w (I_{ani} + 1)} \right] \right\}} \quad (3.28)$$

Because the productivity index (J^*) above the bubble-point pressure is independent of production rate, the IPR curve for single (liquid)-phase reservoir is a straight line. If the bubble-point pressure is 0 psig, the absolute open flow (AOF) is equal to the productivity index (J^*) multiplied by the reservoir pressure.

3-2 Sample problem

Calculate and graph the IPR for a vertical well in an oil reservoir. Consider (1) transient flow at 30 days, (2) steady-state flow, and (3) pseudo—steady-state flow. The following data are given:

Porosity: $\phi = 0.19$

Effective horizontal permeability: $k = 8.2$ md

Pay zone thickness: $h = 53$ ft

Reservoir pressure: p_e or $\bar{p} = 5651$ psia

Bubble-point pressure: $p_b = 50$ psia

Oil formation volume factor: $B_o = 1.1$

Oil viscosity: $\mu_o = 1.7$ cp

Total compressibility: $c_t = 0.0000129$ psi⁻¹

Drainage area: $A = 640$ acres ($r_e = 2980$ ft)

Wellbore radius: $r_w = 0.328$ ft

Skin factor: $S = 0$

Solution

1) For transient flow at 30 days,

$$J^* = \frac{kh}{162.6B_o\mu_o \left(\log t + \log \frac{k}{\phi\mu_o c_t r_w^2} - 3.23 \right)}$$

$$= \frac{(8.2)(53)}{162.6(1.1)(1.7) \left(\log[(30)(24)] + \log \frac{(8.2)}{(0.19)(1.7)(0.0000129)(0.328)^2} - 3.23 \right)}$$

$$= 0.2075 \text{ STB/d - psi}$$

The calculated points are as follows.

p_{wf} (psi)	q_o (STB/day)
50	1162
5651	0

The transient IPR curve is illustrated in Fig. 3.8.

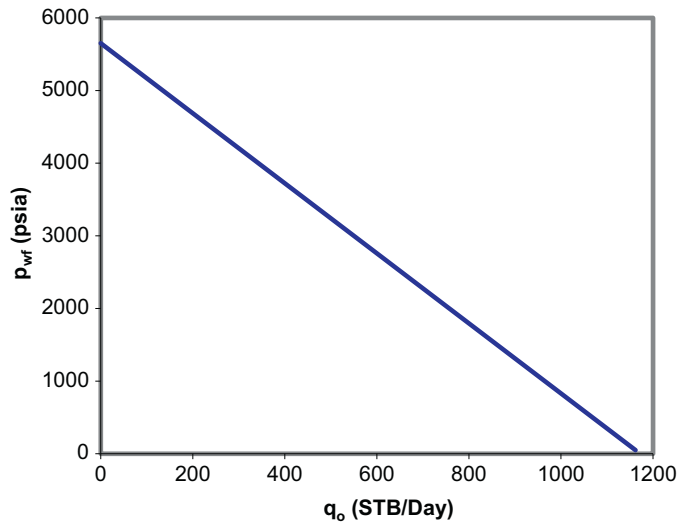


FIGURE 3.8

Transient inflow performance relationship curve for Sample Problem 3-2.

2) For steady-state flow,

$$\begin{aligned}
 J^* &= \frac{kh}{141.2B_o\mu_o \left(\ln \frac{r_e}{r_w} + S \right)} \\
 &= \frac{(8.2)(53)}{141.2(1.1)(1.7) \ln \left(\frac{2980}{0.328} \right)} \\
 &= 0.1806 \text{ STB/d - psi}
 \end{aligned}$$

The calculated points are as follows.

p_{wf} (psi)	q_o (STB/day)
50	1011
5651	0

The steady-state IPR curve is illustrated in Fig. 3.9.

3) For pseudo-steady-state flow,

$$\begin{aligned}
 J^* &= \frac{kh}{141.2B_o\mu_o \left(\ln \frac{r_e}{r_w} - \frac{3}{4} + S \right)} \\
 &= \frac{(8.2)(53)}{141.2(1.1)(1.7) \left(\ln \frac{2980}{0.328} - 0.75 \right)} \\
 &= 0.1968 \text{ STB/d - psi}
 \end{aligned}$$

The calculated points are as follows.

p_{wf} (psi)	q_o (STB/day)
50	1102
5651	0

The pseudo-steady-state IPR curve is illustrated in Fig. 3.10.

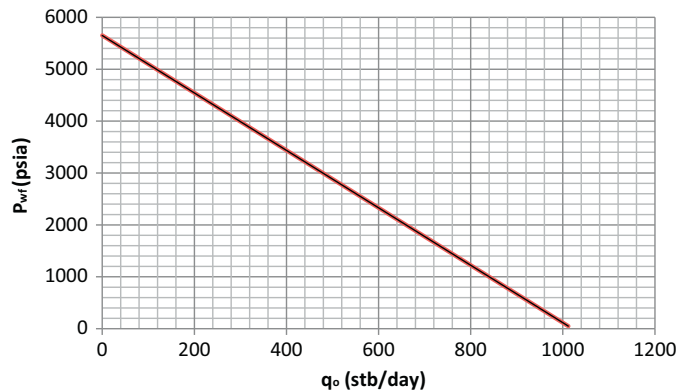


FIGURE 3.9

Steady-state inflow performance relationship curve for Sample Problem 3-2.

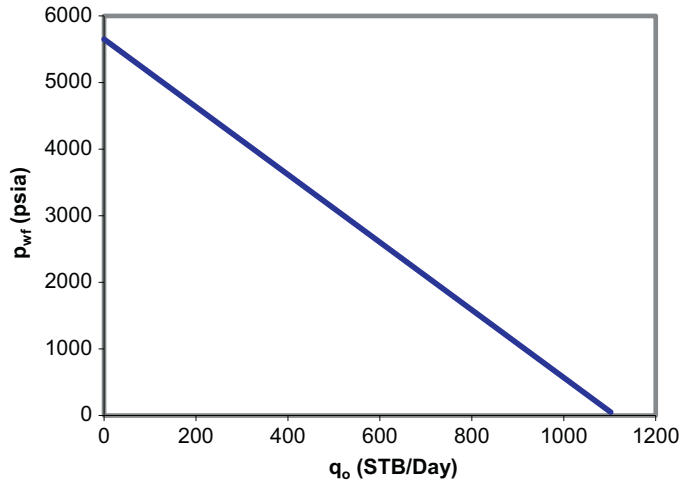


FIGURE 3.10

Pseudo-steady-state inflow performance relationship curve for [Sample Problem 3-2](#).

3.5.2 IPR for two-phase reservoirs

The linear IPR model presented in the last section is valid for pressure values as low as bubble-point pressure. At pressures less than the bubble-point pressure, some solution gas escapes from the oil and becomes free gas, which occupies some portion of available pore space. This reduces oil flow, both because of reduced relative permeability to the oil and because oil viscosity increases as its solution gas content decreases. This combination of decreased relative permeability and increased viscosity results in a lower oil production rate at any given bottom-hole pressure. This causes the IPR curve to deviate from a linear trend at pressures less than the bubble-point pressure, as shown in [Fig. 3.7](#). The lower the pressure, the larger will be the deviation. If the reservoir pressure is less than the initial bubble-point pressure, two-phase oil and gas flow exists in the entire reservoir domain, and it is referred to as a two-phase reservoir.

Only empirically derived equations are available for modeling the IPR of two-phase reservoirs. These include the [Vogel \(1968\)](#) equation as extended by [Standing \(1971\)](#) and those of [Fetkovich \(1973\)](#), [Bandakhlia and Aziz \(1989\)](#), [Chang \(1992\)](#), and [Retnanto and Economides \(1998\)](#). Vogel's equation is still widely used in the industry, expressed as

$$q = q_{\max} \left[1 - 0.2 \left(\frac{P_{wf}}{\bar{p}} \right) - 0.8 \left(\frac{P_{wf}}{\bar{p}} \right)^2 \right] \quad (3.29)$$

or

$$p_{wf} = 0.125\bar{p} \left[\sqrt{81 - 80 \left(\frac{q}{q_{\max}} \right)} - 1 \right] \quad (3.30)$$

where q_{\max} is an empirical constant that represents the maximum possible reservoir deliverability, or AOF. The value of q_{\max} can be estimated theoretically from reservoir pressure and the productivity index at the bubble-point pressure. For pseudo-steady-state flow, it follows that

$$q_{\max} = \frac{J^* \bar{p}}{1.8} \quad (3.31)$$

The derivation of this relation is left to the reader for an exercise. Fetkovich's equation is expressed as

$$q = q_{\max} \left[1 - \left(\frac{p_{wf}}{\bar{p}} \right)^2 \right]^n \quad (3.32)$$

or

$$q = C (\bar{p}^2 - p_{wf}^2)^n \quad (3.33)$$

where C and n are empirical constants and are related to q_{\max} by $C = q_{\max} / \bar{p}^{2n}$. As illustrated in the [Sample Problem 3-6](#), Fetkovich's equation using two constants is more conservative than Vogel's equation for IPR modeling.

Again, [Eqs. \(3.29\) and \(3.33\)](#) are valid if average reservoir pressure \bar{p} is at or less than the initial bubble-point pressure. [Eq. \(3.33\)](#) is often used in gas reservoir applications.

3-3 Sample problem

Calculate and graph the IPR for a vertical well in a saturated oil reservoir using Vogel's equation. The following data are given:

- Porosity: $\phi = 0.19$
- Effective horizontal permeability: $k = 8.2$ md
- Pay zone thickness: $h = 53$ ft
- Reservoir pressure: $\bar{p} = 5651$ psia
- Bubble-point pressure: $p_b = 5651$ psia
- Oil formation volume factor: $B_o = 1.1$
- Oil viscosity: $\mu_o = 1.7$ cp
- Total compressibility: $c_t = 0.0,000,129$ psi⁻¹
- Drainage area: $A = 640$ acres ($r_e = 2980$ ft)
- Wellbore radius: $r_w = 0.328$ ft
- Skin factor: $S = 0$

Solution

$$\begin{aligned}
 J^* &= \frac{kh}{141.2B_o\mu_o \left(\ln \frac{r_e}{r_w} - \frac{3}{4} + S \right)} \\
 &= \frac{(8.2)(53)}{141.2(1.1)(1.7) \left(\ln \frac{2980}{0.328} - 0.75 \right)} \\
 &= 0.1968 \text{ STB/d - psi} \\
 q_{\max} &= \frac{J^* \bar{p}}{1.8} \\
 &= \frac{(0.1968)(5651)}{1.8} \\
 &= 618 \text{ stb/day}
 \end{aligned}$$

The IPR curve is illustrated in Fig. 3.11.
 The points calculated using Eq. (3.29) are as follows.

p_{wf} (psi)	q_o (STB/day)
5651	0
5000	122
4500	206
4000	283
3500	352
3000	413
2500	466
2000	512
1500	550
1000	580
500	603
0	618

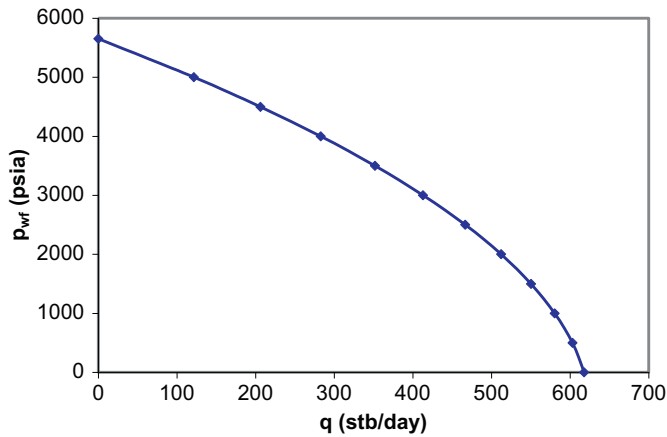


FIGURE 3.11

Inflow performance relationship curve for Sample Problem 3-3.

3.5.3 IPR for partial two-phase oil reservoirs

If the reservoir pressure is greater than the bubble-point pressure and the flowing bottom-hole pressure is less than the bubble-point pressure, a generalized model of Vogel's IPR can be used. The model combines the straight-line IPR model for single-phase flow with Vogel's IPR model for two-phase flow. Fig. 3.12 illustrates the curve derived using the two-part model.

According to the linear IPR model, the flow rate at the bubble-point pressure is

$$q_b = J^*(\bar{p} - p_b) \quad (3.34)$$

Based on Vogel's IPR model, the additional component of flow resulting from the pressure below the bubble-point pressure is expressed as

$$\Delta q = q_v \left[1 - 0.2 \left(\frac{p_{wf}}{p_b} \right) - 0.8 \left(\frac{p_{wf}}{p_b} \right)^2 \right] \quad (3.35)$$

Thus the total flow rate at a given bottom-hole pressure that is less than the bubble-point pressure is expressed as

$$q = q_b + q_v \left[1 - 0.2 \left(\frac{p_{wf}}{p_b} \right) - 0.8 \left(\frac{p_{wf}}{p_b} \right)^2 \right] \quad (3.36)$$

Because

$$q_v = \frac{J^* p_b}{1.8} \quad (3.37)$$

Eq. (3.36) becomes

$$q = J^*(\bar{p} - p_b) + \frac{J^* p_b}{1.8} \left[1 - 0.2 \left(\frac{p_{wf}}{p_b} \right) - 0.8 \left(\frac{p_{wf}}{p_b} \right)^2 \right] \quad (3.38)$$

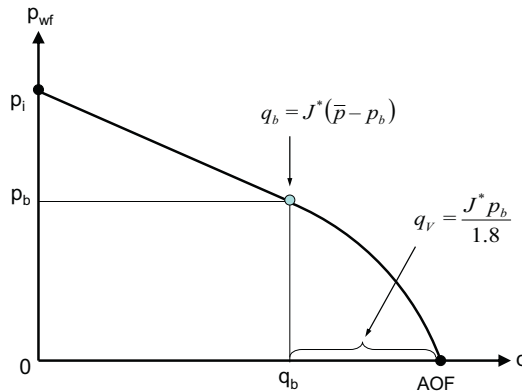


FIGURE 3.12

Generalized Vogel inflow performance relationship model for partial two-phase reservoirs.

3-4 Sample problem

Calculate and graph the IPR of a vertical well in an undersaturated oil reservoir using the generalized Vogel's equation. The following data are given:

- Porosity: $\phi = 0.19$
- Effective horizontal permeability: $k = 8.2$ md
- Pay zone thickness: $h = 53$ ft
- Reservoir pressure: $\bar{p} = 5651$ psia
- Bubble-point pressure: $p_b = 3000$ psia
- Oil formation volume factor: $B_o = 1.1$
- Oil viscosity: $\mu_o = 1.7$ cp
- Total compressibility: $c_t = 0.0000129$ psi⁻¹
- Drainage area: $A = 640$ acres ($r_e = 2980$ ft)
- Wellbore radius: $r_w = 0.328$ ft
- Skin factor: $S = 0$

Solution

$$\begin{aligned}
 J^* &= \frac{kh}{141.2B_o\mu_o \left(\ln \frac{r_e}{r_w} - \frac{3}{4} + S \right)} \\
 &= \frac{(8.2)(53)}{141.2(1.1)(1.7) \left(\ln \frac{2980}{0.328} - 0.75 \right)} \\
 &= 0.1968 \text{ STB/d - psi} \\
 q_b &= J^* (\bar{p} - p_b) \\
 &= (0.1968) (5651 - 3000) \\
 &= 522 \text{ stb/day} \\
 q_v &= \frac{J^* p_b}{1.8} \\
 &= \frac{(0.1968) (3000)}{1.8} \\
 &= 328 \text{ stb/day}
 \end{aligned}$$

The points calculated using Eq. (3.36) are as follows.

p_{wf}	q_o (STB/day)
0	850
565	828
1130	788
1695	729
2260	651
2826	555
3000	522
565	0

The IPR curve is illustrated in Fig. 3.13.

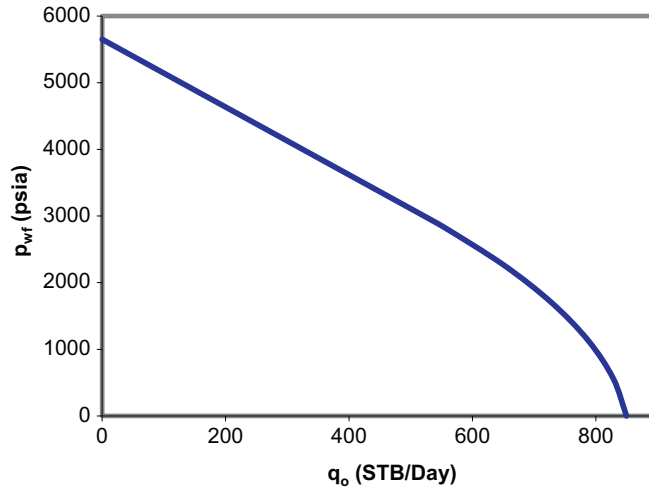


FIGURE 3.13

Inflow performance relationship curve for [Sample Problem 3-4](#).

3.6 Construction of IPR curves using test points

As shown in the last section, well IPR curves can be constructed using formation permeability, pay zone thickness, fluid viscosity, drainage area, wellbore radius, and well skin factor. These parameters determine the constants (such as the productivity index) used in the IPR model. However, actual values for these parameters are not always available in reality. Because of this, reservoir engineers frequently use measured values of production rate and flowing bottom-hole pressure, called test points, to construct IPR curves.

Constructing oil well IPR curves using test points requires the calculation of the productivity index J^* . For a single-phase (undersaturated oil) reservoir, the model constant J^* can be determined by

$$J^* = \frac{q_1}{(\bar{p} - p_{wf1})} \quad (3.39)$$

where q_1 is the tested production rate at actual flowing bottom-hole pressure p_{wf1} .

For a partial two-phase reservoir, the model constant J^* in the generalized Vogel's equation must be determined based on the pressure range in which the tested flowing bottom-hole pressure falls. If the tested flowing bottom-hole pressure is *greater than* the bubble-point pressure, the model constant J^* should be determined by

$$J^* = \frac{q_1}{(\bar{p} - p_{wf1})} \quad (3.40)$$

If the tested flowing bottom-hole pressure is *less than* bubble-point pressure, the model constant J^* should be determined using Eq. (3.38), that is,

$$J^* = \frac{q_1}{\left((\bar{p} - p_b) + \frac{p_b}{1.8} \left[1 - 0.2 \left(\frac{p_{wf1}}{p_b} \right) - 0.8 \left(\frac{p_{wf1}}{p_b} \right)^2 \right] \right)} \quad (3.41)$$

3-5 Sample problem

Calculate and graph the IPR for two wells in an undersaturated oil reservoir using the generalized Vogel's model. The following data are given:

Reservoir pressure: $\bar{p} = 5000$ psia

Bubble-point pressure: $p_b = 3000$ psia

Tested flowing bottom-hole pressure in Well A: $p_{wf1} = 4000$ psia

Tested production rate from Well A: $q_1 = 300$ stb/day

Tested flowing bottom-hole pressure in Well B: $p_{wf1} = 2000$ psia

Tested production rate from Well B: $q_1 = 900$ stb/day

Solution for well A

$$\begin{aligned} J^* &= \frac{q_1}{(\bar{p} - p_{wf1})} \\ &= \frac{300}{(5000 - 4000)} \\ &= 0.3000 \text{ stb/day - psi} \end{aligned}$$

The points calculated using Eq. (3.38) are as follows.

p_{wf} (psia)	q (stb/day)
0	1100
500	1072
1000	1022
1500	950
2000	856
2500	739
3000	600
5000	0

The IPR curve is illustrated in Fig. 3.14.

Solution for well B

$$\begin{aligned} J^* &= \frac{q_1}{\left((\bar{p} - p_b) + \frac{p_b}{1.8} \left[1 - 0.2 \left(\frac{p_{wf1}}{p_b} \right) - 0.8 \left(\frac{p_{wf1}}{p_b} \right)^2 \right] \right)} \\ &= \frac{900}{\left((5000 - 3000) + \frac{3000}{1.8} \left[1 - 0.2 \left(\frac{2000}{3000} \right) - 0.8 \left(\frac{2000}{3000} \right)^2 \right] \right)} \\ &= 0.3156 \text{ stb/day - psi} \end{aligned}$$

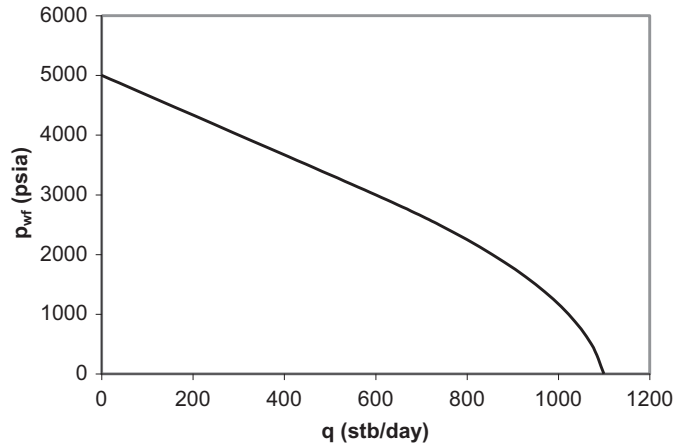


FIGURE 3.14

Inflow performance relationship curves for [Sample Problem 3-5](#), Well A.

The calculated points are as follows.

p_{wf} (psia)	q (stb/day)
0	1157
500	1128
1000	1075
1500	999
2000	900
2500	777
3000	631
5000	0

The IPR curve is illustrated in [Fig. 3.15](#).

For a two-phase (saturated oil) reservoir, if Vogel's equation ([Eq. 3.29](#)) is used for constructing the IPR curve, the model constant q_{max} can be determined by

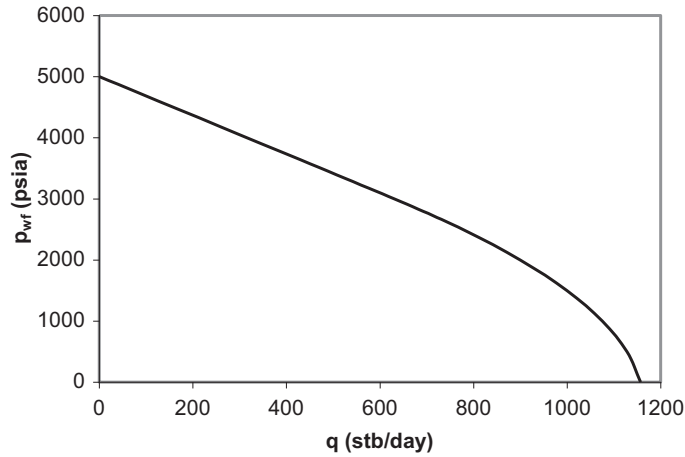
$$q_{max} = \frac{q_1}{1 - 0.2 \left(\frac{p_{wf1}}{\bar{p}} \right) - 0.8 \left(\frac{p_{wf1}}{\bar{p}} \right)^2} \quad (3.42)$$

The productivity index at and above reservoir pressure, if desired, can then be estimated by

$$J^* = \frac{1.8q_{max}}{\bar{p}} \quad (3.43)$$

If Fetkovich's equation is used instead, two test points are required to determine the values of the two model constants:

$$n = \frac{\log \left(\frac{q_1}{q_2} \right)}{\log \left(\frac{\bar{p}^2 - p_{wf1}^2}{\bar{p}^2 - p_{wf2}^2} \right)} \quad (3.44)$$

**FIGURE 3.15**

Inflow performance relationship curves for [Sample Problem 3-5](#), Well B.

and

$$C = \frac{q_1}{(\bar{p}^2 - p_{wf1}^2)^n} \quad (3.45)$$

where q_1 and q_2 are the tested production rates at the actual flowing bottom-hole pressures p_{wf1} and p_{wf2} , respectively.

3-6 Sample problem

Calculate and graph the IPR of a well in a saturated oil reservoir using both Vogel's and Fetkovich's equations. The following data are given:

Reservoir pressure: $\bar{p} = 3000$ psia

Tested flowing bottom-hole pressure: $p_{wf1} = 2000$ psia

Tested production rate at p_{wf1} : $q_1 = 500$ stb/day

Tested flowing bottom-hole pressure: $p_{wf2} = 1000$ psia

Tested production rate at p_{wf2} : $q_2 = 800$ stb/day

Solution using Vogel's equation

$$\begin{aligned} q_{\max} &= \frac{q_1}{1 - 0.2 \left(\frac{p_{wf1}}{\bar{p}} \right) - 0.8 \left(\frac{p_{wf1}}{\bar{p}} \right)^2} \\ &= \frac{500}{1 - 0.2 \left(\frac{2000}{3000} \right) - 0.8 \left(\frac{2000}{3000} \right)^2} \\ &= 978 \text{ stb/day} \end{aligned}$$

The data points calculated using Eq. (3.29) are as follows.

p_{wf} (psia)	q (stb/day)
0	978
500	924
1000	826
1500	685
2000	500
2500	272
3000	0

Solution using Fetkovich's equation

$$\begin{aligned}
 n &= \frac{\log\left(\frac{q_1}{q_2}\right)}{\log\left(\frac{\bar{p}^2 - p_{wf1}^2}{\bar{p}^2 - p_{wf2}^2}\right)} \\
 &= \frac{\log\left(\frac{500}{800}\right)}{\log\left(\frac{(3000)^2 - (2000)^2}{(3000)^2 - (1000)^2}\right)} \\
 &= 1.0 \\
 C &= \frac{q_1}{(\bar{p}^2 - p_{wf1}^2)^n} \\
 &= \frac{500}{\left((3000)^2 - (2000)^2\right)^{1.0}} \\
 &= 0.0001 \text{ stb/day-psi}^{2n}
 \end{aligned}$$

The data points calculated using Eq. (3.33) are as follows.

p_{wf} (psia)	q (stb/day)
0	900
500	875
1000	800
1500	675
2000	500
2500	275
3000	0

The IPR curves are illustrated in Fig. 3.16 and show that Fetkovich's equation with two constants yields more conservative results than Vogel's equation.

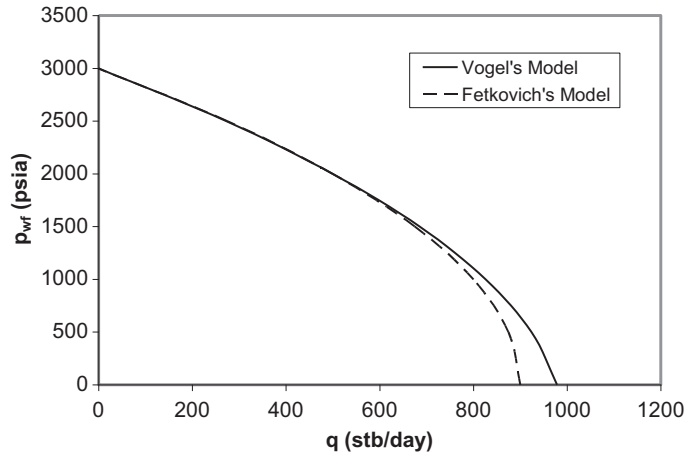


FIGURE 3.16

Inflow performance relationship curves for [Sample Problem 3-6](#).

3.7 Composite IPR of stratified reservoirs

Nearly all producing formations are stratified to some extent. This means that the vertical borehole encounters different rock layers in the production zone with different reservoir pressures, permeabilities, and producing fluids. If there is no communication between these formations other than the wellbore, production will come mainly from the higher permeability layers.

As the well's production rate is gradually increased, the less consolidated layers will begin to produce one after the other at progressively lower gas–oil ratios (GORs), and the overall GOR of production will decrease. If the most highly depleted layers themselves produce at high GORs owing to high free gas saturations, however, the overall GOR will eventually start to rise as the production rate is increased, and this climb will continue even after the most permeable zone has come onto production. Thus, one can expect that a well producing from a stratified formation will exhibit minimum GOR as the rate of liquid production is increased.

One of the major concerns in multilayer systems is that interlayer cross-flow may occur if reservoir fluids are produced from commingled layers of unequal potentials or pressures converted to the datum depth. This cross-flow greatly affects the composite IPR of the well, which may result in an over-optimistic estimate of production rate from the commingled layers.

EI-Banbi and Wattenbarger (1996, 1997) investigated the productivity of commingled gas reservoirs based on matching history of production data. However, no information was given in their papers regarding the generation of IPR curves.

3.7.1 Composite IPR models

The following assumptions are made in this section:

1. Pseudo—steady-state flow prevails in all reservoir layers.
2. Fluids from/into all layers have similar properties.
3. Pressure losses in the wellbore sections between layers are negligible. (These pressure losses are considered when multilateral wells are addressed in Chapter 7.)
4. The IPRs of individual layers are known.

On the basis of assumption 1, under steady flow conditions, the principle of material balance dictates:

Net mass flow rate from layers to the well = mass flow rate at wellhead. That is,

$$\sum_{i=1}^n m_i = m_{wh} \quad (3.46)$$

or

$$\sum_{i=1}^n \rho_i q_i = \rho_{wh} q_{wh} \quad (3.47)$$

where

- m_i = mass flow rate from/into layer i ,
- m_{wh} = mass flow rate at wellhead,
- ρ_i = density of fluid from/into layer i ,
- q_i = flow rate from/into layer i ,
- ρ_{wh} = density of fluid at wellhead,
- q_{wh} = flow rate at wellhead, and
- n = number of layers.

Fluid flow from the wellbore to reservoir is indicated by a negative value for q_i . Using assumption 2 and ignoring the density change from bottom-hole to wellhead, Eq. (3.46) simplifies to

$$\sum_{i=1}^n q_i = q_{wh} \quad (3.48)$$

3.7.1.1 Single-phase liquid flow

For reservoir layers that contain undersaturated oils, if the flowing bottom-hole pressure is greater than the bubble-point pressures of the oils in all layers, then we can expect single-phase flow in all layers. In that case, Eq. (3.48) becomes

$$\sum_{i=1}^n J_i^* (\bar{p}_i - p_{wf}) = q_{wh} \quad (3.49)$$

where J_i^* is the productivity index of layer i at and greater than the bubble-point pressure, and \bar{p}_i and p_{wf} are converted to the datum depth. Thus Eq. (3.49) represents a linear composite IPR of the well. A straight-line IPR can be drawn through two points at AOF and at stabilized shut-in bottom-hole pressure (p_{wfo}) at a datum depth. It is apparent from Eq. (3.49) that

$$AOF = \sum_{i=1}^n J_i^* \bar{p}_i = \sum_{i=1}^n AOF_i \quad (3.50)$$

and

$$p_{wfo} = \frac{\sum_{i=1}^n J_i^* \bar{p}_i}{\sum_{i=1}^n J_i^*} \quad (3.51)$$

It should be borne in mind that p_{wfo} could be a dynamic bottom-hole pressure due to cross-flow between layers.

3.7.1.2 Two-phase flow

For reservoir layers that contain saturated oils, two-phase flow is expected. In that case Eq. (3.49) becomes a polynomial of an order greater than 1. If Vogel's IPR model is used, Eq. (3.49) becomes

$$\sum_{i=1}^n \frac{J_i^* \bar{p}_i}{1.8} \left[1 - 0.2 \left(\frac{p_{wf}}{\bar{p}_i} \right) - 0.8 \left(\frac{p_{wf}}{\bar{p}_i} \right)^2 \right] = q_{wh} \quad (3.52)$$

which gives

$$AOF = \sum_{i=1}^n \frac{J_i^* \bar{p}_i}{1.8} = \sum_{i=1}^n AOF_i \quad (3.53)$$

and

$$p_{wfo} = \frac{\sqrt{80 \sum_{i=1}^n J_i^* \bar{p}_i \sum_{i=1}^n \frac{J_i^*}{\bar{p}_i} + \left(\sum_{i=1}^n J_i^* \right)^2 - \sum_{i=1}^n J_i^*}}{8 \sum_{i=1}^n \frac{J_i^*}{\bar{p}_i}} \quad (3.54)$$

Again, p_{wfo} could be a dynamic bottom-hole pressure at the datum depth due to cross-flow between layers.

3.7.1.3 Partial two-phase flow

The generalized Vogel's IPR model can be used to describe well inflow from multi-layer reservoirs where the reservoir pressures are greater than oil bubble-point pressures, and the wellbore pressure is less. Eq. (3.48) takes the form

$$\sum_{i=1}^n J_i^* \left\{ (\bar{p}_i - p_{bi}) + \frac{p_{bi}}{1.8} \left[1 - 0.2 \left(\frac{p_{wf}}{p_{bi}} \right) - 0.8 \left(\frac{p_{wf}}{p_{bi}} \right)^2 \right] \right\} = q_{wh} \quad (3.55)$$

where all pressures are converted to the datum depth. Eq. (3.45) gives

$$AOF = \sum_{i=1}^n J_i^* (\bar{p}_i - 0.44p_{bi}) = \sum_{i=1}^n AOF_i \quad (3.56)$$

and

$$p_{wfo} = \frac{\sqrt{147 \left[0.56 \sum_{i=1}^n J_i^* p_{bi} + \sum_{i=1}^n J_i^* (\bar{p}_i - p_{bi}) \right] \sum_{i=1}^n \frac{J_i^*}{p_{bi}} + \left(\sum_{i=1}^n J_i^* \right)^2 - \sum_{i=1}^n J_i^*}}{8 \sum_{i=1}^n \frac{J_i^*}{p_{bi}}} \quad (3.57)$$

Once again, p_{wfo} could be a dynamic bottom-hole pressure converted to the datum depth due to cross-flow between layers.

3.7.2 Applications

The equations presented in the previous section can be easily used to generate composite IPR curves if all values for J_i^* are known. Although numerous equations have been proposed to estimate J_i^* for different types of wells, it is always better to determine J_i^* based on actual flow tests of individual strata. If the tested flow rate (q_i) is obtained at a wellbore pressure (p_{wfi}) that is *greater than* the bubble-point pressure in layer i , the productivity index J_i^* can be determined by

$$J_i^* = \frac{q_i}{\bar{p}_i - p_{wfi}} \quad (3.58)$$

If the tested rate (q_i) is obtained at a wellbore pressure (p_{wfi}) that is *less than* the bubble-point pressure in layer i , the productivity index J_i^* should be determined by

$$J_i^* = \frac{q_i}{(\bar{p}_i - p_{bi}) + \frac{p_{bi}}{1.8} \left[1 - 0.2 \left(\frac{p_{wfi}}{p_{bi}} \right) - 0.8 \left(\frac{p_{wfi}}{p_{bi}} \right)^2 \right]} \quad (3.59)$$

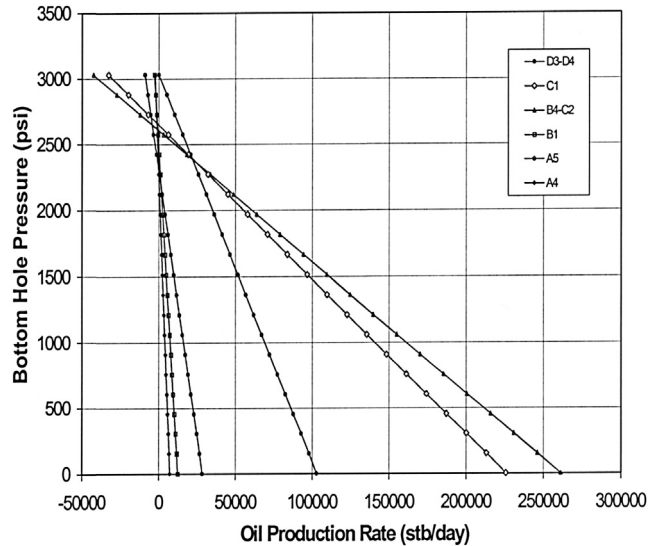
With J_i^* , \bar{p}_i , and p_{bi} known, composite IPR can be generated using Eq. (3.55).

3-7 Sample problem

An exploration well in the South China Sea penetrated eight oil-bearing strata displaying unequal pressures within a short interval. These oil-bearing strata were tested in six groups. Strata B4 and C2 were tested together, and strata D3 and D4 were tested together. The remaining four strata were tested individually. Test data and the calculated productivity indexes (J_i^*) are summarized in Table 3.1. All pressures are converted to a datum depth. The IPR curves of the individual strata are shown in Fig. 3.17, which shows that the productivities of strata A4, A5, and B1 are significantly lower than the others. It is expected that wellbore cross-flow should occur if the bottom pressure (converted to datum depth) is greater than the lowest reservoir pressure of 2254 psi. Strata B4,

Table 3.1 Summary of test points for eight oil-bearing layers.

Layer no.	D3-D4	C1	B4-C2	B1	A5	A4
Strata pressure (psi)	3030	2648	2606	2467	2302	2254
Bubble point (psi)	26.3	4.1	4.1	56.5	31.2	33.8
Test rate (bopd)	3200	3500	3510	227	173	122
Test pressure (psi)	2936	2607	2571	2422	2288	2216
J^* (bopd/psi)	34	85.4	100.2	5.04	12.4	3.2

**FIGURE 3.17**

Inflow performance relationship curves of individual oil-bearing strata.

C1, and C2 should be the major thief zones because of their high injectivities (assumed to be equal to their productivities) and their relatively low pressures.

The composite IPR of these strata is shown in Fig. 3.18, where the net production rate from the well is plotted against bottom-hole pressure. This figure shows that net oil production will not be available unless the bottom-hole pressure is reduced to less than 2658 psi.

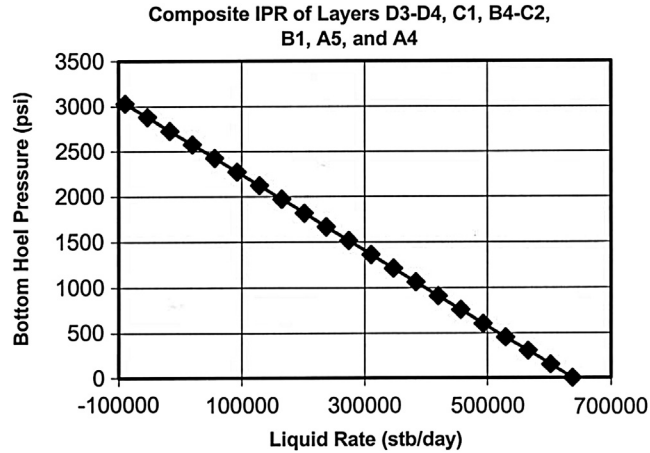
A reservoir engineer inspecting Fig. 3.17 might suggest that the eight oil-bearing strata be produced separately in three groups:

Group 1: Strata D3 and D4

Group 2: Strata B4, C1, and C2

Group 3: Strata B1, A4, and A5

Use Table 3.2 to compare the production rates at several bottom-hole pressures. This comparison indicates that significant production from Group 1 can be achieved at bottom-hole pressures higher than 2658 psi, while Group 2 and Group 3 are shut in. A significant production from Group 1 and Group 2 can be achieved at bottom-hole pressures higher than 2625 psi, while Group 3 is shut in. The grouped-strata production can proceed until the bottom-hole pressure is decreased to less than 2335 psi, at which time Group 3 can be opened for production.

**FIGURE 3.18**

Composite inflow performance relationship (IPR) curve for all strata open to flow.

Table 3.2 Comparison of commingled and strata-grouped productions.

Bottom-hole pressure (psi)	Production rate (stb/day)				
	All strata commingled	Grouped strata			Total
		Group 1	Group 2	Group 3	
2658	0	12,663	Shut in	Shut in	12,663
2625	7866	13,787	0	Shut in	13,787
2335	77,556	23,660	53,896	0	77,556
2000	158,056	35,063	116,090	6903	158,056

3.8 Predicting future IPR

Reservoir deliverability inevitably declines with time during the transient flow period in single-phase reservoirs. This is because the overall pressure gradient in the reservoir drops with time. Graphically, this is because the radius of the pressure funnel, over which the pressure drawdown ($p_i - p_{wf}$) acts, increases with time. During pseudo-steady-state flow, reservoir deliverability decreases due to the depletion of reservoir pressure. In two-phase reservoirs, as the reservoir pressure is depleted, reservoir deliverability decreases due to the reduced relative permeability to oil and the increased oil viscosity. Reservoir engineers use both Vogel's and Fetkovich's methods to predict future IPR.

3.8.1 Using Vogel's method to predict future IPR

Let J_p^* and J_f^* be the present and future productivity indices, respectively. The following relation can be derived:

$$\frac{J_f^*}{J_p^*} = \frac{\left(\frac{k_{ro}}{B_o\mu_o}\right)_f}{\left(\frac{k_{ro}}{B_o\mu_o}\right)_p} \quad (3.60)$$

or

$$J_f^* = J_p^* \frac{\left(\frac{k_{ro}}{B_o\mu_o}\right)_f}{\left(\frac{k_{ro}}{B_o\mu_o}\right)_p} \quad (3.61)$$

Thus,

$$q = \frac{J_f^* \bar{p}_f}{1.8} \left[1 - 0.2 \frac{p_{wf}}{\bar{p}_f} - 0.8 \left(\frac{p_{wf}}{\bar{p}_f} \right)^2 \right] \quad (3.62)$$

where \bar{p}_f is the reservoir pressure at the future time.

3-8 Sample problem

Determine the IPR for a well at a future time when the average reservoir pressure has dropped to 1800 psig. The following data have been obtained from laboratory tests of well fluid samples.

Reservoir properties	Present	Future
Average pressure (psig)	2250	1800
Productivity index J^* (stb/day-psi)	1.01	
Oil viscosity (cp)	3.11	3.59
Oil formation volume factor (rb/stb)	1.173	1.150
Relative permeability to oil	0.815	0.685

Solution

$$\begin{aligned} J_f^* &= J_p^* \frac{\left(\frac{k_{ro}}{B_o\mu_o}\right)_f}{\left(\frac{k_{ro}}{B_o\mu_o}\right)_p} \\ &= 1.01 \frac{\left(\frac{0.685}{3.59(1.150)}\right)}{\left(\frac{0.815}{3.11(1.173)}\right)} \\ &= 0.75 \text{ stb/day} - \text{psi} \end{aligned}$$

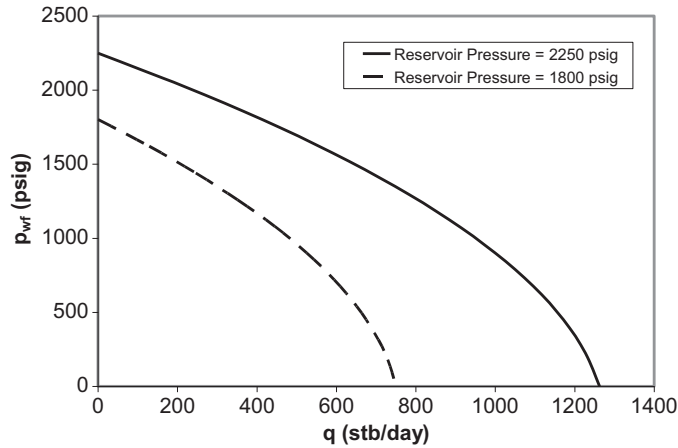


FIGURE 3.19

Inflow performance relationship curves for [Sample Problem 3-8](#).

Using Vogel's equation for future IPR

$$q = \frac{J_f \bar{p}_f}{1.8} \left[1 - 0.2 \frac{p_{wf}}{\bar{p}_f} - 0.8 \left(\frac{p_{wf}}{\bar{p}_f} \right)^2 \right]$$

$$= \frac{(0.75)(1800)}{1.8} \left[1 - 0.2 \frac{p_{wf}}{1800} - 0.8 \left(\frac{p_{wf}}{1800} \right)^2 \right]$$

Calculated data points:

Reservoir pressure = 2250 psig		Reservoir pressure = 1800 psig	
p_{wf} (psig)	q (stb/day)	p_{wf} (psig)	q (stb/day)
2250	0	1800	0
2025	217	1620	129
1800	414	1440	246
1575	591	1260	351
1350	747	1080	444
1125	884	900	525
900	1000	720	594
675	1096	540	651
450	1172	360	696
225	1227	180	729
0	1263	0	750

The present and future IPR curves are illustrated in [Fig. 3.19](#).

3.8.2 Using Fetkovich's method to predict future IPR

The integral form of the reservoir inflow relationship for multiphase flow is expressed as

$$q = \frac{0.007082kh}{\ln\left(\frac{r_e}{r_w}\right)} \int_{p_{wf}}^{p_e} f(p) dp \tag{3.63}$$

where $f(p)$ is a pressure function. The simplest case of two-phase flow is that of a constant pressure p_e at the outer boundary (r_e), with the value of p_e of less than the bubble-point pressure, so that two-phase flow occurs throughout the reservoir. Under these circumstances, $f(p)$ takes the value

$$\frac{k_{ro}}{\mu_o B_o}$$

where k_{ro} is the relative permeability to oil at the saturation conditions in the formation, corresponding to the pressure p . The Fetkovich method makes the key assumption that the expression

$$\frac{k_{ro}}{\mu_o B_o}$$

is a good approximation of a linear function of p and passes through zero. If p_i is the initial formation pressure (i.e., $\sim p_e$), then the straight-line relationship is expressed as

$$\frac{k_{ro}}{\mu_o B_o} = \left(\frac{k_{ro}}{\mu_o B_o} \right) \frac{p}{p_i} \quad (3.64)$$

Substituting Eq. (3.64) into Eq. (3.63) and integrating the latter gives

$$q_o = \frac{0.007082kh}{\ln\left(\frac{r_e}{r_w}\right)} \left(\frac{k_{ro}}{\mu_o B_o} \right) \frac{1}{i^2 p_i} (p_i^2 - p_{wf}^2) \quad (3.65)$$

or

$$q_o = J'_i (p_i^2 - p_{wf}^2) \quad (3.66)$$

where

$$J'_i = \frac{0.007082kh}{\ln\left(\frac{r_e}{r_w}\right)} \left(\frac{k_{ro}}{\mu_o B_o} \right) \frac{1}{i^2 p_i} \quad (3.67)$$

The derivative of Eq. (3.65) with respect to the flowing bottom-hole pressure is

$$\frac{dq_o}{dp_{wf}} = -2J'_i p_{wf} \quad (3.68)$$

This implies that the rate of change of q with respect to p_{wf} is lower at lower values of inflow pressure.

Next, we can modify Eq. (3.63) to take into account the fact that in practice p_e is not constant but decreases with cumulative production. The assumption made is that J'_i will decrease in proportion to the decrease in average reservoir

(drainage area) pressure. Thus, when the static pressure is p_e ($< p_i$), the IPR equation is

$$q_o = J'_i \frac{p_e}{p_i} (p_e^2 - p_{wf}^2) \tag{3.69}$$

or, alternatively,

$$q_o = J' (p_e^2 - p_{wf}^2) \tag{3.70}$$

where

$$J' = J'_i \frac{p_e}{p_i} \tag{3.71}$$

These equations may be used to predict future IPR.

3-9 Sample problem

Using Fetkovich's method, plot the IPR curves for a well in which p_i is 2000 psia and $J'_i = 5 \times 10^{-4}$ stb/day – psia². Predict the IPRs of the well at the well shut in static pressures of 1500 psia and 1000 psia.

Solution

The value of J_o at 1500 psia is

$$\begin{aligned} J'_o &= 5 \times 10^{-4} \left(\frac{1500}{2000} \right) \\ &= 3.75 \times 10^{-4} \text{ day} - (\text{psia})^2 \end{aligned}$$

And the value of J_o at 1000 psia is

$$\begin{aligned} J'_o &= 5 \times 10^{-4} \left(\frac{1000}{2000} \right) \\ &= 2.5 \times 10^{-4} \text{ day} - (\text{psia})^2 \end{aligned}$$

Using the above values for J_o and the accompanying p_e in Eq. (3.54), the following data points can be calculated:

$p_e = 2000$ psig		$p_e = 1500$ psig		$p_e = 1000$ psig	
p_{wf} (psig)	q (stb/day)	p_{wf} (psig)	q (stb/day)	p_{wf} (psig)	q (stb/day)
2000	0	1500	0	1000	0
1800	380	1350	160	900	48
1600	720	1200	304	800	90
1400	1020	1050	430	700	128
1200	1280	900	540	600	160
1000	1500	750	633	500	188
800	1680	600	709	400	210
600	1820	450	768	300	228
400	1920	300	810	200	240
200	1980	150	835	100	248
0	2000	0	844	0	250

The IPR curves are illustrated in Fig. 3.20.

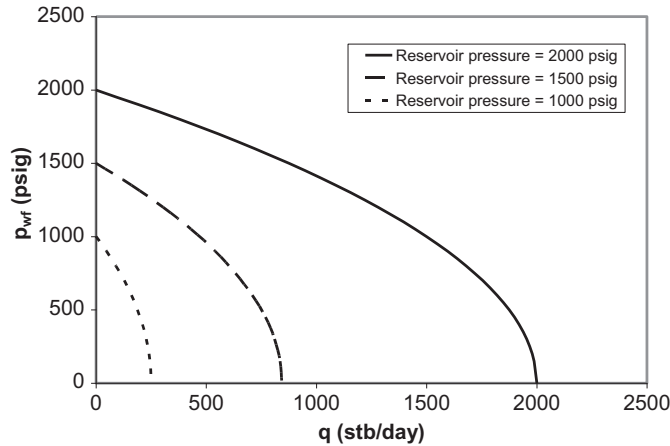


FIGURE 3.20

Inflow performance relationship curves for [Sample Problem 3-9](#).

3.9 Summary

This chapter presented and illustrated several mathematical models for estimating the deliverability of oil and gas reservoirs. Production engineers should choose between the models based on their best estimates of reservoir flow regimes and pressure levels. The selected models should be checked against actual well production rates and bottom-hole pressures. At least one test point is required to validate a straight-line (single-liquid flow) IPR model. At least two test points are required to validate a nonlinear (single-gas flow or two-phase flow) IPR model.

3.10 Problems

3-1 Calculate and graph the IPR of a vertical well in an oil reservoir. Consider (1) transient flow at 30 days, (2) steady-state flow, and (3) pseudo-steady-state flow. The following data are given:

Porosity: $\phi = 0.28$

Effective horizontal permeability: $k = 12$ md

Pay zone thickness: $h = 52$ ft

Reservoir pressure: p_e or $\bar{p} = 5200$ psia

Bubble-point pressure: $p_b = 120$ psia

Fluid formation volume factor: $B_o = 1.2$

Fluid viscosity: $\mu_o = 1.6$ cp

Total compressibility: $c_t = 0.0,000,125$ psi⁻¹

Drainage area: $A = 640$ acres ($r_e = 2980$ ft)

Wellbore radius: $r_w = 0.328$ ft

Skin factor: $S = 8$

- 3-2** A gas reservoir has a permeability of 1.5 md. A vertical well with a radius of 0.328 ft drains the reservoir from the center of an area of 160 acres. If the well is hydraulically fractured to create a 2500-ft long, 0.14-inch wide fracture of 220,000 md permeability around the center of the drainage area, what would be the factor of increase in reservoir deliverability?
- 3-3** Calculate and graph the IPR of a vertical well in a saturated oil reservoir using Vogel's equation, given the following data:
 Porosity: $\phi = 0.24$
 Effective horizontal permeability: $k = 84$ md
 Pay zone thickness: $h = 58$ ft
 Reservoir pressure: $\bar{p} = 4600$ psia
 Bubble-point pressure: $p_b = 4600$ psia
 Fluid formation volume factor: $B_o = 1.15$
 Fluid viscosity: $\mu_o = 1.5$ cp
 Total compressibility: $c_t = 0.000013$ psi⁻¹
 Drainage area: $A = 640$ acres ($r_e = 2980$ ft)
 Wellbore radius: $r_w = 0.328$ ft
 Skin factor: $S = 6$
- 3-4** Calculate and graph the IPR of a vertical well in an unsaturated oil reservoir using the generalized Vogel's equation given the following data:
 Porosity: $\phi = 0.22$
 Effective horizontal permeability: $k = 110$ md
 Pay zone thickness: $h = 53$ ft
 Reservoir pressure: $\bar{p} = 5200$ psia
 Bubble-point pressure: $p_b = 3400$ psia
 Fluid formation volume factor: $B_o = 1.15$
 Fluid viscosity: $\mu_o = 1.4$ cp
 Total compressibility: $c_t = 0.000013$ psi⁻¹
 Drainage area: $A = 640$ acres ($r_e = 2980$ ft)
 Wellbore radius: $r_w = 0.328$ ft
 Skin factor: $S = 5.1$
- 3-5** Calculate and graph the IPR of two wells in an unsaturated oil reservoir using generalized Vogel's equation, given the following data:
 Reservoir pressure: $\bar{p} = 5600$ psia
 Bubble-point pressure: $p_b = 3400$ psia
 Tested flowing bottom-hole pressure in Well A: $p_{wfl} = 4100$ psia
 Tested production rate from Well A: $q_l = 405$ stb/day
 Tested flowing bottom-hole pressure in Well B: $p_{wfl} = 2200$ psia
 Tested production rate from Well B: $q_l = 1100$ stb/day

3-6 Calculate and graph the IPR of a well in a saturated oil reservoir using both Vogel's and Fetkovich's equations, given the following data:

Reservoir pressure: $\bar{p} = 3600$ psia

Tested flowing bottom-hole pressure: $p_{wf1} = 2700$ psia

Tested production rate at p_{wf1} : $q_1 = 620$ stb/day

Tested flowing bottom-hole pressure: $p_{wf2} = 1550$ psia

Tested production rate at p_{wf2} : $q_2 = 940$ stb/day

3-7 Determine the IPR for a well at the time when the average reservoir pressure will be 1500 psig. The following data have been obtained from laboratory tests of well fluid samples:

Reservoir properties	Present	Future
Average pressure (psig)	2210	1510
Productivity index J^* (stb/day-psi)	1.22	
Oil viscosity (cp)	3.05	3.55
Oil formation volume factor (rb/stb)	1.20	1.15
Relative permeability to oil	0.80	0.62

3-8 Using Fetkovich's method, plot the IPR curve for a well in which p_i is 3420 psia and $J_o = 4 \times 10^{-4}$ stb/day- psia^2 . Predict the IPR's of the well at well shut in static pressures of 2500 psia, 2000 psia, 1500 psia, and 1000 psia.

References

- Argawal, R.G., Carter, R.D., Pollock, C.B., March 1979. Evaluation and prediction of performance of low-permeability gas wells stimulated by massive hydraulic fracturing. *Journal of Petroleum Technology* 267, 362–372. Trans. AIME.
- Bandakhlia, H., Aziz, K., 1989. Inflow performance relationship for solution-gas drive horizontal wells. In: Paper SPE 19823 Presented at the 64th SPE Annual Technical Conference and Exhibition (8–11 October, 1989), San Antonio, Texas.
- Chang, M., 1992. Analysis of inflow performance simulation of solution-gas drive for horizontal/slant wells. In: Paper SPE 24352 Presented at the SPE Rocky Mountain Regional Meeting (18–21 May 1992), Casper, Wyoming.
- Cinco-Ley, H., Samaniego, F., September 1981. Transient pressure analysis for fractured wells. *Journal of Petroleum Technology* 1749–1766.
- Dake, L.P., 1978. *Fundamentals of Reservoir Engineering*. Elsevier, New York.
- Dietz, D.N., August 1965. Determination of average reservoir pressure from build-up surveys. *Journal of Petroleum Technology* 955–959.
- Earlougher, R.C., 1977. *Advances in Well Test Analysis*. Society of Petroleum Engineers, Dallas.
- Economides, M.J., Deimbacher, F.X., Brand, C.W., Heinemann, Z.E., December 1991. Comprehensive Simulation of Horizontal Well Performance. SPEFE, pp. 418–426.
- El-Banbi, A.H., Wattenbarger, R.A., 1996. Analysis of commingled tight gas reservoirs. In: Paper SPE 36736 Presented at the SPE Annual Technical Conference and Exhibition (6–9 October 1996), Denver, Colorado.

- El-Banbi, A.H., Wattenbarger, R.A., 1997. Analysis of commingled gas reservoirs with variable bottom-hole flowing pressure and non-Darcy flow. In: Paper SPE 38866 Presented at the SPE Annual Technical Conference and Exhibition (5–8 October 1997), San Antonio, Texas.
- Fetkovich, M.J., 1973. The isochronal testing of oil wells. In: Paper SPE 4529 Presented at the SPE Annual Technical Conference and Exhibition (30 September–3 October 1973), Las Vegas, Nevada.
- Guo, B., Schechter, D.S., July 1999. A simple and rigorous IPR equation for vertical and horizontal wells intersecting long fractures. *Journal of Canadian Petroleum Technology* 46–54.
- Guo, B., Zhou, J., Liu, Y., Ghalambor, A., 2007. A rigorous analytical model for fluid flow in drain holes of finite conductivity applied to horizontal and multilateral wells. In: Paper SPE 106947 Presented at the 2007 Production Operations Symposium (31 March–03 April 2007), Oklahoma City, OK.
- Joshi, S.D., June 1988. Augmentation of well productivity with slant and horizontal wells. *Journal of Petroleum Technology* 729–739.
- Retnanto, A., Economides, M., 1998. Inflow performance relationships of horizontal and multibranch wells in a solution gas drive reservoir. In: Paper SPE 49054 Presented at the 1998 SPE Annual Technical Conference and Exhibition (27–30 September 1998), New Orleans, Louisiana.
- Standing, M.B., September 1971. Concerning the calculation of inflow performance of wells producing from solution gas drive reservoirs. *Journal of Petroleum Technology* 1141–1142 paper SPE 3332.
- Vogel, J.V., January 1968. Inflow performance relationships for solution-gas drive wells. *Journal of Petroleum Technology* 83–92.

Wellbore performance

Chapter outline

4.1 Introduction	93
4.2 Single-phase liquid flow	94
4.3 Multiphase flow in oil wells	99
4.3.1 Flow regimes.....	100
4.3.2 Liquid holdup	100
4.3.3 TPR models	100
4.3.3.1 <i>Homogeneous-flow models</i>	101
4.3.3.2 <i>Separated-flow models</i>	107
4.4 Single-phase gas flow	113
4.4.1 Average temperature and compressibility factor method.....	114
4.4.2 Cullender and Smith method	116
4.5 Mist flow in gas wells	119
4.6 Summary	119
4.7 Problems	119
References	121
Further reading	122

4.1 Introduction

Wellbores provide paths for both petroleum production and fluid injection. Oil and natural gas are usually produced through well strings such as tubing, and the higher the performance of the well strings, the higher the productivity of the wells. A well-designed well string ensures that the flow in the wellbore will not be a limiting factor, or “bottleneck,” during fluid production. This requires that both friction and flow stability (mixing of multiple phases) be considered.

The flow performance of well string depends on the geometry of the string and the properties of the fluids transported through it. The fluids in production wells are usually multiple phases: oil, water, and gas, sometimes with included sand.

Analyzing wellbore performance requires establishing a relationship between tubing size, wellhead and bottom-hole pressures, fluid properties, and fluid production rate. An understanding of wellbore flow performance is vitally important to engineers for designing production wells.

Although oil and natural gas can be produced through tubing, casing, or both, the use of tubing is more common. This is because a tubing string provides a better gas-lift effect than does casing in oil wells, assists in liquid removal in gas wells, and seals better than casing. The properties of American Petroleum Institute (API) tubing are presented in Appendix B. The traditional term *tubing performance relationship* (TPR) is used in this book and is equivalent to other terms from the literature, such as vertical lift performance. Mathematical models are valid for flow in all types of conduits. This chapter focuses on the determination of the pressure profile along the well string and TPR. Both single- and multiphase fluids will be considered. Calculation examples are illustrated using computer spreadsheets. Applications of the TPR will be discussed in Chapters 5–8 in well productivity analyses.

4.2 Single-phase liquid flow

Single-phase oil flow exists in production oil wells only when the wellhead pressure is greater than the bubble-point pressure of the oil. Consider a fluid flowing from point 1 to point 2 in a tubing string of length L and height Δz (Fig. 4.1). The First Law of Thermodynamics yields the following equation for pressure drop:

$$\Delta P = P_1 - P_2 = \frac{g}{g_c} \rho \Delta z + \frac{\rho}{2g_c} \Delta u^2 + \frac{2f_F \rho u^2 L}{g_c D} \quad (4.1)$$

where

- ΔP = pressure drop (lb_f/ft²),
- P_1 = pressure at point 1 (lb_f/ft²),
- P_2 = pressure at point 2 (lb_f/ft²),

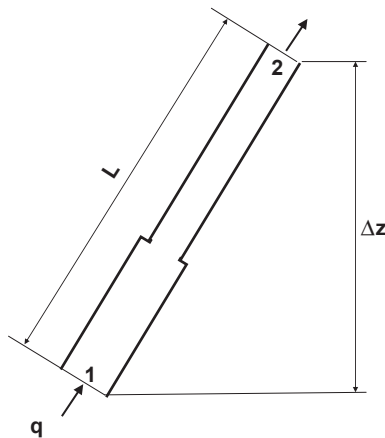


FIGURE 4.1

Parameters used to characterize flow along a tubing string.

g = gravitational acceleration (32.17 ft/s²),
 g_c = unit conversion factor (32.17 lb_m-ft/lb_f-s²),
 ρ = fluid density (lb_m/ft³),
 Δz = elevation increase (ft),
 u = fluid velocity (ft/s),
 f_F = Fanning friction factor,
 L = tubing length (ft), and
 D = tubing inside diameter (ft).

The first, second, and third terms in the right-hand side of Eq. (4.1) represent pressure decrease due to changes in elevation, kinetic energy, and friction, respectively.

The Fanning friction factor (f_F) can be evaluated based on the Reynolds number and the relative roughness of the tubing string interior. The Reynolds number is defined as the ratio of inertial force to viscous force. The Reynolds number is expressed in consistent units as

$$N_{Re} = \frac{Du\rho}{\mu} \quad (4.2)$$

or in US field units as

$$N_{Re} = \frac{1.48q\rho}{d\mu} \quad (4.3)$$

where

N_{Re} = Reynolds number,
 q = fluid flow rate (bbl/day),
 ρ = fluid density (lb_m/ft³),
 d = tubing inside diameter (in), and
 μ = fluid viscosity (cp).

For laminar flow regimes, in which $N_{Re} < 2100$, the Fanning friction factor is inversely proportional to the Reynolds number, or

$$f_F = \frac{16}{N_{Re}} \quad (4.4)$$

For turbulent flow regimes, where $N_{Re} > 2100$, the Fanning friction factor can be estimated empirically. Among numerous correlations developed by different investigators, the one developed by Chen (1979) has an explicit form and gives similar accuracy to the Colebrook–White equation (Gregory and Fogarasi, 1985). The latter was used to generate the friction factor chart widely used in the petroleum industry. Chen's correlation takes the following form:

$$\frac{1}{\sqrt{f_F}} = -4 \log \left\{ \frac{\epsilon}{3.7065} - \frac{5.0452}{N_{Re}} \log \left[\frac{e^{1.1098}}{2.8257} + \left(\frac{7.149}{N_{Re}} \right)^{0.8981} \right] \right\} \quad (4.5)$$

where the relative roughness of the tubing string interior is defined as

$$\varepsilon = \frac{\delta}{d}$$

and δ is the absolute roughness of pipe wall.

The Fanning friction factor can also be obtained from the Darcy–Wiesbach friction factor diagram shown in Fig. 4.2. The Darcy–Wiesbach friction factor might also be referred to as the Moody friction factor (f_M) in the literature. The relationship between these factors is expressed as

$$f_F = \frac{f_M}{4} \tag{4.6}$$

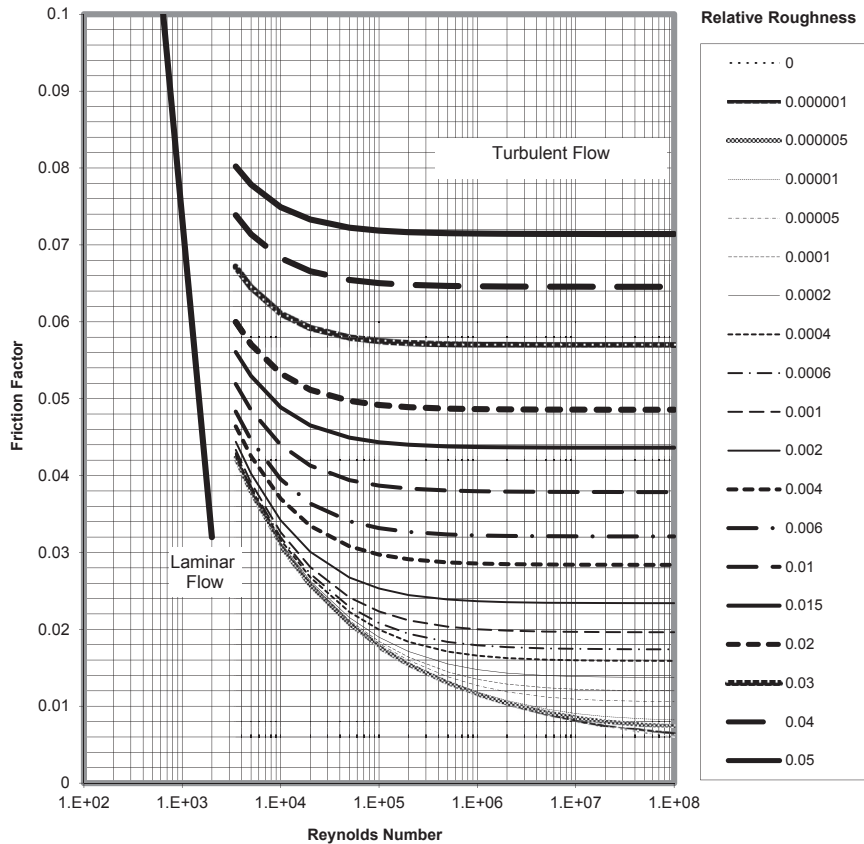


FIGURE 4.2
Darcy–Wiesbach friction factor diagram.

4.1 Sample problem

A well produces 1000 bbl/day of 40 degrees API, 1.2 cp oil, through a 27/8-in., 8.6-lb_m/ft tubing in a borehole with a 15 degrees average inclination angle. The tubing wall relative roughness is 0.001. Assuming that the tubing head pressure is 2000 psia, and the oil bubble-point pressure is 1950 psia, calculate the pressure at the tubing shoe at 1000 ft measured depth.

Solution

Determine the oil-specific gravity:

$$\begin{aligned}\gamma_o &= \frac{141.5}{^\circ\text{API} + 131.5} \\ &= \frac{141.5}{40 + 131.5} \\ &= 0.825\end{aligned}$$

Determine the approximate oil density in tubing:

$$\begin{aligned}\rho &= 62.4\gamma_o \\ &= (62.4)(0.825) \\ &= 51.57 \text{ lbm/ft}^3\end{aligned}$$

Determine the elevation increase:

$$\begin{aligned}\Delta Z &= \cos(\alpha) L \\ &= \cos(15) (1000) \\ &= 966 \text{ ft}\end{aligned}$$

Determine the tubing inside diameter in ft. The 2 7/8-in., 8.6-lb_m/ft tubing has an inside diameter of 2.259 in. Therefore,

$$D = \frac{2.259}{12} = 0.188 \text{ ft}$$

Determine the fluid velocity:

$$\begin{aligned}u &= \frac{4q}{\pi D^2} \\ &= \frac{4(5.615)(1000)}{\pi(0.188)^2 (86400)} \\ &= 2.34 \text{ ft/s}\end{aligned}$$

Determine the Reynolds number:

$$\begin{aligned}N_{\text{Re}} &= \frac{1.48q\rho}{d\mu} \\ &= \frac{1.48(1000)(51.57)}{(2.259)(1.2)} \\ &= 28115 > 2100, \text{ indicating turbulent flow}\end{aligned}$$

Using Chen's correlation, the Fanning friction factor can be calculated by

$$\begin{aligned}\frac{1}{\sqrt{f_F}} &= -4 \log \left\{ \frac{\varepsilon}{3.7065} - \frac{5.0452}{N_{Re}} \log \left[\frac{\varepsilon^{1.1098}}{2.8257} + \left(\frac{7.149}{N_{Re}} \right)^{0.8981} \right] \right\} \\ &= 12.3255 \\ f_F &= 0.006583\end{aligned}$$

If Fig. 4.2 is utilized instead, it gives a Moody friction factor of 0.0265. Thus the Fanning friction factor can then be estimated as

$$\begin{aligned}f_F &= \frac{0.0265}{4} \\ &= 0.006625\end{aligned}$$

The pressure at the tubing shoe can be calculated by

$$\begin{aligned}P_1 &= P_2 + \frac{g}{g_c} \rho \Delta z + \frac{\rho}{2g_c} \Delta u^2 + \frac{2f_F \rho u^2 L}{g_c D} \\ &= (2000)(144) + \frac{32.17}{32.17} (51.57)(966) + \frac{2(0.006625)(51.57)(2.34)^2(1000)}{(32.17)(0.188)} \\ &= 338423 \text{ lbf/ft}^2 \\ &= 2350 \text{ psi}\end{aligned}$$

4.2 Sample problem

In a water-injection well, 1000 bbl/day of water with a specific gravity of 1.05 is injected through a 2 7/8-in., 8.6-lb_m/ft tubing in a well that is 15 degrees from vertical. The water viscosity is 1 cp. The tubing wall relative roughness is 0.001. Assuming that the pressure at the tubing shoe of 1000 ft is 2350 psia, calculate the necessary injection pressure at the tubing head.

Solution

Determine the water density:

$$\begin{aligned}\rho &= 62.4 \gamma_w \\ &= (62.4)(1.05) \\ &= 65.52 \text{ lb}_m/\text{ft}^3\end{aligned}$$

Determine the elevation increase:

$$\begin{aligned}\Delta Z &= \cos(\alpha)L \\ &= \cos(15) (-1000) \\ &= -966 \text{ ft}\end{aligned}$$

Determine the inside diameter of the tubing in ft. The 2 7/8-in., 8.6-lb_m/ft tubing has an inside diameter of 2.259 in. Therefore,

$$\begin{aligned}D &= \frac{2.259}{12} \\ &= 0.188 \text{ ft}\end{aligned}$$

Determine the fluid velocity:

$$\begin{aligned} u &= \frac{4q}{\pi D^2} \\ &= \frac{4(5.615)(1000)}{\pi(0.188)^2(86400)} \\ &= 2.34 \text{ ft/s} \end{aligned}$$

Determine the Reynolds number:

$$\begin{aligned} N_{\text{Re}} &= \frac{1.48q\rho}{d\mu} \\ &= \frac{1.48(1000)(65.52)}{(2.259)(1.0)} \\ &= 42926 > 2100, \text{ indicating turbulent flow} \end{aligned}$$

Using Chen's correlation, the Fanning friction factor can be calculated by

$$\begin{aligned} \frac{1}{\sqrt{f_F}} &= -4 \log \left\{ \frac{\varepsilon}{3.7065} - \frac{5.0452}{N_{\text{Re}}} \log \left[\frac{e^{1.1098}}{2.8257} + \left(\frac{7.149}{N_{\text{Re}}} \right)^{0.8981} \right] \right\} \\ &= 12.7454 \\ f_F &= 0.006156 \end{aligned}$$

The pressure at the tubing shoe can be calculated by

$$\begin{aligned} P_1 &= P_2 + \frac{g}{g_c} \rho \Delta z + \frac{\rho}{2g_c} \Delta u^2 + \frac{2f_F \rho u^2 L}{g_c D} \\ &= (2,350)(144) + \frac{32.17}{32.17} (65.52)(-966) + \frac{2(0.006156)(65.52)(2.34)^2(1000)}{(32.17)(0.188)} \\ &= 275838 \text{ lbf/ft}^2 \\ &= 1916 \text{ psi} \end{aligned}$$

4.3 Multiphase flow in oil wells

In addition to liquid oil, almost all oil wells produce some amount of water, gas, and occasionally sand. These wells are called multiphase oil wells, and the TPR equation for single-phase flow is not valid for them. To analyze the TPR of multiphase oil wells correctly, a multiphase flow model is required.

Multiphase flow is much more complicated than single-phase flow due to the variation of flow regime (or flow pattern). The fluid distribution changes greatly between different flow regimes, which significantly affects the pressure gradient in the tubing.

4.3.1 Flow regimes

At least five flow regimes have been identified in gas–liquid two-phase flow. They are bubble, slug, churn, annular, and mist flow. These flow regimes occur in a progression displaying increasing gas flow rate for any fixed rate of liquid flow. In bubble flow, the gas phase is dispersed in the form of small bubbles within a continuous liquid phase. In slug flow, small gas bubbles coalesce into larger bubbles that eventually fill the entire pipe cross section. Between the large bubbles are slugs of liquid that contain smaller bubbles of entrained gas. In churn flow, the larger gas bubbles become unstable and collapse, resulting in a highly turbulent flow pattern with both phases dispersed. In annular flow, gas becomes the continuous phase, with liquid flowing in an annulus coating the surface of the pipe and as droplets entrained in the gas phase. In mist flow, dispersed liquid droplets move in the continuous gas phase, forming a relatively homogeneous fluid emulsion.

4.3.2 Liquid holdup

In multiphase flow, the volume of pipe occupied by a particular phase is often different from its proportion of the total volumetric flow. This is due to density differences between phases. Gravity causes the denser phases to slip down within the upward flow—that is, the lighter phase rises faster than the denser phase. Because of this, the in-situ volume fraction of the denser phase will be greater than the input volume fraction of the denser phase; the denser phase is “held up” in the pipe relative to the lighter phase. The term liquid “holdup” is defined as

$$y_L = \frac{V_L}{V} \quad (4.7)$$

where

- y_L = liquid holdup (fractional),
- V_L = volume of liquid phase in the pipe segment (ft³), and
- V = volume of the pipe segment (ft³).

Liquid holdup depends on the flow regime, fluid properties, pipe size, and pipe configuration. Its value can only be determined experimentally.

4.3.3 TPR models

Numerous TPR models exist for analyzing multiphase flow in vertical pipes, reviewed by [Brown \(1977\)](#). TPR models for multiphase flow wells fall into two categories: homogeneous flow and separated flow. The homogeneous flow models treat multiphases as a homogeneous mixture and do not consider the effects of liquid holdup (a no-slip assumption). Therefore, these models are less accurate and are usually calibrated against local operating conditions in field applications. Their major

advantage comes from their deterministic nature. They can be constructed to describe gas–oil–water three-phase and gas–oil–water–sand four-phase systems. It is easy to code a deterministic model in computer programs.

The separated flow models are usually presented in the form of empirical correlations developed experimentally. Because they incorporate the effects of liquid holdup (slip) and flow regime automatically, these models are more realistic than the homogeneous flow models. Their major disadvantage is that it is difficult to code them in computer programs because most correlations are presented in graphic form.

4.3.3.1 Homogeneous-flow models

Numerous homogeneous flow models have been developed for analyzing the TPR of multiphase wells since the pioneering works of Poettmann and Carpenter (1952). Poettmann–Carpenter’s model uses an empirical two-phase friction factor for friction pressure-loss calculations, without considering the effect of liquid viscosity. Liquid viscosity was considered by later researchers, including Cicchitti et al. (1960) and Dukler et al. (1964), and a comprehensive review of these models is given by Hasan and Kabir (2002). Recent work addressing gas–oil–water–sand four-phase flow was presented by Guo and Ghalambor (2005).

Assuming no-slip of the liquid phase, Poettmann and Carpenter (1952) presented a simplified gas–oil–water three-phase flow model to compute pressure losses in tubing by estimating mixture density and friction factor. According to Poettmann and Carpenter, the following equation can be used to calculate the pressure profile in vertical tubing when the acceleration term is neglected:

$$\Delta p = \left(\bar{\rho} + \frac{\bar{k}}{\rho} \right) \frac{\Delta h}{144} \quad (4.8)$$

where

$$\begin{aligned} \Delta p &= \text{pressure increment (psi)}, \\ \bar{\rho} &= \text{average mixture density (specific weight) (lb/ft}^3\text{)}, \\ \Delta h &= \text{depth increment (ft)}, \end{aligned}$$

and

$$\bar{k} = \frac{f_{2F} q_o^2 M^2}{7.4137 \times 10^{10} D^5} \quad (4.9)$$

where

$$\begin{aligned} f_{2F} &= \text{Fanning friction factor for two-phase flow,} \\ q_o &= \text{oil production rate (stb/day),} \\ M &= \text{total mass associated with one stb of oil, and} \\ D &= \text{tubing inside diameter (ft).} \end{aligned}$$

The average mixture density $\bar{\rho}$ can be calculated by

$$\bar{\rho} = \frac{\rho_1 + \rho_2}{2} \quad (4.10)$$

where

ρ_1 = mixture density at top of tubing segment (lb/ft³) and
 ρ_2 = mixture density at bottom of segment (lb/ft³).

The mixture density at any given point can be calculated based on mass flow rate and volume flow rate, expressed as

$$\rho = \frac{M}{V_m} \quad (4.11)$$

where

$$M = 350.17(\gamma_o + WOR\gamma_w) + GOR\rho_{air}\gamma_g \quad (4.12)$$

and

$$V_m = 5.615(B_o + WOR B_w) + (GOR - R_s) \left(\frac{14.7}{p} \right) \left(\frac{T}{520} \right) \left(\frac{z}{1.0} \right) \quad (4.13)$$

where

γ_o = oil-specific gravity (1 for freshwater),
 WOR = producing water–oil ratio (bbl/stbv),
 γ_w = water-specific gravity (1 for freshwater),
 GOR = producing gas–oil ratio (scf/stb),
 ρ_{air} = density of air (lb_m/ft³),
 γ_g = gas-specific gravity (1 for air),
 V_m = volume of mixture associated with 1 stb of oil (ft³),
 B_o = formation volume factor of oil (rb/stb),
 B_w = formation volume factor of water (rb/bbl),
 R_s = solution gas–oil ratio (scf/stb),
 p = in situ pressure (psia),
 T = in situ temperature (°R), and
 z = gas compressibility factor at p and T .

If data from direct measurements are not available, the solution gas–oil ratio and formation volume factor of oil can be estimated using Eqs. (2.2) and (2.7), respectively:

$$R_s = \gamma_g \left[\frac{p}{18} \frac{10^{0.0125API}}{10^{0.00091t}} \right]^{1.2048} \quad (4.14)$$

$$B_o = 0.9759 + 0.00012 \left[R_s \left(\frac{\gamma_g}{\gamma_o} \right)^{0.5} + 1.25t \right]^{1.2} \quad (4.15)$$

where t is the in situ temperature in °F. The two-phase friction factor f_{2F} can be estimated graphically, as presented by Poettmann and Carpenter (1952). For easy coding in computer programs, Guo and Ghalambor (2002) developed the following correlation to approximate the chart values:

$$f_{2F} = 10^{1.444 - 2.5 \log(D\rho v)} \tag{4.16}$$

where $(D\rho v)$ is the numerator of the Reynolds number representing inertial force, expressed as

$$(D\rho v) = \frac{1.4737 \times 10^{-5} M q_o}{D} \tag{4.17}$$

Because Poettmann–Carpenter’s model takes a finite-difference form, it is only accurate for a small depth incremental (Δh). For deep wells, therefore, this model should be used in a piecewise manner for accurate results. The tubing string should be divided into segments and the model applied separately to each segment.

Because iterations are required to solve Eq. (4.8) for pressure, a computer spreadsheet program **Poettmann-CarpenterBHP.xls** has been developed and is included in this book.

4.3 Sample problem

For the following given data, calculate the tubing shoe pressure:

Tubing head pressure:	500	Psia
Tubing head temperature:	100	°F
Tubing inside diameter:	1.66	In.
Tubing shoe depth:	5000	ft
Temperature at tubing shoe:	150	°F
Liquid production rate:	2000	stb/day
Water cut:	25	%
Producing gas–liquid ratio:	1000	scf/stb
Oil gravity:	30	°API
Water-specific gravity:	1.05	1 for freshwater
Gas-specific gravity:	0.65	1 for air

Solution

This problem may be solved using spreadsheet program **Poettmann-CarpenterBHP.xls**, as shown in Tables 4.1.

The gas–oil–water–sand four-phase flow model developed by Guo and Ghalambor (2005) assumes no-slip of the denser phases, but takes a closed (integrated) form, which makes it easy to use. It is expressed as follows:

$$144b(p_{ust} - p_{dst}) + \frac{1 - 2bM}{2} \ln \left| \frac{(144p_{ust} + M)^2 + N}{(144p_{dst} + M)^2 + N} \right| - \frac{M + \frac{b}{c}N - bM^2}{\sqrt{N}} \tag{4.18}$$

$$\left[\tan^{-1} \left(\frac{144p_{ust} + M}{\sqrt{N}} \right) - \tan^{-1} \left(\frac{144p_{dst} + M}{\sqrt{N}} \right) \right]$$

$$= a(\cos \theta + d^2 e)L$$

Table 4.1 Results given by spreadsheet program **Poettmann-CarpenterBHP.xls** for [Sample Problem 4.3](#)

Poettman-CarpenterBHP.xls		
Description: This spreadsheet calculates flowing bottom-hole pressure based on tubing head pressure and tubing flow performance using Poettmann–Carpenter method.		
Instruction: (1) Select a unit system; (2) Update parameter values in the “Input Data” section; (3) Click “Solution” button; and (4) View result in the Solution section.		
Input Data:	US field units	
Tubing ID:	1.66	in
Wellhead pressure:	500	psia
Liquid production rate:	2000	stb/d
Producing gas–liquid ratio:	1000	scf/stb
Water cut (WC):	25	%
Oil gravity:	30	°API
Water-specific gravity:	1.05	Freshwater = 1
Gas-specific gravity:	0.65	1 for air
N ₂ content in gas:	0	Mole fraction
CO ₂ content in gas:	0	Mole fraction
H ₂ S content in gas:	0	Mole fraction
Formation volume factor for water:	1.2	rb/stb
Wellhead temperature:	100	°F
Tubing shoe depth:	5000	ft
Bottom-hole temperature:	150	°F
Solution:		
Oil-specific gravity	0.88	Freshwater = 1
Mass associated with 1 stb of oil	495.66	lb
Solution gas ratio at wellhead	78.42	scf/stb
Oil formation volume factor at wellhead	1.04	rb/stb
Volume associated with 1 stb oil at wellhead	45.12	cf
Fluid density at wellhead	10.99	lb/cf
Solution gas–oil ratio at bottom hole =	301.79	scf/stb
Oil formation volume factor at bottom hole =	1.16	rb/stb
Volume associated with 1 stb oil at bottom hole	17.66	cf
Fluid density at bottom hole	28.07	lb/cf
The average fluid density	19.53	lb/cf
Inertial force ($D\rho v$)	79.21	lb/day-ft
Friction factor	0.002	
Friction term	293.12	(lb/cf) ²
Error in depth	0.00	ft
Bottom-hole pressure	1699	psia

where p_{ust} and p_{dst} are the upstream and downstream pressures, respectively, and group parameters are defined as

$$a = \frac{0.0765\gamma_g q_g + 350\gamma_o q_o + 350\gamma_w q_w + 62.4\gamma_s q_s}{4.07T_{av}q_g} \quad (4.19)$$

$$b = \frac{5.615q_o + 5.615q_w + q_s}{4.07T_{av}q_g} \quad (4.20)$$

$$c = 0.00678 \frac{T_{av}q_g}{A} \quad (4.21)$$

$$d = \frac{0.00166}{A} (5.615q_o + 5.615q_w + q_s) \quad (4.22)$$

$$e = \frac{f_M}{2gD_H} \quad (4.23)$$

$$M = \frac{cde}{\cos \theta + d^2e} \quad (4.24)$$

$$N = \frac{c^2e \cos \theta}{(\cos \theta + d^2e)^2} \quad (4.25)$$

where

A = cross-sectional area of conduit (ft²),

D_H = hydraulic diameter (ft),

f_M = Darcy–Wiesbach friction factor (Moody factor),

g = gravitational acceleration (32.17 ft/s²),

L = conduit length (ft),

p = pressure (psia),

p_{hf} = wellhead flowing pressure (psia),

q_g = gas production rate (scf/d),

q_o = oil production rate (bbl/d),

q_s = sand production rate (ft³/day),

q_w = water production rate (bbl/d),

T_{av} = average temperature (°R),

γ_g = specific gravity of gas (air = 1),

γ_o = specific gravity of produced oil (freshwater = 1),

γ_s = specific gravity of produced solid (freshwater = 1), and

γ_w = specific gravity of produced water (freshwater = 1).

The Darcy–Wiesbach friction factor (f_M) can be obtained graphically, as in Fig. 4.2, or by calculating the Fanning friction factor (f_F), obtained from Eq. (4.16). The required relation is $f_M = 4 f_F$.

Because iterations are required to solve Eq. (4.18) for pressure, Guo and Ghalambor developed a computer spreadsheet program, **Guo-GhalamborBHP.xls**.

4.4 Sample problem

From the data given below, estimate the bottom-hole pressure using the Guo–Ghalambor method.

Total measured depth:	7000	ft
The average inclination angle:	20	deg
Tubing inside diameter:	1.995	in
Gas production rate:	1	MMscfd
Gas-specific gravity:	0.7	Air = 1
Oil production rate:	1000	stb/d
Oil-specific gravity:	0.85	H ₂ O = 1
Water production rate:	300	bb/d
Water-specific gravity:	1.05	H ₂ O = 1
Solid production rate:	1	ft ³ /d
Solid-specific gravity:	2.65	H ₂ O = 1
Tubing head temperature:	100	°F
Bottom-hole temperature:	224	°F
Tubing head pressure:	300	psia

Solution

This sample problem is solved with the spreadsheet program **Guo-GhalamborBHP.xls**. The result is shown in [Tables 4.2](#).

Table 4.2 Results given by spreadsheet program **Guo-GhalamborBHP.xls** for [Sample Problem 4.4](#)

Guo-GhalamborBHP.xls		
Description: This spreadsheet calculates flowing bottom-hole pressure based on tubing head pressure and tubing flow performance using Guo–Ghalambor method.		
Instruction: (1) Select a unit system; (2) Update parameter values in the “Input Data” section; (3) Click “Solution” button; and (4) View result in the Solution section.		
Input Data:	US field units	
Total measured depth:	7000	ft
Average inclination angle:	20	deg
Tubing ID:	1.995	in
Gas production rate:	1,000,000	scfd
Gas-specific gravity:	0.7	Air = 1
Oil production rate:	1000	stb/d
Oil-specific gravity:	0.85	H ₂ O = 1
Water production rate:	300	bb/d
Water-specific gravity:	1.05	H ₂ O = 1
Solid production rate:	1	ft ³ /d
Solid-specific gravity:	2.65	H ₂ O = 1
Tubing head temperature:	100	°F
Bottom-hole temperature:	224	°F
Tubing head pressure:	300	psia

Table 4.2 Results given by spreadsheet program **Guo-GhalamborBHP.xls** for **Sample Problem 4.4—cont'd**

Guo-GhalamborBHP.xls		
Solution:		
A	3.1243196	in ²
D	0.16625	ft
T _{av}	622	°R
cos (θ)	0.9397014	
(Dρv)	40.908853	
f _M	0.0415505	
a	0.0001713	
b	2.884E-06	
c	1,349,785.1	
d	3.8942921	
e	0.0041337	
M	20,447.044	
N	6.669E+09	
Bottom-hole pressure, p _{wf}	1682	psia

4.3.3.2 Separated-flow models

Many models for separated flow are available for TPR calculations, including the [Lockhart–Martinelli correlation \(1949\)](#), [Duns–Ros Correlation \(1963\)](#), and [Hagedorn–Brown method \(1965\)](#). Based on comprehensive comparisons, [Ansari et al. \(1994\)](#) and [Hasan and Kabir \(2002\)](#) recommended using the Hagedorn–Brown method with adjustments for near vertical flow.

The modified Hagedorn–Brown method (mH-B) is an empirical correlation based on the original work of [Hagedorn and Brown \(1965\)](#). The recommended modifications to it include assuming zero no-slip liquid holdup whenever the original correlation predicts a liquid holdup value less than the no-slip holdup, and using the Griffith correlation ([Griffith and Wallis, 1961](#)) for the bubble flow regime.

The original Hagedorn–Brown correlation takes the following form:

$$\frac{dP}{dz} = \frac{g}{g_c} \bar{\rho} + \frac{2f_F \bar{\rho} u_m^2}{g_c D} + \bar{\rho} \frac{\Delta(u_m^2)}{2g_c \Delta z} \quad (4.26)$$

Expressed in US field units as

$$144 \frac{dp}{dz} = \bar{\rho} + \frac{f_F M_t^2}{7.413 \times 10^{10} D^5 \bar{\rho}} + \bar{\rho} \frac{\Delta(u_m^2)}{2g_c \Delta z} \quad (4.27)$$

where

M_t = total mass flow rate (lb_m/d),
 $\bar{\rho}$ = in-situ average density (lb_m/ft³),
 u_m = mixture velocity (ft/s),

and

$$\bar{\rho} = y_L \rho_L + (1 - y_L) \rho_G \quad (4.28)$$

$$u_m = u_{SL} + u_{SG} \quad (4.29)$$

where

ρ_L = liquid density (lb_m/ft³),
 ρ_G = in situ gas density (lb_m/ft³),
 u_{SL} = superficial velocity of liquid phase (ft/s), and
 u_{SG} = superficial velocity of gas phase (ft/s).

The superficial velocity of a given phase is defined as the volumetric flow rate of the phase divided by the pipe cross-sectional area. The third term in the right-hand side of Eq. (4.27) represents pressure change due to the change in kinetic energy, which is usually negligible for oil wells.

Obviously, determining the value for liquid holdup y_L is essential in calculating pressures. The mH-B correlation determines liquid holdup from three charts, using the following dimensionless numbers:

Liquid velocity number, N_{vL} :

$$N_{vL} = 1.938 u_{SL}^4 \sqrt{\frac{\rho_L}{\sigma}} \quad (4.30)$$

Gas velocity number, N_{vG} :

$$N_{vG} = 1.938 u_{SG}^4 \sqrt{\frac{\rho_L}{\sigma}} \quad (4.31)$$

Pipe diameter number, N_D :

$$N_D = 120.872 D \sqrt{\frac{\rho_L}{\sigma}} \quad (4.32)$$

Liquid viscosity number, N_L :

$$N_L = 0.15726 \mu_L^4 \sqrt{\frac{1}{\rho_L \sigma^3}} \quad (4.33)$$

where

D = conduit inside diameter (ft),
 σ = liquid-gas interfacial tension (dyne/cm), and
 μ_L = liquid viscosity (cp).

The first chart is used for determining parameter (CN_L) based on N_L . Guo et al. (2007) found that this chart can be replaced by the following correlation with acceptable accuracy:

$$(CN_L) = 10^Y \quad (4.34)$$

where

$$Y = -2.69851 + 0.15841X_1 - 0.55100X_1^2 + 0.54785X_1^3 - 0.12195X_1^4 \quad (4.35)$$

and

$$X_1 = \log(N_L) + 3 \quad (4.36)$$

Once the value of (CN_L) is determined, it can be used to calculate the value of the ratio:

$$\frac{N_{vL}P^{0.1}(CN_L)}{N_{vG}^{0.575}p_a^{0.1}N_D}$$

where p is the absolute pressure at the location where pressure gradient is to be calculated and p_a is atmospheric pressure. The value of this ratio can then be used as an entry in the second chart to determine (y_L/ψ).

Guo et al. (2007) found that the second chart can be represented by the following correlation with acceptable accuracy:

$$\begin{aligned} \left(\frac{y_L}{\psi}\right) = & -0.10307 + 0.61777[\log(X_2) + 6] - 0.63295[\log(X_2) + 6]^2 \\ & + 0.29598[\log(X_2) + 6]^3 - 0.0401[\log(X_2) + 6]^4 \end{aligned} \quad (4.37)$$

where

$$X_2 = \frac{N_{vL}P^{0.1}(CN_L)}{N_{vG}^{0.575}p_a^{0.1}N_D} \quad (4.38)$$

According to Hagedorn and Brown (1965), the value of parameter ϕ can be determined from the third chart, using a value for the ratio:

$$\frac{N_{vG}N_L^{0.38}}{N_D^{2.14}}$$

Guo et al. (2007) found that where

$$\frac{N_{vG}N_L^{0.38}}{N_D^{2.14}} > 0.01$$

the third chart can be replaced by the following correlation with acceptable accuracy:

$$\psi = 0.91163 - 4.82176X_3 + 1232.25X_3^2 - 22253.6X_3^3 + 116174.3X_3^4 \quad (4.39)$$

where

$$X_3 = \frac{N_{vG} N_L^{0.38}}{N_D^{2.14}} \quad (4.40)$$

However, $\psi = 1.0$ should be used if

$$\frac{N_{vG} N_L^{0.38}}{N_D^{2.14}} \leq 0.01$$

Finally, the liquid holdup can be calculated by

$$y_L = \psi \left(\frac{y_L}{\psi} \right) \quad (4.41)$$

The Fanning friction factor in Eq. (4.27) can be determined using either Chen's correlation Eq. (4.5) or Eq. (4.16). The appropriate Reynolds number for multiphase flow can be calculated by

$$N_{Re} = \frac{2.2 \times 10^{-2} m_t}{D \mu_L^{y_L} \mu_G^{(1-y_L)}} \quad (4.42)$$

where m_t is mass flow rate. The modified Hagedorn–Brown method (mH-B) uses the Griffith correlation for the bubble flow regime, which exists where

$$\lambda_G < L_B \quad (4.43)$$

where

$$\lambda_G = \frac{u_{sG}}{u_m} \quad (4.44)$$

and

$$L_B = 1.071 - 0.2218 \left(\frac{u_m^2}{D} \right) \quad (4.45)$$

which is valid for $L_B \geq 0.13$. When the L_B value given by Eq. (4.45) is less than 0.13, $L_B = 0.13$ should be used.

Neglecting the kinetic energy pressure drop term, the Griffith correlation in US field units may be expressed as

$$144 \frac{dp}{dz} = \bar{p} + \frac{f_F m_L^2}{7.413 \times 10^{10} D^5 \rho_L y_L^2} \quad (4.46)$$

where m_L is the mass flow rate of the liquid phase. The liquid holdup in Griffith correlation is given by the following expression:

$$y_L = 1 - \frac{1}{2} \left[1 + \frac{u_m}{u_s} - \sqrt{\left(1 + \frac{u_m}{u_s} \right)^2 - 4 \frac{u_{sG}}{u_s}} \right] \quad (4.47)$$

where $u_s = 0.8$ ft/s. The Reynolds number used to obtain the friction factor is based on the in situ average liquid velocity, expressed as

$$N_{Re} = \frac{2.2 \times 10^{-2} m_L}{D \mu_L} \tag{4.48}$$

To simplify calculations, the Hagedorn–Brown correlation has been coded in the spreadsheet program **HagedornBrownCorrelation.xls**.

4.5 Sample problem

From the data given below, calculate and graph the pressure profile in the tubing string:

Tubing shoe depth:	9700	ft
Tubing inside diameter:	1.995	in
Oil gravity:	40	°API
Oil viscosity:	5	cp
Production gas–liquid ratio:	75	scf/bbl
Gas-specific gravity:	0.7	Air = 1
Flowing tubing head pressure:	100	psia
Flowing tubing head temperature:	80	°F
Flowing temperature at tubing shoe:	180	°F
Liquid production rate:	758	stb/day
Water cut:	10	%
Interfacial tension:	30	dynes/cm
Specific gravity of water:	1.05	H ₂ O = 1

Solution

This sample problem can be solved with the spreadsheet program **HagedornBrownCorrelation.xls**, as shown in [Tables 4.3](#) and [Fig. 4.3](#).

Table 4.3 Result given by spreadsheet program **HagedornBrownCorrelation.xls** for Sample Problem 4.5

HagedornBrownCorrelation.xls		
Description:	This spreadsheet calculates flowing pressures in a single-diameter tubing string based on tubing head pressure using Hagedorn–Brown correlation.	
Instruction:	(1) Select a unit system; (2) Update parameter values in the “Input Data” section; (3) Click “Solution” button; and (4) View result in the Solution section and charts.	
Input Data:	US field units	
Depth (D):	9700	ft
Tubing inner diameter (d_i):	1.995	in
Oil gravity (API):	40	°API
Oil viscosity (μ_o):	5	cp
Production gas–liquid ratio:	75	scf/bbl
Gas-specific gravity (γ_g):	0.7	Air = 1
Flowing tubing head pressure (p_{ht}):	100	psia

Continued

Table 4.3 Result given by spreadsheet program **HagedornBrownCorrelation.xls** for Sample Problem 4.5—*cont'd*

HagedornBrownCorrelation.xls		
Flowing tubing head temperature (t_{ht}):	80	°F
Flowing temperature at tubing shoe (t_{wt}):	180	°F
Liquid production rate (q_L):	758	stb/day
Water cut (WC):	10	%
Interfacial tension (σ):	30	dynes/cm
Specific gravity of water (γ_w):	1.05	H ₂ O = 1

Solution:

Depth (ft)	Pressure		
	(m)	(psia)	(MPa)
0	0	100	0.68
334	102	183	1.24
669	204	269	1.83
1003	306	358	2.43
1338	408	449	3.06
1672	510	543	3.69
2007	612	638	4.34
2341	714	736	5.01
2676	816	835	5.68
3010	918	936	6.37
3345	1020	1038	7.06
3679	1122	1141	7.76
4014	1224	1246	8.48
4348	1326	1352	9.20
4683	1428	1459	9.93
5017	1530	1567	10.66
5352	1632	1676	11.40
5686	1734	1786	12.15
6021	1836	1897	12.90
6355	1938	2008	13.66
6690	2040	2121	14.43
7024	2142	2234	15.19
7359	2243	2347	15.97
7693	2345	2461	16.74
8028	2447	2576	17.52
8362	2549	2691	18.31
8697	2651	2807	19.10
9031	2753	2923	19.89
9366	2855	3040	20.68
9700	2957	3157	21.48

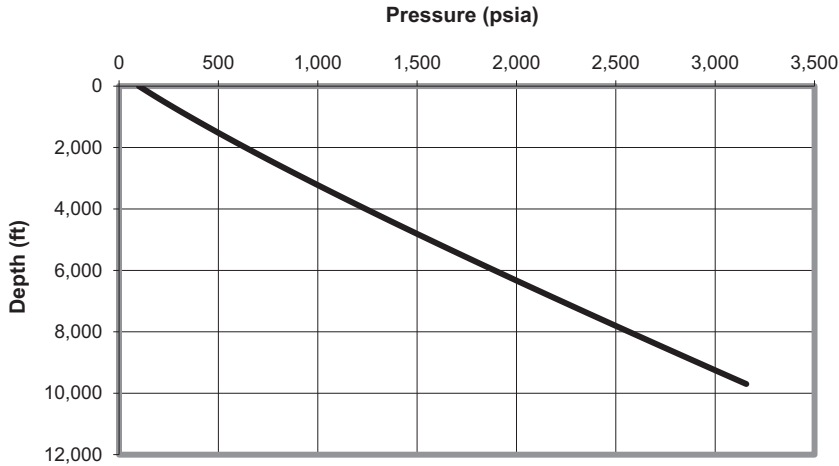


FIGURE 4.3

Pressure profile given by the spreadsheet program HagedornBrownCorrelation.xls for Sample Problem 4.5.

4.4 Single-phase gas flow

The First Law of Thermodynamics (the conservation of energy) governs gas flow in tubing. The effects of kinetic energy changes are usually negligible because the variation in tubing diameter is insignificant in most gas wells. If no shaft work device is installed along the tubing string, the First Law of Thermodynamics yields the following mechanical balance equation:

$$\frac{dP}{\rho} + \frac{g}{g_c} dZ + \frac{f_M v^2 dL}{2g_c D_i} = 0 \quad (4.49)$$

Because $dZ = \cos\theta dL$, $\rho = \frac{29\gamma_g P}{zRT}$, and $v = \frac{4q_{sc} z P_{sc} T}{\pi D_i^2 T_{sc} P}$, Equation can be rewritten as (Eq. 4.49)

$$\frac{zRT}{29\gamma_g} \frac{dP}{P} + \left\{ \frac{g}{g_c} \cos\theta + \frac{8f_M Q_{sc}^2 P_{sc}^2}{\pi^2 g_c D_i^5 T_{sc}^2} \left[\frac{zT}{P} \right]^2 \right\} dL = 0 \quad (4.50)$$

which is an ordinary differential equation governing gas flow in tubing. Although the temperature T can be approximated as a linear function of length L through the geothermal gradient, the compressibility factor z is a function of pressure P and temperature T . This makes it difficult to solve the equation analytically. Fortunately, the pressure P at length L is not strongly affected by the temperature and the compressibility factor, and the petroleum industry has developed approximate solutions to Eq. (4.50).

4.4.1 Average temperature and compressibility factor method

If we assume that the average values of temperature and compressibility factor can be obtained, Eq. (4.50) becomes

$$\frac{\bar{z}R\bar{T}}{29\gamma_g} \frac{dP}{P} + \left\{ \frac{g}{g_c} \cos \theta + \frac{8f_M Q_{cs}^2 P_{sc}^2 \bar{z}^2 \bar{T}^2}{\pi^2 g_c D_i^5 T_{sc}^2 P^2} \right\} dL = 0 \quad (4.51)$$

By separating the variables, Eq. (4.51) can be integrated over the full length of a single-diameter tubing to yield

$$P_1^2 = \text{Exp}(s) P_2^2 + \frac{8f_M [\text{Exp}(s) - 1] Q_{cs}^2 P_{sc}^2 \bar{z}^2 \bar{T}^2}{\pi^2 g_c D_i^5 T_{sc}^2 \cos \theta} \quad (4.52)$$

where

$$s = \frac{58\gamma_g g L \cos \theta}{g_c R \bar{z} \bar{T}} \quad (4.53)$$

Eqs. (4.52) and (4.53) take the following forms when US field units (q_{sc} in Mscf/d) are used (Katz et al., 1959):

$$p_1^2 = \text{Exp}(s) p_2^2 + \frac{6.67 \times 10^{-4} [\text{Exp}(s) - 1] f_M q_{sc}^2 \bar{z}^2 \bar{T}^2}{d_i^5 \cos \theta} \quad (4.54)$$

where

$$s = \frac{0.0375\gamma_g L \cos \theta}{\bar{z} \bar{T}} \quad (4.55)$$

For downward flow in gas-injection wells, Eq. (4.54) takes the following form:

$$p_2^2 = \text{Exp}(-s) \left[p_1^2 + \frac{6.67 \times 10^{-4} [\text{Exp}(s) - 1] f_M q_{sc}^2 \bar{z}^2 \bar{T}^2}{d_i^5 \cos \theta} \right] \quad (4.56)$$

The Darcy–Wiesbach (Moody) friction factor f_M can be determined in the conventional manner for a given tubing diameter, wall roughness, and Reynolds number. However, if one assumes fully turbulent flow, which is the case for most gas wells, then a simple empirical relation may be used for typical tubing strings instead (Katz and Lee, 1990):

$$f_M = \frac{0.01750}{d_i^{0.224}} \quad \text{for } d_i \leq 4.277 \text{ in} \quad (4.57)$$

$$f_M = \frac{0.01603}{d_i^{0.164}} \quad \text{for } d_i > 4.277 \text{ in} \quad (4.58)$$

Guo (2001) used the following Nikuradse (1933) friction factor correlation for fully turbulent flow in rough pipes:

$$f_M = \left[\frac{1}{1.74 - 2 \log \left(\frac{2\delta}{d_i} \right)} \right]^2 \quad (4.59)$$

Because the average compressibility factor is itself a function of pressure, a numerical technique such as the Newton–Raphson iteration is required to solve Eq. (4.54) for bottom-hole pressure. This computation can be performed automatically with the spreadsheet program **AverageTZ.xls**.

4.6 Sample problem

Suppose a vertical well produces 2 MMscf/d of 0.71 gas-specific gravity gas through a 2 7/8-in tubing set into the top of a gas reservoir at a depth of 10,000 ft. At the tubing head, the pressure is 800 psia and the temperature is 150°F. The bottom-hole temperature is 200°F. The relative roughness of tubing is about 0.0006. Calculate the pressure profile along the tubing length and plot the results.

Solution

This sample problem may be solved with the spreadsheet program **AverageTZ.xls**, as shown in Tables 4.4. This table shows the data input and result sections. The calculated pressure profile is illustrated in Fig. 4.4.

Table 4.4 Spreadsheet program **AverageTZ.xls**—Data input and result sections.

AverageTZ.xls		
Description: This spreadsheet calculates tubing pressure traverse for gas wells.		
Instructions:		
Step 1: Input your data in the “Input Data” section.		
Step 2: Click “Solution” button to get results.		
Step 3: View results in table and in graph sheet “Profile.”		
Input Data:		
γ_g	0.71	
d	2.259	in
ϵ/d	0.0006	
L	10,000	ft
θ	0	Deg
P_{hf}	800	psia
T_{hf}	150	°F
T_{wf}	200	°F
Q_{sc}	2000	Mscf/d

Continued

Table 4.4 Spreadsheet program **AverageTZ.xls**—Data input and result sections.—*cont'd*

AverageTZ.xls			
Solution:			
$f_M = 0.017396984$			
Depth (ft)	T(°R)	p(psia)	Z _{av}
0	610	800	0.9028
1000	615	827	0.9028
2000	620	854	0.9027
3000	625	881	0.9027
4000	630	909	0.9026
5000	635	937	0.9026
6000	640	965	0.9026
7000	645	994	0.9026
8000	650	1023	0.9027
9000	655	1053	0.9027
10,000	660	1082	0.9028

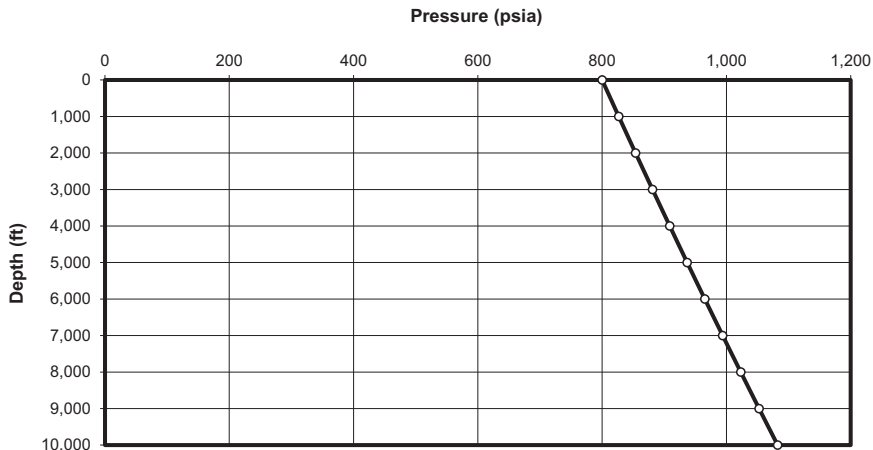


FIGURE 4.4
Calculated tubing pressure profile for [Sample Problem 4.6](#).

4.4.2 Cullender and Smith method

Eq. (4.50) can be solved for bottom pipe pressure using a quick numerical method originally developed by Cullender and Smith (Katz et al., 1959) by rearranging it as

$$\frac{\frac{P}{zT} dp}{\frac{g}{g_c} \cos \theta \left(\frac{P}{zT}\right)^2 + \frac{8f_M Q_{sc}^2 P_{sc}^2}{\pi^2 g_c D_i^5 T_{sc}^2}} = -\frac{29\gamma_g dL}{R} \quad (4.60)$$

That takes an integral form of

$$\int_{P_{wf}}^{P_{nj}} \left[\frac{\frac{P}{zT}}{\frac{g}{g_c} \cos \theta \left(\frac{P}{zT} \right)^2 + \frac{8f_M Q_{sc}^2 P_{sc}^2}{\pi^2 g_c D_i^5 T_{sc}^2}} \right] dp = \frac{29\gamma_g L}{R} \quad (4.61)$$

In US field units (q_{msc} in MMscf/d), Eq. (4.61) takes the following form:

$$\int_{p_2}^{p_1} \left[\frac{\frac{p}{zT}}{0.001 \cos \theta \left(\frac{p}{zT} \right)^2 + 0.6666 \frac{f_M q_{msc}^2}{d_i^5}} \right] dp = 18.75\gamma_g L \quad (4.62)$$

If the integrant is denoted with symbol I , that is,

$$I = \frac{\frac{p}{zT}}{0.001 \cos \theta \left(\frac{p}{zT} \right)^2 + 0.6666 \frac{f_M q_{sc}^2}{d_i^5}} \quad (4.63)$$

Eq. (4.62) becomes

$$\int_{p_2}^{p_1} I dp = 18.75\gamma_g L \quad (4.64)$$

Integrating Eq. (4.64) results in

$$\frac{(p_m - p_2)(I_m + I_2)}{2} + \frac{(p_1 - p_m)(I_1 + I_m)}{2} = 18.75\gamma_g L \quad (4.65)$$

where p_m is the pressure at well mid-depth. The I_2 , I_m , and I_1 are integrant I 's evaluated at p_2 , p_m , and p_1 , respectively. Assuming the first and second terms in the right-hand side of Eq. (4.65) each represent half of the integration, that is,

$$\frac{(p_m - p_2)(I_m + I_2)}{2} = \frac{18.75\gamma_g L}{2} \quad (4.66)$$

$$\frac{(p_1 - p_m)(I_1 + I_m)}{2} = \frac{18.75\gamma_g L}{2} \quad (4.67)$$

The following expressions are obtained:

$$p_m = p_2 + \frac{18.75\gamma_g L}{I_m + I_2} \quad (4.68)$$

$$p_1 = p_m + \frac{18.75\gamma_g L}{I_1 + I_m} \quad (4.69)$$

Because I_m itself is a function of pressure p_m , a numerical technique such as the Newton–Raphson iteration is required to solve Eq. (4.68) for p_m . Once p_m is obtained, p_w can then be calculated from Eq. (4.69). These computations can be performed automatically using the spreadsheet program **Cullender-Smith.xls**.

4.7 Sample problem

Solve the problem in [Sample Problem 4.6](#) using the Cullender and Smith method.

Solution

This sample problem can be solved using the spreadsheet program **Cullender-Smith.xls**. [Table 4.5](#) shows the data input and result sections. The pressures at depths of 5000 ft and 10,000 ft are 937 psia and 1082 psia, respectively. These results are exactly the same as that given by the **AverageTZ.xls**.

Table 4.5 Spreadsheet program **Cullender-Smith.xls**—data input and result sections.

Cullender-SmithBHP.xls					
Description: This spreadsheet calculates bottom-hole pressure with Cullender–Smith method.					
Instructions:					
Step 1: Input your data in the “Input Data” section.					
Step 2: Click “Solution” button to get results.					
Input Data:					
γ_g		0.71			
d		2.259	in		
e/d		0.0006			
L		10,000	ft		
θ		0	Deg		
p_{hf}		800	psia		
T_{hf}		150	°F		
T_{wif}		200	°F		
q_{msc}		2	MMscf/d		
Solution:					
$f_M = 0.017397$					
Depth (ft)	T (°R)	p (psia)	Z	p/ZT	I
0	610	800	0.9028	1.45263	501.137
5000	635	937	0.9032	1.63324	472.581
10,000	660	1082	0.9057	1.80971	445.349

4.5 Mist flow in gas wells

In addition to dry gas, almost all gas wells produce a certain amount of liquids, consisting of formation water and/or gas condensate (light oil). Depending on pressure and temperature, gas condensate may not be seen at the surface in some wells, but it exists in the wellbore. Some gas wells also produce sand and coal particles. All of these wells are called multiphase gas wells. Guo and Ghalambor's (2005) four-phase flow model presented in Section 4.3.3.1 can be applied to mist flow in gas wells. Its applications in liquid loading analysis will be shown in Chapter 5.

4.6 Summary

This chapter presented and illustrated different mathematical models for describing wellbore/tubing performance. Among many models, the modified Hagedorn–Brown (mHB) model has been found to give results with satisfactory accuracy for multiphase flow. Industry practice is to conduct flow gradient (FG) surveys to measure the actual flowing pressures along the tubing string. The FG data are then employed to validate one of the models and to tune the model, if necessary, before use in field applications.

4.7 Problems

- 4.1** Suppose that 1200 bbl/day of 18 °API, 5 cp oil is being produced through 2 7/8-in., 8.6-lb_m/ft tubing in a well that is 3 degrees from vertical. If the tubing wall roughness is 0.003-in., assuming no free gas in tubing string, calculate the pressure drop over a 2000 ft of tubing.
- 4.2** For the following given data, calculate bottom-hole pressure using Poettmann–Carpenter method:

Tubing head pressure:	400 psia
Tubing head temperature:	120°F
Tubing inside diameter:	1.66 in
Tubing shoe depth (near bottom hole):	8200 ft
Bottom-hole temperature:	170°F
Liquid production rate:	2200 stb/day
Water cut:	32%
Producing gas–liquid ratio:	820 scf/stb
Oil gravity:	42 °API
Water-specific gravity:	1.05 1 for freshwater
Gas-specific gravity:	0.72 1 for air

- 4.3** From the data given below, estimate bottom-hole pressure with Guo–Ghalambor method:

Total measured depth:	8200 ft
The average inclination angle:	3 deg
Tubing inside diameter	1.995 in
Gas production rate:	0.5 MMscfd
Gas-specific gravity:	0.75 air = 1
Oil production rate:	2500 stb/d
Oil-specific gravity:	0.82 H ₂ O = 1
Water production rate:	550 bbl/d
Water-specific gravity:	1.05 H ₂ O = 1
Solid production rate:	3 ft ³ /d
Solid-specific gravity:	2.67 H ₂ O = 1
Tubing head temperature:	100°F
Bottom-hole temperature:	175°F
Tubing head pressure:	550 psia

- 4.4** From the data given below, calculate and plot pressure profile in the tubing string using Hagedorn–Brown correlation:

Tubing shoe depth:	6200 ft
Tubing inside diameter:	1.995 in
Oil gravity:	30 ° API
Oil viscosity:	2 cp
Production gas–liquid ratio:	550 scf/bbl
Gas-specific gravity:	0.75 air = 1
Flowing tubing head pressure:	120 psia
Flowing tubing head temperature:	80°F
Flowing temperature at tubing shoe:	142 F
Liquid production rate:	1520 stb/day
Water cut:	30%
Interfacial tension:	30 dyn/cm
Specific gravity of water:	1.05 H ₂ O = 1

- 4.5** Suppose 3 MMscf/d of 0.70 specific gravity gas is produced through a 3 1/2-in tubing string set to the top of a gas reservoir at a depth of 8300 ft. At tubing head, the pressure is 1200 psia and the temperature is 125°F; the bottom-hole temperature is 185°F. The roughness of tubing is about 0.002-in. Calculate the flowing bottom-hole pressure with three methods: (1) the average temperature and compressibility factor method; (2) the Cullender and Smith method; and (3) the four-phase flow method. Make comments on your results.
- 4.6** Solve problem 4.5 for gas production through a K-55, 17 lb/ft, 5 1/2-in casing.

- 4.7** Suppose 2 MMscf/d of 0.7 specific gravity gas is produced through a 2 7/8-in (2.259-in ID) tubing string set to the top of a gas reservoir at a depth of 5200 ft. Tubing head pressure is 400 psia and the temperature is 100°F; the bottom-hole temperature is 155°F. The roughness of tubing is about 0.002 in. Calculate the flowing bottom pressure with the average temperature and compressibility factor method.

References

- Ansari, A.M., et al., May 1994. A comprehensive mechanistic model for upward two-phase flow in wellbores. In: *SPE Production and Facilities*, vol. 143, p. 297. Trans., AIME.
- Brown, K.E., 1977. *The Technology of Artificial Lift Methods*, vol. 1. PennWell Books, Tulsa, OK, pp. 104–158.
- Chen, N.H., 1979. An explicit equation for friction factor in pipe. *Industrial & Engineering Chemistry Fundamentals* 18, 296.
- Cicchitti, A., et al., 1960. Two-phase cooling experiments—pressure drop, heat transfer and burnout measurements. *Energia Nucleare* 7 (6), 407.
- Dukler, A.E., Wicks, M., Cleveland, R.G., 1964. Frictional pressure drop in two-phase flow: a comparison of existing correlations for pressure loss and hold-up. *AIChE Journal* 38–42.
- Duns, H., Ros, N.C.J., 1963. Vertical flow of gas and liquid mixtures in wells. In: *Proceedings of the 6th World Petroleum Congress*, Tokyo, p. 451.
- Guo, B., January 1, 2001. An Analytical Model for Gas-Water-Coal Particle Flow in Coalbed-Methane Production Wells. Society of Petroleum Engineers. <https://doi.org/10.2118/72369-MS>.
- Guo, B., Ghalambor, A., 2002. Gas Volume Requirements for Underbalanced Drilling Deviated Holes. PennWell Corporation, Tulsa, OK, pp. 132–133.
- Guo, B., Ghalambor, A., 2005. *Natural Gas Engineering Handbook*. Gulf Publishing Company, Houston, pp. 59–61.
- Guo, B., Lyons, W.C., Ghalambor, A., 2007. *Petroleum Production Engineering*. Elsevier, Amsterdam, pp. 52–53.
- Gregory, G.A., Fogarasi, M., April 1, 1985. Alternate to standard friction factor equation. *Oil & Gas Journal* 120–127.
- Griffith, P., Wallis, G.B., August 1961. Two-phase slug flow. *Journal of Heat Transfer* 83, 307–320. Trans. ASME, Ser. C.
- Hagedorn, A.R., Brown, K.E., April 1965. Experimental study of pressure gradients occurring during continuous two-phase flow in small-diameter conduits. *Journal of Petroleum Technology* 234, 475–484. Trans. AIME.
- Hasan, A.R., Kabir, C.S., 2002. *Fluid Flow and Heat Transfer in Wellbores*. Society of Petroleum Engineers, Richardson, Texas, pp. 10–15.
- Katz, D.L., Cornell, D., Kobayashi, R., Poettmann, F.H., Vary, J.A., Elenbaas, J.R., Weinaug, C.F., 1959. *Handbook of Natural Gas Engineering*. McGraw-Hill Publishing Company, New York.
- Katz, D.L., Lee, R.L., 1990. *Natural Gas Engineering—Production and Storage*. McGraw-Hill Publishing Company, New York.

- Lockhart, R.W., Martinelli, R.C., 1949. Proposed correlation of data for isothermal two-phase, two-component flow in pipes. *Chemical Engineering Progress* 39.
- Nikuradse, J., October 1933. A new correlation for friction factor. *Forschungshelb* 301–307.
- Poettmann, F.H., Carpenter, P.G., 1952. The multiphase flow of gas, oil, and water through vertical strings. *API Dril. and Prod. Prac.* 257–263.

Further reading

- Goier, G.W., Aziz, K., 1977. *The Flow of Complex Mixtures in Pipes*. Robert E. Drieger Publishing Co., Huntington, New York.

Productivity of wells with simple trajectories

Chapter outline

5.1 Introduction	123
5.2 Principles of well productivity analysis	124
5.3 Deliverability of vertical wells	124
5.3.1 Oil wells in volumetric reservoirs.....	125
5.3.1.1 <i>Transient production</i>	125
5.3.1.2 <i>Pseudo–steady-State Production</i>	127
5.3.1.3 <i>Steady-state production</i>	129
5.3.2 Oil wells in water-/gas-coning reservoirs.....	130
5.3.3 Gas wells in volumetric reservoirs	132
5.3.3.1 <i>Transient production</i>	132
5.3.3.2 <i>Pseudo–steady-State Production</i>	134
5.3.4 Liquid loading in gas wells	136
5.3.4.1 <i>Turner’s method</i>	136
5.3.4.2 <i>Guo’s method</i>	138
5.4 Deliverability of fractured wells	142
5.4.1 Single-fractured oil wells.....	142
5.4.2 Single-fractured gas wells	144
5.5 Deliverability of horizontal wells	145
5.5.1 Oil wells in volumetric reservoirs.....	145
5.5.2 Oil wells in water-/gas-coning reservoirs.....	147
5.5.3 Gas wells in volumetric reservoirs	152
5.6 Summary	154
5.7 Problems	154
References	160
Further reading	161

5.1 Introduction

Well productivity is defined as the deliverability of the well, rather than reservoir, although the latter affects the former. Well deliverability is determined by the combination of well inflow performance described in Chapter 3 and the wellbore flow performance described in Chapter 4. While the former describes reservoir

deliverability, the latter introduces the resistance to flow by the production string. This chapter focuses on the prediction of achievable fluid production rates from various types of reservoirs with given production string characteristics. This technique is called NODAL analysis (a Schlumberger patent). Calculation examples are illustrated using computer spreadsheets.

5.2 Principles of well productivity analysis

Fluid properties change with the location-dependent pressure and temperature in oil and gas production systems. To simulate the fluid flow in a particular system, it is necessary to “break” the system into discrete elements (equipment sections) by nodes. Fluid properties in the elements are then evaluated locally. In petroleum engineering, the techniques for predicting oil and gas production rates and pressure at a specified node are called NODAL analysis.

NODAL analysis is performed on the principle of pressure continuity, i.e., there is only one pressure value at any given node no matter what pressures are indicated by the performance of upstream or downstream equipment. For a given node, the pressure—flow rate relationship for upstream equipment is called the inflow performance relationship (IPR). The relationship for downstream equipment is called the outflow performance relationship (OPR). The equations representing IPR and OPR can be solved mathematically or graphically and yield the operating flow rate and pressure at the specified node.

Although NODAL analysis can be performed using any point in the system as a solution node, it is usually conducted using bottom-hole or the wellhead as the solution node. This is because measured pressure data are normally available for these two points and these data can be used to validate the result of the analysis. This chapter illustrates the principle of NODAL analysis using bottom-hole as the solution node for predicting well productivity. Thus the IPR reflects the flow performance of reservoir from the reservoir boundary to bottom-hole and the OPR reflects the flow performance of the wellbore (tubing) from the bottom-hole to the wellhead (TPR).

5.3 Deliverability of vertical wells

The term *vertical well* in this section is defined as a wellbore penetrating nearly vertically into a nearly horizontal, nonhydraulically fractured pay zone. For multi-layer reservoirs, a composite IPR should be used. All IPR models used in this chapter were presented in Chapter 3.

5.3.1 Oil wells in volumetric reservoirs

A volumetric reservoir is a reservoir surrounded by no-flow boundaries in all directions. As discussed in Chapter 3, the IPR of a vertical well can be described on the basis of flow pattern, that is, transient, steady-state, or pseudo-steady-state flow.

5.3.1.1 Transient production

During the transient production period, as determined using Eq. (3.7) for a theoretical circular boundary, Eq. (3.2) can be used to construct the IPR curve, and the modified Hagedorn–Brown (mHB) correlation described in Chapter 4 can be used to construct the TPR curve. The intersection of these two curves defines the operating point.

5.1 Sample problem

From the data given below, assuming the tubing string is set directly above the pay zone, predict the transient production rate after 30 days:

Reservoir porosity (ϕ):	0.2	
Effective horizontal permeability (k):	10	md
Pay zone thickness (h):	50	ft
Reservoir pressure (p_i):	5500	psia
Oil formation volume factor (B_o):	1.2	rb/stb
Total reservoir compressibility (c_t):	0.000013	psi ⁻¹
Wellbore radius (r_w):	0.328	ft
Skin factor (S):	0	
Well depth (H):	10000	ft
Tubing inner diameter (d):	2.441	in
Oil gravity (API):	30	API
Oil viscosity (μ_o):	1.5	cp
Producing gas–liquid ratio (GLR):	300	scf/bbl
Gas-specific gravity (γ_g):	0.7	Air = 1
Flowing tubing head pressure (p_{hf}):	800	psia
Flowing tubing head temperature (t_{hf}):	150	°F
Flowing temperature at tubing shoe (t_{wf}):	180	°F
Water cut (WC):	10	%
Oil–gas interfacial tension (σ):	30	dynes/cm
Specific gravity of water (γ_w):	1.05	

Solution

This sample problem can be solved using the spreadsheet program **Transient Production Forecast.xls**. [Table 5.1](#) presents calculated data. [Fig. 5.1](#) shows the calculated IPR and TPR curves, which indicate an expected oil production rate of 640 stb/day at a flowing bottom-hole pressure of 2870 psia.

Table 5.1 Data given by the spreadsheet program **Transient Production Forecast.xls**.

q (stb/d)	p _{wf} (psia)	
	Inflow performance relationship	Tubing performance relationship
134	4950	2343
268	4400	2560
402	3850	2702
537	3300	2811
671	2750	2902
805	2200	2982
939	1650	3054
1073	1100	3120
1207	550	3182
1341	0	3241

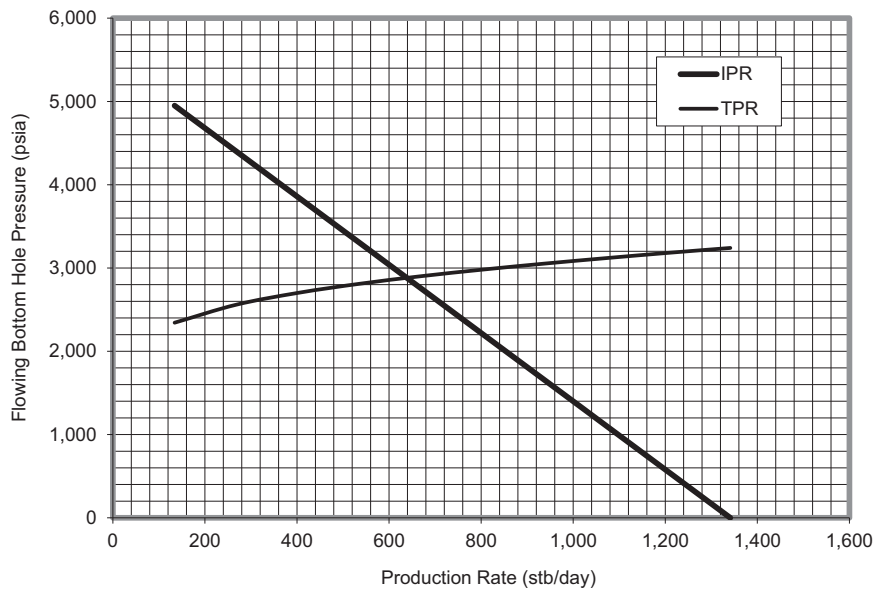


FIGURE 5.1

Inflow performance relationship (IPR) and tubing performance relationship (TPR) curves given by the spreadsheet program **Transient Production Forecast.xls**.

5.3.1.2 Pseudo—steady-State Production

During the pseudo—steady-state production period as determined using Eq. (3.7) for a theoretical circular boundary, Eq. (3.8) can be used to construct the IPR curve, and the mHB correlation, to construct the TPR curve. The intersection of the two curves then defines the operating point.

5.2 Sample problem

From the data given below, assuming the tubing string is set just above the pay zone, predict the pseudo—steady-state production rate:

Initial oil bubble-point pressure (p_b):	4500	psia
Effective horizontal permeability (k):	10	md
Pay zone thickness (h):	50	ft
Average reservoir pressure ($p_{\text{-bar}}$):	2500	Psia
Oil formation volume factor (B_o):	1.2	rb/stb
Well drainage area (A):	320	acres
Wellbore radius (r_w):	0.328	ft
Skin factor (S):	0	
Well depth (H):	8000	Ft
Tubing inner diameter (d):	2.441	in
Oil gravity (API):	30	API
Oil viscosity (μ_o):	1.5	cp
Producing gas—liquid ratio (GLR):	440	scf/bbl
Gas-specific gravity (γ_g):	0.7	Air = 1
Flowing tubing head pressure (p_{hf}):	800	psia
Flowing tubing head temperature (t_{hf}):	150	°F
Flowing temperature at tubing shoe (t_{wf}):	180	°F
Water cut (WC):	10	%
Oil—gas interfacial tension (σ):	30	dynes/cm
Specific gravity of water (γ_w):	1.05	
Shape factor for drainage area (C_A):	31.6	

Solution

This sample problem can be solved using the spreadsheet program **Pseudosteady-2Phase Production Forecast.xls**. Table 5.2 summarizes some calculated data. Fig. 5.2 presents the calculated IPR and TPR curves, which indicate a predicted oil production rate of 136 stb/day at a flowing bottom-hole pressure of 1890 psia.

Table 5.2 Data generated by the spreadsheet program **Pseudosteady-2Phase Production Forecast.xls**.

q (stb/d)	p_{wf} (psia)	
	Inflow performance relationship	Tubing performance relationship
34	2358	1650
68	2207	1752
102	2047	1823
136	1875	1878
170	1688	1924
204	1483	1963
239	1250	1998
273	976	2030
307	625	2058
341	0	2085

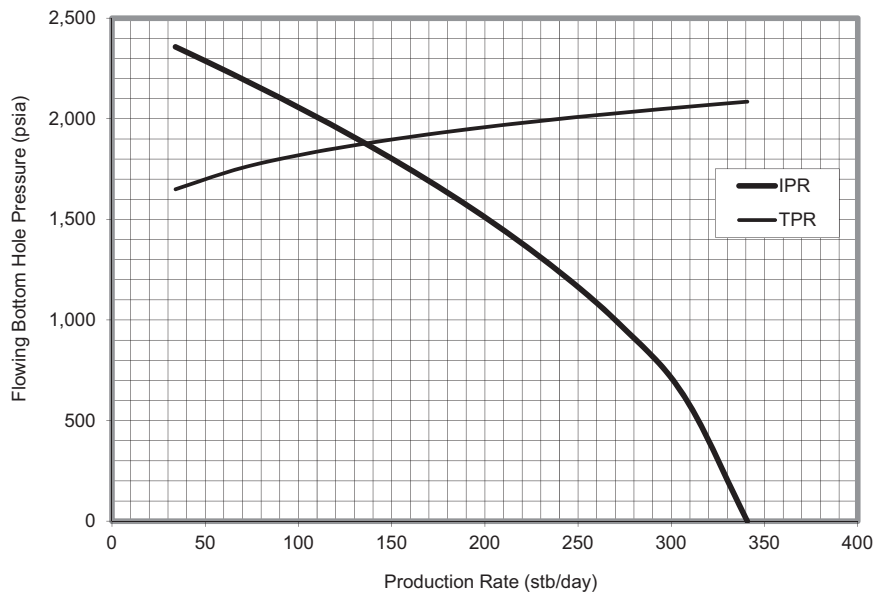


FIGURE 5.2

Inflow performance relationship (IPR) and tubing performance relationship (TPR) curves given by the spreadsheet program Pseudosteady-2Phase Production Forecast.xls.

5.3.1.3 Steady-state production

Steady-state production occurs after a constant-pressure boundary is reached. Eq. (3.5) can be used to construct the IPR curve, and the mHB correlation can be used to construct the TPR curve. The intersection of the two curves then defines the operating point.

5.3 Sample problem

From the data given below, assuming the tubing string is set just above the pay zone, predict the steady-state production rate:

Initial oil bubble-point pressure (p_b):	4000	psia
Effective horizontal permeability (k):	50	md
Pay zone thickness (h):	50	ft
Boundary reservoir pressure (p_e):	4000	psia
Oil formation volume factor (B_o):	1.2	rb/stb
Well drainage area (A):	640	acres
Wellbore radius (r_w):	0.328	ft
Skin factor (S):	0	
Well depth (H):	7000	ft
Tubing inner diameter (d):	2.441	in
Oil gravity (API):	40	API
Oil viscosity (μ_o):	1.5	cp
Producing gas–liquid ratio (GLR):	500	scf/bbl
Gas-specific gravity (γ_g):	0.7	Air = 1
Flowing tubing head pressure (p_{hf}):	1000	psia
Flowing tubing head temperature (t_{hf}):	120	°F
Flowing temperature at tubing shoe (t_{wf}):	170	°F
Water cut (WC):	10	%
Oil–gas interfacial tension (σ):	30	dynes/cm
Specific gravity of water (γ_w):	1.05	

Solution

This sample problem can be solved using the spreadsheet program **Steady-2Phase Production Forecast.xls**. Table 5.3 shows some calculated data. Fig. 5.3 presents the calculated IPR and TPR curves, which indicate an operating oil production rate of 1350 stb/day at a flowing bottom-hole pressure of 2500 psia.

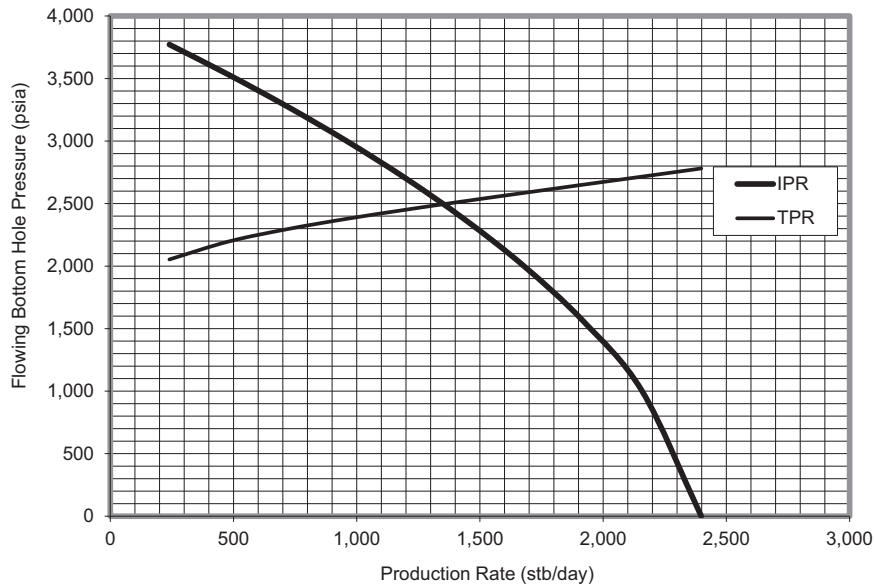
Table 5.3 Data given by the spreadsheet program **Steady-2Phase Production Forecast.xls**.

q(stb/d)	p_{wf} (psia)	
	Inflow performance relationship	Tubing performance relationship
240	3772	2053
480	3531	2196
719	3275	2296
959	3000	2378
1199	2702	2451

Continued

Table 5.3 Data given by the spreadsheet program **Steady-2Phase Production Forecast.xls**.—*cont'd*

q(stb/d)	p_{wf} (psia)	
	Inflow performance relationship	Tubing performance relationship
1439	2372	2520
1679	2000	2586
1919	1562	2651
2158	1000	2716
2398	0	2781

**FIGURE 5.3**

Inflow performance relationship (IPR) and tubing performance relationship (TPR) curves given by the spreadsheet program *Steady-2Phase Production Forecast.xls*.

5.3.2 Oil wells in water-/gas-coning reservoirs

In some reservoirs, oil production rate is limited by water or gas coning. Water breakthrough from the water cone is a result of excessive production drawdown. Reducing the oil production rate can minimize the problem of dealing with large amounts of produced water.

Excess gas production from a gas zone overlaying an oil pay zone can occur due to premature gas breakthrough from the gas cone, also due to excessive production

drawdown. In order to avoid dealing with a large amount of produced gas, and to maintain reservoir pressure, the oil production rate should be reduced to lower levels.

There are a number of methods for predicting the maximum water-free and gas-free production rates (critical rates), including Craft-Hawkins (1959), Schols (1972), Meyer-Gardner-Pirson (1977), Chaperon (1986), Joshi (1988), Hoyland-Papatzacos-Skjaeveland (1989), and Guo-Lee (1992).

The Chaperon, Hoyland-Papatzacos-Skjaeveland, and Guo-Lee methods take into account the effects of vertical permeability on the critical rates, with the Chaperon method giving the most optimistic value of critical rate.

The Chaperon method uses the following equation to predict the critical oil production rate:

$$q_o = 4.888 \times 10^{-4} \frac{k_H h^2 \Delta \rho}{B_o \mu_o} q_c^* \quad (5.1)$$

where

- q_o = critical oil rate (STB/day),
- k_H = horizontal permeability (md),
- h = oil column thickness (ft),
- B_o = oil formation volume factor (rb/STB),
- μ_o = oil viscosity (cp),
- Δ_r = density difference (gm/cc),

and

$$q_c^* = 0.7311 + 1.9434 \alpha'' \quad (5.2)$$

$$\alpha'' = \frac{r_e}{h} \sqrt{\frac{k_v}{k_H}} \quad (5.3)$$

5.4 Sample problem

Calculate the anticipated critical oil production rate using the following data:

Oil column thickness:	80	ft
Horizontal permeability:	70	md
Vertical permeability:	7	md
Oil viscosity:	0.42	cp
Oil density:	0.7	gm/cc
Oil formation volume factor:	1.1	rb/STB
Water or gas density:	1.05	gm/cc
Drainage area:	160	acres

Solution

This problem can be solved using the spreadsheet program **Chaperon Critical Oil Rate.xls**. The result is 176 stb/day.

5.3.3 Gas wells in volumetric reservoirs

Most gas reservoirs are volumetric. As discussed in Chapter 3, the IPR of a vertical gas well depends on whether the flow pattern is transient or pseudo-steady-state.

5.3.3.1 Transient production

During the transient production period, Eq. (3.10) should be used for IPR analysis. Due to the complexity of real-gas pseudo-pressure computations, however, more simplified IPR equations are frequently employed. At pressures lower than 2000 psia, the pseudo-pressure is proportional to the square of the pressure. The following equation is often adopted:

$$q_g = \frac{kh(p_i^2 - p_{wf}^2)}{1638\bar{\mu}_g\bar{z}T \left(\log t + \log \frac{k}{\phi\bar{\mu}_g c_t r_w^2} - 3.23 + 0.87S \right)} \quad (5.4)$$

At pressures greater than 3000 psia, the pseudo-pressure is proportional to pressure. The following equation is often utilized:

$$q_g = \frac{kh(p_i - p_{wf})}{141.2 \times 10^3 \bar{B}_g \bar{\mu}_g \left(\log t + \log \frac{k}{\phi\bar{\mu}_g c_t r_w^2} - 3.23 + 0.87S \right)} \quad (5.5)$$

Because Eq. (5.4) yields a more conservative production rate than Eq. (5.5), use of the former is recommended for pressures between 2000 psia and 3000 psia.

Eq. (4.54) is frequently used for TPR analysis of dry gas wells. Eq. (4.18) can be used for TPR analysis of gas condensate wells and gas wells producing water and/or solids.

5.5 Sample problem

From the data given below, assuming the tubing string is set just above the pay zone, predict the transient production rate of gas after 30 days:

Reservoir permeability (k):	20	md
Pay zone thickness (h):	5	ft
Well skin factor (S):	10	
Porosity (ϕ):	0.2	
Wellbore radius (r_w):	0.328	ft
Gas-specific gravity (γ_g):	0.65	
Gas viscosity (μ_g):	0.01	cp

Tubing inside diameter (D):	3.5	in
Tubing relative roughness (ϵ/D):	0.0006	
Measured depth at tubing shoe (L):	5000	ft
Inclination angle (θ):	0	deg
Wellhead pressure (p_{hf}):	500	psia
Wellhead temperature (T_{hf}):	150	$^{\circ}$ F
Bottom-hole temperature (T_{wf}):	200	$^{\circ}$ F
Initial reservoir pressure (p_i):	2000	psia

Solution

This problem can be solved using the spreadsheet program **Dry Gas Transient Production Forecast.xls**. Table 5.4 shows some calculated data, and Fig. 5.4 illustrates the calculated IPR and TPR curves, which indicate an operating gas production rate of 2371 Mscf/day at a flowing bottom-hole pressure of 565 psia.

Table 5.4 Data given by the spreadsheet program **Dry Gas Production Forecast.xls**.

q_{sc} (Mscf/d)	Inflow performance relationship	Tubing performance relationship
0	2000	556
258	1897	557
515	1789	557
773	1673	557
1031	1549	558
1289	1414	559
1546	1265	560
1804	1095	561
2062	894	563
2319	632	565
2448	447	566
2513	316	566
2545	224	566
2577	0	567
Operating flow rate	2371	Mscf/d
Residual of objective function	3.86463E-05	
Operating pressure	565	psia

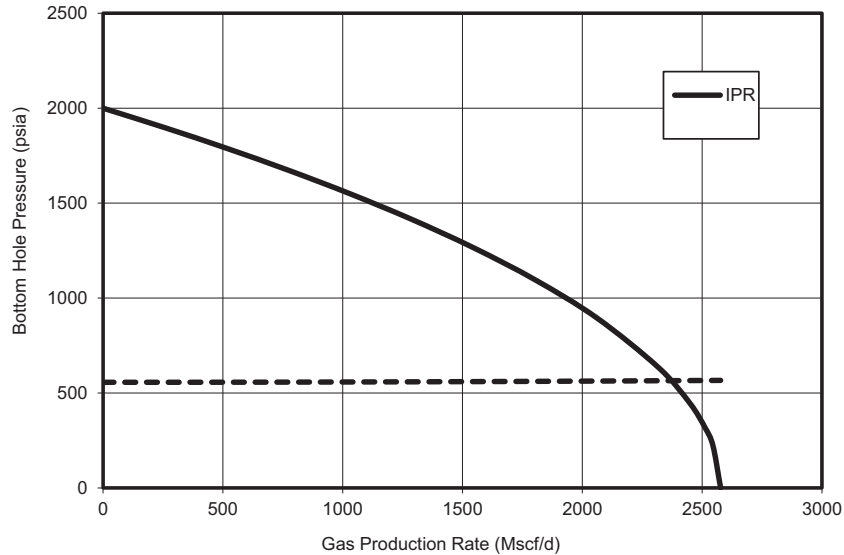


FIGURE 5.4

Inflow performance relationship (IPR) and tubing performance relationship (TPR) curves given by the spreadsheet program Dry Gas Transient Production Forecast.xls.

5.3.3.2 Pseudo—steady-State Production

During the pseudo—steady-state production period as determined by using Eq. (4.7) for a theoretical circular boundary, the appropriate IPR equation is Eq. (4.10). Again, due to the difficulty of pseudo-pressure computations, more simplified IPR equations are frequently used. At pressures lower than 2000 psia, the following equation is often employed:

$$q_g = \frac{kh(\bar{p}^2 - p_{wf}^2)}{1424\bar{\mu}_g\bar{z}T \left(\ln \frac{r_e}{r_w} - \frac{3}{4} + S + Dq_g \right)} \quad (5.6)$$

At pressures higher than 3000 psia, the following equation is often utilized instead:

$$q_g = \frac{kh(\bar{p} - p_{wf})}{141.2 \times 10^3 \bar{B}_g \bar{\mu}_g T \left(\ln \frac{r_e}{r_w} - \frac{3}{4} + S + Dq_g \right)} \quad (5.7)$$

Because Eq. (5.6) gives a more conservative production rate than Eq. (5.7), use of the former is recommended for pressures between 2000 psia and 3000 psia.

Again, Eq. (4.54) is used for the TPR analysis of dry gas wells, and Eq. (4.18) can be used for TPR analysis of gas condensate wells and gas wells producing water and/or solids.

5.6 Sample problem

From the data given below, assuming the tubing string is set just above the pay zone, predict the pseudo-steady gas production rate:

Pay zone thickness:	78	ft
Permeability:	0.17	md
Wellbore radius:	0.328	ft
Darcy skin factor:	5	
Non-Darcy skin coefficient:	0.001	Mscf/day
Reservoir pressure:	4613	psia
Total measured depth:	7000	ft
Average inclination angle:	5	deg
Tubing ID:	1.995	in
Gas-specific gravity:	0.65	Air = 1
Gas viscosity:	0.022	cp
Gas z-factor:	0.958	
Oil production rate:	5	stb/day
Oil-specific gravity:	0.85	H ₂ O = 1
Water cut:	10	%
Water-specific gravity:	1.05	H ₂ O = 1
Solid production rate:	1	ft ³ /d
Solid-specific gravity:	2.65	H ₂ O = 1
Tubing head temperature:	100	°F
Bottom-hole temperature:	180	°F
Tubing head pressure:	1000	psia
Drainage area:	320	acres
Wall roughness:	0.01	in

Solution

This problem can be solved using the spreadsheet program **Wet Gas Pseudosteady Production Forecast.xls**. **Table 5.5** shows some calculated data, which indicates an operating gas production rate of 980 Mscf/day at a flowing bottom-hole pressure of 1189 psia.

Table 5.5 Data given by the spreadsheet program **Wet Gas Pseudosteady Production Forecast.xls**.

A	3.1243196	in ²
D	0.16625	ft
T _{av}	600	°R
cos(θ)	0.9961953	
δ/D	0.0100251	
f ¹ M	0.0303742	
a	2.114E-05	
b	1.346E-08	

Continued

Table 5.5 Data given by the spreadsheet program **Wet Gas Pseudosteady Production Forecast.xls**.—*cont'd*

c	1,275,763.4	
d	0.0171734	
e	0.0028505	
M	62.690286	
N	4.657E+09	
Gas production rate, q	980	Mscf/d
Bottom-hole pressure, p_{wf}	1189	psia

5.3.4 Liquid loading in gas wells

Most gas wells produce wet gas, that is, natural gas carrying condensate and/or liquid water in the form of mist flow. As the gas flow velocity in the well decreases because of reservoir pressure depletion, the carrying capacity of the gas also decreases. When the gas velocity drops to a critical level, liquids begin to accumulate and undergo annular flow and slug flow in the tubing. This accumulation of liquids (liquid loading) increases the bottom-hole pressure and further reduces the gas production rate. The low-gas production rate will in turn cause gas velocity to drop further. Eventually, the well will experience a bubbly flow regime and cease producing.

The liquid loading problem can be solved by using various measures. Artificially foaming the liquid water can enable the gas to lift the water from the well. Using narrower tubing or ensuring a lower wellhead pressure can sometimes maintain adequate mist flow. The well can also be unloaded by gas lifting or by pumping the liquids out of the well. Heating the wellbore can prevent liquid condensation. Down-hole injection of water into an underlying disposal zone is yet another option.

Liquid loading is not always obvious, and recognizing the problem is not an easy task. A thorough diagnostic analysis of well data needs to be performed. The signs to look for include the following:

- Onset of liquid slugs at the surface of the well
- Increasing differential between tubing and casing pressures over time
- Sharp gradient changes on a flowing pressure survey
- Sudden decreases in a production decline curve

Two methods for predicting liquid loading are presented in this section.

5.3.4.1 Turner's method

Turner et al. (1969) pioneered work in analyzing and predicting the minimum gas flow rate that can still prevent liquid loading. They presented two mathematical models describing the liquid loading problem: the film movement model and the entrained droplet movement model. Based on analyses of field data, they concluded that their film movement model did not represent the controlling liquid transport mechanism.

Turner et al.'s entrained drop movement model was derived from the terminal settling velocity of liquid droplets and the maximum droplet diameter corresponding to the critical Weber number of 30. Turner et al.'s terminal slip velocity equation is expressed in US field units as

$$v_{sl} = \frac{1.3\sigma^{1/4}(\rho_L - \rho_g)^{1/4}}{C_d^{1/4} \rho_g^{1/2}} \quad (5.8)$$

According to Turner et al.'s theory, gas will continuously remove liquids from the well until its velocity drops to below the terminal slip velocity. The minimum gas flow rate (in MMcf/D) for a particular pressure and conduit geometry can be calculated using Eqs. (5.8) and (5.9):

$$Q_{gs/MM} = \frac{3.06 p v_{sl} A}{T_z} \quad (5.9)$$

Turner et al. compared their model with actual field data and showed that it underestimated the required gas flow rate. They recommended adjusting the equation-derived values upward by approximately 20% to ensure removal of all droplets. Turner et al. believed that the discrepancy in their model could be attributed to the use of drag coefficients for solid spheres, an assumption of stagnation velocity, and that the critical Weber number was established for droplets falling in air, not in compressed natural gas.

The main problem complicating the use of Turner et al.'s entrained droplet model in gas wells comes from the difficulty of estimating fluid density and pressure accurately. Using an average value for gas-specific gravity (0.6) and gas temperature (120°F), Turner et al. derived an estimate of gas density in lbm/ft³ as 0.0031 times the pressure in psi. However, they did not present a method for calculating the gas pressure in mist flow.

Turner et al.'s entrained droplet movement model was later modified by other researchers. Coleman et al. (1991) suggested using Eq. (5.8) with a lower value of coefficient instead of 1.3. Nosseir et al. (2000) expanded Turner et al.'s entrained droplet model to more than one-flow regimes. Lea and Nickens (2004) made corrections to Turner et al.'s simplified equations. However, the drawbacks of Turner et al.'s original approach neglected transport velocity and multiphase flow pressure still remain unsolved by these later investigators.

5.7 Sample problem

From the data given below, assuming the tubing string is set just above the pay zone, predict the minimum gas production rate that can prevent liquid loading:

Gas-specific gravity (γ_g):	0.6	
Tubing diameter (d):	2.441	in
Tubing shoe pressure (p_{wf}):	530	psia
Tubing shoe temperature (T_{wf}):	116	°F
Liquid density (ρ_l):	67.4	lbm/ft ³
Interfacial tension (σ):	60	dynes/cm

Table 5.6 Result given by the spreadsheet program **TurnerLoading.xls**.

T	576.00	°R
ρ_g	1.49	lbm/ft ³
A	0.0325	ft ²
ρ_{pc}	672.50	psia
T_{pc}	358.50	°R
T_{av}	576.00	°R
ρ_{av}	530.00	psia
ρ_{pr}	0.79	
T_{pr}	1.61	
Z	0.94	
V_{gm}	10.37	ft/s
Q_{gm}	1004	Mscf/d

Solution

This problem can be solved using the spreadsheet program **TurnerLoading.xls**. **Table 5.6** shows some calculated data which indicates the minimum required gas production rate of 1004 Mscf/d.

5.3.4.2 Guo's method

Building on Turner et al.'s entrained droplet model, [Guo et al. \(2006\)](#) determined the minimum kinetic energy of gas required to lift liquids. Applying the minimum kinetic energy criterion to the mist-flow model (see Chapter 4) results in a closed-form analytical equation that can be used to predict the minimum gas flow rate.

Kinetic energy per unit volume of gas can be expressed as

$$E_k = \frac{\rho_g v_g^2}{2g_c} \quad (5.10)$$

Substituting [Eq. \(5.8\)](#) into [Eq. \(5.10\)](#) gives an expression for the minimum kinetic energy required to keep liquid droplets in suspension in the gas:

$$E_{ksl} = 0.026 \sqrt{\frac{\sigma(\rho_L - \rho_g)}{C_d}} \quad (5.11)$$

If the value of the drag coefficient $C_d = 0.44$ recommended by Turner et al. is used, and the effects of gas density are neglected (a conservative assumption), [Eq. \(5.11\)](#) then becomes

$$E_{ksl} = 0.04 \sqrt{\sigma \rho_L} \quad (5.12)$$

In gas wells that produce formation water, typical values for the water–gas interfacial tension and the water density are 60 dynes/cm and 65 lb_m/ft³, respectively. This yields the minimum kinetic energy value of 2.5 lb_f-ft/ft³. In gas wells that

also produce condensate, typical values for the condensate–gas interfacial tension and condensate density are 20 dynes/cm and 45 lb_m/ft³, respectively. This yields the minimum kinetic energy value of 1.2 lb_f-ft/ft³. These results imply that the required minimum gas production rate in water-producing gas wells must be approximately twice that of condensate-producing gas wells.

The minimum gas velocity required for transporting the liquid droplets upward is equal to the minimum gas velocity required for floating the liquid droplets (keeping the droplets in suspension) plus the transport velocity of the droplets, expressed as

$$v_{gm} = v_{sl} + v_{tr} \quad (5.13)$$

The transport velocity v_{tr} may be calculated from estimates of the liquid production rate, conduit geometry, and the liquid volume fraction and is difficult to quantify. Instead of attempting to formulate an expression for the transport velocity v_{tr} , Guo et al. used v_{tr} as an empirical constant to combine the effects of nonstagnation velocity, drag coefficients for solid spheres, and the critical Weber number as established for droplets falling in air. On the basis of Turner et al.'s work, Guo et al. took the value of v_{tr} to be 20% of v_{sl} . Use of this value results in

$$v_{gm} \approx 1.2v_{sl} \quad (5.14)$$

Substituting Eqs. (5.8) and (5.14) into Eq. (5.10) gives the expression for the minimum kinetic energy required for transporting the liquid droplets as

$$E_{km} = 0.0576\sqrt{\sigma\rho_L} \quad (5.15)$$

For typical gas wells producing water, this equation yields a minimum kinetic energy value of 3.6 lb_f-ft/ft³. For typical gas wells producing condensate, this equation results in a minimum kinetic energy value of 1.73 lb_f-ft/ft³. Again, these figures imply that the required minimum gas production rate in water-producing gas wells is approximately twice that of condensate-producing gas wells.

In order to evaluate the gas kinetic energy E_k in Eq. (5.10) at a given gas flow rate and compare it with the minimum required kinetic energy E_{km} in Eq. (5.15), the values of gas density ρ_g and gas velocity v_g need to be determined. Expressions for ρ_g and v_g can be obtained from the ideal gas law:

$$\rho_g = \frac{2.7S_g p}{T} \quad (5.16)$$

$$v_g = 4.71 \times 10^{-2} \frac{TQ_G}{A_i p} \quad (5.17)$$

Substituting Eqs. (5.16) and (5.17) into Eq. (5.10) yields

$$E_k = 9.3 \times 10^{-5} \frac{S_g T Q_G^2}{A_i^2 p} \quad (5.18)$$

Eq. (5.18) indicates that gas kinetic energy decreases with increased pressure. Therefore, the controlling conditions are those at bottom-hole, where the gas has

the highest pressure and lowest kinetic energy. This analysis is consistent with observations from air-drilling operations, during which solid particles accumulate at bottom-hole rather than at the wellhead. However, this contradicts Turner et al.'s results, which indicated that the controlling conditions are generally at the wellhead.

Under the minimum unloaded condition (the last point of the mist-flow regime), Eq. (5.18) becomes

$$E_{km} = 9.3 \times 10^{-5} \frac{S_g T_{bh} Q_{gm}^2}{A_i^2 p} \quad (5.19)$$

which gives

$$p = 9.3 \times 10^{-5} \frac{S_g T_{bh} Q_{gm}^2}{A_i^2 E_{km}} \quad (5.20)$$

Substituting Eq. (5.20) into the mist-flow model of Eq. (5.18) results in

$$144b\alpha_1 + \frac{1 - 2bM}{2} \ln \alpha_2 - \frac{M + \frac{b}{c}N - bM^2}{\sqrt{N}} [\tan^{-1} \beta_1 - \tan^{-1} \beta_2] = \gamma \quad (5.21)$$

where

$$\alpha_1 = 9.3 \times 10^{-5} \frac{S_g T_{bh} Q_{gm}^2}{A_i^2 E_{km}} - p_{hf} \quad (5.22)$$

$$\alpha_2 = \frac{\left(1.34 \times 10^{-2} \frac{S_g T_{bh} Q_{gm}^2}{A_i^2 E_{km}} + M \right)^2}{(144p_{hf} + M)^2 + N} + N \quad (5.23)$$

$$\beta_1 = \frac{1.34 \times 10^{-2} \frac{S_g T_{bh} Q_{gm}^2}{A_i^2 E_{km}} + M}{\sqrt{N}} \quad (5.24)$$

$$\beta_2 = \frac{144p_{hf} + M}{\sqrt{N}} \quad (5.25)$$

$$\gamma = a(1 + d^2 e)L \quad (5.26)$$

All parameters should be evaluated at Q_{gm} . The minimum required gas flow rate Q_{gm} can be determined from Eq. (5.26) using trial and error or numerical methods such as the Bisection method. It can be shown that Eq. (5.26) is a one-to-one function of Q_{gm} for Q_{gm} values greater than zero. Therefore, the Newton–Raphson iteration technique can also be used to determine Q_{gm} . Commercial software packages such as MS Excel with the Goal Seek function programmed in can be used to generate solutions. One such is the spreadsheet program **GasWellLoading.xls**.

5.8 Sample problem

From the data given below, assuming a single-size tubing string is set just above the pay zone, use Guo's method to predict the minimum gas production rate that will prevent liquid loading:

Gas-specific gravity:	0.6	Air = 1
Hole inclination:	0	deg
Tubing shoe depth:	5555	ft
Wellhead pressure:	444	psi
Wellhead temperature:	60	°F
Producing zone temperature:	116	°F
Condensate gravity:	71	API
Condensate make:	1	bbl/MMscf
Water-specific gravity:	1.08	water = 1
Water make:	50	bbl/MMscf
Solid-specific gravity:	2.65	water = 1
Solid make:	0	ft ³ /MMscf
Conduit OD:	2.441	in
Conduit ID:	0	in
Conduit wall roughness:	0.000015	in
Liquid density:	67.4	lb/ft ³
Liquid-gas interfacial tension:	60	dyne/cm

Solution

This problem can be solved using the spreadsheet program **GasWellLoading.xls**. Table 5.7 shows some calculated data which indicates that a minimum gas production rate of 1178 Mscf/d is required. Comparing this and Turner's result (1004 Mscf/d in Sample Problem 5.7) indicates that the Turner method may underestimate the minimum gas flow rate by 17.4%.

Table 5.7 Results given by the spreadsheet program **GasWellLoading.xls**.

Hydraulic diameter:	0.2034	ft
Conduit cross-sectional area:	0.0325	ft ²
Average temperature:	547.775	°R
Minimum kinetic energy:	3.6627	lbf-ft/ft ³
a	2.91508E-05	
b	1.2839E-07	
c	936,406.3493	
d	0.1202439	
e	0.000571676	
f	0.007481992	
M	64.36851023	
N	501,269,364.5	
Critical gas production rate	1178	Mscf/day
Pressure at tubing shoe	530	psia

5.4 Deliverability of fractured wells

The deliverability of hydraulically fractured wells is determined by their individual fracture characteristics. This section addresses productivity of wells with a single fracture. The productivity of wells completed with multiple fractures is discussed in Chapter 7.

5.4.1 Single-fractured oil wells

For steady-state production of a single-fractured oil well, Eq. (3.12) can be used to predict the production index and construct an IPR curve. For pseudo—steady-state production, Eq. (3.18) can be employed. The mHB correlation can be used to construct the TPR curve. The intersection of the two curves defines the operating point.

5.9 Sample problem

From the data given below, assuming that tubing string is set just above the pay zone, predict the pseudo—steady-state production rate:

Fracture half length (x_f):	600	ft
Fracture permeability (k_f):	50000	md
Oil bubble-point pressure (p_b):	5000	psia
Effective horizontal permeability (k):	10	md
Pay zone thickness (h):	50	ft
Average reservoir pressure ($p_{\text{-bar}}$):	4000	psia
Oil formation volume factor (B_o):	1.2	rb/stb
Well drainage area (A):	320	acres
Wellbore radius (r_w):	0.328	ft
Fracture width (w):	0.2	in
Well depth (H):	8000	ft
Tubing inner diameter (d):	2.441	in
Oil gravity (API):	30	API
Oil viscosity (μ_o):	1.5	cp
Producing gas—liquid ratio (GLR):	440	scf/bbl
Gas-specific gravity (γ_g):	0.7	Air = 1
Flowing tubing head pressure (p_{hf}):	800	psia
Flowing tubing head temperature (t_{hf}):	150	°F
Flowing temperature at tubing shoe (t_{wf}):	180	°F
Water cut (WC):	10	%
Oil—gas interfacial tension (s):	30	dynes/cm
Specific gravity of water (γ_w):	1.05	
Shape factor for drainage area (C_A):	31.6	

Solution

This problem can be solved using the spreadsheet program **Pseudosteady Production of Single-Fractured Well.xls**. Table 5.8 shows some calculated data. Fig. 5.5 presents the calculated IPR and TPR curves which indicate an operating oil production rate of 1300 stb/day at a flowing bottom-hole pressure of 2520 psia.

Table 5.8 Data given by the spreadsheet program **Pseudosteady Production of Single-Fractured Well.xls**.

q (stb/d)	Pwf (psia)	
	Inflow performance relationship	Tubing performance relationship
235	3772	1994
469	3531	2171
704	3275	2293
939	3000	2394
1173	2702	2484
1408	2372	2568
1643	2000	2648
1878	1562	2727
2112	1000	2805
2347	0	2883

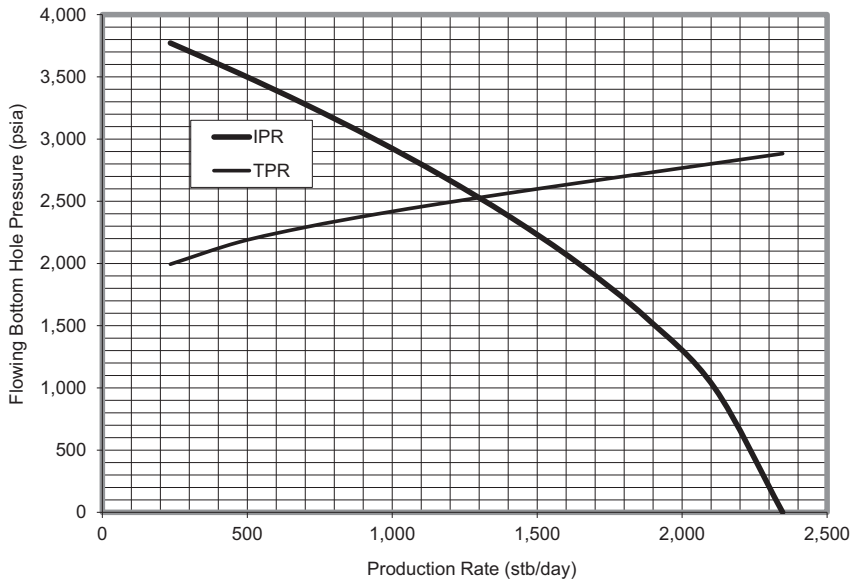


FIGURE 5.5

Curves given by the spreadsheet program **Pseudosteady Production of Single-Fractured Well.xls**. IPR, inflow performance relationship; TPR, tubing performance relationship.

5.4.2 Single-fractured gas wells

For the pseudo–steady-state production of a single-fractured gas well, Eq. (3.10) can be used to construct the IPR curve. However, the total skin factor ($S+Dq_g$) should be replaced by the equivalent fracture skin factor S_f . That is,

$$q_g = \frac{kh(\bar{p}^2 - p_{wf}^2)}{1424\bar{\mu}zT \left(\ln \frac{r_e}{r_w} - \frac{3}{4} + S_f \right)} \quad (5.27)$$

Use Eq. (4.54) for TPR analysis of dry gas wells, and Eq. (4.18) for TPR analysis of gas condensate wells and gas wells with accompanying water and/or solid production.

5.10 Sample problem

From the data given below, assuming that the tubing string is set just above the pay zone, predict the pseudo–steady-state gas production rate:

Pay zone thickness:	78	ft
Permeability:	0.17	md
Wellbore radius:	0.328	ft
Fracture half length:	600	ft
Fracture width:	0.3	in
Fracture permeability:	50000	md
Reservoir pressure:	4613	psia
Total measured depth:	7000	ft
Average inclination angle:	5	deg
Tubing ID:	1.995	in
Gas-specific gravity:	0.65	Air = 1
Gas viscosity:	0.022	cp
Gas z-factor:	0.958	
Oil production rate:	5	stb/day
Oil-specific gravity:	0.85	H ₂ O = 1
Water cut:	10	%
Water-specific gravity:	1.05	H ₂ O = 1
Solid production rate:	1	ft ³ /d
Solid-specific gravity:	2.65	H ₂ O = 1
Tubing head temperature:	100	°F
Bottom-hole temperature:	180	°F
Tubing head pressure:	1000	psia
Drainage area:	320	acres
Wall roughness:	0.01	in

Solution

This problem can be solved using the spreadsheet program **Fractured Gas Well Production Forecast.xls**. Table 5.9 shows the calculated results which indicate an operating gas production rate of 8798 Mscf/day at a flowing bottom-hole pressure of 2705 psia.

Table 5.9 Data given by the spreadsheet program **Fractured Gas Well Production Forecast.xls**.

S_f	-6.9220407	
A	3.1243196	in ²
D	0.16625	ft
T_{av}	600	°R
$\cos(\theta)$	0.9961953	
δ/D	0.0100251	
f_M	0.0303742	
a	2.045E-05	
b	1.498E-09	
c	11,456,002	
d	0.0171734	
e	0.0028505	
M	562.9414	
N	3.755E+11	
Gas production rate, q	8798	Mscf/d
Bottom-hole pressure, p_{wf}	2705	psia

5.5 Deliverability of horizontal wells

Predicting the deliverability of horizontal wells requires considering the hydraulics in the vertical, curved, and horizontal sections. While the hydraulics in the vertical and curved sections can be modeled using the mHB correction (for oil wells) and Guo's mist-flow model (for gas wells), the hydraulics in the horizontal section must be modeled based on reservoir–wellbore cross-flow.

5.5.1 Oil wells in volumetric reservoirs

For horizontal oil wells, use Eq. (3.20) to construct the IPR curve. The mHB correlation described in Chapter 4 can be used to construct the TPR curve. The intersection of the two curves defines the operating point. Because Eq. (3.20) incorporates the correction factor F_o (which depends on production rate itself), the following iterative procedure is recommended:

1. Perform NODAL analysis to predict oil production rate, assuming that $F_o = 1$.
2. Use the predicted operating pressure at heel to calculate F_o value.
3. Perform NODAL analysis to predict the oil production rate using the calculated F_o value.
4. Repeat steps 2 and 3 until the calculated oil production rates converge.

5.11 Sample problem

A horizontal well is to be produced through a 4-in screen. From the data given below, and assuming that the tubing string is set just above the screen, predict pseudo–steady-state oil production rate:

Pay zone thickness (h):	48	ft
Effective horizontal permeability (k_h):	68	md
Effective vertical permeability (k_v):	17	md
Reservoir pressure (pr):	4053	psia
Oil formation volume factor (B_o):	1.1	rb/stb
Well drainage area (A):	640	acres
Horizontal wellbore length (L):	2000	ft
Radius of curvature (ROC):	1000	ft
Total measured well depth (H):	8500	ft
Tubing inner diameter (d):	2.441	in
Oil gravity (API):	42	API
Oil viscosity (μ_o):	1.5	cp
Producing gas–liquid ratio (GLR):	550	scf/bbl
Gas-specific gravity (γ_g):	0.7	Air = 1
Flowing tubing head pressure (p_{hf}):	500	psia
Flowing tubing head temperature (t_{hf}):	125°	F
Flowing temperature at tubing shoe (t_{wf}):	210	°F
Water cut (WC):	10	%
Oil–gas interfacial tension (σ):	30	dynes/cm
Specific gravity of water (γ_w):	1.07	
Wellbore radius (r_w):	0.328	ft

Solution

This problem can be solved using the spreadsheet programs **Pseudo-steady-2Phase Horizontal Well Production Forecast.xls** and **Correction Factor Fo.xls**.

Assuming $F_o = 1.0$, the spreadsheet program **Pseudo-steady-2Phase Horizontal Well Production Forecast.xls** gave IPR and TPR data as shown in [Table 5.10](#). [Fig. 5.6](#) presents the

Table 5.10 Data given by the spreadsheet program **Pseudosteady-2Phase Horizontal Well Production Forecast.xls**.

q (stb/d)	p_{wf} (psia)	
	Inflow performance relationship	Tubing performance relationship
1573	3822	1658
3146	3578	2165
4719	3318	2765
6293	3040	3465
7866	2737	4264
9439	2404	5161
11,012	2027	6154
12,585	1582	7244
14,158	1013	8430
15,732	0	9713

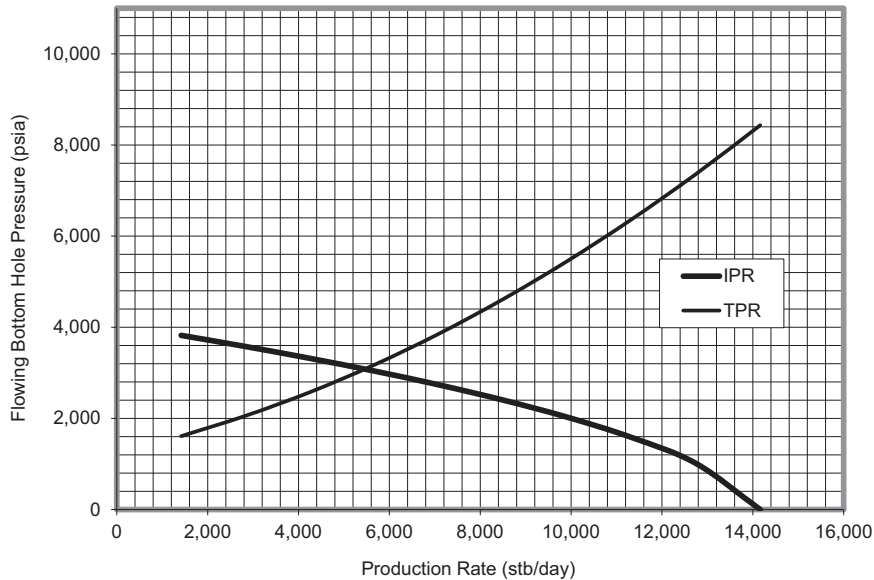


FIGURE 5.6

Curves given by the spreadsheet program *Pseudosteady-2Phase Horizontal Well Production Forecast.xls*. IPR, inflow performance relationship; TPR, tubing performance relationship.

calculated IPR and TPR curves which indicate an operating oil production rate of 5600 stb/day at a flowing pressure at heel of 3200 psia.

1. Using the pressure at a heel of 3200 psia as an input parameter value, the spreadsheet program **Correction Factor Fo.xls** gives a correction factor $F_o = 0.9048$.
2. Substituting $F_o = 0.9048$, the spreadsheet program **Pseudosteady-2Phase Horizontal Well Production Forecast.xls** gives an operating oil production rate of 5500 stb/day at a flowing pressure at heel of 3100 psia.
3. Utilizing this pressure at a heel of 3100 psia as an input parameter value, the spreadsheet program **Correction Factor Fo.xls** gives a correction factor $F_o = 0.9003$.
4. Substituting $F_o = 0.9003$, the spreadsheet program **Pseudo-steady-2Phase Horizontal Well Production Forecast.xls** gives an operating oil production rate of 5510 stb/day, which is only 0.2% higher than the previous value of 5500 stb/day. Thus, the procedure is completed.

5.5.2 Oil wells in water-/gas-coning reservoirs

The deliverability of horizontal oil wells in reservoirs with bottom water and/or gas caps is often limited by water and/or gas coning. Several methods are available for predicting the critical oil production rate, including [Efros \(1963\)](#), [Chaperon \(1986\)](#), [Karcher et al. \(1986\)](#), [Joshi \(1988\)](#), [Giger \(1989\)](#), and [Guo-Lee \(1992\)](#). The Chaperon and Guo—Lee methods incorporate the effects of vertical permeability on the critical rates with the Chaperon method giving the most optimistic value.

The Chaperon method employs the following equation for predicting the critical oil production rate:

$$q_o = 4.888 \times 10^{-4} \frac{Lk_h h^2 \Delta\rho}{B_o \mu_o y_e} F \quad (5.28)$$

where

- q_o = critical oil rate (STB/day),
- L = horizontal wellbore length (ft),
- k_h = horizontal permeability (md),
- h = effective oil column thickness (ft),
- $\Delta\rho$ = density difference (gm/cc),
- B_o = oil formation volume factor (rb/STB),
- μ_o = oil viscosity (cp),
- y_e = half drainage length perpendicular to horizontal wellbore (ft),

and

$$F = 3.9624955 + 0.0616438\alpha'' - 0.000540\alpha''^2 \quad (5.29)$$

$$\alpha'' = \frac{y_e}{h} \sqrt{\frac{k_v}{k_h}} \quad (5.30)$$

5.12 Sample problem

Calculate the anticipated critical oil production rate using following data:

Oil column thickness:	80	ft
Horizontal permeability:	70	md
Vertical permeability:	7	md
Oil viscosity:	0.42	cp
Oil density:	0.7	gm/cc
Oil formation volume factor:	1.1	rb/STB
Water or gas density:	1.05	gm/cc
Drainage area:	160	acres
Horizontal well placement from the no-flow boundary:	8	ft
Horizontal wellbore length:	1640	ft

Solution

This sample problem is solved with the spreadsheet program **Chaperon Critical Oil Rate.xls**. The result is 718 stb/day.

All the methods mentioned in the beginning of this section assume that water/gas approaches the horizontal wellbore uniformly along the horizontal wellbore direction with a crest-shaped phase interface. This is not true in reality partially due to the pressure variation in the wellbore. It is generally believed that water/gas reaches the horizontal wellbore at the heel of the horizontal well first due to the low pressure at heel. Prediction of the water-free production rate requires a numerical model coupling the unevenly distributed reservoir inflow and wellbore hydraulics.

An effective means of delaying water production in horizontal wells is to install inflow control devices (ICDs) along the production string in the horizontal section. The ICDs need to be sized and distributed following a careful design in order to achieve a uniform pressure distribution along the sandface. The following section provides equations that are necessary for developing a numerical simulator to perform design of production strings with ICD installations.

Reservoir influx model. It is generally believed that the reservoir influx is not uniformly distributed along the horizontal wellbore, even for a frictionless wellbore. This is due to the fact that the wellbore sections near the well toe and heel drain more oil from larger areas compared with sections of the same length near the midpoint of the horizontal wellbore. Theoretical studies have shown that the reservoir influx takes a U-shaped distribution with uniform distribution of pressure in the horizontal wellbore (Economides et al., 1996; Ozkan et al., 1999). Based on the result of Papatzacos' (1987) investigation, the author developed the following function for the specific productivity index of horizontal well:

$$J_{sp}(x) = J_{sp}^m \left[1 + 0.005e^{6.7122\left(\frac{x}{L/2}\right)} \right] \quad x \leq L/2 \quad (5.31)$$

where J_{sp}^m is the specific productivity index at the midpoint of the horizontal wellbore and x is the distance from the midpoint. One way of estimating the value of J_{sp}^m is to use Furu'i's et al. (2003) pseudo-linear flow model expressed as

$$J_{sp}^m = \frac{7.08 \times 10^{-3} k_H}{\mu_o B_o \left\{ I_{ani} \ln \left[\frac{h I_{ani}}{r_w (I_{ani} + 1)} \right] + \frac{\pi y_b}{h} - I_{ani} (1.224 - s) \right\}} \quad (5.32)$$

where

$$I_{ani} = \sqrt{\frac{k_H}{k_V}} \quad (5.33)$$

$$y_b = \sqrt{a^2 - (L/2)^2} \quad (5.34)$$

$$a = \left(\frac{L}{2} \right) \left\{ 0.5 + \left[0.25 + \left(\frac{2r_e H}{L} \right)^4 \right]^{0.5} \right\}^{0.5} \quad (5.35)$$

Another way of estimating the value of J_{sp}^m is to derive a relation from a pseudo 3D model. According to Economides et al. (1991), the average specific productivity index is expressed as

$$J_{sp}^J = \frac{7.08 \times 10^{-3} k_H h}{\mu_o B_o L \left\{ \ln \left[\frac{a + \sqrt{a^2 - (L/2)^2}}{(L/2)} \right] + \frac{I_{ani} h}{L} \ln \left[\frac{I_{ani} h}{r_w (I_{ani} - 1)} \right] + S \right\}} \quad (5.36)$$

Volume balance gives

$$2 \int_0^{L/2} J_{sp}(x) dx = J_{sp}^J L. \quad (5.37)$$

Substituting Eq. (5.31) into Eq. (5.37) gives

$$2 \int_0^{L/2} J_{sp}^m \left[1 + 0.005e^{6.7122\left(\frac{x}{L/2}\right)} \right] dx = J_{sp}^J L \quad (5.38)$$

which yields

$$J_{sp}^m L \left[1 + \frac{0.005}{6.7122} (e^{6.7122} - 1) \right] = J_{sp}^J L \quad (5.39)$$

or

$$J_{sp}^m = 0.62J_{sp}^I \quad (5.40)$$

ICD model. Different types of ICDs are used in the industry, including orifice type, nozzle type, and helical channel type. The performance of the orifice-type and nozzle-type ICDs is affected by fluid density and port size. The pressure drop of a liquid across an orifice type or a nozzle type ICD can be estimated by

$$\Delta p = \frac{1.534 \times 10^{-8} \rho q^2}{C_D^2 d_p^4} \quad (5.41)$$

where

ρ = fluid density, lbm/ft³,

Δp = pressure drop, psi,

q = flow rate, bbl/d,

d_p = port diameter, in, and

C_D = discharge coefficient.

The discharge coefficient C_D can be determined based on Reynolds number and choke/pipe diameter ratio from charts or correlations (Guo et al., 2007). The performance of helical channel type ICDs is affected by fluid density, viscosity, and channel design. Their performance curves normally obey the following model:

$$\Delta p = Aq^B \quad (5.42)$$

where the constants A and B are experimentally determined for each ICD design by manufacturers.

5.13 Sample problem

The following data are given for a horizontal well. Calculate pressure and influx distributions in the annulus without ICD (production through screen) and with ICD installations. Assume 20 equal-size nozzles ($C_D = 1.0$) to be installed along the production string with even spacing.

Pay zone thickness:	131.2	ft
Drainage area:	160	acres
Horizontal permeability:	456	md
Vertical permeability:	114	md
Skin factor:	0	
Oil density:	58	lbm/ft ³
Oil viscosity:	0.7	cp
Oil formation volume factor:	1.12	rb/stb
Reservoir pressure:	2533	psi
Drain hole radius to sand face:	0.354	ft
Production string inner diameter:	5.5	in
Bottom-hole pressure at heel:	2,500	psi
Horizontal wellbore length:	2,438	ft
String wall roughness:	0.0024	in

Solution

This sample problem was solved with a spreadsheet program that is not attached to the book and is available from the author upon request. The results are shown in Figs. 5.7 and 5.8. ICD designed ICD sizes and locations are shown in Table 5.11. The total well production rates are predicted to be 10,962 stb/d, and 10,699 stb/d for the wells without and with ICD, respectively.

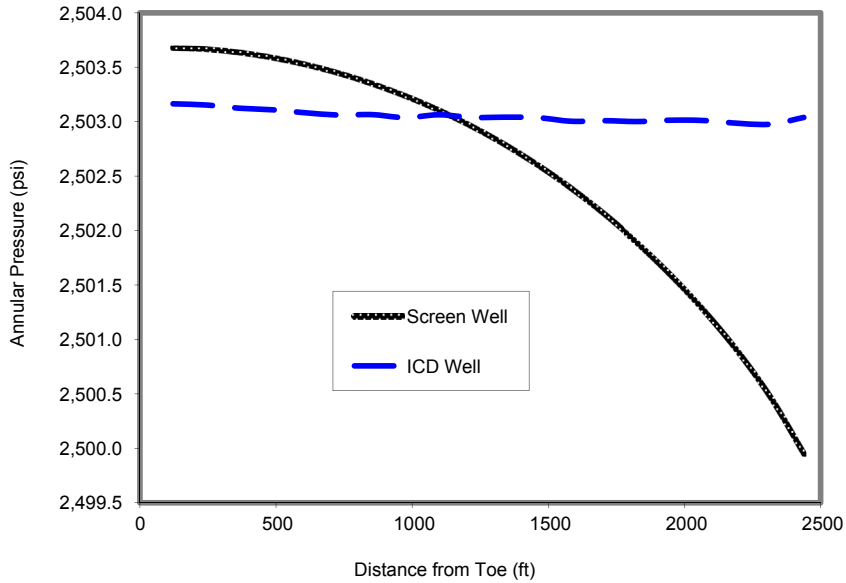


FIGURE 5.7
 Calculated annular pressure distributions with and without inflow control device (ICD) installations.

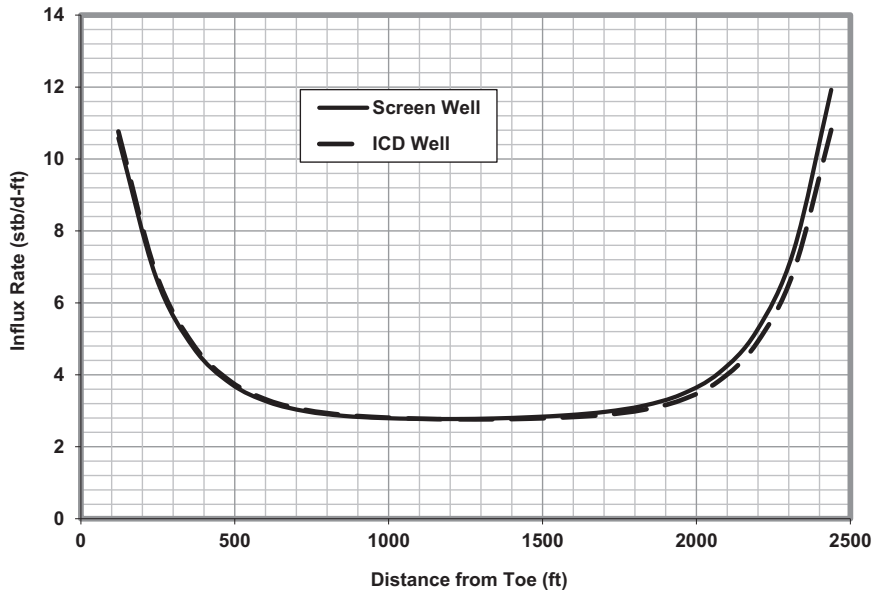


FIGURE 5.8
 Calculated oil influx distributions with and without inflow control device (ICD) installations.

Table 5.11 Designed inflow control device locations and sizes.

Nozzle no.	Segment Center from toe (ft)	Nozzle diameter (in.)
1	60.95	4.00
2	182.85	3.00
3	304.75	2.50
4	426.65	1.50
5	548.55	1.20
6	670.45	1.00
7	792.35	0.85
8	914.25	0.78
9	1036.15	0.70
10	1158.05	0.66
11	1279.95	0.62
12	1401.85	0.59
13	1523.75	0.57
14	1645.65	0.55
15	1767.55	0.54
16	1889.45	0.54
17	2011.35	0.56
18	2133.25	0.61
19	2255.15	0.70
20	2377.05	0.84

5.5.3 Gas wells in volumetric reservoirs

For horizontal gas wells, use Eq. (3.21) to construct the IPR curve and use the mist-flow model of Guo et al. (described in Chapter 4) to construct the TPR curve. The intersection of the two curves defines the operating point. Because Eq. (3.21) involves the correction factor F_g , which depends on production rate itself, the following procedure is recommended:

1. Perform NODAL analysis to predict the gas production rate, assuming $F_g = 1$.
2. Use the predicted pressure at heel to calculate the F_g value.
3. Perform NODAL analysis to predict gas production rate using the calculated F_g value.
4. Repeat steps 2 and 3 until the calculated gas production rates converge.

5.14 Sample problem

For the data given below, assuming tubing string is set right above the pay zone, predict pseudo-steady-state gas production rate:

Pay zone thickness (h):	20	ft
Horizontal permeability (k_h):	5	md
Vertical permeability (k_v):	1	md
Reservoir pressure (p_c):	3458	psia

Reservoir temperature (T):	200	°F
Gas-specific gravity (γ_g):	0.71	
Gas viscosity (μ_g):	0.02	cp
Drainage area (A):	320	acre
Wellbore radius (r_w):	0.328	ft
Horizontal wellbore length (L):	1000	ft
Total well depth (TD):	9000	ft
Kick-off-point (KOP):	6000	ft
Tubing diameter (d):	2.441	in
Tubing relative roughness (ϵ/d):	0.0006	
Tubing head pressure (p_{hf}):	1500	psia
Tubing head temperature (T_{hf}):	150°F	

Solution

This sample problem was solved with the spreadsheet programs **Horizontal Dry Gas Well Production Forecast.xls** and **Correction Factor Fg.xls**.

1. Assuming $F_g = 1.0$, the spreadsheet program **Horizontal Dry Gas Well Production Forecast.xls** gave the IPR and TPR data as shown in **Table 5.12**. **Fig. 5.9** presents the calculated IPR and TPR curves which indicate an operating gas production rate of 13,700 Mscf/day at a flowing pressure at heel of 2600 psia.
2. Using the pressure at a heel of 2600 psia as an input parameter value, the spreadsheet program **Correction Factor Fg.xls** gives a correction factor $F_g = 0.9931$, which is very close to the assumed value of 1.0. Thus, no more computation is necessary.

Table 5.12 Data given by the spreadsheet program **Horizontal Dry Gas Well Production Forecast.xls**.

Flow rate (Mscf/day)	Bottom-hole pressure (psia)	
	Inflow performance relationship	Tubing performance relationship
0	3458	1792
3231	3281	1847
6462	3093	2005
9693	2893	2241
12,924	2679	2533
16,155	2445	2863
19,386	2187	3224
22,617	1894	3608
25,848	1546	4014
29,080	1094	4441
32,310	19	4888

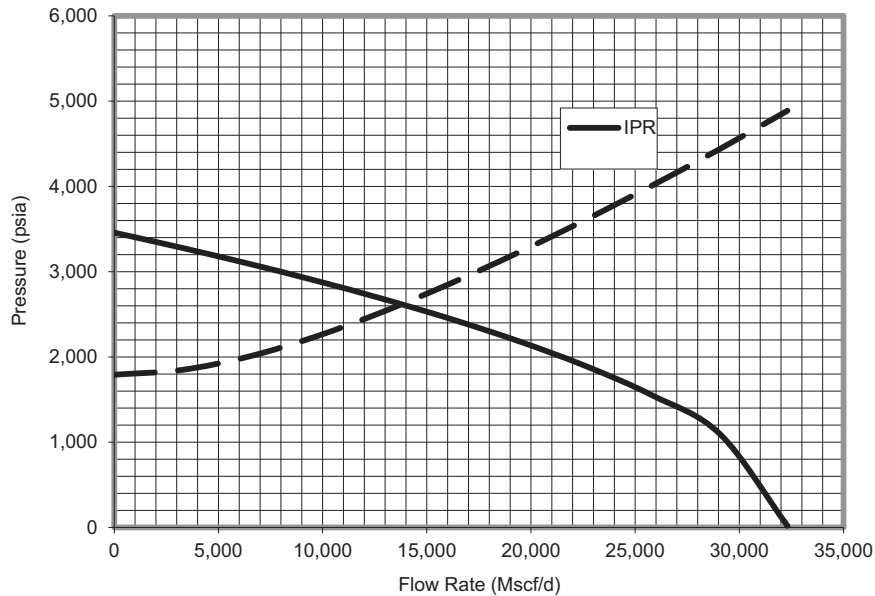


FIGURE 5.9

Curves given by the spreadsheet program Horizontal Dry Gas Well Production Forecast.xls. IPR, inflow performance relationship.

5.6 Summary

This chapter demonstrated methods for predicting the productivities of oil and gas wells with simple trajectories: vertical wells, single-fractured vertical wells, and horizontal wells. The productivities of oil wells with water/gas coning and gas wells with liquid loading were also discussed. The productivity of oil and gas wells with more complex trajectories will be discussed in Chapters 6–8.

5.7 Problems

5.1 From the data given below, assuming the tubing string is set just above the pay zone, predict production rate after 10 days:

Reservoir porosity (ϕ):	0.25	
Effective horizontal permeability (k):	50	md
Pay zone thickness (h):	60	ft
Reservoir pressure (p_i):	5200	psia
Oil formation volume factor (B_o):	1.3	rb/stb
Total reservoir compressibility (c_t):	0.00001	psi ⁻¹

Wellbore radius (r_w):	0.328	ft
Skin factor (S):	5	
Well depth (H):	9000	ft
Tubing inner diameter (d):	2.441	in
Oil gravity (API):	35	API
Oil viscosity (μ_o):	1.2	cp
Producing gas–liquid ratio (GLR):	500	scf/bbl
Gas-specific gravity (γ_g):	0.7	Air = 1
Flowing tubing head pressure (p_{ht}):	500	psia
Flowing tubing head temperature (t_{ht}):	120	°F
Flowing temperature at tubing shoe (t_{wft}):	160	°F
Water cut (WC):	15	%
Oil–gas interfacial tension (σ):	35	dynes/cm
Specific gravity of water (γ_w):	1.04	

5.2 From the data given below, assuming the tubing string is set just above the pay zone, predict the pseudo–steady-state production rate:

Initial oil bubble-point pressure (p_b):	4300	psia
Effective horizontal permeability (k):	35	md
Pay zone thickness (h):	40	ft
Average reservoir pressure (p_{-bar}):	2800	psia
Oil formation volume factor (B_o):	1.25	rb/stb
Well drainage area (A):	160	acres
Wellbore radius (r_w):	0.328	ft
Skin factor (S):	6	
Well depth (H):	8200	ft
Tubing inner diameter (d):	2.441	in
Oil gravity (API):	40	API
Oil viscosity (μ_o):	1.45	cp
Producing gas–liquid ratio (GLR):	560	scf/bbl
Gas-specific gravity (γ_g):	0.7	Air = 1
Flowing tubing head pressure (p_{ht}):	600	psia
Flowing tubing head temperature (t_{ht}):	120	°F
Flowing temperature at tubing shoe (t_{wft}):	160	°F
Water cut (WC):	15	%
Oil–gas interfacial tension (σ):	40	dynes/cm
Specific gravity of water (γ_w):	1.06	
Shape factor for drainage area (C_A):	31.6	

5.3 From the data given below, assuming the tubing string is set just above the pay zone, predict the steady-state production rate:

Initial oil bubble-point pressure (p_b):	4200	psia
Effective horizontal permeability (k):	70	md
Pay zone thickness (h):	55	ft
Boundary reservoir pressure (p_b):	4200	psia
Oil formation volume factor (B_o):	1.3	rb/stb

Well drainage area (A):	320	acres
Wellbore radius (r_w):	0.328	ft
Skin factor (S):	3	
Well depth (H):	7200	ft
Tubing inner diameter (d):	2.441	in
Oil gravity (API):	45	API
Oil viscosity (μ_o):	2.5	cp
Producing gas—liquid ratio (GLR):	700	scf/bbl
Gas-specific gravity (γ_g):	0.75	air = 1
Flowing tubing head pressure (p_{htf}):	900	psia
Flowing tubing head temperature (t_{htf}):	130	°F
Flowing temperature at tubing shoe (t_{wtf}):	180	°F
Water cut (WC):	20	%
Oil—gas interfacial tension (σ):	40	dynes/cm
Specific gravity of water (γ_w):	1.03	

5.4 Calculate the anticipated critical oil production rate, using the following data:

Oil column thickness:	50	ft
Horizontal permeability:	60	md
Vertical permeability:	9	md
Oil viscosity:	0.45	cp
Oil density:	0.8	gm/cc
Oil formation volume factor:	1.2	rb/STB
Water or gas density:	1.06	gm/cc
Drainage area:	320	acres

5.5 From the data given below, assuming the tubing string is set just above the pay zone, predict the transient production rate after 10 days:

Reservoir permeability (k):	30	md
Pay zone thickness (h):	5	ft
Well skin factor (S):	10	
Porosity (ϕ):	0.2	
Wellbore radius (r_w):	0.328	ft
Gas-specific gravity (γ_g):	0.65	
Gas viscosity (μ_g):	0.01	cp
Tubing inside diameter (D):	3.5	in
Tubing relative roughness (ϵ/D):	0.0006	
Measured depth at tubing shoe (L):	5000	ft
Inclination angle (θ):	0	Deg
Wellhead pressure (p_{htf}):	500	psia
Wellhead temperature (T_{htf}):	150	°F
Bottom-hole temperature (T_{wtf}):	200	°F
Initial reservoir pressure (p_i):	2000	psia

5.6 From the data given below, assuming the tubing string is set just above the pay zone, predict the pseudo—steady gas production rate:

Pay zone thickness:	50	ft
Permeability:	0.5	md
Wellbore radius:	0.328	ft
Darcy skin factor:	5	
Non-Darcy skin coefficient:	0.001	day/Mscf
Reservoir pressure:	4620	psia
Total measured depth:	7100	ft
Average inclination angle:	0	deg
Tubing ID:	2.441	in
Gas-specific gravity:	0.70	Air = 1
Gas viscosity:	0.02	cp
Gas z-factor:	0.96	
Oil production rate:	4	stb/day
Oil-specific gravity:	0.8	H ₂ O = 1
Water cut:	12	%
Water-specific gravity:	1.04	H ₂ O = 1
Solid production rate:	0.5	ft ³ /d
Solid-specific gravity:	2.65	H ₂ O = 1
Tubing head temperature:	110	°F
Bottom-hole temperature:	190	°F
Tubing head pressure:	900	psia
Drainage area:	160	acres
Wall roughness:	0.005	in

5.7 From the data given below, assuming a single-size tubing string is set just above the pay zone, use Guo's method to predict the minimum gas production rate that prevents liquid loading:

Gas-specific gravity:	0.66	Air = 1
Hole inclination:	0	Deg
Tubing shoe depth:	5600	ft
Wellhead pressure:	400	psi
Wellhead temperature:	90	°F
Producing zone temperature:	130	°F
Condensate gravity:	70	API
Condensate make:	2	bb/MMscf
Water-specific gravity:	1.05	water = 1
Water make:	40	bb/MMscf
Solid-specific gravity:	2.65	water = 1
Solid make:	1	ft ³ /MMscf
Conduit OD:	1.995	in
Conduit ID:	0	in
Conduit wall roughness:	0.00015	in
Liquid density:	64	lb/ft ³
Liquid—gas interfacial tension:	55	dyne/cm

5.8 From the data given below, assuming the tubing string is set just above the pay zone, predict the pseudo—steady-state production rate:

Fracture half length (x_f):	800	ft
Fracture permeability (k_f):	60,000	md
Oil bubble-point pressure (p_b):	5200	psia
Effective horizontal permeability (k):	10	md
Pay zone thickness (h):	50	ft
Average reservoir pressure ($p_{\text{-bar}}$):	4500	psia
Oil formation volume factor (B_o):	1.25	rb/stb
Well drainage area (A):	160	acres
Wellbore radius (r_w):	0.328	ft
Fracture width (w):	0.25	in
Well depth (H):	8200	ft
Tubing inner diameter (d):	2.441	in
Oil gravity (API):	35	API
Oil viscosity (μ_o):	2.2	cp
Producing gas—liquid ratio (GLR):	600	scf/bbl
Gas-specific gravity (γ_g):	0.75	Air = 1
Flowing tubing head pressure (p_{htf}):	850	psia
Flowing tubing head temperature (t_{htf}):	140	°F
Flowing temperature at tubing shoe (t_{wft}):	170	°F
Water cut (WC):	15	%
Oil—gas interfacial tension (σ):	35	dynes/cm
Specific gravity of water (γ_w):	1.04	
Shape factor for drainage area (C_A):	31.6	

5.9 From the data given below, assuming the tubing string is set just above the pay zone, predict the pseudo—steady-state gas production rate:

Pay zone thickness:	70	ft
Permeability:	0.22	md
Wellbore radius:	0.328	ft
Fracture half length:	800	ft
Fracture width:	0.25	in
Fracture permeability:	80000	md
Reservoir pressure:	4655	psia
Total measured depth:	7200	ft
Average inclination angle:	0	deg
Tubing ID:	2.441	in
Gas-specific gravity:	0.75	Air = 1
Gas viscosity:	0.025	cp
Gas z-factor:	0.97	
Oil production rate:	3	stb/day
Oil-specific gravity:	0.75	H ₂ O = 1
Water cut:	15	%
Water-specific gravity:	1.06	H ₂ O = 1
Solid production rate:	1	ft ³ /d
Solid-specific gravity:	2.65	H ₂ O = 1

Tubing head temperature:	120	°F
Bottom-hole temperature:	180	°F
Tubing head pressure:	900	psia
Drainage area:	160	acres
Wall roughness:	0.001	in

5.10 A horizontal well is to be produced through a 4-in screen. For the data given below, assuming the tubing string is set just above the screen, predict the pseudo—steady-state oil production rate:

Pay zone thickness (h):	460	ft
Effective horizontal permeability (k_h):	80	md
Effective vertical permeability (k_v):	20	md
Reservoir pressure (p_r):	4080	psia
Oil formation volume factor (B_o):	1.15	rb/stb
Well drainage area (A):	320	acres
Horizontal wellbore length (L):	1800	ft
Radius of curvature (ROC):	1200	ft
Total measured well depth (H):	8700	ft
Tubing inner diameter (d):	2.441	in
Oil gravity (API):	46	API
Oil viscosity (μ_o):	0.8	cp
Producing gas—liquid ratio (GLR):	550	scf/bbl
Gas-specific gravity (γ_g):	0.75	Air = 1
Flowing tubing head pressure (p_{ht}):	400	psia
Flowing tubing head temperature (t_{ht}):	120	°F
Flowing temperature at tubing shoe (t_{wft}):	200	°F
Water cut (WC):	15	%
Oil—gas interfacial tension (σ):	35	dynes/cm
Specific gravity of water (γ_w):	1.05	
Wellbore radius (r_w):	0.328	ft

5.11 Calculate the anticipated critical oil production rate, using the following data:

Oil column thickness:	60	ft
Horizontal permeability:	75	md
Vertical permeability:	15	md
Oil viscosity:	0.40	cp
Oil density:	0.65	gm/cc
Oil formation volume factor:	1.2	rb/STB
Water or gas density:	1.065	gm/cc
Drainage area:	320	acres
Horizontal well placement from the no-flow boundary:	10	ft
Horizontal wellbore length:	1500	ft

5.12 For the data given below, assuming the tubing string is set right above the pay zone, predict the pseudo—steady-state gas production rate:

Pay zone thickness (h):	40	ft
Horizontal permeability (k_h):	10	md
Vertical permeability (k_v):	3	md
Reservoir pressure (p_e):	34,708	psia
Reservoir temperature (T):	210	°F
Gas-specific gravity (γ_g):	0.76	
Gas viscosity (μ_g):	0.015	cp
Drainage area (A):	320	acre
Wellbore radius (r_w):	0.328	ft
Horizontal wellbore length (L):	1200	ft
Total well depth (TD):	9200	ft
Kick-off-point (KOP):	6500	ft
Tubing diameter (d):	2.441	in
Tubing relative roughness (ϵ/d):	0.001	
Tubing head pressure (p_{htf}):	1200	psia
Tubing head temperature (T_{htf}):	120	°F

References

- Chaperon, I., 1986. Theoretical study of coning toward horizontal and vertical wells in anisotropic formations: subcritical and critical rates. In: Paper SPE 15377, Presented at the SPE Annual Technical Conference and Exhibition (5–8 October 1986), New Orleans, Louisiana.
- Coleman, S.B., Clay, H.B., McCurdy, D.G., Norris III, L.H., March 1991. A new look at predicting gas well loading-up. *Journal of Petroleum Technology* 291, 329. Trans. AIME.
- Craft, B.C., Hawkins, M.F., 1959. *Applied Petroleum Reservoir Engineering*. Prentice-Hall, Englewood Cliffs, New Jersey.
- Economides, M.J., Deimbacher, F.X., Brand, C.W., Heinemann, Z.E., December 1991. Comprehensive simulation of horizontal well performance. *Study of Political Economy and Free Enterprise* 418.
- Economides, M.J., Brand, C.W., Frick, T.P., December 1996. Well configurations in anisotropic reservoirs. *SPE Formation Evaluation* 257.
- Efros, D.A., 1963. *Study of Multiphase Flows in Porous Media*. Gastoptexizdat, Leningrad.
- Furui, K., Zhu, D., Hill, A.D., August 1, 2003. A rigorous formation damage skin factor and reservoir inflow model for a horizontal well. *SPE production & Facilities* 18 (03), 151–157.
- Giger, F.M., 1989. Analytic 2-D models for water cresting before breakthrough for horizontal wells. *SPE Reservoir Engineering* 409–416.
- Guo, B., Lee, R.L., January 1992. Determination of the maximum water-free production rate of a horizontal well with water/oil/interface cresting. In: *SPE Rocky Mountain Regional Meeting*. Society of Petroleum Engineers.
- Guo, B., Ghalambor, A., Xu, C., 2006. A systematic approach to predicting liquid loading in gas well. *SPE Production & Operations* 21 (1), 81–88.

- Guo, B., Lyons, W.C., Ghalambor, A., 2007. *Petroleum Production Engineering—A Computer-Assisted Approach*. Elsevier, Amsterdam.
- Hoyland, L.A., Papatzacos, P., Skjaeveland, S.M., November 1989. Critical rate for water coning: correlation and analytical solution. *SPE Reservoir Engineering* 495–502.
- Joshi, S.D., June 1988. Augmentation of well productivity using slant and horizontal wells. *Journal of Petroleum Technology* 729–739.
- Karcher, B.J., Giger, F.M., Combe, J., 1986. Some practical formulas to predict horizontal well behavior. In: Paper SPE 15430, Presented at the SPE Annual Technical Conference and Exhibition (5–8 October 1986), New Orleans, Louisiana.
- Lea, J.F., Nickens, H.V., April 2004. Solving gas-well liquid-loading problems. *SPE Production and Facilities* 30.
- Meyer, H.L., Gardner, A.O., November 1954. Mechanics of two immiscible fluids in porous media. *Journal of Applied Physics* 25 (11), 1400.
- Nosseir, M.A., Darwich, T.A., Sayyouh, M.H., Sallaly, M.E., Nov. 2000. A new approach for accurate prediction of loading in gas wells under different flowing conditions. *SPE Production and Facilities* 15 (4), 245.
- Ozkan, E., Sarica, C., Haci, M., September 1999. Influence of pressure drop along the wellbore on horizontal-well productivity. *SPE Journal* 288.
- Papatzacos, P., May 1987. Exact solutions for infinite-conductivity wells. *SPE Reservoir Engineering* 217.
- Schols, R.S., January 1972. An empirical formula for the critical oil production rate. *Erdoel Erdgas Z* 88 (1), 6–11.
- Turner, R.G., Hubbard, M.G., Dukler, A.E., November 1969. Analysis and prediction of minimum flow rate for the continuous removal of liquids from gas wells. *Journal of Petroleum Technology* 246, 1475. *Trans. AIME*.

Further reading

- Horne, R.N., 1995. *Modern Well Test Analysis: A Computer-Aided Approach*. Petroway Publishing, New York.
- Lee, J.W., Rollins, J.B., Spivey, J.P., 2003. *Pressure Transient Testing*. Society of Petroleum Engineers, Richardson, Texas.
- Pirson, S.J., 1977. *Oil Reservoir Engineering*. Robert E. Krieger Publishing Company, Huntington, New York.

Productivities of modern well types

2

This section of book presents additional knowledge necessary for predicting productivity of oil and gas wells with modern well structures.

Chapter 6 presents methods for predicting productivity of multilateral wells including fishbone-type multilaterals and root-type multilaterals.

Chapter 7 provides methods for predicting productivity of multifractured wells for unconventional oil and gas reservoirs such as tight sands and shale plays.

Chapter 8 illustrates methods for predicting productivity of radial-fractured wells completed with blast fracturing and high-energy gas fracturing.

Productivity of multilateral wells

Chapter outline

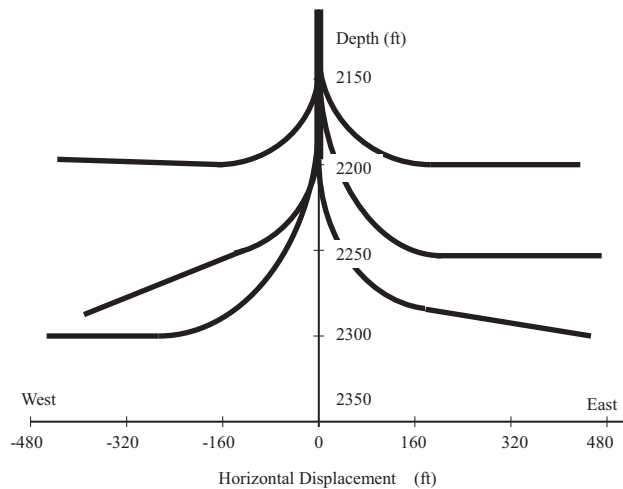
6.1 Introduction	165
6.2 Fishbone wells	165
6.2.1 Oil wells	167
6.2.2 Gas wells	170
6.3 Root wells	171
6.4 Summary	179
6.5 Problems	180
References	181

6.1 Introduction

A multilateral well is defined, in general, as a well with multiple branches in the lower borehole, targeting oil and gas reserves in the same or in different strata. These branches are called “laterals.” The primary, or main wellbore, from which the laterals are drilled out can be vertical or horizontal. Lateral bores extending from vertical wellbores are usually used to reach different pay zones, while the laterals drilled out from horizontal wellbores are usually intended to reach different areas of the same pay zone. In this book, multilateral wells with laterals drilled from vertical main wellbores are called “root wells” (Fig. 6.1). Multilateral wells with the laterals drilled out from horizontal main wellbores are called “fishbone wells” (Fig. 6.2). The prediction of fishbone well productivity is relatively simple because all laterals (rib holes) share approximately the same pressure in the main wellbore (backbone hole). Prediction of root well productivity is more complicated because the pressures in the laterals can be significantly different and wellbore hydraulics plays an important role.

6.2 Fishbone wells

The initial flow regime in a fishbone well may be pseudolinear before the rib holes begin to interfere with each other. Pseudoradial flow may prevail later if the drainage area is large in proportion to the drilled region of the reservoir.

**FIGURE 6.1**

Schematic of a typical root well.

**FIGURE 6.2**

Schematic of a reservoir section drained by a fishbone well.

Raghavan and Joshi (1993) presented a mathematical model that can be used to predict the productivities of root wells. The model uses effective wellbore radius (horizontal radial flow) to simulate fluid flow to the horizontal drain holes. Retnanto and Economides (1996) published a simple formulation of multilateral well productivity for pseudo-steady-state flow. They derived their formulation by combining a one-dimensional linear flow model with a two-dimensional radial

flow model to cover the whole drainage area. Larsen (1996) proposed a mathematical model similar to that of Raghavan and Joshi (1993) in the sense that horizontal drain holes are simulated by vertical wellbores located at the midpoints of the well elements.

A pseudolinear-radial-combined model is described in this section. The model assumes two regions within the reservoir—an inner drilled region and an outer non-drilled region. The model assumes the inner region to be dominated by pseudo-steady-state pseudolinear flow between the rib holes, and the outer region to be dominated by pseudo-steady-state radial flow.

6.2.1 Oil wells

Following Furui et al. (2003), for uniformly distributed rib holes in the inner region, the deliverability of n rib holes is expressed as

$$q = \sum_{i=1}^n \frac{7.08 \times 10^{-3} k_H L_i (p_{PL} - p_{wf})}{\mu_o B_o \left\{ I_{ani} \ln \left[\frac{h I_{ani}}{r_{wi} (I_{ani} + 1)} \right] + \frac{\pi y_{bi}}{h} - I_{ani} (1.224 - s_i) \right\}} \quad (6.1)$$

where L_i , r_{wi} , y_{bi} , and s_i are length, radius, drainage distance, and skin factor of rib hole i , respectively. The permeability anisotropy I_{ani} is defined as

$$I_{ani} = \sqrt{\frac{k_H}{k_V}} \quad (6.2)$$

The p_{PL} is defined as the average pressure at the edge of the inner region. The radial flow in the outer region can be described by

$$q = \frac{k_H h (\bar{p} - p_{PL})}{141.2 B_o \mu_o \left(\frac{1}{2} \ln \frac{4A}{\gamma C_A r_{PL}^2} \right)} \quad (6.3)$$

It is understood that this equation is valid only when the inner region is much smaller than the drainage area so that the argument of the logarithm is greater than unity.

Combining Eqs. (6.1) and (6.3) to eliminate p_{PL} gives

$$q = \frac{1}{\left(\frac{1}{J_{PL}} + \frac{1}{J_R} \right)} (\bar{p} - p_{wf}) \quad (6.4)$$

where

$$J_{PL} = \sum_{i=1}^n \frac{7.08 \times 10^{-3} k_H L_i}{\mu_o B_o \left\{ I_{ani} \ln \left[\frac{h I_{ani}}{r_{wi} (I_{ani} + 1)} \right] + \frac{\pi y_{bi}}{h} - I_{ani} (1.224 - s_i) \right\}} \quad (6.5)$$

and

$$J_R = \frac{k_H h}{141.2 B_o \mu_o \left(\frac{1}{2} \ln \frac{4A}{\gamma C_A r_{PL}^2} \right)} \quad (6.6)$$

The equivalent radius of the inner region may be estimated by

$$r_{PL} = \sqrt{\frac{2(n+1)\bar{y}_b \bar{L}}{\pi}} \quad (6.7)$$

where \bar{y}_b and \bar{L} are the average rib hole drainage distance and rib hole length, respectively. The drainage area shape factor C_A can be estimated based on the shape of drainage area and the location of the inner region at the center of the drainage area. The aspect ratio (length to width) of the drainage area may be taken as

$$R_A = \frac{(n+1)\bar{y}_b}{2\bar{L}} \quad (6.8)$$

The shape factor may be estimated by $C_A = 39.51 - 8.5214R_A$.

Because all the above equations are deterministic, they can be used for predicting actual well inflow performance relationship (IPR).

The tubing performance relationship (TPR) of fishbone wells can be modeled using different correlations that depend on the fluid type. The Hagedorn–Brown correlation is used in the following example.

6.1 Sample problem

For the data given below, assuming the tubing string is set just above the pay zone, predict the pseudo–steady-state liquid production rate:

Average rib hole spacing ($2y_b$):	1000	ft
Average rib hole length (L):	1000	ft
Average rib hole skin factor (s):	5	
Oil bubble-point pressure (p_b):	5000	psia
Effective horizontal permeability (k_H):	10	md
Pay zone thickness (h):	50	ft
Average reservoir pressure (p_{bar}):	4000	psia
Oil formation volume factor (B_o):	1.2	rb/stb
Well drainage area (A):	320	acres
Average rib hole radius (r_w):	0.328	ft
Vertical permeability (k_v):	2	md
Well vertical depth (H):	8000	ft
Tubing inner diameter (d):	4	in

Oil gravity (API):	30	API
Oil viscosity (μ_o):	1.5	cp
Producing gas—liquid ratio (GLR):	500	scf/bbl
Gas-specific gravity (γ_g):	0.7	Air = 1
Flowing tubing head pressure (p_{th}):	800	psia
Flowing tubing head temperature (t_{th}):	150	°F
Flowing temperature at tubing shoe (t_{wf}):	180	°F
Water cut (WC):	10	%
Oil—gas interfacial tension (σ):	30	dynes/cm
Specific gravity of water (γ_w):	1.05	
Number of rib holes (n):	7	
Drainage area shape factor (C_A) based on aspect ratio:	5.38	

Solution

This problem can be solved using the spreadsheet program **Pseudosteady Production of Fishbone Oil Well.xls**. Fig. 6.3 indicates that the expected liquid production rate is 1540 stb/day at a flowing bottom-hole pressure of 1905 psia.

Using this spreadsheet, it can be shown that the productivity of fishbone wells does not increase in proportion to the number of rib holes. The solution to the problem is left to the reader as an exercise in using the spreadsheet.

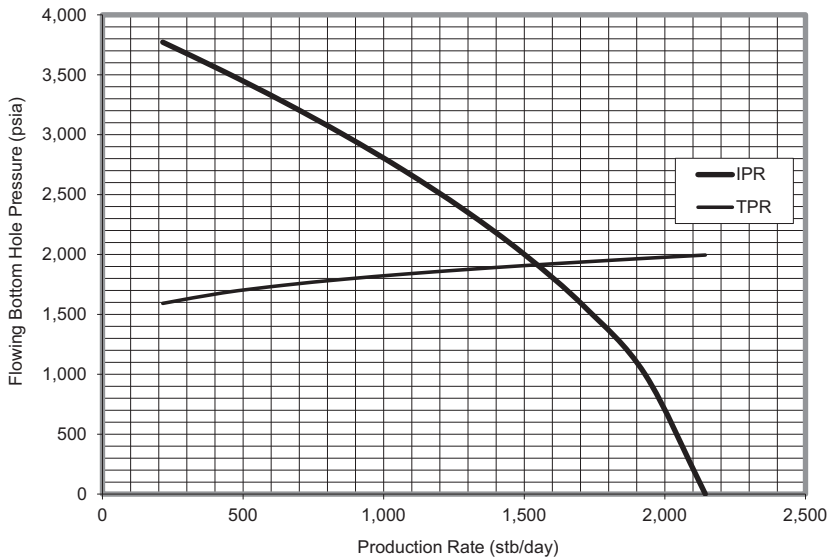


FIGURE 6.3

Curves given by the spreadsheet program **Pseudosteady Production of Fishbone Oil Well.xls**. *IPR*, inflow performance relationship; *TPR*, tubing performance relationship.

6.2.2 Gas wells

Following the work of [Furui et al. \(2003\)](#), for uniformly distributed rib holes in the inner region, the gas deliverability of n rib holes is expressed as

$$q = \sum_{i=1}^n \frac{k_H L_i (p_{PL}^2 - p_w^2)}{1424 \bar{\mu}_g \bar{z} T \left\{ I_{ani} \ln \left[\frac{h I_{ani}}{r_{wi} (I_{ani} + 1)} \right] + \frac{\pi y b_i}{h} - I_{ani} (1.224 - (s_i + Dq)) \right\}} \quad (6.9)$$

The p_{PL} is defined as the average pressure at the edge of the inner region. The radial flow in the outer region can be described by

$$q = \frac{k_H h (\bar{p}^2 - p_{PL}^2)}{1424 \bar{\mu}_g \bar{z} T \left(\frac{1}{2} \ln \frac{4A}{\gamma C_A r_{PL}^2} \right)} \quad (6.10)$$

Again it is understood that this equation is valid only when the inner region is much smaller than the drainage area so that the argument of the logarithm is greater than unity.

Combining [Eqs. \(6.9\) and \(6.10\)](#) to eliminate p_{PL} gives

$$q = \frac{1}{\left(\frac{1}{J_{PL}} + \frac{1}{J_R} \right)} (\bar{p}^2 - p_{wf}^2) \quad (6.11)$$

where

$$J_{PL} = \sum_{i=1}^n \frac{k_H L_i}{1424 \bar{\mu}_g \bar{z} T \left\{ I_{ani} \ln \left[\frac{h I_{ani}}{r_{wi} (I_{ani} + 1)} \right] + \frac{\pi y b_i}{h} - I_{ani} (1.224 - (s_i + Dq)) \right\}} \quad (6.12)$$

and

$$J_R = \frac{k_H h}{1424 \bar{\mu}_g \bar{z} T \left(\frac{1}{2} \ln \frac{4A}{\gamma C_A r_{PL}^2} \right)} \quad (6.13)$$

where C_A can be estimated in the same way as for oil wells.

Because all the above equations are deterministic, they can be used for predicting actual well IPR.

The TPR of fishbone wells can be modeled using different correlations for gas flow in the wellbores. The Guo–Ghalambor model expressed by [Eq. \(4.13\)](#) for mist flow is used in the following example.

6.2 Sample problem

For the data given below, assuming tubing string is set just above the pay zone, predict the pseudo-steady-state gas production rate:

Pay zone thickness:	30	ft
Horizontal permeability:	1	md
Wellbore radius:	0.328	ft
Average Darcy skin factor:	5	
Non-Darcy skin coefficient:	0.001	day/Mscf
Reservoir pressure:	4613	psia
Total measured depth:	7000	ft
Average inclination angle:	0	deg
Tubing ID:	3.5	in
Gas-specific gravity:	0.65	Air = 1
Gas viscosity:	0.022	cp
Gas z-factor:	0.958	
Oil production rate:	1	stb/day
Oil-specific gravity:	0.85	H ₂ O = 1
Water cut:	10	%
Water-specific gravity:	1.05	H ₂ O = 1
Solid production rate:	1	ft ³ /d
Solid-specific gravity:	2.65	H ₂ O = 1
Tubing head temperature:	100	°F
Bottom-hole temperature:	180	°F
Tubing head pressure:	2000	psia
Drainage area:	640	acres
Average wall roughness:	0.01	in
Number of rib holes:	4	
Average rib hole length:	500	ft
Average rib hole spacing (2y _b):	1000	ft
Vertical permeability:	0.25	md

Solution

This problem is solved using the spreadsheet program **Pseudosteady Production of Fishbone Gas Well.xls**. Table 6.1 indicates that the expected gas production rate is 12,092 Mscf/d at a flowing bottom-hole pressure of 2427 psia.

6.3 Root wells

The lower section of a root well is an integration of several horizontal wells. However, because of pressure drops in the wellbore sections, the productivity of a root well is not simply the sum of the productivities of the individual laterals, unless the IPRs of all the laterals are properly integrated with an understanding of the wellbore hydraulics.

Table 6.1 Results given by spreadsheet **Program Pseudosteady Production of Fishbone Gas Well.xls**.

f_M	2.58E-02	l_{ana}	2	
a	2.04E-05	r_{PL}	892	ft
b	2.45E-10	J_{PL}	0.00115	Mscf/d-psi ²
c	5.12E+06	J_R	0.00250	Mscf/d-psi ²
d	1.25E-03	J	0.00079	Mscf/d-psi ²
e	1.37E-03			
M	8.82E+00			
N	3.60E+10			
	Gas production rate, q		12,092	Mscf/d
	Bottom-hole pressure, p_{wf}		2427	psia

Fig. 6.4 shows a generalized root well structure. The root well can be viewed as a few well branches linked in series, each having three sections: vertical, curved, and horizontal sections. The symbols H , R , and L stand for the vertical length; the radius-of-curvature; and the horizontal length of the vertical, curved, and horizontal sections, respectively.

Fig. 6.5 illustrates the parameters used to characterize a root well. The notations K , h , and \bar{P} represent the respective permeability, thickness, and average pressure in the reservoir area drained by a lateral branch. The pressures at heel and kick-off point are denoted by P_{wf} and P_{kf} , respectively. The symbols P_{hf} and q represent well-head pressure and well production rate. The following trial-and-error procedure can be used to predict the productivity of a root well with n roots.

1. At the given wellhead flowing pressure $p_{hf\ n}$, assume a value of the total well flow rate q_t , and calculate the pressure at the kick-off point of lateral n and p_{kfn} using the TPR function \mathfrak{S}_n :

$$p_{kfn} = \mathfrak{S}_n(p_{hf_n}, q_t) \tag{6.14}$$

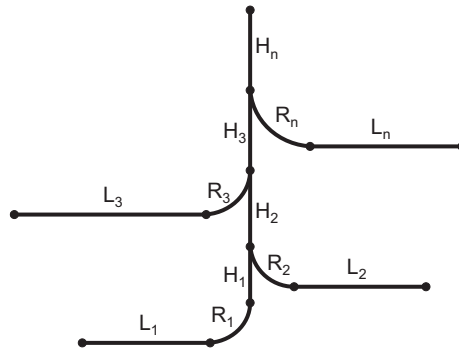
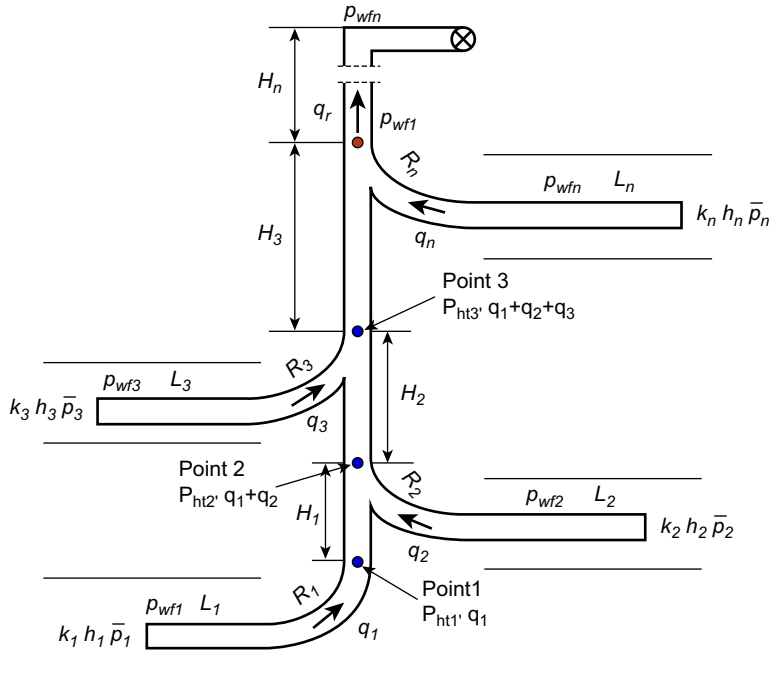


FIGURE 6.4

A simplified multilateral well structure.


FIGURE 6.5

Symbols used to describe a multilateral well.

2. Perform an inflow–outflow analysis for lateral n to calculate the production rate. Do this by combining the TPR of the curved section and the IPR of the horizontal section by solving for q_n from the following two relations:

$$p_{wfn} = \mathfrak{N}_n(\bar{p}_n, q_n) \quad (6.15)$$

$$p_{wfn} = \mathfrak{R}_n(p_{kfn}, q_n) \quad (6.16)$$

where \mathfrak{N}_n and \mathfrak{R}_n are IPR and TPR (curved section) functions for the lateral n , respectively.

3. Calculate the flowing pressure at the kick-out point of lateral $n-1$ and p_{kfn-1} using the TPR function of the vertical section with flow rate $(q_t - q_n)$, that is:

$$p_{kfn-1} = \mathfrak{S}_{n-1}(p_{kf n}, q_t - q_n) \quad (6.17)$$

4. Perform an inflow–outflow analysis for lateral $n-1$ to calculate the production rate from that lateral. This is done by combining the TPR of the curved section and the IPR of the horizontal section, and then solving for q_{n-1} from the following two relations:

$$p_{wfn-1} = \mathfrak{N}_{n-1}(\bar{p}_{n-1}, q_{n-1}) \quad (6.18)$$

$$p_{wfn-1} = \mathfrak{R}_{n-1}(p_{kfn-1}, q_{n-1}) \quad (6.19)$$

5. Calculate the flowing pressure at the kick-out point of lateral $n-2$ and P_{kfn-2} using the TPR function of the vertical section with flow rate $(q_t - q_n - q_{n-1})$, that is,

$$p_{kfn-2} = \mathfrak{S}_{n-2}(p_{kfn-1}, q_t - q_n - q_{n-1}) \quad (6.20)$$

6. Perform an inflow–outflow analysis for lateral $n-2$ to calculate the production rate from that lateral. Do this by combining the TPR of the curved section and the IPR of the horizontal section by solving for q_{n-2} from the following two relations:

$$p_{wfn-2} = \mathfrak{K}_{n-1}(\bar{p}_{n-2}, q_{n-2}) \quad (6.21)$$

$$p_{wfn-2} = \mathfrak{R}_{n-2}(p_{kfn-2}, q_{n-2}) \quad (6.22)$$

7. Repeat the procedure shown in steps 3 through 6 until the flow rate from lateral 1 (q_1) is calculated.

Compare the calculated total flow rate $(q_1 + q_2 + \dots + q_n)$ with the assumed total flow rate q_t . If the $(q_1 + q_2 + \dots + q_n) - q_t$ is greater than the specified tolerance, use the value of $(q_1 + q_2 + \dots + q_n)$ as a new assumption for the total flow rate q_t and repeat steps 1–6. If $(q_1 + q_2 + \dots + q_n) - q_t$ is less than the specified tolerance, exit the loop. Then the q_t is a prediction of production rate of the root well.

For oil wells, the Hagedorn–Brown correlation presented in Chapter 4 can be employed to generate the tubing performance functions \mathfrak{S} and \mathfrak{R} . The lateral IPR function \mathfrak{K} can be chosen from different IPR models for horizontal oil wells presented in Chapter 3.

For gas wells, Guo’s mist flow model presented in Chapter 4 can be employed to generate the tubing performance functions \mathfrak{S} and \mathfrak{R} . The lateral IPR function \mathfrak{K} can be chosen from different IPR models for horizontal oil wells given in Chapter 3.

One of the difficulties in predicting the productivity of root wells lies in accommodating the mixed properties of fluids (oil, water, and gas) from all roots in the hydraulics computations for different wellbore sections. The mixing rule can be applied to all stages of the trial-and-error procedure.

6.3 Sample problem

A planned root-type oil well has four laterals penetrating four oil reservoir sections. From the data given in Table 6.2, predict the pseudo–steady-state oil production rate at wellhead pressure 1500 psi and temperature 100°F.

Solution

This problem can be solved using the spreadsheet program **Multilateral Oil Well Deliverability.xls**. The result is 796 stb/d, 598 stb/d, 476 stb/d, and 165 stb/d from laterals 1, 2, 3, and 4, respectively. The total predicted well flow rate is 2035 stb/d.

Table 6.2 Given data for a four-lateral root-type oil well.

Lateral no.	1	2	3	4	
Reservoir Pressure (p -bar)	3700	3500	3300	2800	psia
Oil formation Factor (B_o)	1.20	1.15	1.10	1.1	stb/rb
Water formation Factor (B_w)	1.00	1.00	1.00	1.00	stb/rb
Bottom-hole temperature (T)	270	260	250	230	°F
Gas compressibility factor (z)	0.85	0.90	0.95	0.98	
Gas-specific gravity (γ_g)	0.85	0.83	0.80	0.75	Air = 1
Oil-specific gravity (γ_o)	0.80	0.78	0.87	0.85	Water = 1
Water-specific gravity (γ_w)	1.07	1.06	1.05	1.04	Water = 1
Water-oil ratio (WOR)	0.10	0.40	0.20	0.30	stb/stb
Gas-oil ratio (GOR)	1000	1500	2000	2500	scf/stb
Solution gas-oil ratio (R_s)	800	1200	1500	2000	scf/stb
Productivity index (J)	1	0.8	0.7	0.6	stb/d/psi
Curvic sections:					
Lateral no.	1	2	3	4	
Radius of curve (R)	200	200	200	200	ft
Inclination angle (θ)	45	45	45	45	°
Tubing diameter (d_i)	3	3	3	3	in
Pipe roughness (e)	0.0018	0.0018	0.0018	0.0018	in
Vertical sections:					
Lateral no.	1	2	3	4	
Interval length (H)	500	400	300	3000	ft
Tubing diameter (d_i)	3	3.5	4	4.5	in
Pipe roughness (e)	0.0018	0.0018	0.0018	0.0018	in

6.4 Sample problem

A planned root well has 10 roots penetrating 10 multiphase reservoir sections. From the data given in Table 6.3–6.7, predict the pseudo–steady-state oil production rate.

Solution

This problem can be solved using the spreadsheet program **Multilateral Oil Well.xls**. The result is presented in Table 6.8.

Table 6.3 Reservoir property data.

Lateral no.	Reservoir pressure (psia)	Temperature (°F)	Horizontal permeability (md)	Vertical permeability (md)	Thickness (ft)
1	1200	120	5	1.67	50
2	1400	125	6	2.00	51
3	1600	130	7	2.33	52
4	1800	135	8	2.67	53
5	2000	140	9	3.00	54
6	2200	145	10	3.33	55
7	2400	150	11	3.67	56
8	2600	155	12	4.00	57
9	2800	160	13	4.33	58
10	3000	165	14	4.67	59

Table 6.4 Fluid property data.

Lateral no.	Oil gravity (API)	Oil viscosity (cp)	Oil formation volume factor (rb/stb)	Solution gas ratio (scf/stb)	Water cut (%)
1	65	0.5	1.4	5000	33
2	60	1	1.35	4000	34
3	55	1.5	1.3	3000	35
4	50	2	1.25	2000	36
5	45	2.5	1.2	1000	37
6	40	3	1.15	500	38
7	35	3.5	1.13	300	39
8	30	4	1.1	200	40
9	25	4	1.07	100	60
10	20	4	1.05	50	80

Table 6.5 Well data for vertical sections.

Lateral no.	Kick-off point (ft)	Inclination angle (deg)	Tubing diameter (in)	Wall roughness (in)
1	3000	0	9	0.0001
2	3500	0	6	0.0001
3	4000	0	6	0.0001
4	4500	0	6	0.0001
5	5000	0	6	0.0001
6	5500	0	6	0.0001
7	6000	0	6	0.0001
8	6500	0	6	0.0001
9	7000	0	6	0.0001
10	7500	0	6	0.0001

Table 6.6 Well data for curved sections.

Lateral no.	Radius of curvature (ft)	Plane inclination angle (deg)	Tubing diameter (in)	Wall roughness (in)
1	500	0	4	0.0001
2	550	0	4	0.0001
3	600	0	4	0.0001
4	650	0	4	0.0001
5	700	0	4	0.0001
6	750	0	4	0.0001
7	800	0	4	0.0001
8	850	0	4	0.0001
9	900	0	4	0.0001
10	950	0	4	0.0001

Table 6.7 Well data for horizontal sections.

Lateral no.	Lateral length (ft)	Inclination angle (deg)	Tubing diameter (in)	Wall roughness (in)	Open hole radius (ft)	Drainage area (acre)
1	2000	90	4	0.0001	0.328	160
2	1900	90	4	0.0001	0.328	160
3	1800	90	4	0.0001	0.328	160
4	1700	90	4	0.0001	0.328	160
5	1600	90	4	0.0001	0.328	160
6	1500	90	4	0.0001	0.328	160
7	1400	90	4	0.0001	0.328	160
8	1300	90	4	0.0001	0.328	160
9	1200	90	4	0.0001	0.328	160
10	1100	90	4	0.0001	0.328	160

Table 6.8 Summary of calculated lateral and well production rates.

Lateral no.	Heel pressure (psi)	Liquid production rate (stb/day)	Oil production rate (stb/day)	Water production rate (bbl/day)	Gas production rate (Mscf/day)
1	808	743	498	245	2489
2	1020	443	292	151	1170
3	1224	346	225	121	675
4	1424	298	191	107	381
5	1623	265	167	98	167
6	1842	227	141	86	70
7	2065	182	111	71	33
8	2299	132	79	53	16
9	2556	104	42	62	4
10	2818	56	11	45	1
Total:		2796	1756	1040	5006

6.5 Sample problem

A planned root-type gas well has four laterals penetrating four gas reservoir sections. From the data given in Table 6.9, predict the pseudo–steady-state oil production rate at wellhead pressure 2000 psi and temperature 100°F.

Solution

This problem can be solved using the spreadsheet program **Multilateral Gas Well Deliverability (Radial-Flow IPR).xls**. The result is 1052 Mscf/d, 419 Mscf/d, –280 Mscf/d, and 253 Mscf/d from laterals 1, 2, 3, and 4, respectively. The negative number represents the flow by lateral 3. The total predicted well flow rate is 1444 Mscf/d.

Table 6.9 Given data for a four-lateral root-type gas well.

Lateral no.:	Horizontal sections:				
	1	2	3	4	
Length of horizontal section (L)	1200	1000	800	900	ft
Initial guess for bottom-hole pressure (p _{wf})	2224	2211	2187	2179	psia
Horizontal permeability (k)	5	3	10	7	md
Net pay thickness (h)	80	80	60	50	ft
Reservoir pressure (p-bar)	3700	3500	1800	2800	psia
Radius of drainage (r _{eh})	2000	2500	1700	2100	ft
Gas viscosity (μ _g)	0.02	0.02	0.02	0.02	cp

Table 6.9 Given data for a four-lateral root-type gas well.—*cont'd*

Horizontal sections:					
Lateral no.:	1	2	3	4	
Wellbore diameter (di)	8.00	8.00	8.00	8.00	in
Bottomhole temperature (T)	270	260	250	230	°F
Gas compressibility factor (z)	0.85	0.90	0.95	0.98	
Gas-specific gravity (γ_g)	0.85	0.83	0.80	0.75	Air = 1
Curvic sections:					
Lateral no.	1	2	3	4	
Radius of curve (R)	250	300	200	270	ft
Average inclination angle (θ)	45	45	45	45	°
Tubing diameter (di)	3	3	3	3	in
Pipe roughness (e)	0.0018	0.0018	0.0018	0.0018	in
Vertical sections:					
Lateral no.	1	2	3	4	
Interval length (H)	250	300	200	3000	ft
Tubing diameter (di)	3	3	3	3	in
Pipe roughness (e)	0.0018	0.0018	0.0018	0.0018	in

6.4 Summary

This chapter presented practical methods for predicting the productivities of multi-lateral oil and gas wells including fishbone wells and root wells. The IPR's of fishbone wells can be estimated using simple models that allow solutions to be obtained by hand calculations. The productivity prediction of root wells requires computer programs due to the complex procedure of coupling the root inflow and wellbore hydraulics.

6.5 Problems

6.1 A planned fishbone well will have 10 laterals penetrating 10 reservoir sections. From the data given in the following tables, predict the pseudo—steady-state oil production rate:

Lateral no.	Reservoir pressure (psia)	Temperature (°F)	Horizontal permeability (md)	Vertical permeability (md)	Thickness (ft)
1	1200	120	5	2	50
2	1400	125	5	2	50
3	1600	130	5	2	50
4	1800	135	5	2	50
5	2000	140	5	2	50
6	2200	145	10	4	55
7	2400	150	10	4	55
8	2600	155	10	4	55
9	2800	160	10	4	55
10	3000	165	10	4	55

Lateral no.	Oil gravity (API)	Oil viscosity (cp)	Oil formation volume factor (rb/stb)	Solution gas ratio (scf/stb)	Water cut (%)
1	65	0.5	1.4	5000	30
2	60	1	1.35	4000	30
3	55	1.5	1.3	3000	35
4	50	2	1.25	2000	35
5	45	2.5	1.2	1000	35
6	40	3	1.15	500	38
7	35	3.5	1.13	300	38
8	30	4	1.1	200	40
9	25	4	1.07	100	50
10	20	4	1.05	50	60

Lateral no.	Kick-off point (ft)	Inclination angle (deg)	Tubing diameter (in)	Wall roughness (in)
1	3000	0	7	0.0001
2	3500	0	4	0.0001
3	4000	0	4	0.0001
4	4500	0	4	0.0001
5	5000	0	4	0.0001
6	5500	0	4	0.0001
7	6000	0	4	0.0001
8	6500	0	4	0.0001
9	7000	0	4	0.0001
10	7500	0	4	0.0001

Lateral no.	Radius of curvature (ft)	Plane inclination angle (deg)	Tubing diameter (in)	Wall roughness (in)
1	500	0	4	0.0001
2	500	0	4	0.0001
3	600	0	4	0.0001
4	600	0	4	0.0001
5	700	0	4	0.0001
6	700	0	4	0.0001
7	800	0	4	0.0001
8	800	0	4	0.0001
9	900	0	4	0.0001
10	900	0	4	0.0001

Lateral no.	Lateral length (ft)	Inclination angle (deg)	Tubing diameter (in)	Wall roughness (in)	Open hole radius (ft)	Drainage area (acre)
1	2100	90	4	0.0001	0.328	160
2	2000	90	4	0.0001	0.328	160
3	1900	90	4	0.0001	0.328	160
4	1800	90	4	0.0001	0.328	160
5	1700	90	4	0.0001	0.328	160
6	1600	90	4	0.0001	0.328	160
7	1500	90	4	0.0001	0.328	160
8	1400	90	4	0.0001	0.328	160
9	1300	90	4	0.0001	0.328	160
10	1200	90	4	0.0001	0.328	160

References

- Furui, K., Zhu, D., Hill, A.D., August 2003. A rigorous formation damage skin factor and reservoir inflow model for a horizontal well. SPERE 151.
- Larsen, L., 1996. Productivity computations for multilateral, branched, and other generalized and extended well concepts. In: Paper SPE 36754 Presented at the SPE Annual Technical Conference & Exhibition (6–9 October 1996), Denver, Colorado.
- Raghavan, R., Joshi, S.D., March 1993. Productivity of multiple drainholes or fractured horizontal wells. SPE Formation Evaluation 11–16.
- Retnanto, A., Economides, M.J., May 1996. Performance of multilateral horizontal well laterals in low- to medium-permeability reservoirs. SPE Reservoir Engineering 7–77.

Productivity of multifractured horizontal wells

Chapter outline

7.1 Introduction	183
7.2 Multifractured horizontal wells	185
7.2.1 Oil wells	185
7.2.2 Gas wells	189
7.3 Volume-fractured horizontal wells	190
7.3.1 Oil wells	191
7.3.2 Gas wells	192
7.4 Summary	194
7.5 Problems	194
References	196

7.1 Introduction

Some horizontal wells are purposely drilled in parallel to the direction of the minimum horizontal stress in the formation. This specific wellbore orientation allows multiple transverse fractures to be hydraulically created for enhancing productivity. Fig. 7.1 shows two regions of the reservoir. The inner region is the fractured region, and the outer region is the nonfractured region. Linear flow may exist initially before fractures begin to influence each other. Radial flow may prevail later if the drainage area is sufficiently large compared with the fractured region of the reservoir. Fig. 7.2 illustrates flow in the fracture near the wellbore. Flow convergence and the reduced fracture conductivity due to proppant loss and stress concentration cause well productivity to drop.

Raghavan and Joshi (1993) presented a mathematical model that can predict the productivities of horizontal wells with multiple transverse fractures. The model uses the effective wellbore radius (in radial flow) to simulate fluid flow toward the fractured well. Flow within the fracture itself was not considered.

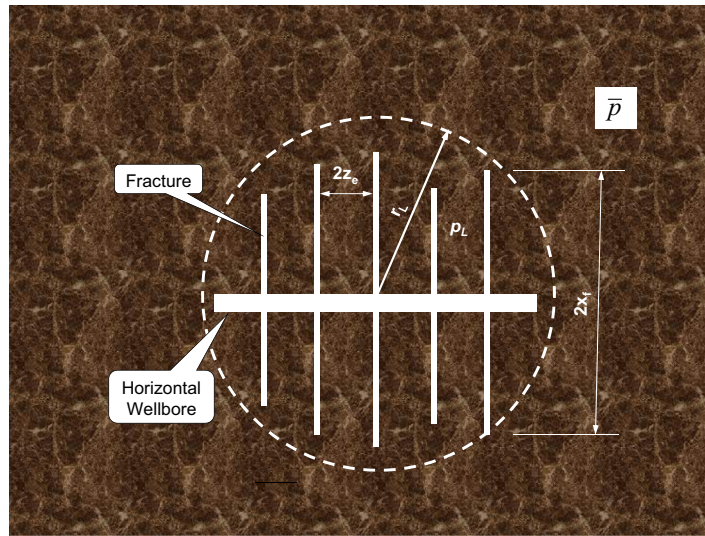


FIGURE 7.1

A reservoir section drained by a multifractured horizontal wellbore.

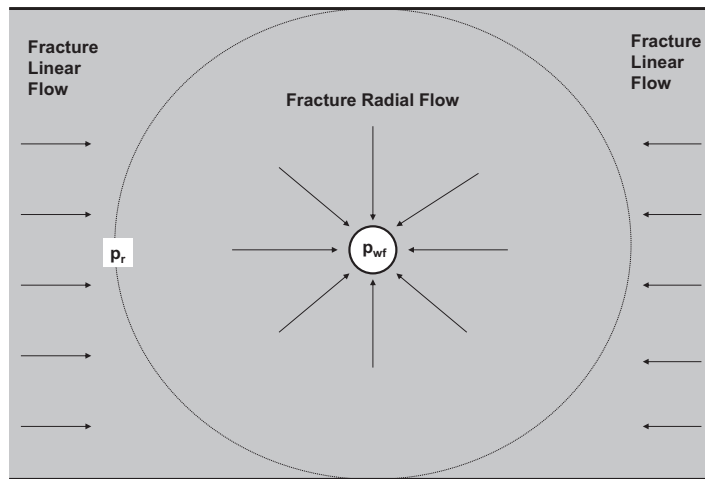


FIGURE 7.2

Fluid flow in a fracture to a horizontal wellbore.

Li et al. (1996) presented an analytical model for predicting productivities of horizontal wells with multiple transverse fractures. The model incorporates the following:

- Linear flow from the fractured reservoir region to the fractures
- Linear flow within the fractures
- Radial flow within the fractures to the horizontal wellbore
- Flow from the fractured region directly to the horizontal wellbore

Most fractured horizontal wells are drilled in low-permeability reservoirs in which fluid flow from the unfractured regions directly to the horizontal wellbore is often negligible. As demonstrated by Guo and Yu (2008), predictions of the long-term productivity of multifractured horizontal wells must consider the following sequence:

1. Reservoir radial flow within the drainage boundary to the fractured region of reservoir
2. Reservoir linear flow between fractures in the reservoir to the fracture faces
3. Fracture linear flow in the fracture to the near-wellbore region
4. Wellbore radial flow in the fracture to the wellbore, where a “choking” effect occurs

7.2 Multifractured horizontal wells

The multifractured horizontal wells considered in this section include those wells in tight oil and gas sands where long transverse fractures are created with multistage hydraulic fracturing techniques. They can be oil or gas wells.

7.2.1 Oil wells

Consider a reservoir characterized by pseudo–steady-state radial flow in the outer region (Fig. 7.1). The total oil flow rate can then be described by

$$q = \frac{7.08 \times 10^{-3} k_H h (\bar{p} - p_L)}{B_o \mu_o \left(\frac{1}{2} \ln \frac{4A}{\gamma C_A r_L^2} \right)} \quad (7.1)$$

where p_L is defined as the pressure at the outer boundary of the inner region and r_L is the equivalent radius of the inner region that can be estimated by

$$r_L = \sqrt{\frac{4n\bar{z}_e\bar{x}_f}{\pi}} \quad (7.2)$$

where \bar{z}_e and \bar{x}_f are the average half-distances between fractures and the average fracture half-length, respectively.

If the multifractured well is used to drain an entire reservoir characterized by physical no-flow boundaries, the drainage area shape factor C_A can be estimated based on reservoir shape and the location of the reservoir's inner region. If the multifractured well is employed to drain a portion of a reservoir, then the C_A should be estimated based on the shape of the drainage area, with the location of the inner region centered in the drainage area. The aspect ratio (length to width) of the drainage area may be taken as

$$R_A = \frac{n\bar{z}_e}{\bar{x}_f}$$

and the shape factor may be estimated as $C_A = 39.51 - 8.5214R_A$.

It is understood that this equation is valid only when the inner region is much smaller than the drainage area so that the argument of the logarithm is greater than unity.

For the reservoir-fracture cross-flow, [Guo and Schechter's \(1997\)](#) model, modified by [Guo and Yu \(2008\)](#), links reservoir linear flow and fracture linear flow. For uniformly distributed fractures, according to this model, the deliverability of n fractures can be expressed as

$$q = \sum_{i=1}^n \frac{4.5 \times 10^{-3} h}{B_o \mu \sqrt{c_i} \left[\frac{(z_{ei} - z_{si})}{k_H} + \frac{z_{si}}{k_{si}} \right]} \left(1 - e^{-\sqrt{c_i x_{fi}}} \right) (p_L - p_r) \quad (7.3)$$

where

$$c_i = \frac{24}{k_{fi} w_i \left[\frac{(z_{ei} - z_{si})}{k_H} + \frac{z_{si}}{k_{si}} \right]} \quad (7.4)$$

z_{ei} is half the distance between the i th and $(i+1)$ th fractures, z_{si} is the depth of the altered zone near the surface of fracture i , k_{si} is the permeability of the altered zone near the surface of fracture i , and p_r represents the pressure in the fracture before the onset of flow convergence to wellbore ([Fig. 7.2](#)).

The linear-radial flow model of [Furui et al. \(2003\)](#) can be used to couple the fracture linear flow and the fracture radial flow. According to this model, well deliverability through n uniformly distributed fractures can be expressed as

$$q = \sum_{i=1}^n \frac{5.9 \times 10^{-4} k_{fwi} w_{wi} (p_r - p_{wf})}{\mu_o B_o \left\{ \ln \left[\frac{h}{2r_{wi}} \right] + \pi - (1.224 - s_i - Dq) \right\}} \quad (7.5)$$

where p_{wf} is the flowing bottom-hole pressure. The k_{fwi} is the fracture permeability in the near-wellbore region and w_{wi} is the width of the i th fracture in the near-wellbore region. These two parameters, plus the non-Darcy flow coefficient D , can be used to simulate choked fractures.

Combining Eqs. (7.1–7.5) gives the reservoir deliverability equation:

$$q = \frac{1}{\left(\frac{1}{J_R} + \frac{1}{J_L} + \frac{1}{J_r}\right)} (\bar{p} - p_{wf}) \quad (7.6)$$

where

$$J_R = \frac{7.08 \times 10^{-3} k_H h}{B_o \mu_o \left(\frac{1}{2} \ln \frac{4A}{\gamma C_A r_L^2}\right)} \quad (7.7)$$

$$J_L = \sum_{i=1}^n \frac{4.5 \times 10^{-3} h}{B_o \mu \sqrt{c_i} \left[\frac{(z_{ei} - z_{si})}{k_H} + \frac{z_{si}}{k_{si}}\right]} (1 - e - \sqrt{c_i x_{fi}}) \quad (7.8)$$

$$J_r = \sum_{i=1}^n \frac{5.9 \times 10^{-4} k_{fwi} w_{wi}}{\mu_o B_o \left\{ \ln \left[\frac{h}{2r_{wi}} \right] + \pi - (1.224 - s_i - Dq) \right\}} \quad (7.9)$$

The tubing performance relationship of multifractured wells can be modeled using different correlations, depending on the fluid type. The Hagedorn–Brown correlation will be used in the following sample calculations.

7.1 Sample problem

From the data given below, assuming no formation damage near the fractures and that the tubing string is set just above the pay zone, predict the pseudo-steady-state production rate:

Fracture spacing ($2z_e$):	1000	ft
Fracture half-length (x_f):	1000	ft
Fracture permeability (k_f):	50,000	md
Oil bubble-point pressure (p_b):	5000	psia
Effective horizontal permeability (k):	10	md
Pay zone thickness (h):	60	ft
Average reservoir pressure (p_{bar}):	4000	psia
Oil formation volume factor (B_o):	1.2	rb/stb
Well drainage area (A):	320	acres
Well radius (r_w):	0.328	ft
Fracture width (w):	0.3	in
Well vertical depth (H):	8000	ft
Tubing inner diameter (d):	4	in
Oil gravity (API):	40	API
Oil viscosity (μ_o):	1.5	cp

Producing gas–liquid ratio (GLR):	500	scf/bbl
Gas-specific gravity (γ_g):	0.7	Air = 1
Flowing tubing head pressure (p_{hf}):	800	psia
Flowing tubing head temperature (t_{hf}):	150	$^{\circ}\text{F}$
Flowing temperature at tubing shoe (t_{wf}):	180	$^{\circ}\text{F}$
Water cut (WC):	10	%
Near-wellbore fracture width (w_w):	0.2	in
Total skin factor (S):	0	
Number of fractures (n):	4	
Near-wellbore fracture permeability (k_{fw}):	50,000	md

Solution

This problem can be solved using the spreadsheet program **Pseudosteady Production of Multi-Fractured Well.xls**. Fig. 7.3 indicates that the expected liquid production rate is 1700 stb/day at a flowing bottom-hole pressure of 1900 psia.

It can be shown that the productivity of multifractured wells does not increase in proportion to the number of fractures. This is left to the reader to determine as an exercise using the spreadsheet.

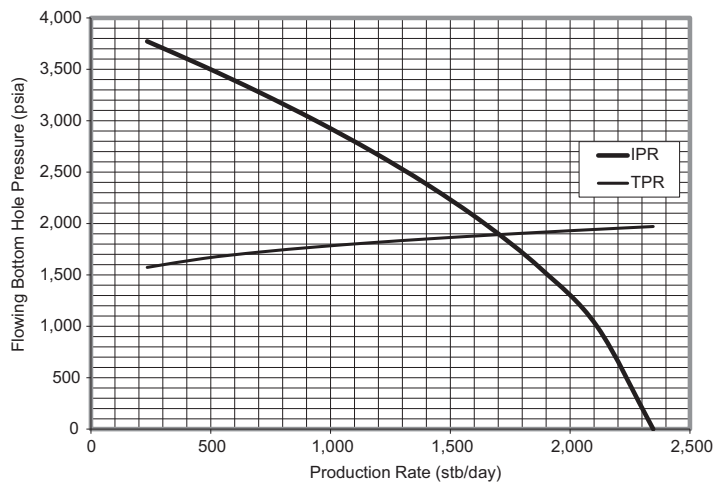


FIGURE 7.3

Curves given by spreadsheet program Pseudosteady Production of Multi-Fractured Well.xls. *IPR*, inflow performance relationship; *TPR*, tubing performance relationship.

7.2.2 Gas wells

Similar to oil wells, the total gas flow rate can then be described by

$$q = \frac{k_H h (\bar{p}^2 - p_{PL}^2)}{1424 \bar{\mu}_g \bar{z} T \left(\frac{1}{2} \ln \frac{4A}{\gamma C_A r_{PL}^2} \right)} \quad (7.10)$$

Guo and Yu (2008) links reservoir linear flow and fracture linear flow. For uniformly distributed fractures, according to this model, the deliverability of n fractures can be expressed as

$$q = \sum_{i=1}^n \frac{4.475 \times 10^{-4} h}{\bar{\mu}_g \bar{z} T \sqrt{c_i} \left[\frac{(z_{ei} - z_{si})}{k_H} + \frac{z_{si}}{k_{si}} \right]} \left(1 - e^{-\sqrt{c_i} x_{fi}} \right) (p_L^2 - p_r^2) \quad (7.11)$$

The linear-radial flow model of Furui et al. (2003) can be used to couple the fracture linear flow and the fracture radial flow. According to this model, well deliverability through n uniformly distributed fractures can be expressed as

$$q = \sum_{i=1}^n \frac{5.85 \times 10^{-5} k_{fwi} w_{wi} (p_r^2 - p_{wf}^2)}{\bar{z} \bar{\mu}_g T \left\{ \ln \left[\frac{h}{2r_{wi}} \right] + \pi - (1.224 - s_i - Dq) \right\}} \quad (7.12)$$

Combining Eqs. (7.10–7.12) gives the reservoir deliverability equation:

$$q = \frac{1}{\left(\frac{1}{J_R} + \frac{1}{J_L} + \frac{1}{J_r} \right)} (\bar{p}^2 - p_{wf}^2) \quad (7.13)$$

where

$$J_R = \frac{k_H h}{1424 \bar{z} \bar{\mu}_g T \left(\frac{1}{2} \ln \frac{4A}{\gamma C_A r_L^2} \right)} \quad (7.14)$$

$$J_L = \sum_{i=1}^n \frac{4.475 \times 10^{-4} h}{\bar{\mu}_g \bar{z} T \sqrt{c_i} \left[\frac{(z_{ei} - z_{si})}{k_H} + \frac{z_{si}}{k_{si}} \right]} \left(1 - e^{-\sqrt{c_i} x_{fi}} \right) \quad (7.15)$$

$$J_r = \sum_{i=1}^n \frac{5.85 \times 10^{-5} k_{fwi} w_{wi}}{\bar{z} \bar{\mu}_g T \left\{ \ln \left[\frac{h}{2r_{wi}} \right] + \pi - (1.224 - s_i - Dq) \right\}} \quad (7.16)$$

The tubing performance relationship of multifractured wells can be modeled using different correlations appropriate to the fluid type. Guo–Ghalambor's four-phase flow model may be used.

7.3 Volume-fractured horizontal wells

Volume fracturing is a special technique of multistage hydraulic fracturing where a large volume of fracturing fluids is pumped into closely spaced perforation clusters along a horizontal wellbore at high pressure and high flow rate. This technique is widely used for fracturing horizontal wells in unconventional oil and gas reservoirs, especially shale oil and gas reservoirs. Volume fracturing creates multiple fractures and fracture branches in the reservoir volume near the horizontal wellbore owing to the failure of brittle shale formations. Prediction of productivity of volume-fractured horizontal wells is difficult because the distribution of fractures and fracture branches is not known. Oil and gas production of the volume-fractured horizontal wells is believed to be mainly from the stimulated reservoir volume (SRV). If the fractures and fracture branches from a given perforation cluster are defined as a fracture trend, well productivity can be described using analytical models.

Volume fracturing is carried out on horizontal wells in multiple stages separated by packers. A few clusters of perforations are created in each stage. The explosive energy during perforating should induce microcracks from the perforations. When fracturing fluid is forced to go through the perforations, multiple fractures may be initiated from the microcracks. The orientations of the fractures in the near-wellbore area are complicated because the wellbore and perforations alter the state of stress in this area as depicted in Fig. 7.4 (Guo et al., 2017). A number of fracture propagation mechanisms may exist. Fractures may reorientate from the perforations toward preferred fracture planes owing to stress anisotropy. Fractures may also interact with and dilate natural fracture if the latter exists. As a result, multiple

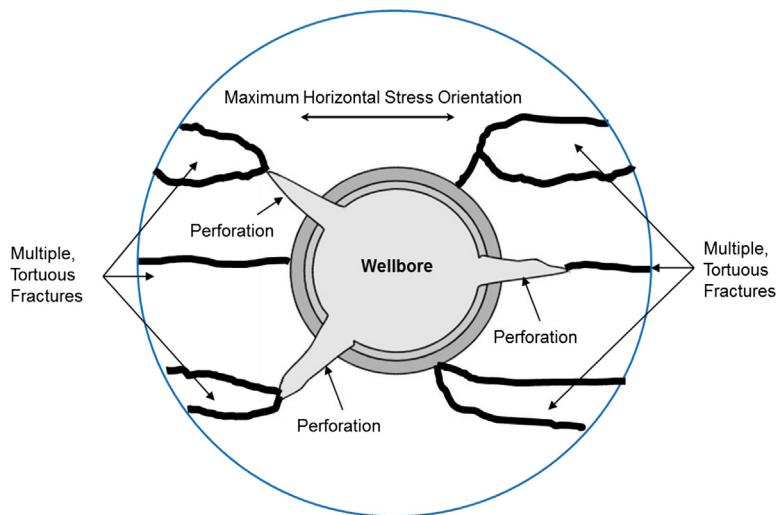


FIGURE 7.4

Tortuous fractures in the near-wellbore area (Guo et al., 2017).

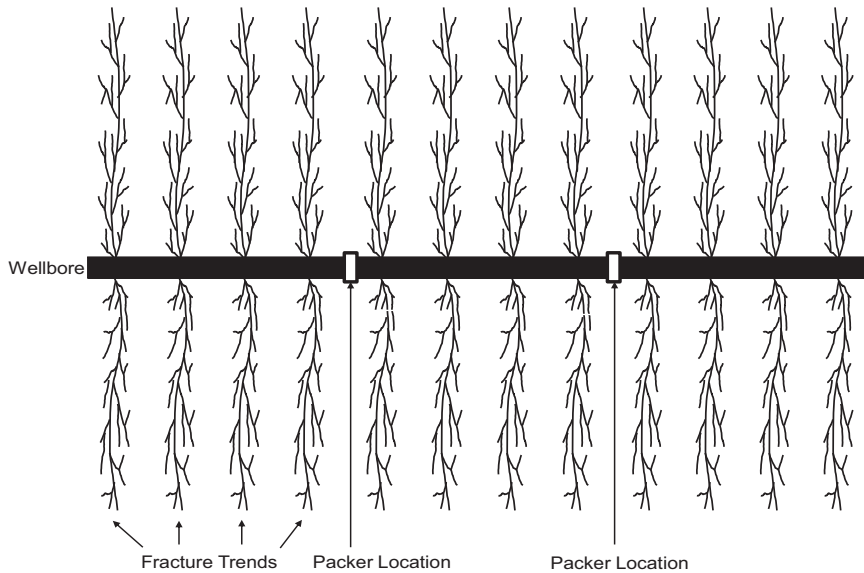


FIGURE 7.5

Twelve fracture trends developed from 12 perforation clusters in three stages of fracturing.

and tortuous fractures are anticipated in the near-wellbore area. When these initial fractures propagate away from the near-wellbore area, they may converge or diverge depending on stress field and natural fractures. A single fracture may develop branches due to shale heterogeneities. All the fractures initiated from a perforation cluster should form a fracture trend in the direction of the maximum horizontal stress to achieve the minimum strain energy in the shale. Twelve fracture trends created from 12 perforation clusters are depicted in Fig. 7.5. Fracture spacing is defined as the distance between the centerlines of two adjoined fracture trends which is expected to be equal to the distance between the two adjoined perforation clusters.

7.3.1 Oil wells

Unlike conventional multifractured horizontal wells that experience reservoir linear flow in the inner region and pseudoradial flow in the outer region, volume-fractured horizontal wells normally experience boundary-dominated flow in the SRV. The mathematical model presented by Li et al. (2019) may be used for predicting the initial productivity of volume-fractured horizontal oil wells:

$$Q_o = \frac{5.91 \times 10^{-3} n_f k_m h_f (\bar{p} - p_w)}{B_o \mu_o S_f \sqrt{c} \left(\frac{1}{1 - e^{-\sqrt{c} x_f}} - \frac{1}{3 x_f \sqrt{c}} \right)} \quad (7.17)$$

where c is expressed as

$$c = \frac{96k_m}{k_f w S_f} \quad (7.18)$$

where Q_o is the oil production rate in stb/d, n_f is the number of perforation clusters (hydraulic fracture trends), k_m is the matrix permeability in md, h_f is the fracture trend height in ft, \bar{p} is the average formation pressure in psia, p_w is the wellbore pressure in psia, μ_o is the gas viscosity in cp, B_o is the oil formation factor in rb/stb, S_f is the fracture trend spacing in ft, e is the exponential function, x_f is the fracture trend half-length in ft, k_f is the fracture trend permeability in md, and w is the average fracture trend net-width in inch.

7.2 Sample problem

From the data given below for a volume-fractured horizontal oil well, predict the initial oil production rate:

Pay zone thickness	135	ft
Shale porosity	0.15	
Shale permeability	0.0001–0.01	md
Reservoir pressure	6,000	psi
Oil formation volume factor	1.5	rb/stb
Oil viscosity	0.5	cp
Total compressibility	0.00001	psi ⁻¹
Number of perforation clusters	993	
Perforation cluster spacing	5–75	ft
Fracture trend half-length	300	ft
Fracture trend height	101	ft
Fracture trend permeability	1500	md
Volume of proppant	1000	ft ³
Wellbore pressure	4000	psi

Solution

This problem can be solved using the spreadsheet program **Volume-Fractured Oil Well.xls**. Fig. 7.6 shows that well productivity can be greatly improved when the fracture spacing (perforation cluster spacing) is reduced.

7.3.2 Gas wells

Li et al.'s (2019) analytical model may be used for predicting the initial productivity of volume-fractured horizontal gas wells under boundary-dominated flow conditions:

$$Q_g = \frac{5.87 \times 10^{-5} n_f k_m h (\bar{p}^2 - p_w^2)}{\mu T S_f \sqrt{c} \left[\frac{1}{1 - e^{-\sqrt{c} x_f}} - \frac{1}{3 x_f \sqrt{c}} \right]} \quad (7.19)$$

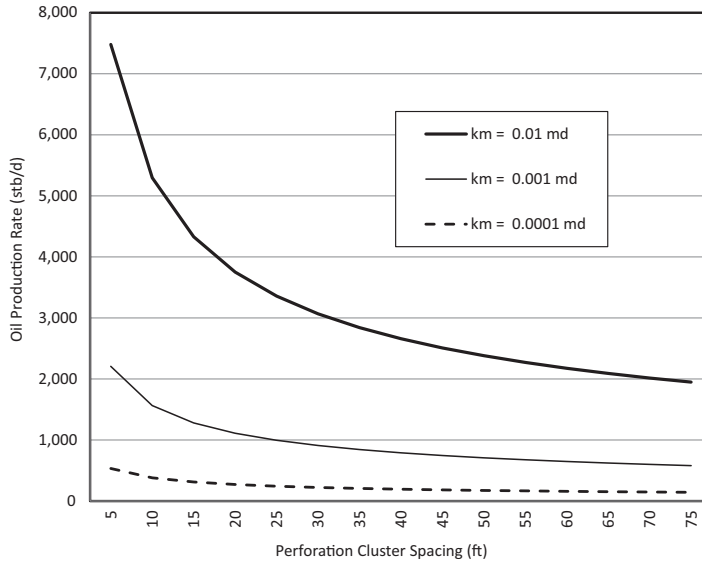


FIGURE 7.6

Model-predicted well productivity curves for a volume-fractured horizontal oil well given by spreadsheet program Volume-Fractured Oil Well.xls.

where Q_g is the gas production rate in Mscf/d, T is the formation temperature in $^{\circ}\text{R}$, and c is still given by Eq. (7.18).

7.3 Sample problem

From the data given below for a volume-fractured horizontal gas well, predict the initial production rate:

Pay zone thickness	300	ft
Shale permeability	0.00001–0.001	md
Reservoir pressure	6000	psi
Reservoir temperature	560	R
Gas viscosity	0.01	cp
Number of fractures	20	ft
Fracture half-length	500	ft
Fracture height	300	ft
Fracture permeability	1000	md
Volume of proppant	1000	ft ³
Wellbore pressure	2,000	psi

Solution

This problem can be solved using the spreadsheet program **Volume-Fractured Gas Well.xls**. Fig. 7.7 shows the result indicating that well productivity can be significantly enhanced when the fracturing spacing (perforation cluster spacing) is reduced.

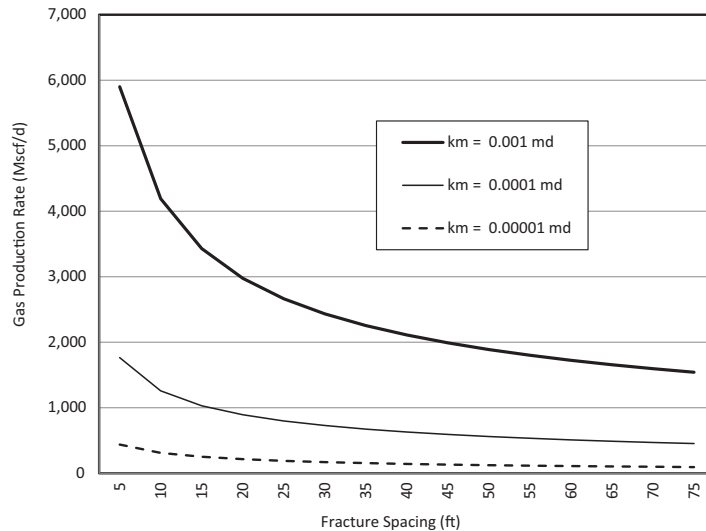


FIGURE 7.7

Model-predicted well productivity curves for a volume-fractured horizontal gas well given by spreadsheet program Volume-Fractured Gas Well.xls.

7.4 Summary

This chapter presented methods for predicting the productivities of fractured horizontal wells including multifractured horizontal wells in tight oil and gas sands and volume-fractured horizontal wells in unconventional shale gas and oil reservoirs. Productivity of conventional multifractured horizontal wells depends on fracture-reservoir cross-linear flow and pseudoradial flow in the drainage area. Productivity of unconventional volume-fractured horizontal wells is controlled by the boundary-dominated flow in the SRV. Reducing fracture spacing (perforation cluster spacing) can significantly enhance well productivity.

7.5 Problems

7.1 From the data given below, and assuming that the tubing string is set just above the pay zone, predict the pseudo—steady-state production rate of the oil well:

Fracture spacing ($2z_e$):	1200	ft
Fracture half-length (x_f):	800	ft
Fracture permeability (k_f):	40,000	md
Oil bubble-point pressure (p_b):	4000	psia
Effective horizontal permeability (k):	20	md
Pay zone thickness (h):	40	ft

Average reservoir pressure (p_{-bar}):	3000	psia
Oil formation volume factor (B_o):	1.2	rb/stb
Well drainage area (A):	320	acres
Well radius (r_w):	0.328	ft
Fracture width (w):	0.3	in
Well vertical depth (H):	6000	ft
Tubing inner diameter (d):	3.5	in
Oil gravity (API):	40	API
Oil viscosity (μ_o):	1.2	cp
Producing gas—liquid ratio (GLR):	800	scf/bbl
Gas-specific gravity (γ_g):	0.65	air = 1
Flowing tubing head pressure (p_{ht}):	600	psia
Flowing tubing head temperature (t_{ht}):	120	°F
Flowing temperature at tubing shoe (t_{wt}):	150	°F
Water cut (WC):	15	%
Near-wellbore fracture width (w_w):	0.2	in
Total skin factor (S):	1	
Number of fractures (n):	5	
Near-wellbore fracture permeability (k_{fw}):	50,000	md

7.2 From the data given below for a volume-fractured horizontal oil well, predict and plot the initial oil production rate curves:

Pay zone thickness	115	ft
Shale porosity	0.12	
Shale permeability	0.0001–0.01	md
Reservoir pressure	9,000	psi
Oil formation volume factor	1.8	rb/stb
Oil viscosity	0.5	cp
Total compressibility	0.00001	psi ⁻¹
Number of perforation clusters	800	
Perforation cluster spacing	5–60	ft
Fracture trend half-length	200	ft
Fracture trend height	100	ft
Fracture trend permeability	1500	md
Volume of proppant	2000	ft ³
Wellbore pressure	6,500	psi

7.3 From the data given below for a volume-fractured horizontal gas well, predict and plot the initial production rate curves:

Pay zone thickness	200	ft
Shale permeability	0.00001–0.001	md
Reservoir pressure	7000	psi
Reservoir temperature	550	R
Gas viscosity	0.01	cp
Number of fractures	30	ft
Fracture half-length	400	ft
Fracture height	200	ft
Fracture permeability	1500	md

Volume of proppant	2000	ft ³
Fracture spacing	15–75	ft
Wellbore pressure	4000	psi

References

- Guo, B., Liu, X., Tan, X., 2017. *Petroleum Production Engineering*, second ed. Elsevier, Cambridge.
- Guo, B., Schechter, D.S., 1997. A simple and rigorous mathematical model for estimating inflow performance of wells intersecting long fractures. In: Paper SPE 38104 Presented at the SPE Asia Pacific Oil and Gas Conference and Exhibition (14–16 April 1997). Kuala Lumpur, Malaysia.
- Guo, B., Yu, X., 2008. A simple and accurate mathematical model for predicting productivity of multifractured horizontal wells. In: Paper SPE 114452 Presented at the CIPC/SPE Gas Technology Symposium 2008 Joint Conference (16–19 June 2008). Canada, Calgary.
- Furui, K, Zhu, D, Hill, AD, Aug 2003. A rigorous formation damage skin factor and reservoir inflow model for a horizontal well. *SPE production & Facilities* 18 (03), 151–157.
- Li, G., Guo, B., Li, J., Wang, M., January 2019. A mathematical model for predicting long-term productivity of modern multifractured shale gas/oil wells. *SPE Drilling and Completion Journal*. <https://doi.org/10.2118/194495-PA>.
- Li, H., Jia, Z., Wei, Z., 1996. A new method to predict performance of fractured horizontal wells. In: Paper SPE 37051 Presented at the SPE International Conference on Horizontal Well Technology (18–20 November 1996), Calgary, Canada.
- Raghavan, R., Joshi, S.D., March 1993. Productivity of multiple drainholes or fractured horizontal wells. *SPE Formation Evaluation* 11–16.

Productivity of radial-fractured wells

8

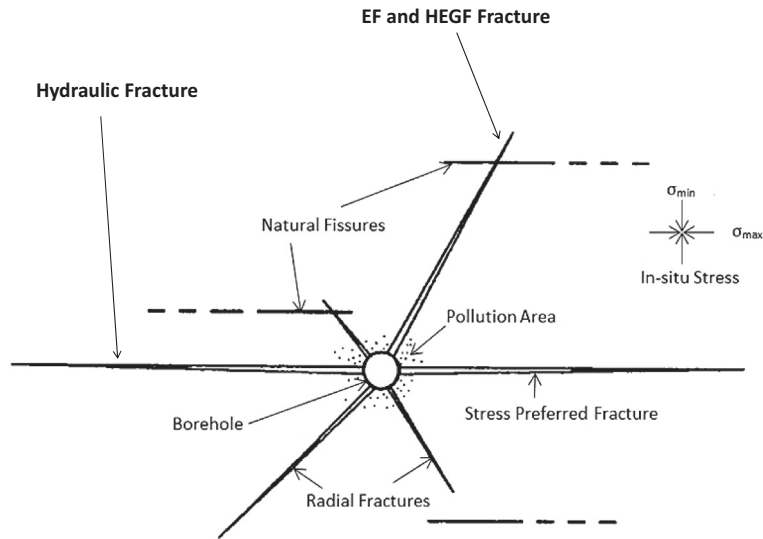
Chapter outline

8.1 Introduction	197
8.2 Steady-state production	199
8.2.1 Radial-fractured oil wells	199
8.2.2 Radial-fractured gas wells	200
8.3 Pseudo–steady-state production	201
8.3.1 Radial-fractured oil wells	201
8.3.2 Radial-fractured gas wells	202
8.4 Summary	203
8.5 Problems	203
References	204

8.1 Introduction

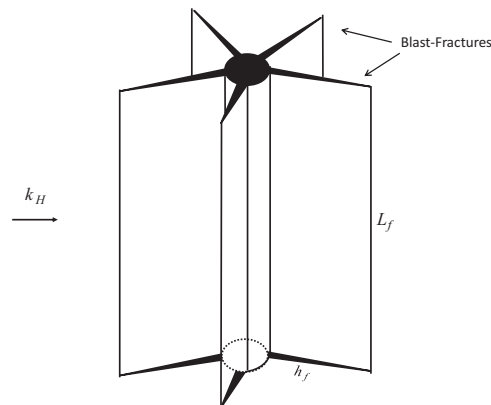
Fractures can be initiated at wellbore and propagated in the radial direction in some well completion and stimulation operations. Such operations include blast or explosive fracturing, high-energy gas fracturing (HEGF), and hydraulic refracturing treatment of oil and gas wells.

Hydraulic fracturing releases energy in minutes, generating pressures up to 5000 psi. The low rate of energy release allows hydraulic fractures to propagate in a single direction perpendicular to the minimum formation stress, not crossing low-permeability streaks (Fig. 8.1). This limits the areal coverage of reservoir in the near-wellbore region by the fractures and thus well productivity. Explosive blast releases energy in microseconds, generating pressures of over 1,000,000 psi (Jaimes Plata et al., 2012). Blast fracturing in wellbore creates radial fractures regardless of formation stresses and heterogeneities. The radial fractures can connect formation streaks with flow channels, and then, if desired, these streaks may be hydraulically fractured through these flow channels (Eakin and Miller, 1967). The fracture distance has been found to be proportional to the cubic root of the weight of the explosives. The coefficient of proportionality is rock-type-dependent, 5 for sandstone and 7 for limestone. A 3-lb nitroglycerin explosive can produce a fracture of only 10.8 ft in limestone (Dysart et al., 1969). HEGF releases energy in milliseconds, generating pressures over 20,000 psia (Jaimes Plata et al., 2012). It creates relatively longer

**FIGURE 8.1**

Radial propagation of fractures in EF and HEGF (Levey, 1967). *EF*, explosive fracturing; *HEGF*, high-energy gas fracturing.

radial fractures and thus higher well productivity than blast fracturing. This technology has gained momentum in recent years (Li et al., 2018). Fig. 8.2 depicts radial fractures created in explosive blast and HEGF operations. Radial fractures also exist in hydraulic refractured oil and gas wells (Shan et al., 2018). As illustrated in Fig. 8.3, hydraulic refracturing usually creates four radial fractures with or without right angles.

**FIGURE 8.2**

A sketch of radial fractures created in blast fracturing (Guo et al., 2014).

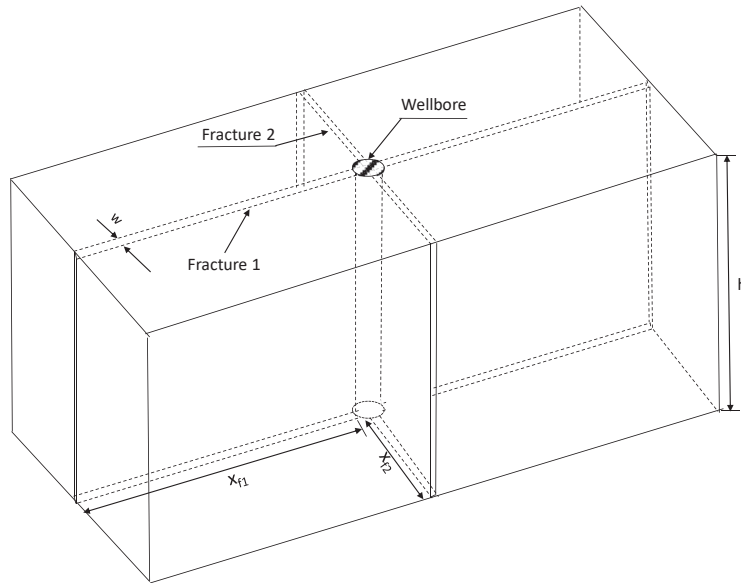


FIGURE 8.3

A sketch of radial fractures created in hydraulic re-fracturing (Shan et al., 2018).

8.2 Steady-state production

Radial-fractured wells produce oil under steady-state flow condition when they are surrounded by water injection wells or active aquifers. Gas wells normally do not produce under steady-state flow condition unless the well is very close to very active aquifers. Guo et al. (2014) presented a closed-form solution for steady productivity of blast-fractured wells in liquid-rich shale gas formations. Derivation of the solution is briefly summarized in Appendix F.

8.2.1 Radial-fractured oil wells

Assuming that radial fractures have infinite conductivities, Guo et al. (2014) showed that, for vertical oil wells, production rate under steady-state condition is expressed as follows:

$$Q_o = \frac{2.255 \times 10^{-3} n k_H L_f (p_e - p_f)}{\mu_o B_o \tan\left(\frac{\pi}{n}\right)} \ln\left(\frac{r_w + h_f}{r_w}\right) \quad (8.1)$$

where Q_o is the oil production rate in stb/d, n is the number of identical fractures created in a single borehole, k_H is the horizontal permeability in md, L_f is the

fracture length which is assumed to be equal to the length of wellbore packed with explosives, p_e is the reservoir pressure at outer boundary in psia, p_f is the pressure in the fracture in psia (same pressure in the wellbore), r_w is the wellbore radius in ft, h_f is the fracture penetration in ft, μ_o is the liquid viscosity in cp, and B_o is the formation volume factor in rb/stb. The values of the number of fractures and fracture penetration may be predicted using commercial software such as LS-DYNA. For horizontal oil wells, the horizontal oil permeability k_H should be replaced by the mean permeability $\bar{k} = \sqrt{k_H k_V}$ where k_V is vertical oil permeability.

8.2.2 Radial-fractured gas wells

Guo et al.'s (2014) solution for productivity of blast-fractured gas wells takes a closed-form if radial fractures have infinite conductivity. For vertical gas wells, production rate under steady-state condition is expressed as

$$Q_g = \frac{2.24 \times 10^{-4} n k_H L_f (p_e^2 - p_f^2)}{\mu_g z T \tan\left(\frac{\pi}{n}\right)} \ln\left(\frac{r_w + h_f}{r_w}\right) \quad (8.2)$$

where Q_g is the natural gas production rate in Mscf/d, μ_g is the gas viscosity in cp, z is the gas compressibility factor in psi^{-1} , and T is the reservoir temperature in $^{\circ}\text{F}$. For horizontal gas wells, the horizontal gas permeability k_H should be replaced by the mean permeability $\bar{k} = \sqrt{k_H k_V}$ where k_V is vertical gas permeability.

8.1 Sample problem

From the data given below for a blast-fractured vertical oil well, plot productivity index versus fracture penetration:

Horizontal permeability (k_H)	0.01	md
Permeability anisotropy ratio (k_V/k_H)	1	
Liquid viscosity (μ_o)	0.5	cp
Liquid formation volume factor (B_o)	1.5	rb/stb
Wellbore radius (r_w)	7.875	in
Fracture length (L_f)	200	ft
Fracture penetration (h_f)	5–35	ft
Number of identical fractures (n)	6	

Solution

This problem can be solved with Eq. (8.1). The result is given in Fig. 8.4, which indicates that the effect of fracture penetration on the well productivity of blast-fractured wells levels off as the fracture penetration increases.

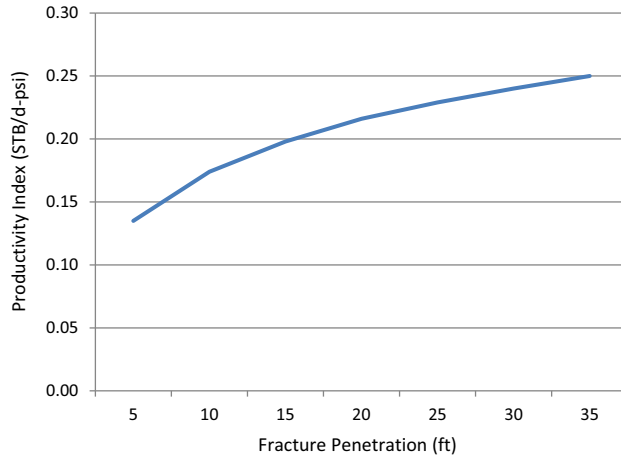


FIGURE 8.4
Effect of fracture penetration on productivity index of a blast-fractured oil well.

8.3 Pseudo—steady-state production

Radial-fractured wells produce oil and gas under pseudo—steady-state flow condition when they are surrounded by other production wells or sealing faults. Li et al. (2018) presented a sophisticated mathematical model to predict productivity of radial-fractured wells considering fractures of finite conductivity. Derivation of the model is shown in Appendix F.

8.3.1 Radial-fractured oil wells

Li et al.’s (2018) mathematical model takes the following form for radial-fractured oil wells:

$$Q_o = \frac{5.51 \times 10^{-3} n \bar{k} L_f}{\mu \tan(\alpha)} \int_{r_w}^{h_f} \frac{p_d}{x} dx \tag{8.3}$$

where

$$p_d = C_1 \sqrt{x} J_1(2i\sqrt{c} \sqrt{x}) + C_2 \sqrt{x} N_1(2i\sqrt{c} \sqrt{x}) \tag{8.4}$$

where J_1 is the Bessel function of the first kind in the order of 1 and N_1 is the Bessel function of the second kind in the order of 1. The constants C_1 and C_2 are determined based on the boundary conditions to be

$$C_1 = -\frac{p_d^* T_{12}}{T_{02} T_{11} - T_{12} T_{01}} \tag{8.5}$$

$$C_2 = \frac{p_d^* T_{11}}{T_{02} T_{11} - T_{12} T_{01}} \quad (8.6)$$

where

$$p_d^* = \bar{p} - p_w \quad (8.7)$$

$$T_{01} = \sqrt{r_w} J_1(2i\sqrt{c} \sqrt{r_w}) \quad (8.8)$$

$$T_{02} = \sqrt{r_w} N_1(2i\sqrt{c} \sqrt{r_w}) \quad (8.9)$$

$$T_{11} = \sqrt{h_f} J_1(2i\sqrt{c} \sqrt{h_f}) \quad (8.10)$$

$$T_{12} = \sqrt{h_f} N_1(2i\sqrt{c} \sqrt{h_f}). \quad (8.11)$$

where \bar{p} is the average reservoir pressure in psia and p_w is wellbore pressure.

8.3.2 Radial-fractured gas wells

According to Li et al. (2018), the pseudosteady production of radial-fractured gas well is expressed as

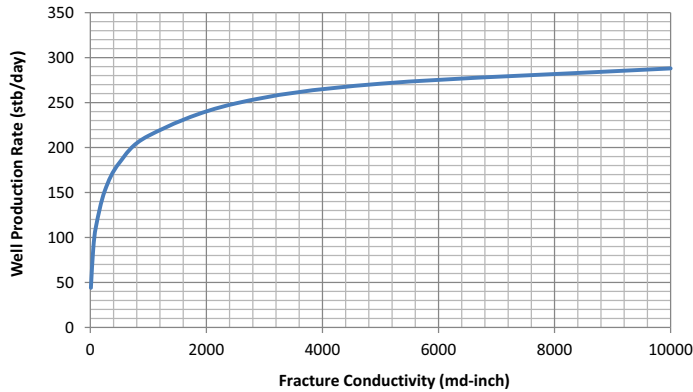
$$Q_g = \frac{4.48 \times 10^{-4} n \bar{k} L_f (\bar{p} + p_w)}{\mu_g z T \tan(\alpha)} \int_{r_w}^{h_f} \frac{p_d}{x} dx \quad (8.12)$$

where Q_g is the natural gas production rate in Mscf/d, μ_g is the gas viscosity in cp, z is the gas compressibility factor in psi^{-1} , T is the reservoir temperature in $^{\circ}\text{F}$, and p_d is still given by Eq. (8.4).

8.2 Sample problem

From the data given below for an HEGF vertical oil well, plot well production rate versus fracture conductivity:

Horizontal permeability:	0.08	md
Fluid viscosity:	0.01	cp
Wellbore radius:	0.328	ft
Number of fractures:	4	
Fracture length:	20	ft
Fracture depth:	4.5	ft
Fracture width:	0.1	inch
Fracture permeability:	1000	md
Reservoir pressure:	12472	psia
Wellbore pressure:	5339	psia
Formation temperature:	80	F
Z-factor:	1.1	

**FIGURE 8.5**

Effect of fracture conductivity on productivity of a high-energy gas fracturing oil well.

Solution

This problem can be solved with spreadsheet program *HEGF-Prod.xlsx*. The result is given in Fig. 8.5, which indicates that the effect of fracture conductivity on the well productivity levels off as the fracture conductivity increases.

8.4 Summary

This chapter presented methods for predicting the productivities of radial-fractured oil and gas wells under steady-state and pseudo–steady-state flow conditions. The method can be applied to both vertical and horizontal radial-fractured wells. Example calculations show that well productivity levels out as fracture penetration and conductivity increase.

8.5 Problems

8.1 From the data given below for a blast-fractured horizontal oil well, assuming infinite fracture conductivity, predict oil production rate:

Horizontal permeability (k_H)	0.01	md
Permeability anisotropy ratio (k_V/k_H)	0.3	
Liquid viscosity (μ_o)	0.8	cp
Liquid formation volume factor (B_o)	1.4	rb/stb
Wellbore radius (r_w)	7.875	in
Fracture length (L_f)	500	ft
Fracture penetration (h_f)	10	ft
Number of identical fractures (n)	4	
Reservoir pressure (p_e)	5000	psi
Wellbore/fracture pressure (p_w)	3000	psi

8.2 From the data given below for an HEGF vertical gas well, predict gas production rate:

Horizontal permeability	0.05	md
Fluid viscosity	0.01	cp
Wellbore radius	0.328	ft
Number of fractures	6	
Fracture length	15	ft
Fracture depth	6	ft
Fracture width	0.1	inch
Fracture permeability	2000	md
Reservoir pressure:	10,000	psia
Wellbore pressure	6,000	psia
Formation temperature	90	F
Z-factor	0.95	

References

- Dysart, G.R., Spencer, A.M., Anderson, A.L., April 1969. Blast-fracturing. In: Paper Presented at the Spring Meeting of the Mid-continent District, API Division of Production.
- Eakin, J.L., Miller, J.S., November 1967. Explosives research to improve flow through low permeability rock. *Journal of Petroleum Technology* 1431.
- Guo, B., Shan, J., Feng, Y., April 14, 2014. Productivity of blast-fractured wells in liquid-rich shale gas formations. *Journal of Natural Gas Science and Engineering* 18C, 360–367. <https://doi.org/10.1016/j.jngse.2014.03.018>.
- Jaimes Plata, M., Castillo, R.D., Mendoza, S.A., January 1, 2012. High energy gas fracturing: a technique of hydraulic prefracturing to reduce the pressure losses by friction in the near wellbore - a Colombian field application. Society of Petroleum Engineers. <https://doi.org/10.2118/152886-MS>.
- Levey, D., August 1967. Explosive Stimulation Report. The Western Company Publication, Report.
- Li, J., Cao, L., Guo, B., Zhang, X., 2018. Prediction of productivity of high energy gas-fractured oil wells. *Journal of Petroleum Science and Engineering* 160, 510–518.
- Shan, L., Guo, B., Weng, D., Liu, Z., Chu, H., 2018. Posteriori assessment of fracture propagation in re-fractured vertical oil wells by pressure transient analysis. *Journal of Petroleum Science and Engineering* 168, 8–16.

Unit conversion factors

A

Quantity	US field unit	To SI unit	To US field unit	SI unit
Length	Feet (ft)	0.3084	3.2808	meter (m)
	Mile (mi)	1.609	0.6214	Kilometer (km)
	Inch (in)	25.4	0.03937	Millimeter (mm)
Mass	Ounce (oz)	28.3495	0.03527	Gram (g)
	Pound (lb)	0.4536	2.205	Kilogram (kg)
	lbm	0.0311	32.17	Slug
Volume	Gallon (gal)	0.003785	264.172	Meter ³ (m ³)
	Cubic feet (ft ³)	0.028317	35.3147	Meter ³ (m ³)
	Barrel (bbl)	0.15899	6.2898	Meter ³ (m ³)
	Mcf (1000 ft ³ , 60°F, 14.7 psia)	28.317	0.0353	Nm ³ (15°C, 101.325 kPa)
Area	Square feet (ft ²)	9.29×10^{-2}	10.764	Meter ² (m ²)
	acre	4.0469×10^3	2.471×10^{-4}	Meter ² (m ²)
	sq mile	2.59	0.386	(km) ²
Pressure	lb/in ² (psi)	6.8948	0.145	kPa (1000 Pa)
	psi	0.068	14.696	Atm
	psi/ft	22.62	0.0442	kPa/m
	inch Hg	3.3864×10^3	0.2953×10^{-3}	Pa
Temp.	F	0.5556 (F-32)	1.8C+ 32	C
	Rankine (°R)	0.5556	1.8	Kelvin (K)
Energy (work)	Btu	252.16	3.966×10^{-3}	cal
	Btu	1.0551	0.9478	Kilojoule (kJ)
	ft-lbf	1.3558	0.73766	Joule (J)
	hp-hr	0.7457	1.341	kW-hr
Viscosity (μ)	cp	0.001	1000	Pa·s
	lb/ft·sec	1.4882	0.672	kg/(m·sec) or (Pa·s)
	lbf-s/ft ²	479	0.0021	dyne-s/cm ² (poise)
Density (ρ)	lbm/ft ³	16.02	0.0624	kg/m ³
Permeability (k)	md	0.9862	1.0133	mD (=10 ⁻¹⁵ m ²)
	md (=10 ⁻³ darcy)	9.8692×10^{-16}	1.0133×10^{15}	m ²

Minimum performance
properties of API tubing

B

Nom., in	Outside diameter (OD), in	Grade	Weight per feet With couplings, lb		Inside diameter, in	Drift diameter, in	OD of upset, in	OD of c, in		Collapse resistance, psi	Internal yield pressure, psi	Joint yield strength, llb	
			Non upset	Upset				Non upset	Upset			Non upset	Upset
3/4	1.050	F-25	—	1.20	0.824	0.730	1.315	—	1.660	5960	4710	—	8320
		H-40	—	1.20	0.824	0.730	1.315	—	1.660	7680	7530	—	13,300
		J-55	—	1.20	0.824	0.730	1.315	—	1.660	10,560	10,360	—	18,290
		C-75	1.14	1.20	0.824	0.730	1.315	1.313	1.660	14,410	14,120	11,920	24,950
		N-80	—	1.20	0.824	0.730	1.315	—	1.660	15,370	15,070	—	26,610
1	1.315	F-25	—	1.80	1.049	0.955	1.469	—	1.900	5540	4430	—	12,350
		H-40	—	1.80	1.049	0.955	1.469	—	1.900	7270	7080	—	19,760
		J-55	—	1.80	1.049	0.955	1.469	—	1.900	10,000	9730	—	27,160
		C-75	1.70	1.80	1.049	0.955	1.469	1.660	1.900	13,640	13,270	20,540	37,040
		N-80	—	1.80	1.049	0.955	1.469	—	1.900	14,650	14,160	—	39,510
1 1/4	1.660	F-25	—	2.40	1.380	1.286	1.812	—	2.200	4400	3690	—	16,710
		H-40	—	2.40	1.380	1.286	1.812	—	2.200	6180	5910	—	26,740
		J-55	—	2.40	1.380	1.286	1.812	—	2.200	8490	8120	—	36,770
		C-75	2.30	2.40	1.380	1.286	1.812	2.054	2.200	11,580	11,070	29,120	50,140
		N-80	—	2.40	1.380	1.286	1.812	—	2.200	12,360	11,800	—	53,480
1 1/2	1.900	F-25	2.75	2.90	1.610	1.516	2.094	2.200	2.500	3920	3340	11,930	19,900
		H-40	2.75	2.90	1.610	1.516	2.094	2.200	2.500	5640	5350	19,090	31,980
		J-55	2.75	2.90	1.610	1.516	2.094	2.200	2.500	7750	7350	26,250	43,970
		C-75	2.75	2.90	1.610	1.516	2.094	2.200	2.500	10,570	10,020	35,800	59,960
		N-80	2.75	2.90	1.610	1.516	2.094	2.200	2.500	11,280	10,680	38,180	63,960

2	2.375	F-25	4.00	2.041	1.947	2.875	3530	3080	18,830				
		F-25	4.60	4.70	1.995	1.901	2.594	2.875	3.063	4160	3500	22,480	32,600
		H-40	4.00	2.041	1.947	2.875	5230	4930	30,130				
		H-40	4.60	4.70	1.995	1.901	2.594	2.875	3.063	5890	5600	35,960	52,170
		J-55	4.00	2.041	1.947	2.875	7190	6770	41,430				
		J-55	4.60	4.70	1.995	1.901	2.594	2.875	3.063	8100	7700	49,440	71,730
		C-75	4.00	2.041	1.947	2.875	9520	9230	56,500				
		C-75	4.60	4.70	1.995	1.901	2.594	2.875	3.063	11,040	10,500	67,430	97,820
		C-75	5.80	5.95	1.867	1.773	2.594	2.875	3.063	14,330	14,040	96,560	126,940
		N-80	4.00	2.041	1.947	2.875	9980	9840	60,260				
		N-80	4.60	4.70	1.995	1.901	2.594	2.875	3.063	11,780	11,200	71,920	104,340
		N-80	5.80	5.95	1.867	1.773	2.594	2.875	3.063	15,280	14,970	102,980	135,400
		P-105	4.60	4.70	1.995	1.901	2.594	2.875	3.063	15,460	14,700	94,400	136,940
		P-105	5.80	5.95	1.867	1.773	2.594	2.875	3.063	20,060	19,650	135,170	177,710
2 1/2	2.875	F-25	6.40	6.50	2.441	2.347	3.094	3.500	3.668	3870	3300	32,990	45,300
		H-40	6.40	6.50	2.441	2.347	3.094	3.500	3.668	5580	5280	52,780	72,480
		J-55	6.40	6.50	2.441	2.347	3.094	3.500	3.668	7680	7260	72,570	99,660
		C-75	6.40	6.50	2.441	2.347	3.094	3.500	3.668	10,470	9910	98,970	135,900
		C-75	8.60	8.70	2.259	2.165	3.094	3.500	3.668	14,350	14,060	149,360	186,290
		N-80	6.40	6.50	2.441	2.347	3.094	3.500	3.668	11,160	10,570	105,560	144,960
		N-80	8.60	8.70	2.259	2.165	3.094	3.500	3.668	15,300	15,000	159,310	198,710
		P-105	6.40	6.50	2.441	2.347	3.094	3.500	3.668	14,010	13,870	138,550	190,260
		P-105	8.60	8.70	2.259	2.165	3.094	3.500	3.668	20,090	19,690	209,100	260,810

Continued

—cont'd

Nom., in	Outside diameter (OD), in	Grade	Weight per feet With couplings, lb		Inside diameter, in	Drift diameter, in	OD of upset, in	OD of c, in		Collapse resistance, psi	Internal yield pressure, psi	Joint yield strength, lb	
			Non upset	Upset				Non upset	Upset			Non upset	Upset
3	3.500	F-25	7.70		3.068	2.943		4.250		2970	2700	40,670	
		F-25	9.20	9.3	2.992	2.867	3.750	4.250	4.500	3680	3180	49,710	64,760
		F-25	10.20		2.922	2.797		4.250		4330	3610	57,840	
		H-40	7.70		3.068	2.943		4.250		4630	4320	65,070	
		H-40	9.20	9.3	2.992	2.867	3.750	4.250	4.500	5380	5080	79,540	103,610
		H-40	10.20		2.922	2.797		4.250		6060	5780	92,550	
		J-55	7.70		3.068	2.943		4.250		5970	5940	89,470	
		J-55	9.20	9.3	2.992	2.867	3.750	4.250	4.500	7400	6980	109,370	142,460
		J-55	10.20		2.922	2.797		4.250		8330	7940	127,250	
		C-75	7.70		3.068	2.943		4.250		7540	8100	122,010	
		C-75	9.20	9.3	2.992	2.867	3.750	4.250	4.500	10,040	9520	149,140	194,260
		C-75	10.20		2.922	2.797		4.250		11,360	10,840	173,530	
		C-75	12.70	12.95	2.750	2.625	3.750	4.250	4.500	14,350	14,060	230,990	276,120
		N-80	7.70		3.068	2.943		4.250		7870	8640	130,140	
		N-80	9.20	9.3	2.992	2.867	3.750	4.250	4.500	10,530	10,160	159,080	207,220
		N-80	10.20		2.922	2.797		4.250		12,120	11,560	185,100	
		N-80	12.70	12.95	2.750	2.625	3.750	4.250	4.500	15,310	15,000	246,390	294,530
		P-105	9.20	9.3	2.992	2.867	3.750	4.250	4.500	13,050	13,340	208,790	271,970
		P-105	12.70	12.95	2.750	2.625	3.750	4.250	4.500	20,090	19,690	323,390	386,570

3 1/2	4.000	F-25	9.50		3.548	3.423		4.750		2630	2470	15,000	
		F-25		11.00	3.476	3.351	4.250		5.000	3220	2870		76,920
		H-40	9.50		3.548	3.423		4.750		4060	3960	72,000	
		H-40		11.00	3.476	3.351	4.250		5.000	4900	4580		123,070
		J-55	9.50		3.548	3.423		4.750		5110	5440	99,010	
		J-55		11.00	3.476	3.351	4.250		5.000	6590	6300		169,220
		C-75	9.50		3.548	3.423		4.750		6350	7420	135,010	
		C-75		11.00	3.476	3.351	4.250		5.000	8410	8600		230,760
4	4.500	N-80	9.50		3.548	3.423		4.750		6590	7910	144,010	
		N-80		11.00	3.476	3.351	4.250		5.000	8800	9170		246,140
		F-25	12.60	12.75	3.958	3.833	4.750	5.200	5.563	2.870	2.630	65,230	90,010
		H-40	12.60	12.75	3.958	3.833	4.750	5.200	5.563	4500	4220	104,360	144,020
		J-55	12.60	12.75	3.958	3.833	4.750	5.200	5.563	5720	5790	143,500	198,030
		C-75	12.60	12.75	3.958	3.833	4.750	5.200	5.563	7200	7900	195,680	270,030
		N-80	12.60	12.75	3.958	3.833	4.750	5.200	5.563	7500	8440	208,730	288,040

Nom, Nominal size.

Mathematical model for obtaining oil rate correction factor f_o

C

The oil rate correction factor for wellbore friction is defined as

$$F_o = \frac{Q_{oH,Friction}}{Q_{oH,No-friction}} \quad (C.1)$$

where $Q_{oH,Friction}$ and $Q_{oH,No-friction}$ are the oil production rates predicted by mathematical models with and without considering wellbore friction. The $Q_{oH,No-friction}$ can be estimated using the inflow model of [Furui et al. \(2003\)](#) that was derived assuming a fully penetrated box-shaped reservoir:

$$Q_{oH,No-friction} = J_{sp,o}L(p_e - p_{wf}) \quad (C.2)$$

where

$$J_{sp,o} = \frac{7.08 \times 10^{-3}k_H}{\mu_o B_o \left\{ I_{ani} \ln \left[\frac{hI_{ani}}{r_w(I_{ani} + 1)} \right] + \frac{\pi y_b}{h} - I_{ani}(1.224 - s) \right\}} \quad (C.3)$$

and

$$I_{ani} = \sqrt{\frac{k_H}{k_V}} \quad (C.4)$$

where

- L = length of drain hole, ft,
- p_e = reservoir pressure, psi,
- p_{wf} = flowing bottom-hole pressure psi,
- h = pay zone thickness, ft,
- k_H = horizontal permeability, md,
- k_V = vertical permeability, md,
- y_b = distance of boundary from drain hole, ft,
- s = skin face, dimensionless,
- B_o = oil formation volume factor, rb/stb, and
- μ_o = oil viscosity, cp.

The $Q_{oH,Friction}$ for a fully penetrated box-shaped reservoir was presented by Guo et al. (2007):

$$Q_{oH,Friction} = Q_{oc} + \frac{J_{sp,o}}{2b} \left[\frac{1}{(a + bx_c)^2} - \frac{1}{(a + bL)^2} \right] \quad (C.5)$$

where

$$Q_{oc} = 1351.34 \frac{\mu_o d_h}{\rho_o} \quad (C.6)$$

$$a = \frac{1}{\sqrt[3]{P_r - P_{wH}}} + 0.2752 C_1^{\frac{2}{3}} L \quad (C.7)$$

$$b = -0.2752 C_1^{\frac{2}{3}} \quad (C.8)$$

$$C_1 = \frac{2C_1'}{\sqrt{\frac{6g_c d_h}{f_f \rho_o}}} \quad (C.9)$$

$$C_1' = \frac{0.012 J_{sp,o}}{d_h^2} \quad (C.10)$$

where

P_{wH} = pressure at the heel of drain hole, psi,

d_h = equivalent diameter of the drain hole, in,

f_f = Fanning friction factor, dimensionless,

g_c = gravitational conversion factor, 32.17 lbf-ft/lbf-s², and

ρ_o = oil density, lb_m/ft³.

Reference

- Guo, B., Zhou, J., Liu, Y., Ghalambor, A., 2007. A rigorous analytical model for fluid flow in drain holes of finite conductivity applied to horizontal and multilateral wells. In: Paper SPE 106947, Presented at the SPE 2007 Production Operations Symposium in Oklahoma City, OK, Held 31 March–03 April 2007.
- Furui, K., Zhu, D., Hill, A.D., Aug 2003. A rigorous formation damage skin factor and reservoir inflow model for a horizontal well. SPE production & facilities 18 (3), 151–157.

Mathematical model for obtaining gas rate correction factor f_g

D

The gas rate correction factor for wellbore friction is defined as

$$F_g = \frac{Q_{gH,Friction}}{Q_{gH,No-friction}} \quad (D.1)$$

where $Q_{gH,Friction}$ and $Q_{gH,No-friction}$ are the gas production rates predicted by mathematical models with and without considering wellbore friction. The $Q_{gH,No-friction}$ can be estimated using the inflow model of [Furui et al. \(2003\)](#), which was derived assuming a fully penetrated box-shaped reservoir:

$$Q_{gH,No-friction} = J_{sp,g} L (p_e^2 - p_{wf}^2) \quad (D.2)$$

where

$$J_{sp,g} = \frac{k_H}{1424 \bar{\mu}_g \bar{z} T \left\{ I_{ani} \ln \left[\frac{h}{r_w (I_{ani} + 1)} \right] + \frac{\pi y_b}{h} - I_{ani} (1.224 - s) \right\}} \quad (D.3)$$

and

$$I_{ani} = \sqrt{\frac{k_H}{k_V}} \quad (D.4)$$

where

- L = length of drain hole, ft,
- p_e = reservoir pressure, psi,
- p_{wf} = flowing bottom-hole pressure psi,
- h = pay zone thickness, ft,
- k_H = horizontal permeability, md,
- k_V = vertical permeability, md,
- y_b = distance of boundary from drain hole, ft,
- s = skin face, dimensionless,
- T = reservoir temperature, °R,
- \bar{z} = gas compressibility factor, dimensionless, and
- $\bar{\mu}_g$ = gas viscosity, cp.

The $Q_{gH,Friction}$ for a fully penetrated box-shaped reservoir was presented by Guo et al. (2007):

$$Q_{gH,Friction} = \frac{3J_{sp}p_r}{\left(\frac{3}{C}\right)^{2/3}} \{2[F_1(z_0) - F_1(z)] - [F_2(z_0) - F_2(z)]\} \quad (D.5)$$

where

$$z = \frac{p_e}{3} \left[C_2 - \left(\frac{3}{C}\right)^{2/3} L \right] \quad (D.6)$$

$$z_0 = \frac{p_e C_2}{3} \quad (D.7)$$

$$F_1(z) = 3^{-1/3} \left\{ \begin{array}{l} \log(z + 3^{-1/3}) - \frac{1}{2} \log(z^2 - 3^{-1/3}z + 3^{-2/3}) \\ + 3^{1/2} \arctan \left[\frac{3^{1/2}}{3} (2 \times 3^{1/3}z - 1) \right] \end{array} \right\} \quad (D.8)$$

$$F_1(z_0) = 3^{-1/3} \left\{ \begin{array}{l} \log(z_0 + 3^{-1/3}) - \frac{1}{2} \log(z_0^2 - 3^{-1/3}z_0 + 3^{-2/3}) \\ + 3^{1/2} \arctan \left[\frac{3^{1/2}}{3} (2 \times 3^{1/3}z_0 - 1) \right] \end{array} \right\} \quad (D.9)$$

$$F_2(z) = 2F_1(z) + \frac{3z}{3z^3 + 1} \quad (D.10)$$

$$F_2(z_0) = 2F_1(z_0) + \frac{3z_0}{3z_0^3 + 1} \quad (D.11)$$

$$C = \frac{140.86}{J_{sp}} \sqrt{\frac{p_{wH} d_h^5}{f_f \gamma_g T}} \quad (D.12)$$

$$C_2 = \left(\frac{3}{C}\right)^{2/3} L + \frac{3}{p_e} \left(\frac{p_e - \frac{1}{3}(p_e - p_{wH})}{p_e - p_{wH}} \right)^{1/3} \quad (D.13)$$

where

- p_{wH} = pressure at the heel of drain hole, psi,
- d_h = equivalent diameter of the drain hole, in,
- f_f = Fanning friction factor, dimensionless,
- g_c = gravitational conversion factor, 32.17 lbf-ft/lbf-s², and
- γ_g = gas-specific gravity, air = 1.

Reference

- Guo, B., Zhou, J., Ghalambor, A., 2007. Effects of friction in drain hole on productivity of horizontal and multilateral wells. In: Paper SPE 106948, Presented at the SPE 2007 Asia Pacific Oil and Gas Conference & Exhibition (APOGCE) in Jakarta, Indonesia, Held 30 October–01 November 2007.
- Furui, K., Zhu, D., Hill, A.D., Aug 2003. A rigorous formation damage skin factor and reservoir inflow model for a horizontal well. *SPE production & facilities* 18 (3), 151–157.

Derivation of a mathematical model for predicting long-term productivity of modern multifractured horizontal wells

E

This section provides a derivation of an analytical model for predicting long-term productivity of modern multifractured shale gas/oil wells. Gas and oil wells are distinguished in the model by using different compressibility factors and the real gas law.

E.1 ASSUMPTIONS

The following assumptions are made in this model formulation. They are explained after being listed.

1. The oil- and gas-bearing formations are isotropic.
2. Pseudo—steady-state flow condition is reached within the well drainage area.
3. Linear flow prevails from rock matrix to the fractures.
4. Darcy's law dominates the fluid flow in the matrix and fractures.
5. Fracture skin is negligible.
6. Hydraulic fractures are identical and uniformly distributed in the drainage area.
7. Single oil-phase flow in undersaturated oil reservoirs and single gas-phase flow in dry gas reservoirs.

E.2 GOVERNING EQUATIONS

Consider a fluid flowing from matrix to one of the fractures as shown in [Figure E.1](#). Productivity of one fracture can be formulated on the basis of linear flow from the shaded quadrant of the fracture drainage area to the fracture.

Under pseudo—steady-state flow conditions compressible fluids move because of expansion in the depressurization process. Consider the fluid in a volume element V expressed as

$$V = \frac{1}{2} \phi h S_f \Delta x \quad (\text{E.1})$$

Based on the definition of compression coefficient

$$C = -\frac{1}{V} \left(\frac{\partial V}{\partial p} \right) \quad (\text{E.2})$$

Differentiation of [Eq. \(E.1\)](#) with respect to time gives an expression of the flow rate from the volume V :

$$CV \frac{\partial p}{\partial t} = -\frac{\partial V}{\partial t} = -q(x) \quad (\text{E.3})$$

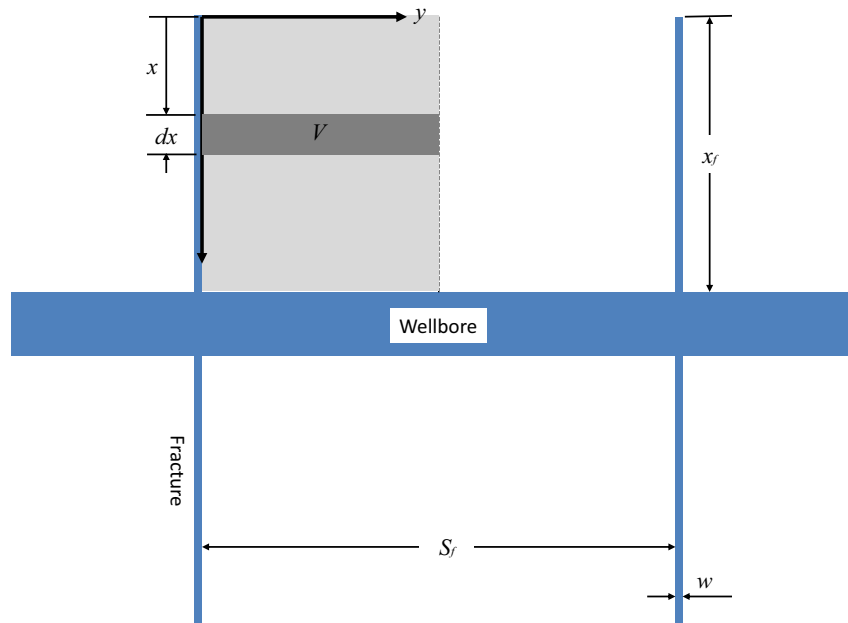


FIGURE E.1

A planar schematic of fluid flow from a quadrant of matrix volume V to a fracture.

Using Eq. (E.1), the pressure decline rate $\frac{\partial p}{\partial t}$ in Eq. (E.3) is then expressed as

$$\frac{\partial p}{\partial t} = -\frac{q(x)}{CV} = -\frac{2q(x)}{C\phi h S_f \Delta x} \quad (\text{E.4})$$

The following equation governs linear flow in porous media (Dake, 1978):

$$\frac{\partial^2 p}{\partial y^2} = \frac{\phi \mu C}{k_m} \frac{\partial p}{\partial t} \quad (\text{E.5})$$

Substituting Eq. (E.4) into Eq. (E.5) yields:

$$\frac{\partial^2 p}{\partial y^2} = -\frac{2\mu q(x)}{k_m h S_f \Delta x} \quad (\text{E.6})$$

Integrating Eq. (E.6) one time yields:

$$\frac{\partial p}{\partial y} = -\frac{2\mu q(x)}{k_m h S_f \Delta x} y + c_1 \quad (\text{E.7})$$

where c_1 is an integration constant and can be determined using the no-flow boundary condition

$$\left(\frac{\partial p}{\partial y} \right)_{y=S_f/2} = 0 \quad (\text{E.8})$$

Applying Eq. (E.8) to Eq. (E.7) gives:

$$c_1 = \frac{\mu q(x)}{k_m h \Delta x} \quad (\text{E.9})$$

Substituting Eq. (E.9) into Eq. (E.7) yields

$$\frac{\partial p}{\partial y} = \frac{\mu q(x)}{k_m h \Delta x} \left[1 - \frac{2y}{S_f} \right] \quad (\text{E.10})$$

Separating variables, Eq. (E.10) is changed to

$$\int dp = \int \frac{\mu q(x)}{k_m h \Delta x} \left[1 - \frac{2y}{S_f} \right] dy + c_2 \quad (\text{E.11})$$

Integration of Eq. (E.11) obtains

$$p = \frac{\mu q(x)}{k_m h \Delta x} \left[y - \frac{y^2}{S_f} \right] + c_2 \quad (\text{E.12})$$

where the integration constant c_2 can be determined using the boundary condition at the fracture face:

$$p|_{y=0} = p_f(x) \quad (\text{E.13})$$

where $p_f(x)$ is the pressure in the fracture at point x . Applying Eq. (E.13) to Eq. (E.12) gives

$$c_2 = p_f(x) \quad (\text{E.14})$$

Substituting Eq. (E.14) into Eq. (E.12) results in

$$p = p_f(x) + \frac{\mu q(x)}{k_m h \Delta x} \left[y - \frac{y^2}{S_f} \right] \quad (\text{E.15})$$

Along the no-flow boundary $y = \frac{S_f}{2}$, where the pressure is p_e , Eq. (E.15) demands

$$q(x) = \frac{4k_m h \Delta x}{\mu S_f} [p_e - p_f(x)] \quad (\text{E.16})$$

The Darcy velocity in the matrix in the y -direction at the fracture face at point x can thus be expressed as

$$v(x) = \frac{q(x)}{h \Delta x} = \frac{4k_m}{\mu S_f} [p_e - p_f(x)] \quad (\text{E.17})$$

The cumulative flow rate of fluid collected in a fracture interval between fracture tip and point x can be determined based on $v(x)$ as

$$Q(x) = 2 \int_0^x v(x) h dx = \int_0^x \frac{8k_m h}{\mu S_f} [p_e - p_f(x)] dx \quad (\text{E.18})$$

If the average width of the fracture is w , Darcy velocity $v_f(x)$ in the fracture can be formulated by dividing Eq. (E.18) by the cross-sectional area of the fracture:

$$v_f(x) = \frac{Q(x)}{wh} \quad (\text{E.19})$$

Applying Darcy's law to the flow along the fracture gives

$$v_f(x) = -\frac{k_f}{\mu} \frac{dp_f(x)}{dx} \quad (\text{E.20})$$

Coupling Eqs. (E.19) and (E.20) yields

$$\frac{Q(x)}{wh} = -\frac{k_f}{\mu} \frac{dp_f(x)}{dx} \quad (\text{E.21})$$

Substituting Eq. (E.18) into Eq. (E.21) and rearranging the latter gives

$$\frac{dp_f(x)}{dx} = -\int_0^x \frac{8k_m}{k_f w S_f} [p_e - p_f(x)] dx \quad (\text{E.22})$$

Differentiation of Eq. (22) with respect to x yields

$$\frac{d^2 p_f(x)}{dx^2} = -\frac{8k_m}{k_f w S_f} [p_e - p_f(x)] \quad (\text{E.23})$$

Defining p_d as the pressure drawdown at point x in the fracture:

$$p_d = p_e - p_f(x) \quad (\text{E.24})$$

and c is expressed in Darcy units as

$$c = \frac{8k_m}{k_f w \Delta_f} \quad (\text{E.25})$$

Substituting Eq. (E.24) and Eq. (E.25) into Eq. (E.23) gives

$$\frac{d^2 p_d(x)}{dx^2} = c p_d \quad (\text{E.26})$$

E.3 BOUNDARY CONDITIONS

The first boundary condition is expressed as

$$p_d|_{x=x_f} = p_d^* = p_e - p_w \quad (\text{E.27})$$

The second boundary condition may be expressed as

$$\left(\frac{dp_d}{dx} \right)_{p_d=0} = 0 \quad (\text{E.28})$$

E.4 SOLUTION

Let

$$p'_d = \frac{dp_d}{dx} \quad (\text{E.29})$$

then

$$\frac{d^2 p_d}{dx^2} = \frac{dp'_d}{dx} = \frac{dp'_d}{dp_d} \frac{dp_d}{dx} = p'_d \frac{dp'_d}{dp_d} \quad (\text{E.30})$$

Substituting Eq. (E.30) into Eq. (E.26) yields

$$p'_d \frac{dp'_d}{dp_d} = c p_d \quad (\text{E.31})$$

By separation of variables, a solution to Eq. (E.31) yields

$$\frac{1}{2} p_d'^2 = \frac{1}{2} c p_d^2 + c_3 \quad (\text{E.32})$$

Using the boundary condition Eq. (E.28), c_3 can be obtained:

$$c_3 = 0 \quad (\text{E.33})$$

Substituting Eq. (E.33) into Eq. (E.32) yields

$$p'_d = \sqrt{c} p_d \quad (\text{E.34})$$

Substituting Eq. (E.29) into Eq. (E.34) gives

$$\frac{dp_d}{dx} = \sqrt{c} p_d \quad (\text{E.35})$$

Integrating Eq. (E.35) yields

$$\ln p_d = \sqrt{c} x + c_4 \quad (\text{E.36})$$

Using the boundary condition of Eq. (E.27), c_4 can be obtained:

$$c_4 = \ln p_d^* - \sqrt{c} x_f \quad (\text{E.37})$$

Substituting Eq. (E.37) into Eq. (E.36) yields

$$\ln \left(\frac{p_d}{p_d^*} \right) = \sqrt{c} (x - x_f) \quad (\text{E.38})$$

or

$$p_d = p_d^* e^{\sqrt{c}(x-x_f)} \quad (\text{E.39})$$

Substitution of Eq.(E.24) and Eq.(E.27) into Eq.(E.39) results in an equation for pressure drawdown distribution in the fracture:

$$p_e - p_f(x) = (p_e - p_w) e^{\sqrt{c}(x-x_f)} \quad (\text{E.40})$$

The equation for pressure distribution in the fracture is then found to be

$$p_f(x) = p_e - (p_e - p_w) e^{\sqrt{c}(x-x_f)} \quad (\text{E.41})$$

To obtain an influx function of closed form, substituting Eq. (E.40) into Eq. (E.18) yields

$$Q(x) = \int_0^x \frac{8k_m h}{\mu S_f} (p_e - p_w) e^{\sqrt{c}(x-x_f)} dx \quad (\text{E.42})$$

which can be integrated resulting in the following inflow performance relationship

$$Q(x_f) = \frac{8k_m h}{\mu S_f \sqrt{c}} (p_e - p_w) \left(1 - e^{-\sqrt{c} x_f} \right) \quad (\text{E.43})$$

Then the production rate from one fracture is expressed as

$$Q_F = 2Q(x_f) = \frac{16k_m h}{\mu S_f \sqrt{c}} (p_e - p_w) \left(1 - e^{-\sqrt{c} x_f} \right) \quad (\text{E.44})$$

To obtain an expression for pressure distribution in the matrix, substituting Eq. (E.16) and Eq. (E.41) into Eq. (E.15) gives

$$p = p_e - (p_e - p_w)e^{\sqrt{c}(x-x_f)} + \frac{4}{S_f}(p_e - p_w)e^{\sqrt{c}(x-x_f)} \left[y - \frac{y^2}{S_f} \right] \quad (\text{E.45})$$

The average reservoir pressure, \bar{p} , may be taken as the average pressure in the matrix owing to the small volume of fractures:

$$\bar{p} = \frac{\int p dV}{\int dV} = \frac{\phi h \int_0^{x_f} \int_0^{S_f/2} p dy dx}{\phi h x_f (S_f/2)} \quad (\text{E.46})$$

Substituting Eq. (E.45) into Eq. (E.46) and integrating the later yields

$$\bar{p} = p_e - \frac{p_e - p_w}{3x_f\sqrt{c}} \left(1 - e^{-\sqrt{c}x_f} \right) \quad (\text{E.47})$$

which gives

$$p_e - p_w = \frac{\bar{p} - p_w}{1 - \frac{1 - e^{-\sqrt{c}x_f}}{3x_f\sqrt{c}}} \quad (\text{E.48})$$

Substituting Eq. (E.48) into Eq. (E.44) results in

$$Q_F = \frac{16k_m h (\bar{p} - p_w)}{\mu S_f \sqrt{c} \left[\frac{1}{1 - e^{-\sqrt{c}x_f}} - \frac{1}{3x_f\sqrt{c}} \right]} \quad (\text{E.49})$$

The productivity rate for a well with n_f identical fractures is expressed as

$$Q = \frac{16n_f k_m h (\bar{p} - p_w)}{\mu S_f \sqrt{c} \left[\frac{1}{1 - e^{-\sqrt{c}x_f}} - \frac{1}{3x_f\sqrt{c}} \right]} \quad (\text{E.50})$$

E.5 UNIT CONVERSION

Eq. (E.50) is a general inflow equation in Darcy units for wells with any single-phase fluid flow inside reservoirs. For oil wells, this equation, converted in US field units, is expressed as

$$Q_o = \frac{5.91 \times 10^{-3} n_f k_m h (\bar{p} - p_w)}{B_o \mu S_f \sqrt{c} \left[\frac{1}{1 - e^{-\sqrt{c}x_f}} - \frac{1}{3x_f\sqrt{c}} \right]} \quad (\text{E.51})$$

where c is expressed in US field units as

$$c = \frac{96k_m}{k_f w S_f} \quad (\text{E.52})$$

For gas wells, the flow rate in Eq. (E.53) is converted to surface condition using the real gas law:

$$\left[\frac{(\bar{p} + p_w)}{2} \right] \frac{Q}{zT} = \frac{p_{sc} Q_{sc}}{z_{sc} T_{sc}} \quad (\text{E.53})$$

Substituting $p_{sc} = 14.696$ psia, $z_{sc} = 1.0$, $T_{sc} = 520$ °R, and Q_{cs} in Mscf/d into this equation gives

$$Q_{sc} \frac{0.01769(\bar{p} + p_w) Q}{zT} \quad (\text{E.54})$$

Substituting Eq. (E.50) into Eq. (E.54) and rearranging the latter in US field units give an inflow equation for gas wells as

$$Q_g = \frac{5.87 \times 10^{-5} n_f k_m h (\bar{p}^2 - p_w^2)}{\mu T S_f \sqrt{c} \left[\frac{1}{1 - e^{-\sqrt{c} x_f}} - \frac{1}{3 x_f \sqrt{c}} \right]} \quad (\text{E.55})$$

where c is still given by Eq. (E.52).

Derivation of a mathematical model for predicting steady productivity of radial-fractured wells

F

This section documents the derivation of a mathematical model for describing productivity of radial fracture which is characterized by its length L_f , depth h_f , width w , and permeability k_G .

F.1 ASSUMPTIONS

The following assumptions are made in deriving a well inflow model:

1. The rock in the pay zone is homogeneous and anisotropic.
2. Linear flow of fluid governed by Darcy's law prevails in the rock.
3. All fractures are identical in geometry.
4. Pressure drop in the fractures is negligible.
5. Fluid flow from the rock directly to the wellbore is negligible.
6. Steady-state flow in the pay zone.

F.2 GOVERNING EQUATION

Fig. F.1 shows a sketch of fracture configuration around a wellbore. Consider a fluid particle at point P which is on the line of stagnation where $PA = PB$. The flow distance to fracture A is expressed as

$$PA = x \tan(\alpha) \quad (\text{F.1})$$

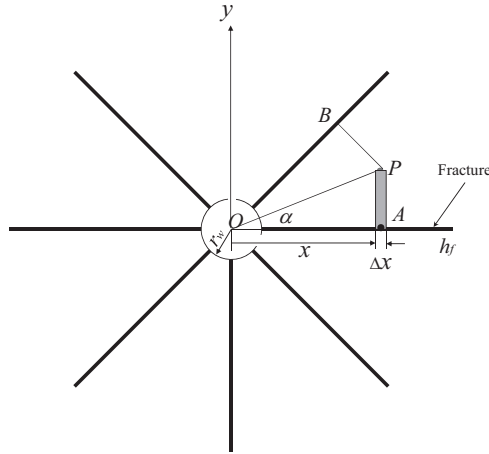


FIGURE F.1

A sketch of radial fracture configuration around a wellbore.

where the angle α relates to the number of fractures n ($n > 2$) around the wellbore by

$$\alpha = \frac{2\pi}{n} / 2 = \frac{\pi}{n}. \quad (\text{F.2})$$

where n is the number of fractures around the wellbore.

Consider the fluid flowing from point P to a fracture segment of width dx . According to Darcy's law, the fluid influx rate to the fracture segment can be expressed as

$$dq = \frac{kL_f(p_e - p_f)}{\mu(PA)} dx \quad (\text{F.3})$$

where k is the mean permeability of rock, L_f is the fracture length along the wellbore, \bar{p} is the reservoir pressure, p_f is the pressure in the fracture, and μ is the fluid viscosity. Substituting Eqs. (F.1) and (F.2) into Eq. (F.3) gives

$$dq = \frac{kL_f(p_e - p_f)}{\mu x \tan\left(\frac{\pi}{n}\right)} dx \quad (\text{F.4})$$

F.3 BOUNDARY CONDITION

Assuming linear flow of fluid to the fracture surface with a length of L_f and a total width between $x = r_w$ and $x = h_f$, the fluid influx rate to the fracture is null at $x = r_w$, i.e.,

$$q = 0 \quad \text{at } x = r_w \quad (\text{F.5})$$

F.4 SOLUTION

Integration of Eq. (F.4) using the boundary condition (F.5) gives

$$q = \int_{r_w}^{r_w+h_f} \frac{kL_f(p_e - p_f)}{\mu x \tan\left(\frac{\pi}{n}\right)} dx \quad (\text{F.6})$$

which results in

$$q = \frac{kL_f(p_e - p_f)}{\mu \tan\left(\frac{\pi}{n}\right)} \ln\left(\frac{r_w + h_f}{r_w}\right) \quad (\text{F.7})$$

Since each fracture has two faces, the total fluid influx rate into n fractures is expressed as

$$Q = 2nq = \frac{2nkL_f(p_e - p_f)}{\mu \tan\left(\frac{\pi}{n}\right)} \ln\left(\frac{r_w + h_f}{r_w}\right) \quad (\text{F.8})$$

F.5 UNIT CONVERSION

Eq. (F.8) is valid in Darcy's units. In US field units, it becomes

$$Q = \left[\frac{(60)(60)(24)cm^3 \text{ sec}}{(2.54)^3(12)^3ft^3 \text{ day}} \right] \times \frac{2nk \left[\frac{\text{Darcy}}{1000md} \right] L_f \left[\frac{(12)(2.54)}{ft} \right] (p_e - p_f) \left[\frac{\text{Atm}}{14.696psi} \right]}{\mu \tan\left(\frac{\pi}{n}\right)} \ln\left(\frac{r_w + h_f}{r_w}\right) \quad (\text{F.9})$$

or

$$Q = 0.01266 \frac{nkL_f(p_e - p_f)}{\mu \tan\left(\frac{\pi}{n}\right)} \ln\left(\frac{r_w + h_f}{r_w}\right) \quad (\text{F.10})$$

where the permeability is in md, viscosity is in cp, pressures are in psia, lengths are in ft, and fluid flow rate is in cubic feet per day in reservoir condition (rcfd).

If the reservoir fluid is natural gas liquid, or oil, the flow rate should be converted to stb/d:

$$Q_{NGL} = \frac{0.01266}{5.615} \frac{nkL_f(p_e - p_f)}{\mu_o B_o \tan\left(\frac{\pi}{n}\right)} \ln\left(\frac{r_w + h_f}{r_w}\right) \quad (\text{F.11})$$

or

$$Q_{NGL} = \frac{2.255 \times 10^{-3} nkL_f (p_e - p_f)}{\mu_o B_o \tan\left(\frac{\pi}{n}\right)} \ln\left(\frac{r_w + h_f}{r_w}\right) \quad (\text{F.12})$$

If the reservoir fluid is gas, the flow rate should be converted to Mscf/d using real gas law:

$$\left[\frac{(p_e + p_f)}{2}\right] \frac{Q}{zT} = \frac{p_{sc} Q_{sc}}{z_{sc} T_{sc}} \quad (\text{F.13})$$

Substituting $p_{sc} = 14.696$ psia, $z_{sc} = 1.0$, $T_{sc} = 520$ °R, and Q_{cs} in Mscf/d into this equation gives

$$Q_{sc} \frac{0.01769(p_e + p_f)Q}{zT} \quad (\text{F.14})$$

Substituting Eq. (F.10) into Eq. (F.12) results in

$$Q_{sc} = \frac{2.24 \times 10^{-4} nkL_f (p_e^2 - p_f^2)}{\mu_g zT \tan\left(\frac{\pi}{n}\right)} \ln\left(\frac{r_w + h_f}{r_w}\right) \quad (\text{F.15})$$

Derivation of a mathematical model for predicting pseudosteady productivity of radial-fractured wells

G

This section documents the derivation of a mathematical model for describing productivity of radial fracture which is characterized by its length L_f , depth h_f , width w , and permeability k_G .

G.1 ASSUMPTIONS

The following assumptions are made in deriving a well inflow model:

1. The rock in the pay zone is homogeneous.
2. Reservoir pressure is above bubble point so that single phase liquid flow dominates.
3. Linear fluid flow governed by Darcy's law prevails in the rock.
4. All fractures are identical in geometry and are uniformly distributed around the wellbore based on the tests made by previous investigators (Dysart et al., 1969) which shows that explosive fractures can propagate in all directions.
5. Fluid flow from the rock directly to the wellbore is negligible.
6. Pseudo—steady-state flow prevails in the fractured region.

G.2 GOVERNING EQUATION

Figure F.1 shows a sketch of radial fractures around a wellbore. It can be shown that the half-angle between fractures is $\alpha = \frac{\pi}{n}$ where n is the number of fractures.

Consider the fluid flow from point P to point A at a radial distance x from the wellbore centerline. The fluid flow rate $q(x)$ over a short interval of fracture dx can be formulated. Under pseudo-steady-state flow condition, the fluid production is driven by the expansion of fluid and rock in the reservoir. The total compressibility of reservoir is defined as

$$c_t = -\frac{1}{V} \left(\frac{\partial V}{\partial p} \right) \quad (\text{G.1})$$

Differentiation of Eq. (G.1) with respect to time gives an expression of the flow rate

$$c_t V \frac{\partial p}{\partial t} = -\frac{\partial V}{\partial t} = -q(x) \quad (\text{G.2})$$

where the fluid volume is expressed as

$$V = \phi \left[\frac{x \tan(\alpha) + (x + \Delta x) \tan(\alpha)}{2} \right] \Delta x L_f \approx \phi L_f \tan(\alpha) x \Delta x \quad (\text{G.3})$$

The pressure decline rate $\frac{\partial p}{\partial t}$ in Eq. (G.2) is then expressed as

$$\frac{\partial p}{\partial t} = -\frac{q(x)}{c_t V} = -\frac{q(x)}{c_t \phi L_f \tan(\alpha) x \Delta x} \quad (\text{G.4})$$

It is well known that the following equation governs linear flow in porous media:

$$\frac{\partial^2 p}{\partial y^2} = \frac{\phi \mu c_t}{\bar{k}} \frac{\partial p}{\partial t} \quad (\text{G.5})$$

where the effective permeability in the y -direction perpendicular to the fracture orientation can be estimated based on horizontal and vertical permeabilities, i.e., $\bar{k} = \sqrt{k_h k_v}$.

Substituting Eq. (G.4) into Eq. (G.5) yields

$$\frac{\partial^2 p}{\partial y^2} = -\frac{\mu q(x)}{\bar{k} L_f \tan(\alpha) x \Delta x} \quad (\text{G.6})$$

Integrating Eq. (G.6) one time yields

$$\frac{\partial p}{\partial y} = -\frac{\mu q(x)}{\bar{k} L_f \tan(\alpha) x \Delta x} y + c_1 \quad (\text{G.7})$$

where c_1 is an integration constant and can be determined using the no-flow boundary condition

$$\left(\frac{\partial p}{\partial y} \right)_{y=x \tan(\alpha)} = 0 \quad (\text{G.8})$$

Applying Eq. (G.8) to Eq. (G.7) gives

$$c_1 = \frac{\mu q(x)}{\bar{k}L_f \Delta x} \quad (\text{G.9})$$

Substituting Eq. (G.9) into Eq. (G.7) gives

$$\frac{\partial p}{\partial y} = \frac{\mu q(x)}{\bar{k}L_f \Delta x} \left[1 - \frac{y}{x \tan(\alpha)} \right] \quad (\text{G.10})$$

Separating variables, Eq. (G.10) is changed to

$$\int dp = \int \frac{\mu q(x)}{\bar{k}L_f \Delta x} \left[1 - \frac{y}{x \tan(\alpha)} \right] dy \quad (\text{G.11})$$

which is integrated to get

$$p = \frac{\mu q(x)}{\bar{k}L_f \Delta x} \left[y - \frac{y^2}{2x \tan(\alpha)} \right] + c_2 \quad (\text{G.12})$$

where the integration constant c_2 can be determined using the boundary condition at the fracture face

$$p|_{y=0} = p_f(x) \quad (\text{G.13})$$

where $p_f(x)$ is the pressure in the fracture at point x . Applying Eq. (G.13) to Eq. (G.12) gives

$$c_2 = p_f(x) \quad (\text{G.14})$$

Substituting Eq. (G.14) into Eq. (G.12) results in

$$p = p_f(x) + \frac{\mu q(x)}{\bar{k}L_f \Delta x} \left[y - \frac{y^2}{2x \tan(\alpha)} \right] \quad (\text{G.15})$$

Along the no-flow boundary $y = x \tan(\alpha)$, the pressure is \bar{p} . Eq. (G.15) demands

$$q(x) = \frac{2\bar{k}L_f \Delta x}{\mu x \tan(\alpha)} [\bar{p} - p_f(x)] \quad (\text{G.16})$$

The fluid velocity in the matrix in the y -direction at the fracture face at point x can thus be expressed as

$$v(x) = \frac{q(x)}{L_f \Delta x} = \frac{2\bar{k}}{\mu x \tan(\alpha)} [\bar{p} - p_f(x)] \quad (\text{G.17})$$

The cumulative flow rate of fluid collected by a fracture interval between wellbore and point A can be determined based on $v(x)$ as

$$Q(x) = 2 \int_x^{h_f} v(x) L_f dx = -2 \int_{h_f}^x \frac{2\bar{k}L_f}{\mu x \tan(\alpha)} [\bar{p} - p_f(x)] dx \quad (\text{G.18})$$

If the average width of the fracture is w , Darcy velocity $v_f(x)$ in the fracture can be formulated by dividing Eq. (G.18) by the cross-sectional area of the fracture:

$$v_f(x) = \frac{Q(x)}{wL_f} \quad (\text{G.19})$$

Applying Darcy's law to the flow along the fracture gives

$$v_f(x) = -\frac{k_f}{\mu} \frac{dp_f(x)}{dx} \quad (\text{G.20})$$

Coupling Eq. (G.20) and Eq. (G.19) yields

$$\frac{Q(x)}{wL_f} = -\frac{k_f}{\mu} \frac{dp_f(x)}{dx} \quad (\text{G.21})$$

Substituting Eq. (G.18) into Eq. (G.21) and rearranging the latter give

$$\frac{dp_f(x)}{dx} = 2 \int_{h_f}^x \frac{2\bar{k}}{wk_f x \tan(\alpha)} [\bar{p} - p_f(x)] dx \quad (\text{G.22})$$

Differentiation of Eq. (G.22) with respect to x yields

$$\frac{d^2 p_f(x)}{dx^2} = \frac{4\bar{k}}{wk_f x \tan(\alpha)} [\bar{p} - p_f(x)] \quad (\text{G.23})$$

Defining p_d as the pressure drawdown at point x in the fracture:

$$p_d = \bar{p} - p_f(x) \quad (\text{G.24})$$

and

$$c = \frac{4\bar{k}L_f}{wk_f \tan(\alpha)} \quad (\text{G.25})$$

Substituting Eqs. (G.24) and (G.25) into Eq. (G.23) yields

$$\frac{d^2 p_d}{dx^2} = \frac{c}{x} p_d \quad (\text{G.26})$$

G.3 BOUNDARY CONDITIONS

The first boundary condition is expressed as

$$p_d|_{x=r_w} = p_d^* = \bar{p} - p_w \quad (\text{G.27})$$

The second boundary condition is given at the wellbore and expressed as

$$p_d|_{x=h_f} = 0 \quad (\text{G.28})$$

G.4 SOLUTION

The general solution to Eq. (G.26) is

$$p_d = C_1 \sqrt{x} J_1(2i\sqrt{c} \sqrt{x}) + C_2 \sqrt{x} N_1(2i\sqrt{c} \sqrt{x}) \quad (\text{G.29})$$

where J_1 is the Bessel function of the first kind in the order of 1 and N_1 is the Bessel function of the second kind in the order of 1. The constants C_1 and C_2 are determined based on the boundary conditions to be:

$$C_1 = -\frac{p_d^* T_{12}}{T_{02} T_{11} - T_{12} T_{01}} \quad (\text{G.30})$$

$$C_2 = \frac{p_d^* T_{11}}{T_{02} T_{11} - T_{12} T_{01}} \quad (\text{G.31})$$

where

$$T_{01} = \sqrt{r_w} J_1(2i\sqrt{c} \sqrt{r_w}) \quad (\text{G.32})$$

$$T_{02} = \sqrt{r_w} N_1(2i\sqrt{c} \sqrt{r_w}) \quad (\text{G.33})$$

$$T_{11} = \sqrt{h_f} J_1(2i\sqrt{c} \sqrt{h_f}) \quad (\text{G.34})$$

$$T_{12} = \sqrt{h_f} N_1(2i\sqrt{c} \sqrt{h_f}) \quad (\text{G.35})$$

Substituting Eq. (G.24) into Eq. (G.18) results in

$$Q(x) = -\int_{h_f}^x \frac{4\bar{k}L_f}{\mu x \tan(\alpha)} p_d dx \quad (\text{G.36})$$

The expression for fluid production from a whole fracture is obtained by setting $x = r_w$, or

$$Q_1 = -\int_{h_f}^{r_w} \frac{4\bar{k}L_f}{\mu x \tan(\alpha)} p_d dx \quad (\text{G.37})$$

or

$$Q_1 = \frac{4\bar{k}L_f}{\mu \tan(\alpha)} \int_{r_w}^{h_f} \frac{p_d}{x} dx \quad (\text{G.38})$$

The expression for fluid production from n fracture is

$$Q = \frac{4n\bar{k}L_f}{\mu \tan(\alpha)} \int_{r_w}^{h_f} \frac{p_d}{x} dx \quad (\text{G.39})$$

where p_d is given by Eq. (G.29).

G.5 UNIT CONVERSION

Eq. (G.39) is valid in Darcy's units. In US field units, it becomes

$$Q = \left[\frac{(60)(60)(24) \text{ cm}^3 \text{ sec}}{(2.54)^3 (12)^3 \text{ ft}^3 \text{ day}} \right] \frac{4n\bar{k} \left[\frac{\text{Darcy}}{1000 \text{ md}} \right] L_f \left[\frac{(12)(2.54)}{\text{ft}} \right]}{\mu \tan(\alpha)} \int_{r_w}^{h_f} \frac{p_d \left[\frac{\text{Atm}}{14.696 \text{ psi}} \right]}{x} dx \quad (\text{G.40})$$

or

$$Q = 0.02532 \frac{n\bar{k}L_f}{\mu \tan(\alpha)} \int_{r_w}^{h_f} \frac{p_d}{x} dx \quad (\text{G.41})$$

where the flow rate is in standard cubic foot per day in reservoir condition, permeability is in md, viscosity is in cp, pressures are in psia, and lengths are in ft.

If the reservoir fluid is oil, the flow rate should be converted to stb/d:

$$Q_o = \frac{0.02532}{5.615} \frac{n\bar{k}L_f}{\mu \tan(\alpha)} \int_{r_w}^{h_f} \frac{p_d}{x} dx \quad (\text{G.42})$$

or

$$Q_o = \frac{5.51 \times 10^{-3} n\bar{k}L_f}{\mu \tan(\alpha)} \int_{r_w}^{h_f} \frac{p_d}{x} dx \quad (\text{G.43})$$

If the reservoir fluid is gas, the flow rate should be converted to Mscf/d using real gas law:

$$\left[\frac{(\bar{p} + p_w)}{2} \right] \frac{Q}{zT} = \frac{p_{sc} Q_{sc}}{z_{sc} T_{sc}} \quad (\text{G.44})$$

Substituting $p_{sc} = 14.696$ psia, $z_{sc} = 1.0$, $T_{sc} = 520$ °R, and Q_{cs} in Mscf/d into this equation gives

$$Q_{sc} \frac{0.01769(\bar{p} + p_w) Q}{zT} \quad (\text{G.45})$$

Substituting Eq. (G.41) into Eq. (G.45) results in

$$Q_{sc} = \frac{4.48 \times 10^{-4} n\bar{k}L_f (\bar{p} + p_w)}{\mu_g z T \tan(\alpha)} \int_{r_w}^{h_f} \frac{p_d}{x} dx \quad (\text{G.46})$$

Reference

Dysart, G.R., Spencer, A.M., Anderson, A.L., 1969. Blast-fracturing. In *Drilling and Production Practice*. American Petroleum Institute.

Index

Note: Page numbers followed by “f” indicate figures, “t” indicate tables and “b” indicate boxes.

A

Absolute open flow (AOF), 66–68
Absolute permeability, 38
Acidizing, 11
American Petroleum Institute (API), 8, 94
 performance properties of API tubing,
 208t–211t
Analytical model, 185
Annular flow, 100, 136
AOF. *See* Absolute open flow (AOF)
API. *See* American Petroleum Institute (API)
Atmospheric pressure, 109
Average compressibility factor, 115
Average temperature, 114–115

B

Blast fracturing, 197–198, 198f
Bottom-water drive reservoirs, 4–5
Bubble flow, 100

C

Calcite (CaCO_3), 36
Carbonate rocks, 36
Casing
 hanger, 8
 head, 8
Cemented sleeves, 12
Chalk, 36
Chen’s correlation, 95–96, 99
“Christmas Tree”, 8, 10f
Churn flow, 100
Colebrook–White equation, 95–96
Composite IPR of stratified reservoirs,
 79–83
 applications, 82–83
 partial two-phase flow, 81–82
 single-phase liquid flow, 80–81
 two-phase flow, 81
Compressibility factor, 113
 method, 114–115
Compression coefficient, 220
Constant-bottom-hole pressure solution, 56
Constant-rate solution, 54–55
Conventional well completions, 11
Correction factor, 152–153
Crude oil, 18
Cullender and Smith method, 116–118, 118t

D

Darcy velocity, 222
Darcy’s law, 56–58, 222, 228, 234
Darcy–Wiesbach friction factor, 96–99, 105,
 114
 diagram, 96f
Deliverability
 of fractured wells, 142–144
 of horizontal wells, 145–153
 of vertical wells, 124–141
Density, 33
Deviation factor. *See* Gas compressibility—factor
Discharge coefficient, 150
Dissolved-gas drive reservoir, 5, 7f
Dolomite ($\text{CaMg}(\text{CO}_3)_2$), 36
Down-hole chokes, 9
Dynamic viscosity, 26

E

Edge-water drive reservoirs, 4–5
Effective permeability, 38–43
 determination, 41–43
 flow regimes, 40–41
Entrained droplet movement model, 136
Explosive blast fractures, 197–198

F

Fanning friction factor, 95–99, 105, 110
Fetkovich’s method, 86–88
Fetkovich’s equation, 70
Film movement model, 136
First Law of Thermodynamics, 94–95, 113
Fishbone type for multilateral wells, 11–12
Fishbone wells, 165–171, 166f
 gas wells, 170–171
 oil wells, 167–169
Flow regimes, 40–41, 100, 165
 horizontal linear flow, 40
 horizontal pseudo-linear flow, 41
 horizontal pseudo-radial flow, 41
 horizontal radial flow, 40
 laminar, 95
 turbulent, 95
 vertical radial flow, 40–41
Fluid injection, 93
Fluid interfacial tension, 34–36, 35t
Fluid-productive sandstones, 37

- Four-phase flow model, 189
- Fracture(s), 197
 penetration, 199–200, 200b
 spacing, 190–191
- Fractured wells, 59–63, 142–144
 Argawal et al. (1979), 59–61
 Cinco-Ley and Samaniego (1981), 59–63
 fracture conductivity, 62–63
 single-fractured gas wells, 144
 single-fractured oil wells, 142
 Valko et al. (1997), 62–63
- Fully penetrated box-shaped reservoir, 213–217
- G**
- Garbage-in, garbage-out (GIGO), 14
- Gas
 condensate, 3
 coning reservoirs, 11, 11f
 density, 30–31
 expansion factor, 32
 formation volume factor, 32
 phase, 100
 pseudocritical pressure and temperature, 24–25
 rate correction factor (F_g), 215–216
 viscosity, 26–27
 Carr, Kobayashi, and Burrows, 27
 Dean-Stiel (1958), 27
 Dempsey (1965), 26–27
 dynamic viscosity, 26
 kinematic viscosity, 26
 Lee-Gonzalez-Eakin (1966), 27
 wells, 3–9, 11
 liquid loading in, 136–141
 mist flow in, 119
 in volumetric reservoirs, 132–135, 152–153
- Gas compressibility, 33
 factor, 28–33
 Brill and Beggs's correlation, 29–30
- Gas-cap drive reservoirs, 5, 6f
- Gas-injection wells, 114
- Gas-saturated crude oil, 21–22
- Gas-specific gravity, 23–24
- Gas–liquid two-phase flow, 100
- Gas–oil ratio (GOR), 3, 19, 79
- Gas–oil–water three-phase system, 100–101
- Gas–oil–water–sand four-phase system, 100–101
- GIGO. *See* Garbage-in, garbage-out (GIGO)
- GOR. *See* Gas–oil ratio (GOR)
- Griffith correlation, 107
- Guo and Schechter's model, 186
- Guo–Ghalambor method, 106, 170–171
 four-phase flow model, 189
- Guo's method, 138–141
- Guo's mist-flow model, 145, 174
- H**
- Hagedorn–Brown correlation, 107, 111, 168–169, 174, 187–188
- Hemispherical flow regime, 41–42
- High-energy gas fracturing (HEGF), 197
- Homogeneous-flow models, 101–106
 spreadsheet program Poettmann-CarpenterBHP, xls, 104t, 106t–107t
- Horizontal linear flow, 40
- Horizontal pseudo-linear flow, 41
- Horizontal pseudo-radial flow, 41
- Horizontal radial flow, 40
- Horizontal wellbore length, 11
- Horizontal wells, 11, 12f, 63–64, 145–153, 183, 185. *See also* Modern multifractured horizontal wells; Multifractured horizontal wells; Vertical wells
- Economides et al. (1991), 63–64, 149
 gas wells in volumetric reservoirs, 152–153
 Guo et al. (2007), 63–64, 150
- ICDs, 149
- Joshi (1988), 63–64, 147
 multifractured, 12
 oil wells
 in volumetric reservoirs, 145–147
 in water-/gas-coning reservoirs, 147–150
 volume-fractured, 190–193, 192b
 gas wells, 192–193
 oil wells, 191–192
- Hydraulic fracturing, 11, 197
- Hydraulic refracturing, 197–198
- Hydrocarbon phase diagram, 3–4, 5f
- I**
- ICDs. *See* Inflow control devices (ICDs)
- IFT. *See* Interfacial tension (IFT)
- Igneous rocks, 36–37
- Impermeable formations, 38
- In-situ volume fraction, 100
- Inflow control devices (ICDs), 149, 151f, 152t
- Inflow model, 213–216
- Inflow performance relationship (IPR), 1, 14, 32, 54, 65–73, 124, 126f, 128f, 130f, 134f, 168

- composite IPR of stratified reservoirs, 79–83
 - future, 84–88
 - Fetkovich's method, 86–88
 - Vogel's method, 85–86
 - for partial two-phase oil reservoirs, 72–73
 - partial two-phase reservoir, 74
 - productivity index, 65–68, 74, 82
 - reservoir inflow models, 65
 - single phase reservoir, 65–68
 - test points, 65, 74–78
 - two-phase reservoirs, 69–71
 - Bandakhlia and Aziz (1989), 69–70
 - Chang (1992), 69–70
 - Fetkovich (1973), 69–70
 - Retnanto and Economides (1998), 69–70
 - Standing (1971), 69–70
 - Vogel (1968), 69–70
 - Vogel's IPR model, 72, 85–86
 - Inflow–outflow analysis, 173
 - Interfacial tension (IFT), 34–35
 - Iteration procedure, 14
- J**
- Joshi's equation, 63–64
- K**
- Kinematic viscosity, 26
- L**
- Laminar flow regimes, 95
 - Lava, 36–37
 - Linear flow, 183, 185
 - Linear IPR model, 69
 - Linear-radial flow model, 186
 - Liquid
 - droplets, 139
 - holdup, 100
 - loading, 136–141
 - analysis, 119
 - annular flow, 136
 - entrained droplet movement model, 137–138
 - Guo's method, 138–141
 - slug flow, 136
 - solutions, 140–141
 - transport velocity, 139
 - Turner's method, 136–138
 - phase, 101
 - viscosity, 101
 - volume fraction, 139
 - Lithology, 18
- M**
- Magma, 36–37
 - Mathematical models, 63–64, 94
 - Metamorphic rocks, 37
 - mHB correlation. *See* Modified Hagedorn–Brown correlation (mHB correlation)
 - Microcracks, 190–191
 - Mist flow, 100
 - in gas wells, 119
 - model, 138
 - Mixing rule, 26
 - Modern multifractured horizontal wells. *See also* Horizontal wells; Multifractured horizontal wells
 - assumptions, 219
 - boundary conditions, 223
 - governing equations, 220–223
 - solution, 223–225
 - unit conversion, 225–226
 - Modern well type productivities, 163
 - Modified Hagedorn–Brown correlation (mHB correlation), 107, 110, 125
 - Moody friction factor, 96–99
 - Multifractured horizontal wells, 12, 13f, 185–189.
 - See also* Horizontal wells; Modern multifractured horizontal wells
 - drainage area shape, 186
 - Furui (2003) model, 186
 - gas wells, 189
 - Guo and Schechter's model (1997), 186
 - Guo and Yu (2008), 185, 189
 - Li et al. (1996), 185
 - oil wells, 185–188
 - Raghavan and Joshi (1993), 183
 - Multilateral wells, 11–12, 165
 - fishbone wells, 165–171, 166f
 - Furui et al. (2003), 167
 - mixed properties of fluids, 174
 - pseudolinear-radial-combined model, 167
 - root wells, 165, 166f, 171–178
 - symbols in, 173f
 - Multiphase flow
 - Brown (1977), 100–101
 - Guo and Ghalambor (2005), 103
 - liquid holdup, 100
 - in oil wells, 99–111
 - flow regimes, 100
 - Poettmann and Carpenter (1952), 101
 - single-phase gas flow, 113–118
 - single-phase liquid flow, 94–99
 - TPR models, 100–111

- Multiphase flow (*Continued*)
 homogeneous-flow models, 101–106
 separated-flow models, 107–111
- Multiphase fluid, 94
- Multiphase gas wells, 119
- N**
- Natural gas, 18
 properties, 23–27
 gas compressibility factor, 28–33
 gas pseudocritical pressure and temperature, 24–25
 gas viscosity, 26–27
 gas-specific gravity, 23–24
 sample problem, 24b–25b
- Naturally flowing well, 3, 4f
- Newton–Raphson’s iterative method, 30, 140–141
- No-flow boundary condition, 57–58, 232
- NODAL analysis, 14, 123–124
 principle in well productivity forecast, 2
- Non-Darcy flow coefficient (D), 186
- O**
- Oil, 3–9
 compressibility, 22
 density, 19–20
 formation volume factor, 20–21
 and natural gas, 93
 properties, 19–22
 rate correction factor (F_o), 213–214
 reservoirs, 4
 sample problem, 22b
 solution GOR, 19
 viscosity, 21–22
- Oil wells, 6, 7f, 11
 multiphase flow in, 99–111
 in volumetric reservoirs, 125–129, 145–147
 in water-/gas-coning reservoirs, 130–131, 147–150
- Open-hole logs, 36
- Outflow performance relationship (OPR), 124
- P**
- Packers, 8
- Partial two-phase flow, composite IPR, 81–82
- Partial two-phase oil reservoirs, IPR for, 72–73
- Pay zone thickness, 11
- Pay zones, 165
- Perforation cluster, 190
- Permeability, 18
- Permeable formations, 38
- Petroleum fluids, 18
 composition, 18t
- Petroleum production, 93
 wells, 1
- Petroleum reservoir properties
 reservoir fluid properties, 18–36
 reservoir rock properties, 36–47
- PI. *See* Productivity index (PI)
- “Plug and perf” method, 12
- Poettmann–Carpenter’s model, 101
- Porosity, 18
- Pressure–flow rate relationship, 124
- Produced water, 18
 properties, 33–34
 density, 33
 salinity, 33
 specific gravity, 33
 water compressibility, 34
 water formation volume factor, 34
 water viscosity, 33
- Production casing, 8
- Production liner, 8
- Production tubing, 8
- Productivity index (PI), 65–68, 74, 82
- Pseudolinear-radial-combined model, 167
- Pseudoradial flow, 165
- Pseudosteady productivity of radial-fractured wells, 231. *See also* Steady productivity of radial-fractured wells
 assumptions, 231
 boundary conditions, 234
 governing equation, 231–234
 solution, 235
 unit conversion, 236
- Pseudo–steady-state flow, 57–58
- Pseudo–steady-state production, 127, 128t, 134–135, 144, 146b–147b
 of radial-fractured wells, 201–203
- R**
- Radial flow, 183
- Radial fractured wells, 12, 13f
- Radial fractures, 197–198
- Radial-fractured wells
 productivity
 HEGF vertical oil well, 202b–203b
 pseudo–steady-state production, 201–203
 steady-state production, 199–200
 pseudosteady productivity of, 231
 assumptions, 231
 boundary conditions, 234

- governing equation, 231–234
 - solution, 235
 - unit conversion, 236
 - steady productivity of, 227
 - assumptions, 227
 - boundary condition, 229
 - governing equation, 228
 - solution, 229
 - unit conversion, 229–230
 - Relative permeability, 38–39
 - Reservoir rock properties, 36–47
 - lithology, 36–37
 - carbonate rocks, 36
 - igneous rocks, 36–37
 - metamorphic rocks, 37
 - sedimentary rocks, 36
 - pay zone, 36
 - porosity, 37
 - reservoir permeability, 38–39
 - effective permeability, 38–43
 - relative permeability, 38–39
 - skin factor, 44–47
 - total compressibility, 37–38
 - Reservoir(s), 3–9
 - deliverability, 53, 123–124
 - equation, 187
 - fractured wells, 59–63
 - horizontal wells, 63–64
 - inflow performance relationship, 65–73
 - vertical wells, 54–58
 - fluid properties, 18–36
 - fluid interfacial tension, 34–36
 - natural gas properties, 23–27
 - oil properties, 19–22
 - produced water properties, 33–34
 - influx model, 149
 - productivity, 14
 - Reynolds number, 95
 - Root type for multilateral wells, 11–12
 - Root wells, 165, 166f, 171–178
- S**
- Salinity, 33
 - Saturated oil, 3–4
 - Sedimentary rocks, 36
 - Separated-flow models, 107–111
 - pressure profile, 113f
 - spreadsheet program HagedornBrownCorrelation.xls, 111t–112t
 - Shape factor, 58, 59f–60f
 - Single phase reservoir, IPR for, 65–68
 - Single-fractured gas wells, 144
 - Single-fractured oil wells, 142
 - Single-phase
 - flow, 3–4
 - fluid, 94
 - gas flow, 113–118
 - average temperature and compressibility factor method, 114–115
 - Cullender and Smith method, 116–118
 - liquid flow, 94–99
 - composite IPR, 80–81
 - Skin factor, 44–47
 - Slug flow, 100, 136
 - Solution gas–oil ratio (Solution GOR), 19, 102–103
 - Solution-gas drive reservoir. *See* Dissolved-gas drive reservoir
 - Specific gravity, 33
 - SRV. *See* Stimulated reservoir volume (SRV)
 - Standard temperature and pressure (STP), 19
 - Steady productivity of radial-fractured wells, 227.
 - See also* Pseudosteady productivity of radial-fractured wells
 - assumptions, 227
 - boundary condition, 229
 - governing equation, 228
 - solution, 229
 - unit conversion, 229–230
 - Steady-state flow, 56–57
 - Steady-state production, 129, 129t–130t
 - of radial-fractured wells, 199–200
 - Stimulated reservoir volume (SRV), 190
 - Stock tank conditions (STP), 20–21
 - STP. *See* Standard temperature and pressure (STP); Stock tank conditions (STP)
 - Superficial velocity, 108
 - Surface casing, 8
 - Surface chokes, 8–9
- T**
- Total compressibility of reservoir, 232
 - TPR. *See* Tubing performance relationship (TPR)
 - Transient flow, 54–56
 - Dake (1978), 54–55
 - Earlougher (1977), 56
 - Transient production, 125, 126t, 132–133
 - Transport velocity, 139
 - Trial-and-error method, 14, 172–178
 - Tubing head, 8
 - Tubing performance relationship (TPR), 94, 134–135, 134f, 168–169, 187–188, 188f
 - models, 100–111
 - homogeneous-flow models, 101–106

- Tubing performance relationship (TPR) (*Continued*)
 - separated-flow models, 107–111
 - Tubing string, 8, 94f, 103, 111
 - interior, 95–96
 - Tubing/wellbore performance relationship (TPR), 1
 - Tufa, 36
 - Turbulent flow
 - pattern, 100
 - regimes, 95
 - Turner's method, 136–138
 - Two-phase flow, 3–4
 - composite IPR, 81
 - Two-phase friction factor, 102–103
 - Two-phase reservoirs, IPR for, 69–71
- U**
- Unconventional well completions, 11–12
 - Undersaturated crude oil, 22
 - Undersaturated oil, 3–4
 - Unit conversion factors, 205t
- V**
- Vertical radial flow, 40–41
 - Vertical wells, 11, 54–58. *See also* Horizontal wells
 - deliverability of, 124–141
 - gas wells in volumetric reservoirs, 132–135
 - liquid loading in gas wells, 136–141
 - oil wells in volumetric reservoirs, 125–129
 - oil wells in water-/gas-coning reservoirs, 130–131
 - pseudo-steady-state flow, 57–58
 - steady-state flow, 56–57
 - transient flow, 54–56
 - Vogel's method, 85–86
 - Vogel's IPR model, 72
 - Volume-fractured horizontal wells, 190–193
 - Volumetric flow rate, 108
 - Volumetric reservoirs
 - gas wells in, 152–153
 - oil wells in, 125–129, 145–147
- W**
- Water
 - compressibility, 34
 - cone, 130
 - coning reservoirs, 11, 11f
 - drive reservoirs, 4–5, 6f
 - formation volume factor, 34
 - viscosity, 33
 - water-/gas-coning reservoirs, oil wells in, 130–131, 147–150
 - water-free production rate, 148
 - water-specific gravity, 33
 - Well completions, 9–12
 - conventional, 11
 - unconventional, 11–12
 - Well deliverability, 123–124
 - Well inflow performance, 123–124
 - Well productivity, 14, 123–124, 165, 190
 - basics, 1
 - deliverability
 - of fractured wells, 142–144
 - of horizontal wells, 145–153
 - of vertical wells, 124–141
 - gas wells in volumetric reservoirs, 132–135
 - oil wells
 - in volumetric reservoirs, 125–129, 145–147
 - in water-/gas-coning reservoirs, 130–131, 147–150
 - principles, 124
 - transient production, 125, 132–133
 - Well strings, 93
 - Wellbore, 93, 119, 165
 - flow performance, 123–124
 - lateral bores, 165
 - performance, 93
 - WellFlo, 44–47
 - Wellhead, 8, 9f
 - pressure, 94–95
- Z**
- Z-factor. *See* Gas compressibility—factor

Well Productivity Handbook, Second Edition

Vertical, Fractured, Horizontal, Multilateral,
Multi-fractured, and Radial-Fractured Wells

Boyun Guo

Reservoir and production engineers address challenging issues in development of oil and gas fields using complex well structures in today's energy industry.

Well Productivity Handbook, 2nd edition, provides updated example solutions to deliverability of various types of modern well structures. Improved to address productivity models of both simple and complex well completions, this reference presents petroleum engineers the full scope of productivity simulation through well modeling solutions with computer-aided examples. Starting from estimating fluid properties and estimation of reservoir properties, the content discusses modeling of inflow performance of simple well structures producing different types of fluids, describes the principle of well productivity analysis, and extends the principle from simple traditional well structures to modern complex well structures including multilateral, multifractured, and radial fractured horizontal wells. Rounding out with sample problems to solve and future references to pursue, *Well Productivity Handbook, 2nd edition* continues to give reservoir and production engineers the tools needed to tackle the full spectrum of well completion types.

Key Features

- Covers the full range of well completion types, from conventional to unconventional including multilateral, multifractured, and radial fractured well deliverability.
- Delivers practical elements including well model review, illustrative examples, chapter summary, future references, and exercise problems at the end of each chapter.
- Updated with complex well structures, new case studies, and essential derivations.

About the Author

Dr. Boyun Guo is well known for his contributions to the oil and gas industry in horizontal well drilling and completion engineering. He is currently a professor at the University of Louisiana at Lafayette in the Petroleum Engineering Department and Director of the Center for Optimization of Petroleum Systems. He has over 35 years of work experience in the oil and gas industry and academia including China National Petroleum Corporation, New Mexico Institute of Mining and Technology, Edinburgh Petroleum Services, and Intec Engineering. He holds a BS degree from Daqing Petroleum Institute, an MS degree from Montana College of Mineral Science and Technology, and a PhD from New Mexico Institute of Mining and Technology, all in Petroleum Engineering. Dr. Guo has authored over 150 technical papers and published 10 books of which 9 reside with Elsevier.

Related titles

Petroleum Production Engineering, 2nd Edition by Guo, Liu, and Tan/978-0-12-809374-0

Advanced Production Decline Analysis and Application by Sun/978-0-12-802411-9

Advanced Well Completion, 3rd Edition by Renpu/978-0-12-385868-9

Technology and Engineering / Petroleum



Gulf Professional Publishing

An imprint of Elsevier

elsevier.com/books-and-journals

ISBN 978-0-12-818264-2



9 780128 182642